Quantum properties of ultra-short pulses generated by SPOPOs: multi-mode squeezing and entanglement

Giuseppe Patera

Université Pierre et Marie Curie-Paris6
Laboratoire Kastler Brossel

Universitá degli Studi dell'Insubria
Facoltá di Scienze, Como
Dipartimento di Fisica e Matematica

Thèse de doctorat UPMC en co-tutelle avec Università dell'Insubria présentée par
Tesi di dottorato dell'Universitá dell'Insubria in cotutela con UPMC presentata da

Giuseppe Patera

Quantum properties of ultra-short pulses generated by SPOPOs: multi-mode squeezing and entanglement

Soutenue le 5 novembre 2008 devant le jury composé de:
Sostenuta il 5 novembre 2008 davanti la commissione composta da:

M. Claude FABRE	**Directeur de thèse**
M. Marco GENOVESE	**Rapporteur**
M. Luigi A. LUGIATO	**Directeur de thèse**
M. Emmanuel ROSENCHER	**Rapporteur**
M. Germán de VALCARCEL	**Examinateur**

Contents

Introduction

The intrinsic statistical behavior of light, arising from its quantum nature, induces fluctuations which degrade the precision of the measurements. Such fluctuations are unavoidable even when all other sources of noise have been canceled and are usually referred to as *quantum noise*. The quantum noise level associated to usual light sources, in which the photons are randomly distributed, is known as *shot-noise* or *standard quantum limit*. For a classical field the shot-noise represents the ultimate precision permitted in a measurement of one of the field quadrature, but since the 70's the existence of states of the light for which quantum fluctuations are below the shot-noise was experimentally demonstrated. In fact Heisenberg's principle is a constraint only for the product of the variances of two conjugate observables (i.e. two field quadratures), which means that the fluctuations of one observable can be reduced below the shot-noise provided that, at the same time, the noise on the conjugate observable is enhanced.

After the first pioneering works in the '70, the possibility of controlling and manipulating quantum fluctuations was soon predicted then experimentally demonstrated. The existence of such non-classical states permits to exploit them as sources to beat the limit of the shot-noise in many applications involving the detection of light. The reduction (or squeezing) of the fluctuations of a particular quadrature of the electromagnetic field has been proposed for increasing the sensitivity of phase-sensitive measurements beyond the quantum limit, for example in high sensitivity spectroscopy and interferometric measurements for the detection of gravitational waves.

The interest in manipulating quantum fluctuations does not only reside in squeezing quantum noise. In 1935, Einstein, Podolsky and Rosen pointed out the paradoxical fact that for a special class of states, say *entangled*, quantum theory could predict correlations stronger than the ones predictable by any other theory obeying "local realism" and this led them to conclude that quantum theory was incomplete. In 1964, J. S. Bell derived his well-known inequalities which fix an upper limit to the strength of correlations for theories obeying local realism and permitted to test experimentally quantum theory. After 1964, an increasing number of experimental tests supported the consistency of quantum entanglement and, after *quantum teleportation* was demonstrated, entangled states began to be considered as the main resource in quantum communication protocols.

The generation, investigation and manipulation of quantum states has been, so far, essentially performed in single mode systems. In recent years, it has become more and more appealing to exploit optical systems supporting multi-mode electromagnetic fields for reasons that are grounded both on a fundamental and practical point of view. Well known since the beginnings of the laser physics, complex phenomena connected to the presence of

several (temporal or spatial) modes of the electromagnetic field inside laser cavities have been considered undesirable because they are not easy to handle: for this reason filters were used in order to reduce their number. After the 80's the interest in complex systems led to reassess the multi-modal phenomena arising in laser systems, now regarded as paradigms of what happens in more complex systems such as fluids, chemistry and biology [Haken]. Self-organization, in general, stems out each time that several number of modes are let to compete by means of a non-linear interaction. Therefore non-linear laser systems are the best candidates for putting in evidence these phenomena in optical domain: pattern formation in the space domain and self phase-modulation in time domain are among the most known examples. On the other side, applications like the mode-locking of laser fields, the need to exchange informations through communication channels of higher and higher capacities, the capability to extract information from complex signals (like a radio signal or an image from a CCD camera) require devices exploiting a larger number of modes.

An optical image corresponds to a specific light distribution that can be recorded onto our retina or onto a detection device such as the CCD detector of a camera. The classical criterion of Rayleigh sets a lower limit, of the order of a detected light wavelength, to the resolution power of optical devices ascribing it to diffraction, but the great improvement reached in processing of detected images permits to go beyond this classical limit. The quantum nature of light will manifest as a shot-noise by limiting the quality of the detected signal. In order to account for the transverse spatial distribution of quantum fluctuations a complete quantum multi-mode description of the field is needed. Inside this picture the concept of noise reduction or signal amplification can be transferred from mono-mode to multi-mode beams so that concepts such as local squeezing [Kolobov1989] or the amplification of several transverse modes [Kolobov1995] can be introduced. The investigation of ultimate performance limits in optical imaging imposed by the quantum nature of light and the conciliation of this description of the electromagnetic field with imaging processing are among the principal goals of *quantum imaging* [Lugiato1995].

Sources producing highly multi-mode fields are needed not only in image processing experiments but also because multi-modal aspect of quantum imaging allows to greatly increase the information capacity of several quantum information protocols such as, for example, quantum teleportation and quantum dense coding. Most of the proposition for producing non-classical spatial multi-mode beams involve the parametric down conversion effect in nonlinear crystals and the two main systems in which these effects have been studied, theoretically and experimentally, are the optical parametric amplifier (OPA) [Kolobov1999, Lugiato2002] and the optical parametric oscillator (OPO) [Lopez2005, Fabre2007].

At the same time, a great number of experiments have obtained extraordinary performances combining image processing techniques to the use of high precision detectors. For example precisions of the order of nanometer have been achieved in the measure of position of a laser beam by means of a double quadrant detector [Boccara1980, Charbonnier1990, Putman1992, Kojima1997]. It is possible to show that, whereas a mono-mode squeezed beam cannot improve the measurement [Fabre2000], squeezed fluctuations in an appropriate mode can be used to beat the standard quantum limit [Treps2002].

Nowadays protocols for standard communication or for extraction of information from complex signals are rather based on the exchange of broadband light in a well defined

transverse spatial mode (for example the guided mode of an optical fiber), in which the information is conveyed by the temporal variation of the light amplitude and phase, in an analog or digital way. In this case the multimode optical system considered is the set of all the possible temporal shapes of the light pulses. Temporal multi-mode laser sources gain the same appeal as spatial multi-mode devices in the measure they are employed to beat quantum standard limit. For example, like the quantum laser pointer, a multi-mode pulsed source of squeezed light could be exploited for beating the shot-noise in measures of time delay with very high sensibility. Implementation for parallel transfer of quantum communication by means of several temporal modes can be envisaged too.

It is clear that for implementing these applications, sources of temporal multi-mode non-classical light are required. Parametric down conversion in concomitance with a pulsed pump field is at the base for such a sources. The simplest device is made up of a single pass amplifier (OPA) pumped by means of one short pump pulse [Wasilewski2006a]. As a consequence, in the Fourier space, temporal modes are described by a continuous spectrum. Since perfect quantum properties are achieved only when the pump power goes to infinity, systems combining high peak pump powers (obtained for examples from Q-switched or mode-locked lasers) with the feedback of the cavities are more efficient than OPAs. Such systems are the synchronously pumped optical parametric oscillators (SPOPO) which are OPO cavities pumped by a c.w. train of ultra-short (femtoseconds) pump pulses generated by a mode-locked laser whose cavity free spectral range is adjusted in order to be equal to the OPO free spectral range (synchronization). SPOPO devices have been used in order to generate ultrashort optical pulses of tunable wavelength or to efficiently control the pulse compression, and their temporal properties have been theoretically investigated [Cheung1991] but, at the best of our knowledge, their properties have not been studied yet on the quantum point of view.

The goal of this thesis is to extend to the time and frequency degrees of freedom of an optical beam the multi-modal approach so far adopted in the context of quantum imaging. Indeed, the analogy between the spatial and time/frequency degrees of freedom immediately appears by observing that as like an optical image can be regarded as a coherent superposition of several transverse modes, a frequency comb is a coherent superposition of optical frequencies. Such combs are produced by means of mode-locked lasers and, in a temporal picture, they correspond to a train of pulses which are mutually coherent. For these reasons, a good choice for a temporal multi-modal analysis is represented by a SPOPO. We, therefore, present here the complete quantum multi-mode model of SPOPO cavities. Starting from the equations of the motion for the intra-cavity field operators, the classical problem of the steady state solutions below threshold will first be approached, thus permitting a detailed study of the classical functioning of the device. This problem depends on the solution of an eigenvalue equation from the spectrum of which it is possible to extract information about the threshold and the spectral shape of the temporal modes that will oscillate. On the other hand, the quantum analysis shows not only that SPOPOs are able to produce non-classical states, for example squeezed states, but also that a whole set of temporal modes (say “super-modes”) own non-classical properties. Finally, we illustrate that, thanks to their multi-modal character, SPOPOs could be exploited as a compact source of multi-mode entangled states which can be useful in quantum communication protocols.

In the first chapter of this thesis, we will resume the fundamental theoretical aspects of the quantum optics such as the notion of continuous variables, the Heisenberg inequalities for conjugate observables and the statistical properties of the field fluctuations that characterize squeezed or entangled states. The second chapter is dedicated to a brief introduction of the basic functioning of synchronously pumped OPOs. It will be introduced, also, a formal description of mode-locked laser beams, both from a classical and quantum point of view. Being made of a large number of longitudinal modes of the laser cavity, we address the question whether or not mode-locked beams are multi-mode and introduce some tools, developed in the context of quantum imaging, for discerning multi-mode from single-mode light. In the third chapter we will present a complete multi-mode quantum model for different typologies of degenerate type I SPOPOs. We will consider both ring and linear geometries and both singly resonant (for the signal field) and doubly resonant configurations for the resonator. The fourth chapter is dedicated to the study of the classical linearized dynamics of the SPOPO in the below threshold regime, with a particular attention to the influence of the typology of the non-linearity and of other experimental parameters on the dynamics of the device. Finally in the fifth chapter we will approach, from the quantum point of view, the multi-mode characterization of the output field of SPOPOs. Starting, then, from the evidence of its multi-mode non classical character, we will finally illustrate a general scheme for the engineering of multi-mode quantum states.

CHAPTER 1

Quantum optics in continuum variables

Contents

Quantum fluctuations and correlations of variables of the electromagnetic field with a continuous spectrum have been extensively studied in the field of quantum optics. The capacity of manipulating them is witnessed by results such as squeezing of light [Slusher1987], generation of twin beams [Heidmann1987, Fabre1989], quantum non-destructive measurements [Roch1997, Grangier1998].

The great variety of practical applications of quantum systems to the exchange and treatment of the information has lead, in the past years, to the birth of the domain of quantum information and communication. Initially, protocols adapted to this purpose were realized by manipulating systems for which the possible results of a measurement can assume only discrete values, like as particles of spin 1/2, two level atoms or the polarization of a photon. Nevertheless, more recently, the possibility of coding an information by means of the quadratures of the electromagnetic field (phase or amplitude, for example) or by means of the collective angular momentum of an ensemble of atoms made quantum systems with continuous variables more and more appealing. This was confirmed

by the experimental demonstration of teleportation, dense coding and entanglement with continuous variables systems, which presents different advantages with respect to discrete variables like as the simplicity to produce, manipulate and detect the corresponding quantum states.

In this chapter we will shortly introduce some basic aspects of quantum optics in continuous variables with a particular attention to non-classical two-mode correlations.

1.1 Quantization of e.m. field in continuum variables

A single mode of the electromagnetic field corresponding to a plane wave propagating and polarized along well established directions and oscillating at a frequency ω can be classically described as the real part of a complex number:

$$E(t) = E_0(t)\,\mathrm{e}^{-i\omega t} + E_0^*(t)\,\mathrm{e}^{i\omega t} \tag{1.1}$$

where $E_0 = |E_0(t)|\,\mathrm{e}^{-i\phi(t)}$ is its slowly varying complex envelope at the carrying frequency ω. This expression can be recasted after the introduction of the two terms in quadrature $X(t)$ and $P(t)$:

$$E(t) = X(t)\cos(\omega t) + P(t)\sin(\omega t) \tag{1.2}$$

where:

$$\begin{aligned} X(t) &= |E_0(t)|\cos(\phi(t)) \\ P(t) &= |E_0(t)|\sin(\phi(t)) \end{aligned}$$

In Heisenberg's representation, the description of a quantized field is made by means of the construction and destruction operators $\hat{a}$ and $\hat{a}^\dagger$ associated to the considered e.m. mode:

$$\hat{E}(t) = \hat{a}(t)\,\mathrm{e}^{-i\omega t} + \hat{a}^\dagger(t)\,\mathrm{e}^{i\omega t} \tag{1.3}$$

where $\hat{a}(t)$ and $\hat{a}^\dagger(t)$ satisfy the commutation relation:

$$\left[\hat{a}(t), \hat{a}^\dagger(t')\right] = \delta(t - t') \tag{1.4}$$

The choice of the quadrature components is arbitrary because it corresponds to a particular definition of the Fresnel reference frame. In this way it is possible to define, in a general manner, a couple of conjugated quadratures as:

$$\begin{aligned} \hat{X}_\theta(t) &= \hat{a}(t)\,\mathrm{e}^{-i\theta} + \hat{a}^\dagger(t)\,\mathrm{e}^{i\theta} \\ \hat{P}_\theta(t) &= -i\left(\hat{a}(t)\,\mathrm{e}^{-i\theta} - \hat{a}^\dagger(t)\,\mathrm{e}^{i\theta}\right) \end{aligned} \tag{1.5}$$

In the case where the field has a non-null average, the couple of conjugated quadratures for $\theta = \phi$ is privileged respect to the others and corresponds respectively to the amplitude and phase quadrature.

Quadrature operators are simply dimensionless form of position and momentum operators corresponding to the harmonic oscillator associated to the field mode during the quantization formalism. Their commutation relation is:

$$\left[\hat{X}(t), \hat{P}(t')\right] = 2i\,\delta(t - t') \tag{1.6}$$

1.2 Fluctuations of the e.m. field

A non-null commutator implies a lower limit to the product of the variances which implies the existence of a Heisenberg's uncertainty relation for the two conjugate quadrature operators:

$$\langle \Delta^2 \hat{X}_\theta \rangle \langle \Delta^2 \hat{P}_\theta \rangle \geq 1 \tag{1.7}$$

This means that, even in principle, it is not possible to measure at the same time with an arbitrary precision the two quadratures as a consequence of the fact that quantum fluctuations are an intrinsic property of physical observables.

In the Fresnel reference frame, a classical field like the one in Eqs. (1.1) and (1.2) is represented by means of its quadrature components X_θ and P_θ as a vector whose the norm and angle represent respectively the field amplitude and phase (see figure). The quantum nature of the light, however, is at the origin of fluctuations around the mean value represented by the classical amplitude and phase of the field thus producing a distribution in the Fresnel reference frame for repeated measurements. The properties of such a distribution is completely determined by means of its moments, but in general for the states that will be presented in the following it is enough the first and the second moments, respectively the mean value and the variance of the distribution. In general the distribution is not homogeneous, therefore variances of all quadratures should be determined by performing a *tomography* of the specific state.

1.2.1 Vacuum and coherent states

The quantification of the electromagnetic field brings to an exact parallelism between the dynamics of each electromagnetic mode and the dynamics of a harmonic oscillator. Classically speaking, the state corresponding to the minimum allowed energy is referred to as vacuum state in the sense that there is absence of any excitation. In a quantum framework, even if the expectation values of position and momentum operators in the vacuum state are zero, Heisenberg's inequalities fix a minimum bound for the product of their variances. Zero-point fluctuations have a number of consequences such as spontaneous emission, the Casimir effect, the Van-Der Waals bonds, the Lamb shift, all phenomena experimentally tested with success.

The vacuum state is a *minimal incertitude* state for which Eq. (1.7) becomes an equality and all the quadrature components have the same variance $\Delta^2 \hat{X}_\theta = \Delta^2 \hat{P}_\theta = 1$. The fluctuations corresponding to the vacuum state are referred to as the standard quantum limit or shot-noise and are reference for a long time considered an ultimate limit now overcome by non-classical states.

To the class of minimal incertitude states belong in general the *coherent states* of which vacuum state is a particular case. Differently from the latter, their mean photon number is not zero. Introduced by Glauber in 1963 [Glauber1963], coherent states are the one whose properties better approach that of the classical field of stable amplitude and fixed phase. According to the idea that a coherent state corresponds to the vacuum state but of a non zero excitation, their formal expression can be obtained by applying the *displacement* operator:

$$\hat{D}(\alpha) = \mathrm{e}^{\alpha \hat{a}^\dagger - \alpha^* \hat{a}} \tag{1.8}$$

where $\alpha \in \mathbb{C}$, to the vacuum state $|0\rangle$:

$$|\alpha\rangle = \hat{D}(\alpha)|0\rangle \tag{1.9}$$

The first and second moment for the number operator $\hat{N} = \hat{a}^\dagger \hat{a}$ are:

$$\langle \hat{N} \rangle = |\alpha|^2 \tag{1.10}$$

$$\left\langle \Delta^2 \hat{N} \right\rangle = \langle \hat{N} \rangle^2 + \langle \hat{N} \rangle \tag{1.11}$$

Eq. (1.10) clarify how $|\alpha|$ is connected to the amount of excitation (the number of photons) of the considered e.m. mode, while Eq. (1.11) is the typical expression for poissonian probability distributions. In fact the probability of finding n photons in the mode is given by:

$$P(n) = |\langle n \mid \alpha \rangle|^2 = \mathrm{e}^{-\langle \hat{N} \rangle} \frac{\langle \hat{N} \rangle^n}{n!} \tag{1.12}$$

that is the typical distribution of completely aleatory events.

1.2.2 Squeezed states

If Heisenberg's inequality fixes a lower bound for the product of the variances for a given field state, on the other side it does not fix any constraint on the individual variances. The homogeneity of conjugated quadratures respect to any choice of the angle θ can be then not verified and state for which one of the two quadratures presents fluctuations below the shot-noise are possible at the price that the conjugated quadrature presents fluctuation amplified at least as much the fluctuations of the other quadrature have been reduced respect the standard quantum limit. Such states are called *squeezed states* and their fluctuations in the Fresnel reference frame have a Gaussian distribution characterized by the two widths corresponding to the variances respectively of the reduced and the amplified quadratures (see figure). In this case the probability of finding n photons in a squeezed state has a sub-Poissonian distribution. Squeezed states can be formally obtained applying the squeeze operator:

$$\hat{S}(\Lambda) = \mathrm{e}^{\frac{1}{2}\left(\Lambda^* \hat{a}^2 - \Lambda\, \hat{a}^{\dagger\, 2}\right)} \tag{1.13}$$

with $\Lambda \in \mathbb{C}$, to a general coherent state $|\alpha\rangle = \hat{D}(\alpha)|0\rangle$. As an example results only for the vacuum state will be reported without loosing generality since the action of the $\hat{D}$-operator produce only a displacement proportional to the absolute value of the complex number α. The expectation values of the quadrature operators defined in (1.5) for vacuum squeezed state $|\Lambda\rangle = \hat{S}(\Lambda)|0\rangle$ are:

$$\langle \Lambda | \hat{X}_\theta | \Lambda \rangle = \langle \Lambda | \hat{P}_\theta | \Lambda \rangle = 0 \tag{1.14}$$

and, setting $\Lambda = \zeta \mathrm{e}^{i\vartheta}$, the corresponding variances are:

$$\langle \Delta^2 X_\theta \rangle = \mathrm{e}^{2\zeta} \sin^2\left(\tfrac{\vartheta}{2} - \theta\right) + \mathrm{e}^{-2\zeta} \cos^2\left(\tfrac{\vartheta}{2} - \theta\right) \tag{1.15}$$

$$\langle \Delta^2 Y_\theta \rangle = \mathrm{e}^{2\zeta} \cos^2\left(\tfrac{\vartheta}{2} - \theta\right) + \mathrm{e}^{-2\zeta} \sin^2\left(\tfrac{\vartheta}{2} - \theta\right) \tag{1.16}$$

1.2.3 GHZ states

Greenberger-Horne-Zeilinger states (GHZ) are states that involve many subsystems (for example particles) and have extremely non-classical properties. For an ensemble of N qubits states, if the Hilbert space of the k-th subsystem is $\mathcal{H}_k$, a GHZ state living in the space $\mathcal{H}_k = \mathcal{H}_1 \otimes \ldots \otimes \mathcal{H}_N$ can be expressed:

$$|GHZ\rangle_N = \frac{1}{\sqrt{2}} \left(|0 \ldots 0\rangle + |1 \ldots 1\rangle \right). \tag{1.17}$$

1.3 Quantum correlations

In 1935, Einstein, Podolsky and Rosen proposed a thought experiment by means of which, using a special two-particle quantum state owing perfect correlations in position and momentum, they raised the problem of the completeness of quantum mechanics. The EPR experiment, in fact, brings to the dichotomy according to which either the measurements performed of one part A of the quantum state has a non-local effect on the physical reality of the other distant part, in the sense that quantum mechanics can predict outcomes of some measurements carried out at B, or quantum mechanics is incomplete in the sense that some element of physical reality corresponding to the cannot be accounted for by quantum mechanics (that is, some extra variable is needed to account for it).

If the hypothesis of the incompleteness of quantum mechanics is accepted, "hidden" variables obeying to some classical probability distribution law should be introduced in order to complete the theory. As proven by Bell [Bell1964] and after confirmed in many experiments [Aspect1981, Aspect1982, Incompleteness], local causality cannot be maintained even considering a local hidden variables model.

The consequence is that quantum mechanics is a non-local theory and *entangled* quantum states such the one proposed in the thought experiment by EPR reveal to be an essential resource in information processing.

The following is a rapid summary of the more complete review [Treps2004] of some criteria commonly used to recognize quantum correlations.

1.3.1 Twin states

Let's consider two modes 1 and 2 that can be spatially separated and the two corresponding quadratures $\hat{X}_i$, $i = 1, 2$.

The variance on the difference operator $\hat{X}_- = \hat{X}_1 - \hat{X}_2$ defines a quantity known as "gemellity" ("twinship") that is a measure of correlations that exist between the fluctuation of the two quadratures:

$$G = \frac{\langle \Delta^2 \hat{X}_- \rangle}{2} = \frac{\langle \Delta^2 (\hat{X}_1 - \hat{X}_2) \rangle}{2} \tag{1.18}$$

If $G < 1$, or equivalently the gemellity is below the quantum standard limit, the measured correlation cannot be explained by a model involving only classical fluctuations and the two modes are said to be *twin*.

1.3.2 QND-correlated states

A QND measurement consists in performing a measure on a first system highly correlated to a second one in order to extract information from the latter without perturbing it. If the quadratures $\hat{X}_1$ and $\hat{X}_2$ of two distinguishable modes of the e.m. field are perfectly correlated, a QND measure will thus permit to obtain without incertitude the expectation value of $\hat{X}_2$ by measuring the first quadrature.

The estimator for a QND measure is given by the conditional variance of $\hat{X}_2$:

$$\langle \Delta^2(\hat{P}_2|\hat{P}_1)\rangle = \langle \Delta^2 \hat{P}_2\rangle - \frac{\langle \delta\hat{P}_1 \delta\hat{P}_2\rangle^2}{\langle \Delta^2 \hat{P}_1\rangle} \tag{1.19}$$

where $\delta\hat{P}_i = \hat{P}_i - \langle \hat{P}_i\rangle$. If $\langle \Delta^2(\hat{P}_2|\hat{P}_1)\rangle$ lower than the shot-noise then the measure is QND and it is the mark that there are quantum correlations between the two modes.

1.3.3 EPR correlations and Reid's criterion

The paradox as originally proposed by EPR considered two causally separated particles whose position and momentum operators (represented by $\hat{X}_A$, $\hat{P}_A$, $\hat{X}_B$ and $\hat{P}_B$) are, respectively, perfectly correlated and anti-correlated. By virtue of their correlation, a measure of $\hat{X}_A$ gives with certainty the position of the particle B without perturbing the system. Thus, it must exist an element of reality associated to the position of B. An analogous reasoning imply that also the momentum $\hat{P}_B$ has a predetermined value. But in quantum mechanics the position and momentum of a system cannot have definite values at the same time: the paradoxical situation led EPR to conclude that quantum mechanics is not complete.

The EPR thought experiment was, after, extended by Reid [Reid1989] to continuum variables optical systems envisaging an experimental implementation. According to Reid's argument, EPR paradox can be directly obtained by means of not maximal correlations/anti-correlations between the conjugated quadratures of two optical modes. In this case there will be an error in deducing information about the first system by a measure on the second one. However, it is still possible to obtain a paradox provided that the product of the inferred variances on the conjugated quadratures is small enough compared to the Heisenberg's uncertainty bound. This is equivalent to require that:

$$\langle \Delta^2(\hat{X}_2|\hat{X}_1)\rangle \langle \Delta^2(\hat{P}_2|\hat{P}_1)\rangle < 1 \tag{1.20}$$

1.3.4 Inseparable states

A more general class of quantum states whose EPR states are a subset are the non-separable states. A bipartite system completely characterized by its density matrix ρ is said to be not separable if:

$$\hat{\rho} \neq \sum_i p_i \, \hat{\rho}_{i_1} \otimes \hat{\rho}_{i_2} \tag{1.21}$$

where $\hat{\rho}_{i_1}$ and $\hat{\rho}_{i_2}$ are the density matrices of modes 1 and 2 and p_i the associated probabilities. Several criteria have been proposed to investigate separability of the mixed states for continuum variables systems [Duan2000, Simon2000, Mancini2002] and a unifying criterion has been proposed by Giovannetti *et al.* [Giovannetti2003].

1.3.5 Squeezing and entanglement

There is a close connection between squeezing and entanglement. Let's consider a 50/50 beam splitter on which are mixed two beams represented by destruction operators $\hat{a}_1$ and $\hat{a}_2$. The transformation induced by the beam splitter is:

$$\hat{a}_{(+)} = \frac{\hat{a}_1 + \hat{a}_2}{\sqrt{2}} \tag{1.22}$$

$$\hat{a}_{(-)} = \frac{\hat{a}_1 - \hat{a}_2}{\sqrt{2}} \tag{1.23}$$

The variances of the two conjugated quadrature operators of the sum and difference modes are therefore:

$$\langle \Delta^2 \hat{P}_{(-)} \rangle = \frac{\langle \Delta^2 (\hat{P}_1 - \hat{P}_2) \rangle}{2} \tag{1.24}$$

$$\langle \Delta^2 \hat{X}_{(+)} \rangle = \frac{\langle \Delta^2 (\hat{X}_1 + \hat{X}_2) \rangle}{2} \tag{1.25}$$

If the modes 1 and 2 are EPR correlated then $\langle \Delta^2 (\hat{P}_1 - \hat{P}_2) \rangle \to 0$ and $\langle \Delta^2 (\hat{X}_1 + \hat{X}_2) \rangle \to 0$, and the sum and difference modes result squeezed. Inverting the relation (1.22), it is easy to show that two EPR correlated states can be obtained by mixing at a 50/50 beam splitter two squeezed modes.

Let's consider, now, the *photon-pair operator*

$$\hat{S}_2(\Lambda) = \mathrm{e}^{\Lambda\left(\hat{a}_1^\dagger \hat{a}_2^\dagger - \hat{a}_1 \hat{a}_2\right)} \tag{1.26}$$

with $\Lambda \in \mathbb{R}$. Eq. (1.26) is a generalization at two field modes of Eq. (1.13) and it creates a pair of entangled photons in the modes 1 and 2. Its action on the vacuum state $|0\rangle \equiv |0_1, 0_2\rangle$ produce the entangled state [Banaszek1999]:

$$|\psi\rangle = \frac{1}{\cosh \Lambda} \sum_{n=0}^{\infty} (\mathrm{tgh}\, \Lambda)^n |n, n\rangle \tag{1.27}$$

which is the eigenstate of the operators $\hat{X}_1 + \hat{X}_2$ and $\hat{P}_1 - \hat{P}_2$. For $\Lambda \to +\infty$, $|\psi\rangle$ converges to a maximally entangled state that is the continuum variables parallel of a bidimensional GHZ state (1.17) [Walls, vanEnk1999]:

$$|\psi\rangle \to \int \mathrm{d}x |x\rangle_1 |x\rangle_2 = \int \mathrm{d}p |p\rangle_1 |-p\rangle_2 = \sum_{n=0}^{\infty} |n\rangle_1 |n\rangle_2 \tag{1.28}$$

It corresponds exactly to the state used by EPR in their paper of 1935 [EPR].

1.4 Parametric generation of non-classical states

The first example of non-classical state can be even dated back to 1927, when Kennard [Kennard1927] considered the evolution on time of a generic Gaussian wavepacket. However only after applications for squeezed light were proposed in the 1980's squeezing was studied in more detail. There has been a whole variety of successful demonstrations of squeezed states in several non-linear physical systems, such as four-wave mixing, optical

parametric amplifier, optical fiber, cold atomic vapors. The first demonstration have been done by Slusher *et al.* in 1985 using four wave mixing in a sodium vapor [Slusher1985]. The latest best result reported amounts to 10dB [Vahlbruch2008].

In general, the propagation of e.m. field through a dielectric medium induces the macroscopic polarization whose components are given by the convergent series of powers of the electric field:

$$P_i = \epsilon_0 \sum_j \chi^{(1)}_{ij} E_j + \epsilon_0 \sum_{j,k} \chi^{(2)}_{ijk} E_j E_k + \epsilon_0 \sum_{j,k,l} \chi^{(3)}_{ijkl} E_j E_k E_l + \dots \tag{1.29}$$

for $i, j, k, l \in \{x, y, z\}$, and where ϵ_0 is the dielectric permittivity of vacuum. The first term $\chi^{(1)}$ is connected to the linear properties of the medium such as its refraction and absorption index. For low intensities, the $\chi^{(1)}E$ term is bigger the the others terms of the series and the propagation of e.m. field is linear. For high intensities, instead, the others terms cannot be neglected and non-linear phenomena of wave mixing (sum and difference generation, harmonic generation) become more relevant. Since polarization behaves as a source term for the e.m. field, $n > 1$ order terms induce a non-symmetric dynamics and modify the statistics of its components. Therefore non-linear crystals behaves as a phase-sensitive amplifiers and can produce deamplification (squeezing) or amplification (anti-squeezing) of fluctuations of the field quadratures.

Among a whole variety of non-linear processes (based on second- and third-order non-linearities), an interesting case is the *parametric down conversion*, where a strong pump field at frequency ω_p and a weak field (*seed*) at frequency ω_s are injected into a non-linear crystal. Due to $\chi^{(2)}$ non-linear effect, the two field "mix" inside the crystal and a weak field at frequency $\omega_i = \omega_p - \omega_s$ is generated by the polarization:

$$P^{(2)}(\omega_p - \omega_s) = \epsilon_0 \chi^{(2)} E_p E_s^* \tag{1.30}$$

In a quantum picture, the same process can be depicted as the absorption by the crystal of the pump photon that excites a virtual level and the successive decay by two photon emission at frequency ω_s and ω_i stimulated by the presence of the weak seed field. The energy and momentum conservation requires the generated photons to satisfy the relations:

$$\omega_p = \omega_s + \omega_i \tag{1.31}$$

$$\vec{k}_p = \vec{k}_s + \vec{k}_i \tag{1.32}$$

In the interaction picture, the Hamiltonian describing the quantum evolution of parametric conversion involves a destruction operator of one pump photon $\hat{a}_p$ and two construction operators of a signal and a idler photons, respectively $\hat{a}_s^\dagger$ and $\hat{a}_i^\dagger$ mediated by the non-linear interaction parameter $\chi^{(2)}$:

$$\hat{H}_{int} = i\hbar\chi^{(2)} \left(\hat{a}_p \hat{a}_s^\dagger \hat{a}_i^\dagger - \hat{a}_p^\dagger \hat{a}_s \hat{a}_i \right) \tag{1.33}$$

In many practical cases pump field can be considered a classical one in the limit its intrinsic fluctuations and the fluctuations induced by the down-conversion in signal and idler photons are negligible respect to its intensity. That amount to require the hypothesis of strong coherent pump field and low depletion of the pump field. In such eventuality, the quantum operator $\hat{a}_p$ can be substituted by a "classical" complex number A_p because pump field is a strong coherent and the Hamiltonian is linearized in:

$$\hat{H}_{int} = i\hbar\chi^{(2)}\left(A_p\hat{a}_s^\dagger\hat{a}_i^\dagger - A_p^*\hat{a}_s\hat{a}_i\right) \tag{1.34}$$

Therefore, the unitary evolution of a vacuum input state $|0\rangle = |0_s, 0_i\rangle$ will produce an entangled state as the one (1.26) discussed in subsection 1.3.5. In an analogous way, if signal and idler modes are indistinguishable, thus $\hat{a}_i \equiv \hat{a}_s$, the unitary evolution of a vacuum input state will produce a signal squeezed state like the one in (1.13) discussed in section 1.2.2.

The quantum properties we summarized here for the case of single-mode beams, in particular entanglement and squeezing, are at the basis of the quantum effects in multi-mode systems we are going to discuss in the following chapters.

CHAPTER 2

Quantum optics with trains of ultra-short pulses

Contents

In this introductory chapter we briefly introduce synchronously pumped OPOs and tools useful to describe quantum effects in SPOPOs. We will see that, in condition of synchronization, when a OPO cavity is pumped by a mode-locked laser, its properties of inter-pulse coherence are preserved inside the cavity and the intra-cavity fields generated by parametric conversion can still be considered mode-locked. Then, their description can be made, in a compact way, by means of frequency combs that are the coherent superposition of optical frequencies. This picture is extended to the quantum domain, by the introduction of appropriate monochromatic operators. Being the superposition of several modes (which are the degrees of freedom of the system), we address the question whether or not a frequency comb is multi-mode. In analogy with the study of "multimodicity" of images in the context of quantum imaging [Treps2005], we find that, from a classical point of view, a mode-locked beam can always be depicted by a single mode, but that the answer is not trivial from a quantum point of view, being this last case the object of a deeper study in Chapter 5.

2.1 Synchronously Pumped Optical Parametric Oscillators

Optical Parametric Oscillators are among the best sources of squeezed [Wu1986], [Takeno2007, Vahlbruch2008], correlated [Heidmann1987, Laurat2003] and entangled [Ou1992] light in the so-called continuous variable regime. They have allowed physicists to successfully implement demonstration experiments for high sensitivity optical measurements and quantum information protocols. In order to maximize the quantum effects, one needs to optimize the parametric down-conversion process. This has been achieved so far by using either intense pump lasers or resonant cavities. Having in mind that the parametric process is an almost instantaneous one, femtosecond mode-locked lasers are the best pump sources in this respect, as they generate very high peak optical powers with high coherence properties. Furthermore, they minimize the thermal effects in the linear crystal which often hamper the normal operation of parametric devices.

Mode-locked lasers have been already used extensively to generate non classical light, either to pump a parametric crystal [Slusher1987, Shelby1992] or an optical fiber [Rosenbluh1991]. However in such single-path configurations, perfect quantum properties are only obtained when the pump power goes to infinity. This is the reason why mode-locking is often associated to Q-switching and pulse amplification [Levenson1993] in order to reach even higher peak powers, at the expense of a loss in the coherence properties between the successive pump pulses. In contrast, intracavity devices produce perfect quantum properties for a finite power, namely the oscillation threshold of the device. It is therefore tempting to consider devices in which one takes advantage of the beneficial effects of both high peak powers and resonant cavity build-up. Such devices exist: they are the so-called synchronously pumped OPOs or SPOPOs (see Figure 2.1). In a SPOPO the cavity round-trip time is equal to that of the pumping mode-locked laser, so that the effect of the successive intense pump pulses add coherently, thus reducing considerably its oscillation threshold.

Such SPOPOs have already been implemented as efficient sources of tunable ultrashort pulses [Piskarskas1988, Edelstein1989, Mak1992, Maker1990, Ebrahimzadeh1991, McCarty1992] and their temporal properties have been theoretically investigated [Cheung1991, McCarty1993, Becker1974]. Let us mention that mode-locked OPOs have also been developed: in such devices, the cavity is resonant only for the signal modes and idler modes, and the pump pulses are not re-circulating. Mode-locked OPOs have been used to generate picosecond pulsed squeezed light in a degenerate configuration

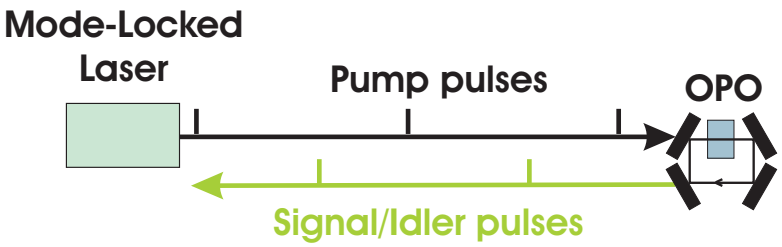

Figure 2.1: Synchronously pumped OPO.

[Shelby1992] or in quasi-degenerate configurations [Forget2006].

In this thesis we will present a complete multi-mode quantum analysis of degenerate SPOPOs and show theoretically that these devices are very efficient to produce squeezed states and that squeezing is effective not just in a single frequency mode but instead in a whole set of "super-modes", which are well defined linear combinations of signal modes of different frequency.

2.1.1 Experimental implementation of a SPOPO

The theoretical study presented in this manuscript has been developed in the context of a more general analysis about dynamical and quantum properties of SPOPOs. In this same context, indeed, Olivier Pinel, Benoit Chalopin and Nicolas Treps, from the quantum optic group directed by Prof. Claude Fabre at Laboratoire Kastler Brossel, are experimentally implementing a synchronously pumped OPO. It is quite natural, therefore, that both the theoretical and the experimental works benefited from an intense mutual support. From the point of view of this work, the experimental setup represented a guide line in all those choices that are involved in modeling of a real system. Hence, it is worth to present in this section a brief description of the SPOPO device experimentally implemented and sketched in Figure 2.2. The experimental device is based on a Ti:Sa mode-locked laser generating a c.w. train of 100fs pulses at 800nm with a repetition rate of about 80MHz. A part of its output is doubled by a simple passage frequency double based on a bismuth borate BiB_3O_6 (BIBO) crystal. The 400nm beam produced is then used for pumping a 2m linear cavity OPO which exploits the nonlinearity of a BIBO crystal. A critical point for the functioning of a SPOPO is the synchronization between the pumping laser and the OPO cavity. In the time picture, the round trip time of the signal pulse circulating inside the cavity has to be equal to the temporal inter-pulse separation of the mode-locked pump. If this condition is satisfied, the signal field will benefit not only from the cavity feed-back but also from the coherent superposition of successive pump pulses. As an effect, the efficiency of the device increases and the threshold lowers. In this condition, a description

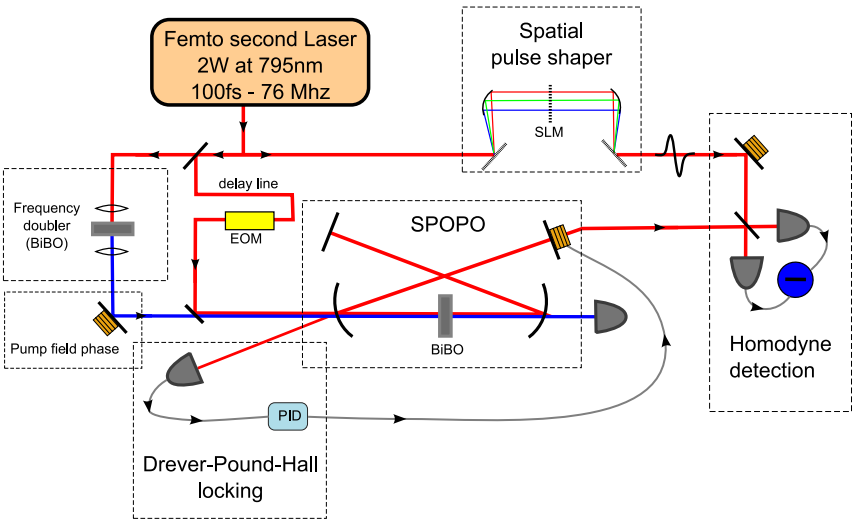

Figure 2.2: Experimental implementation of a Synchronously pumped OPO (This figure has been kindly provided by O. Pinel).

in terms of frequency combs is allowed also inside the cavity. It is clear, then, that the synchronization condition, in the frequency domain, corresponds to requiring the signal field comb to be resonant with the cavity. This synchronization is performed by locking the OPO cavity length to the mode-locked cavity length by means of the Drever-Pound-Hall method [Drever1983]. However, for ultra-short pulses the dispersion caused by the nonlinear crystal represents a serious problem because their broadband spectrum. The solution consists in introducing in the cavity some dispersive elements (like prisms or gratings) in order to compensate the crystal dispersion.

Differently from what we considered in the model, the experimental realization of the SPOPO considers also a small injection of the field at 800nm (the signal field). This solution has two practical implications: it makes easier both the alignment of the cavity, since the signal field is not in the vacuum state, and the configuration of the OPO working point. Therefore another small part of the Ti:Sa laser is sent into the cavity through a delay line which is needed for synchronizing the pump pulse and the seed pulse. Instead, by means of a piezoelectric crystal, it is possible to control the relative phase between the pump and the seed and, thus, change the quadrature of the signal field that is amplified.

The output signal field is detected, then, by means of a classical homodyne detection scheme where the local oscillator consists of a third part of the output of the Ti:Sa mode-locked laser. In order to detect with the best efficiency the quantum properties of the signal field, the frequency comb describing the local oscillator field has to be matched to its frequency comb. The mode matching is realized by means of a pulse shaper. It consist of a first dispersive element such as a grating or a prism that spatially separates the frequency constituting the incoming optical pulse. Then a spatial light modulator can control, for each frequency[1] component, the phase and/or the amplitude of the beam in order to give it the wanted spectral shape. Then the frequency components are recombined at a second dispersive element.

Up to now, the goals that have been successfully achieved are the frequency doubling of 400nm beam, the synchronization between the OPO and the Ti:Sa laser cavity and the phase-sensitive amplification of the seed beam.

2.1.2 Mode-locked laser sources

The use of the output field of a mode-locked laser for pumping an OPO cavity reveals the double advantage of producing broadband non-classical field and increasing the efficiency of the parametric conversion thanks to the coherence properties between each pulse of mode-locked beam. In this section we will present the main features of mode-locked field and show that, thanks to their inter-pulse coherence, they can be described in a compact way by means of a comb of frequencies in the Fourier space.

In a simple laser, generally, each of the lasing longitudinal modes oscillate independently with no fixed relationship between them and with randomly varying phase. Consequently, their incoherent interference will produce a averaged almost constant output intensity known as c.w. operation. On the other hand, mode-locked lasers generate a train of short optical pulses by establishing a fixed phase relationship between all of the lasing longitudinal modes. Having well established phase relations, these modes will con-

[1] In fact, since the spatial light modulator is made of a discrete number of pixels, it modulates the phase/amplitude over a small interval of spectral frequencies.

structively interfere generating a beating effect that, for a huge number of lasing modes, will result in a train of very intense and short pulses equally spaced in time with period T_{rep}.

The output field can be depicted, in the temporal domain, by an optical wave with carrier frequency ω_c and envelope $A(t)$:

$$E(t) = A(t)\mathrm{e}^{-i\omega_{\text{c}}t} + \text{c.c.} \tag{2.1}$$

Since the train of pulses is periodic in time $A(t) = A(t - T_{\text{rep}})$, one can decompose it on a discrete Fourier basis:

$$E(t) = \sum_m A_m \mathrm{e}^{-i(\omega_{\text{c}}+m\omega_{\text{rep}})t} + \text{c.c.}, \tag{2.2}$$

where A_m are the Fourier components of $A(t)$ and $\omega_{\text{rep}} = 2\pi/T_{\text{rep}}$. The spectrum of the output of a mode-locked field is, therefore, represented by a comb of equally separated frequencies around ω_{c}:

$$\omega_m \equiv \omega_{\text{c}} + m\omega_{\text{rep}}. \tag{2.3}$$

Notice that this result have been obtained under the assumption of identical pulses. Generally, for any pulse shape, there exists a carrier-envelope phase $\Delta\phi_{\text{ce}}$ that corresponds to the phase shift between the peak of the envelope and a given wavefront of the carrier wave. In presence of dispersive material, the difference between group and phase velocities is at the origin of $\Delta\phi_{\text{ce}}$. After a round-trip, in fact, the phase accumulated between the envelope and the carrier is:

$$\Delta\phi_{\text{ce}} = \left(\frac{1}{v_{\text{g}}} - \frac{1}{v_{\text{p}}}\right) L\omega_{\text{c}} \bmod 2\pi, \tag{2.4}$$

where v_{g} and v_{p} are, respectively, the group and phase velocities and L is the length of the laser cavity. The consequence is that the phase carrier-envelope induces a rigid shift of the frequencies of the comb by an amount ω_{ce} that is linked to ω_{c} through the relation:

$$\omega_{\text{ce}} = \frac{\omega_{\text{c}}}{2\pi}\Delta\phi_{\text{ce}}. \tag{2.5}$$

There exist different mechanisms for locking the phases of lasing longitudinal modes based on active or passive phase modulators. Currently the generation of ultra-short pulses is dominated by the Kerr-lens mode-locking. This method exploits the variation of the refraction index inside the gain medium (usually Ti:Sa) across the beam profile by optical Kerr effect. For a Gaussian beam (as found in laser resonators), then, the center of the beam will experience a greater refractive index than the low intensity tails, thus inducing a greater focalization. In this way, the amplification of short intense pulses will be favored with respect to the c.w. solutions.

2.1.3 Quantum description of c.w. trains of pulses in time domain

The evolution of a linearly polarized electric field operator $\hat{\vec{E}}(\vec{r}, z, t)$ in the Heisenberg representation [Cohen-Tannoudji] can be described in terms of its positive frequency part and its Hermitian conjugate as follows:

$$\hat{\vec{E}}\,(\vec{r}, t) = \mathbf{u}_{\text{e}}\left[\hat{E}^{(+)}\,(\vec{r}, t) + \hat{E}^{(+)\,\dagger}\,(\vec{r}, t)\right], \tag{2.6}$$

where $\mathbf{u}_e$ refers to the direction of polarization. Since we will consider in this manuscript a field that propagates as a plane wave along the axis $\mathbf{u}_z$ at the frequency ω_0 and with a transverse dimension of A, the field operator can be written in the form:

$$\hat{E}^{(+)}(z,t) = \hat{\mathcal{E}}^{(+)}(z,t)\, \mathrm{e}^{-i\omega_0\left(t-\frac{z}{c}\right)}, \tag{2.7}$$

where the quantity $\mathrm{e}^{-i\omega_0\left(t-\frac{z}{c}\right)}$ is the carrier for a wave propagating in vacuum along the z axis at the speed of light c and $\hat{\mathcal{E}}^{(+)}(z,t)$ is the envelope field operator.

The quantization of the electric field in the free (one-dimensional) space is given by the corresponding operator:

$$\hat{E}^{(+)}(\vec{r},t) = i\sqrt{\frac{\hbar}{2\epsilon_0 A}} \int \frac{\mathrm{d}k}{\sqrt{2\pi}} \sqrt{\omega(k)}\, \hat{a}(k) \mathrm{e}^{ik(z-ct)}, \tag{2.8}$$

where $\hat{a}(k)$ and $\hat{a}^\dagger(k)$ are the annihilation and creation operators of a photon with wave number k. These operators satisfy the following commutation rules:

$$\begin{aligned} \left[\hat{a}(k), \hat{a}^\dagger(k')\right] &= \delta(k-k'), \\ \left[\hat{a}(k), \hat{a}(k')\right] &= 0, \\ \left[\hat{a}^\dagger(k), \hat{a}^\dagger(k')\right] &= 0. \end{aligned} \tag{2.9}$$

Then, by writing, for an electric field propagating with carrier $\mathrm{e}^{-ik_0(z-ct)}$, its envelope as:

$$\hat{\mathcal{E}}^{(+)}(z,t) \equiv i\sqrt{\frac{\hbar\omega_0}{2\epsilon_0 A}}\, \hat{a}(z,t), \tag{2.10}$$

the expression of the operators $\hat{a}(z,t)$ can be derived from Eq. (2.8):

$$\hat{a}(z,t) = \int \frac{\mathrm{d}k}{\sqrt{2\pi}} \sqrt{\frac{\omega(k)}{\omega_0}}\, \hat{a}(k) \mathrm{e}^{i((k-k_0)(z-ct)}. \tag{2.11}$$

The corresponding commutation rules are straightforwardly obtained from Eq. (2.9):

$$\left[\hat{a}(z,t), \hat{a}^\dagger(z',t')\right] = \int \frac{\mathrm{d}k}{\sqrt{2\pi}} \frac{\omega(k)}{\omega_0} \mathrm{e}^{i(k-k_0)((z-z')-c(t-t'))}. \tag{2.12}$$

Since we will deal only with c.w. mode-locked optical beams, it is worth to adapt the notation for the quantized fields to the notation for frequency combs. We have to pass, thus, to a discrete formulation of the operator $\hat{a}(z,t)$. Let's write the integral as a sum over intervals of width Δk and centered at $k_r = k_0 + r\Delta k$, being $r \in \mathbb{Z}$. Thus (2.11) becomes:

$$\hat{a}(z,t) = \mathrm{e}^{-ik_0(z-ct)} \sum_r \int_{k_r-\frac{\Delta k}{2}}^{k_r+\frac{\Delta k}{2}} \frac{\mathrm{d}k}{\sqrt{2\pi}}\, \hat{a}(k) \mathrm{e}^{ik(z-ct)}. \tag{2.13}$$

Let's define, now, new operators:

$$\mathrm{e}^{ik_r(z-ct)} \hat{a}_r(z,t) \equiv \int_r \frac{\mathrm{d}k}{\sqrt{2\pi}}\, \hat{a}(k) \mathrm{e}^{ik(z-ct)}, \tag{2.14}$$

where the subscript r of the integral denotes the interval $[k_r - \Delta k/2, k_r + \Delta k/2]$. They verify the usual boson commutation rule:

$$\begin{aligned}\left[\hat{a}_r(z_1,t_1), \hat{a}^\dagger_{r'}(z_2,t_2)\right] &= \frac{1}{2\pi}\mathrm{e}^{-i(k_r-k_{r'})(z_1-z_2-c(t_1-t_2))} \times \\ &\times \int_r \mathrm{d}k \int_{r'} \mathrm{d}k' \left[\hat{a}(k), \hat{a}^\dagger(k')\right] \mathrm{e}^{ik(z_1-ct_1)}\mathrm{e}^{-ik'(z_2-ct_2)} \\ &= \frac{1}{2\pi}\mathrm{e}^{-ik_r(z_1-z_2-c(t_1-t_2))}\delta_{r,r'}\int_r \mathrm{d}k\, \mathrm{e}^{ik[z_1-z_2-c(t_1-t_2)]} \\ &= \delta_{r,r'}\frac{\sin\left[\frac{\Delta k}{2}\left(z_1-z_2-c(t_1-t_2)\right)\right]}{\pi\left(z_1-z_2-c(t_1-t_2)\right)} \\ &\simeq \delta_{r,r'}\delta\left(z_1-z_2-c(t_1-t_2)\right). \end{aligned} \tag{2.15}$$

In order to arrive to Eq. (2.15) we used Eq. (2.9) and kept in mind that the $\delta_{r,r'}$ term appears because the double integral vanishes if $r \neq r'$ since the integration domains in k and k' are not overlapping in that case. Hence the operators (2.11) can be expressed as a discrete superposition of the boson operators $\hat{a}_r(z,t)$:

$$\hat{a}\left(z,t\right) = \sum_r \hat{a}_r \mathrm{e}^{i(k_r-k_0)(z-ct)}, \tag{2.16}$$

that used in Eqs. (2.7) and (2.8) gives the electric field:

$$\hat{E}^{(+)}(z,t) = i\sqrt{\frac{\hbar\omega_0}{2\epsilon_0 A}}\sum_r \hat{a}_r \mathrm{e}^{ik_r(z-ct)}, \tag{2.17}$$

which is consistent with the classical expression for the mode-locked field (2.2).

2.1.4 A different modal decomposition of the electromagnetic field: the temporal Gaussian modes

Either in space or time or space-time domain, the wave equation in a dielectric medium for electric components admits, for propagation in vacuum (or linear propagation in a dielectric medium), a modal decomposition of the electric field on several complete set of functions $\{u_k\}$ which correspond to the monochromatic solutions of the Maxwell equations for given boundary conditions. While the previous method does not keep in account the propagative aspects of a e.m. field, it is possible quantize it by associating to each eigenmode of the propagation a quantum operator [Walls]. In time domain the linear propagation in a dispersive medium along the z-axis of the slowly varying field envelope $\mathcal{E}^{(+)}(z,\eta)$ in the plane wave approximation is given by:

$$\left(i\frac{g}{2}\frac{\partial^2}{\partial\eta^2} + \frac{\partial}{\partial z}\right)\mathcal{E}\left(z,\eta\right) = 0 \tag{2.18}$$

where $\eta = t - z/v$ is the reduced time in a frame of reference co-propagating with the e.m. wave-packet, v is the velocity of light for the considered dispersive medium and g is the group velocity dispersion evaluated at the carrier frequency. Together with the boundary conditions imposed by a usual optical cavity, Eq. (2.18) admits a complete set of modes $\{u_k\left(z,\eta\right)\}$ that are given by the 1-dimensional Gauss-Hermite functions:

$$u_k(z,\eta) = \left(\frac{2}{\pi}\right)^{1/4}\left(2^k k!\right)^{1/2}\frac{1}{\sqrt{w(z)}}H_k\left(\frac{\sqrt{2}\,\eta}{w(z)}\right)\mathrm{e}^{-\frac{\eta^2}{w^2(z)}+i\frac{\eta^2}{2gR(z)}+i(n+1)\psi(z)}, \tag{2.19}$$

where:

$$\begin{aligned} w(z) &= w_0\sqrt{1+\left(\frac{z}{z_{\mathrm{R}}}\right)^2}, \\ R(z) &= z+\frac{z_{\mathrm{R}}^2}{z}, \\ \psi(z) &= \arctan\left(\frac{z}{z_{\mathrm{R}}}\right), \\ z_{\mathrm{R}} &= \frac{w_0^2}{2g}. \end{aligned} \tag{2.20}$$

These modes are orthogonal to each other:

$$\int_{-\infty}^{+\infty} \mathrm{d}\,\eta u_k^*(z,\eta)u_l(z,\eta) = \delta_{k,l}, \tag{2.21}$$

and satisfy the relation of completeness:

$$\sum_k u_k^*(z,\eta)u_l(z,\eta') = \delta(z-z')\delta(\eta-\eta'). \tag{2.22}$$

The field envelope can be, thus, expanded on this basis:

$$\mathcal{E}^{(+)}(z,\eta) = \sum_k a_k u_k(z,\eta). \tag{2.23}$$

In a quantum picture, each mode $u_k(z,\eta)$ can be associated with an independent quantum oscillator so that the complex coefficients a_k are replaced by the operators $i\sqrt{\frac{\hbar\omega_k}{2\epsilon_0}}\,\hat{a}_k$ where $\hat{a}_k$ and $\hat{a}_k^\dagger$ is the set of photon creation/annihilation operators in each mode. Then, from Eq. (2.7), the modal decomposition for the electric field reads:

$$\hat{\mathcal{E}}\,(z,\eta) = i\sum_k \sqrt{\frac{\hbar\omega_k}{2\epsilon_0}}\hat{a}_k u_k\,(z,\eta)\,. \tag{2.24}$$

Therefore, in a general way, the e.m. field can be decomposed into a linear superposition of several modes as many as the number of degrees of freedom needed for giving a complete description of it. Is such number the least dimension of the Hilbert space in which the field "lives" needed? The answer to this question will clarify the differences that occur between simple-modal systems and multi-modal ones and provide a criterium for distinguishing the two cases.

2.2 Multi-mode light

In the domain of the continuous variables (CV) quantum optics, the use of macroscopic intense optical beams involves a huge number of photons so that they cannot be individually distinguished, and a statistical characterization of their quantum fluctuations has to be privileged. Therefore, with respect to regimes with a very small number of photons, a larger variety of non-classical states can be produced like, for example, squeezed or entangled states usually by means of sources based on the non-linear parametric interaction. To

this purpose, the most reliable and exploited sources are the optical parametric oscillators. However, the non-linearities involved and the detection techniques adopted usually allows for no more than small quantum fluctuation, thus preventing the possibility to realize quantum states with negative Wigner function. Nevertheless, the richness of quantum states that can be generated by OPO based sources and of the number of applications can be enlarged, in spite of this limitation, by multiplying the number of "modes" or degree of freedom at stake in the process of detection. This is the domain of the multi-mode quantum optics.

On one hand, the multimodal complexity has great potentialities for applications concerning the quantum treatment of the information like, for example, the increasing of storage and transfer of information, the generation of more robust entangled states, the parallel treatment of the information. On the other hand, multi-mode optical systems can improve the precision measurements in the domains of imaging and metrology.

During recent years, spatial quantum optical effects, usually called quantum imaging effects, has witnessed a growing interest since the generation of spatial correlations of spatial squeezing in the transverse plane can find application in the detection of small transverse displacement and tilt of an optical beam surpassing the standard quantum noise limit [Treps2002, Treps2003, Delaubert2006], detection of weak phase images [Lugiato2002], quantum teleportation of optical information [Sokolov2001], transverse spatial quantum correlation for transmission of images [Gigan2006] and noiseless image amplification [Kolobov1995, Lopez2008]. On the other hand, it was already known that that the introduction of spatial features in the transverse plane of laser beams can lead to parallel information processing and multichannel operations [Caves1994], thus allowing the implementation of quantum protocols such as quantum entanglement, quantum cryptography, dense coding and quantum teleportation [Lassen2007] that already have been demonstrated in the simple-mode regime [Ou1992, Silberhorn2001, Mattle1996].

In problems concerning the characterization of an optical image and the extraction of as much as possible of details from it, without knowing where they are placed, it is necessary the use of detectors with a great number of pixels and and of superresolution techniques [Kolobv2000]. In these cases, differently from the detection of small displacements and tilt, where a small number of degrees of freedom are involved, the absence of an *a priori* information does not allow to know the form of the modes in order to optimize the signal-to-noise ratio. Consequently, one needs to simultaneously reduce the noise in all the degrees of freedom of the optical beam. Such situation can be reproduced in configurations of degeneracy with respect to all the modes involved. In the context of optical images, a successfully scheme, exploited for obtaining this, concerns OPO cavities which are degenerate for a large number of transverse modes [Gigan2005, Martinelli2003, Lopez2005, Lopez2008]. For these systems, the amplification/de-amplification, affected by a noise lower than the standard quantum limit, of an optical image prove their quantum multi-modal character. The results obtained in Section 2.1 authorize to depict the output field of a mode-locked laser by means of a comb of optical frequencies which, in the time domain, corresponds to a train of short pulses that are coherent each other. From the point of view of the frequencies, then, there is a perfect analogy with the optical images, since an image can be considered as the coherent superposition of several transverse modes. In the light of these considerations, a synchronously pumped OPO is a device potentially multi-mode since it

is completely degenerate for all the frequencies of the comb that resonate simultaneously. It is the goal of this work to understand whether or not a SPOPO is a multi-mode system and complete, at least in part, the analogy with spatial multi-mode systems.

2.2.1 Single mode or multi-mode light

In this section we report a brief resume of a criterium which permits to precisely characterize intrinsic single-mode and multi-mode light [Treps2005].

Classical approach

For a number greater than one of non null coefficients a_k, modal decomposition (2.23) could induce to think that the field is multi-mode. In effect, if the a_k coefficients are a coherent superposition (and not a statistical one), it is always possible to define a new mode:

$$v_0 = \frac{1}{\sqrt{\sum_k |a_k|^2}} \sum_i a_k u_k \tag{2.25}$$

and build a basis $\{v_k\}$ in which v_0 is the first element. Therefore, on a classical point of view, an intrinsic multi-mode description of the e.m. field cannot exist, because, at least for coherent modes superposition, it is always possible to find a new basis in which the field is mono-mode. On the other hand, for a statistical superposition of modes the vector $v_0(\zeta)$ cannot be defined and the multi-mode character assumes an intrinsic meaning. In time domain, for example, a mode-locked laser is a mono-mode system because it is the coherent superposition of many temporal modes.

Single mode or multi-mode light: quantum approach

Let's consider the most general state of the field in the Fock state basis $|N_1, N_2, \ldots, N_k, \ldots\rangle$, where N_k stands for the number of photons in the field mode u_k. It reads:

$$|\psi\rangle = \sum_{N_1,\ldots,N_k,\ldots} C_{N_1,\ldots,N_k,\ldots} |N_1, N_2, \ldots, N_k, \ldots\rangle, \tag{2.26}$$

where $\{C_{N_1,\ldots,N_k,\ldots}\}$ are complex coefficients of the decomposition in the Fock state basis. Then, the mean value of the field envelope operator (2.17) (or (2.24)) can be written:

$$\langle\psi|\hat{\mathcal{E}}|\psi\rangle = i\sqrt{\frac{\hbar\omega_k}{2\epsilon_0 A}} \sum_k \sqrt{N_k} \left(\sum_{N_1,\ldots,N_k,\ldots} C^*_{N_1,\ldots,N_{k-1},\ldots} C_{N_1,\ldots,N_k,\ldots} \right) u_k \tag{2.27}$$

Using these notations, we can give a definition of a single mode beam:

Definition 1 *A state is single mode is there exists a mode basis $\{v_0, v_1, \ldots\}$ in which it can be written:*

$$|\psi\rangle = |\phi\rangle \otimes |0, \ldots, 0, \ldots\rangle \tag{2.28}$$

where $|\phi\rangle$ is the field state in the first mode.

But does it exist quantum states that cannot be written as in Eq. (2.28)? The answer to this question is given by the following proposition:

Proposition 1 *A quantum state of the field is single mode if and only if the action on it of all the annihilation operators of a given basis gives proportional vectors.*

Leaving the details of the demonstration to the paper [Treps2005], let's consider, here, an example. Assuming that a state $|\psi\rangle$ with respect to the basis $\{u_k, \hat{a}_k\}$ reads as:

$$|\psi\rangle = |\phi_1\rangle \otimes \ldots \otimes |\phi_k\rangle \otimes \ldots \tag{2.29}$$

the action of the annihilation operators on it gives:

$$\hat{a}_k = |\phi_1\rangle \otimes \ldots \otimes (\hat{a}_k|\phi_k\rangle) \otimes \ldots \tag{2.30}$$

Consequently, there are only two possibilities to have all these states proportional: (i) either only one of the projection is different from zero, which means we are already in the basis in which the state is single mode, (ii) or all the states are coherent states. If, for instance, one considers the superposition of several field modes, if at least one of them is a non-coherent state, one gets a multi-mode quantum state.

One can characterize a beam which is not single-mode, by its degree N:

Definition 2 *For a beam $|\psi\rangle$, the minimum number of modes necessary to describe it (or the minimum number of non-vacuum modes in its modal decomposition), reached by choosing the appropriate basis, is called the degree N of a multi-mode beam. Any corresponding basis is called a minimum basis for the field $|\psi\rangle$.*

Accordingly, it can be shown that a quantum field is in a N-mode state if and only if the action of all the annihilation operators belongs to the same N-dimensional sub-space.

Among all the possible minimal basis, it exists a special one that will be called *eigen-basis* or *mean-field basis* that verifies the following proposition

Proposition 2 *For a state $|\psi\rangle$ of degree N, it is always possible to find a basis $\{v_k, \hat{b}_k\}$ such that the mean value of the electric field is nonzero only in the first mode and it is a minimum basis.*

Starting from a minimal basis $\{u_k, \hat{a}_k\}$, such a basis can be obtained by means of the following combinations:

$$v_0 = \frac{1}{\sqrt{\sum_{k=0}^{N-1} \langle \hat{a}_k \rangle^2}} \sum_{k=0}^{N-1} \langle \hat{a}_k \rangle \, u_k \tag{2.31}$$

$$v_{k,0<k<N} = \sum_{l=0}^{N-1} c_{kl} \, u_l \tag{2.32}$$

$$v_{k,k\geq N} = u_k \tag{2.33}$$

where the coefficients $\{c_{ij}\}$ are chosen in order to get an orthonormal basis. Definition (2.31) apply also for the annihilation operators $\hat{b}_k$.

In a classical sense the mean field is single mode because the only non null expectation value is the one corresponding to the first mode while all the other modes have zero mean value. However, the energy lying in all the modes labeled from 1 to N-1 is not necessarily

zero. These states, in fact, are not necessarily traditional vacuum states. Although their electric field mean value is zero, they can still correspond to squeezed vacuum states or correlated vacuum states. Therefore, for a multi-mode beam, this description shows that some of the modes orthogonal to the mean fields are sources of noise but do not contribute to the mean value and, consequently, that the noise distribution in the profile of the field is independent of the one of the mean field.

In the specific case of a SPOPO, from a classical point of view, if all the terms contributing to the phase diffusion affecting a laser radiation and others technical noises can be neglected, we can conclude that the intra-cavity mode-locked fields can always be depicted by means of the mode corresponding to the mean field mode (2.25). On the other hand, in a quantum picture, the multi-modal character of the fields has to be thoroughly investigated, since the modes orthogonal to v_0 can independently contribute to the temporal distribution of quantum fluctuation.

CHAPTER 3

Quantum model for Synchronously Pumped OPOs

Contents

Synchronously pumped OPOs or SPOPOs, in the recent past, have been used for generating ultrashort optical pulses of tunable wavelength or for efficient controlling of the pulse compression and their temporal properties have been theoretically investigated (see for example Cheung *et al.* [Cheung1991]). A different application could be addressed for the generation of non-classical states and implement demonstration experiments for high sensitivity optical measurements and quantum information protocols. Mono-mode cw OPOs have been already used for this purpose by exploiting the coherence properties of the interaction (i.e. parametric down conversion) between a non-linear medium and strong e.m. fields; in this way, squeezed, correlated, entangled light has been produced in the so-called continuous variable regime. In order to maximize the quantum effects, one needs to optimize the non-linear coupling. This has been achieved, so far, by using either intense pump lasers or resonant cavities. In the first case, due to the fact that parametric process is an almost instantaneous one, femtosecond mode-locked lasers are the best sources because they generate very high peak optical powers with high coherence properties. Therefore, such a sources have been extensively used to generate non classical light either by pumping a parametric crystal or an optical fiber. However in such single-path configurations, perfect quantum properties are obtained only when the pump power goes to infinity. On the other side, intracavity devices produce perfect quantum properties for a finite power, say the oscillation threshold of the device. SPOPO devices take advantage of the effects of both high peak powers and resonant cavity build-up. This is efficiently achieved when the repetition rate of the pumping mode-locked laser is synchronized to the round-trip time of the pump pulses inside the OPO cavity because of their coherent superposition.

In this chapter the complete quantum model for a single-transverse mode, synchronously pumped optical parametric oscillator (SPOPO) is addressed. We will consider high finesse optical cavities, of either ring or linear geometry, pumped by a c.w. train of femtosecond pulses (about 100 fs). Two possibilities for pumping have been envisaged: either (i) the pump is also resonated inside the cavity (doubly resonant case) or (ii) the cavity is transparent for the pump (singly resonant case). For sake of simplicity, we will consider quasi-degenerate collinear type I interaction in a $\chi^{(2)}$ non-linear crystal placed inside optical cavity which is assumed to be dispersion compensated be intracavity dispersive elements. This hypothesis will permit to assume all signal cavity modes equally spaced by a common free spectral range.

In the below threshold regime and in the linear approximation, both singly resonant and doubly resonant cases are described by formally identical models, so the results obtained are in fact more general. We will extend our analysis to non-chirped pumps as chirping requires another, more general treatment, as will be presented in the last section.

3.1 Doubly resonant ring cavity

Let's consider quasi-degenerate collinear type I interaction, by means of which the pumping frequency comb, at frequencies around $2\omega_0$, is converted by a nonlinear $\chi^{(2)}$ crystal into

multi-mode signal radiation at frequencies around ω_0 and vice-versa, being $2\omega_0$ and ω_0 the two frequencies at which phase matching occurs, i.e. $n(2\omega_0) = n(\omega_0) \equiv n_0$, being n the crystal refractive index. The nonlinear crystal is placed inside a high finesse optical cavity of length L which is assumed to be dispersion compensated by intracavity dispersive elements, so that all signal cavity modes are equally spaced by a common free spectral range Ω, which is made equal to that of the pumping laser Ω_p. This ensures that the pulse-to-pulse delay of the pump beam coincides with the cavity round-trip time and successive pump and signal pulses superpose in time thus maximizing the strength of the interaction. As we will be concerned with femtosecond lasers (pulse durations around 100 fs) and cavity lengths around $1-4$ m, the number of pump modes will be typically on the order of $10^4 - 10^5$.

3.1.1 Longitudinal modes of the resonator

Let's consider a ring resonator of length L where the intracavity field is supposed to be a superposition of plane waves propagating along the positive direction of $\mathbf{u}_z$ axis of the resonator. This implies that the nonlinear crystal is assumed to be broadband antireflection coated. Plane wave assumption is still approximately valid for Gaussian beams as far as the thin crystal is placed at the (common) beam waist of pump and signal, and the Rayleigh lengths are much longer than the crystal length l. Taking the crystal entrance facet at $z = -l/2$, any resonator mode $U_m(z,t)$ can be written as:

$$U_m^{\text{ring}}(z,t) = \begin{cases} \frac{1}{\sqrt{n(\omega_m)}}\, u_m e^{i(k_m z - \omega_m t)} + \text{c.c.}, & z \in \left[-\frac{l}{2}, \frac{l}{2}\right] \\ u_m e^{i(k_m^{\text{vac}} z - \omega_m t)} e^{i\phi_m} + \text{c.c.}, & z \notin \left[-\frac{l}{2}, \frac{l}{2}\right] \end{cases}, \tag{3.1}$$

where $k_m^{\text{vac}} = \omega_m/c$ is the wavenumber in vacuum, $k_m = n(\omega_m)\, k_m^{\text{vac}}$, $n(\omega_m)$ is the refractive index of the crystal at frequency ω_m, u_m is a classical complex amplitude, the transmission factor $1/\sqrt{n(\omega_m)}$ is due to the flux conservation keeping in count that reflection at the entrance facet is absent, and ϕ_m is a suitable phase. If the crystal is the only refractive element inside the cavity, the frequencies ω_m verify the following resonance condition:

$$\omega_m = m\, \frac{2\pi c}{[n(\omega_m) - 1]\, l + L}, \tag{3.2}$$

with $m \in \mathbb{N}$. This expression keep accounts for the dispersion of the nonlinear crystal that produces a nonuniform free spectral range across the broadband frequency comb propagating inside the cavity. When the phase-matching is not of type I, pump, signal and idler feel e different dispersion owing to the different refraction index. This can be a serious problem for the synchronization of the three resonating fields and an external dispersion compensation is needed. For the case, that will be considered here, of type I phase-matching the problem is less severe, but in any case a resonator compensated by intracavity dispersive elements (such as prisms or diffraction gratings) will be admitted.

Calling $\omega_{p,0}$ and $\omega_{s,0}$ the two cavity modes closest to pump and signal carrying frequencies $2\omega_0$ and ω_0 respectively, the cavity modal frequencies can be written as:

$$\omega_{\text{p},m} = \omega_{\text{p},0} + m\Omega \tag{3.3}$$

$$\omega_{\text{s},m} = \omega_{\text{s},0} + m\Omega \tag{3.4}$$

where Ω is the cavity free spectral range, equal for signal and pump, because of the hypothesis of dispersion compensation, and $m \in \mathbb{Z}$ because by convention $m = 0$ corresponds to the cavity modes $\omega_{\mathrm{p},0}$ and $\omega_{\mathrm{s},0}$. Therefore the assumption that ω_0 and $2\omega_0$ are phase-matched forces the equality $\omega_{\mathrm{p},0} = 2\omega_{\mathrm{s},0}$. Note that according to (3.2) the hypothesis of constant cavity free spectral range Ω is valid only in presence of intracavity dispersive elements for dispersion compensation, otherwise terms in Ω of order larger than the first in (3.3) and (3.4) should be considered.

The expansion of the external pump field on the same base of longitudinal plane modes, instead, reads:

$$E_{\mathrm{ext}}(t) = i\sqrt{\frac{P}{2\epsilon_0 c}} \sum_m \alpha_m e^{-i(2\omega_0 + m\Omega_{\mathrm{p}})t} + \mathrm{c.c.}, \tag{3.5}$$

which is a classical, phase-locked multi-mode coherent field. Here P is the average laser irradiance (power per unit area), α_m is the normalized ($\sum_m |\alpha_m|^2 = 1$) complex spectral component of longitudinal mode labeled by the integer index m, and $m = 0$ corresponds to the phase-matched mode.

3.1.2 The fields

Since type I operation is assumed, let's take pump and signal fields, respectively E_p and E_s, polarized along two orthogonal directions, for example $\mathbf{u}_y$ and $\mathbf{u}_x$. The total field can be written as:

$$\hat{\mathbf{E}}(z,t) = \hat{E}_p(z,t)\,\mathbf{u}_y + \hat{E}_s(z,t)\,\mathbf{u}_x. \tag{3.6}$$

Inside the nonlinear crystal, which extends from $z = -l/2$ to $z = +l/2$, the fields are written, in the Schrödinger picture, as:

$$\hat{E}_{\mathrm{p}}(z,t) = i\sum_m \mathcal{E}_{\mathrm{p},m}\left(\hat{p}_m(t)\,e^{ik_{\mathrm{p},m}z} - \hat{p}_m^\dagger(t)\,e^{ik_{\mathrm{p},m}z}\right), \tag{3.7}$$

$$\hat{E}_{\mathrm{s}}(z,t) = i\sum_m \mathcal{E}_{\mathrm{s},m}\left(\hat{s}_m(t)\,e^{ik_{\mathrm{s},m}z} - \hat{s}_m^\dagger(t)\,e^{ik_{\mathrm{s},m}z}\right), \tag{3.8}$$

where $\mathcal{E}_{\mathrm{f},m} = \sqrt{\frac{\hbar\omega_{\mathrm{f},m}}{2\epsilon_0 n(\omega_{\mathrm{f},m}) A_{\mathrm{f}} L}}$, $\mathrm{f} = \mathrm{p}, \mathrm{s}$ are single photon fields, and A_{f} is the transverse area of pump ($\mathrm{f} = \mathrm{p}$) or signal ($\mathrm{f} = \mathrm{s}$) fields. The boson operators $\hat{p}_j$ and $\hat{s}_m$ verify usual commutation relations:

$$\left[\hat{s}_m(t), \hat{s}_n^\dagger(t)\right] = \left[\hat{p}_m(t), \hat{p}_n^\dagger(t)\right] = \delta_{m,n}, \tag{3.9}$$

$$\left[\hat{p}_m(t), \hat{s}_n^\dagger(t)\right] = \left[\hat{s}_m(t), \hat{s}_n(t)\right] = \left[\hat{p}_m(t), \hat{p}_n(t)\right] = 0. \tag{3.10}$$

3.1.3 The interaction Hamiltonian

A phenomenological approach to quantization of nonlinear optics permits to use the following form for the interaction Hamiltonian:

$$\hat{H}_{\mathrm{I}} = -\int_{V_{\mathrm{I}}} \mathrm{d}\vec{r}\,\hat{\mathbf{E}}\cdot\hat{\mathbf{P}}, \tag{3.11}$$

where V_{I} is the volume inside the crystal where the pump and signal fields overlaps. In the situation where only plane waves are considered, the fields do not depend on the transverse

coordinates (x, y) and the integral (3.11) becomes:

$$\hat{H}_{\mathrm{I}} = -A_{\mathrm{I}} \int_{-l/2}^{l/2} \mathrm{d}z \, \hat{\mathbf{E}} \cdot \hat{\mathbf{P}}, \tag{3.12}$$

being A_{I} the surface of the crystal in the transverse plane xOy. In the case of Gaussian beams, under the hypothesis that the crystal thickness is smaller than the Rayleigh range of the pump and signal beams, the interaction volume can be approximated as a cylinder of thickness l along $\mathbf{u}_z$ and transverse section A_{I} given by the overlapping integral between the three Gaussian transverse modes $u_{\mathrm{p}}(x,y)u_{\mathrm{s}}^2(x,y)$, with $u_{\mathrm{p}}(x,y) = \exp\left\{-\pi\left(x^2+y^2\right)/A_{\mathrm{p}}\right\}$ and $u_{\mathrm{s}}(x,y) = \exp\left\{-\pi\left(x^2+y^2\right)/A_{\mathrm{s}}\right\}$:

$$A_{\mathrm{I}} = \int \mathrm{d}x\mathrm{d}y \; u_{\mathrm{p}}(x,y)\, u_{\mathrm{s}}(x,y)\, u_{\mathrm{s}}(x,y) = \left(\frac{2}{A_{\mathrm{s}}} + \frac{1}{A_{\mathrm{p}}}\right)^{-1}, \tag{3.13}$$

where A_{p} and A_{s} are the transverse section of the pump and signal beams, respectively.

Returning to Eq. (3.12), the nonlinear polarization $\hat{\mathbf{P}}$ can be written as:

$$\hat{\mathbf{P}}(z,t) = \hat{P}_{\mathrm{p}}(z,t)\,\mathbf{u}_y + \hat{P}_{\mathrm{s}}(z,t)\,\mathbf{u}_x. \tag{3.14}$$

and $\hat{P}_{\mathrm{s}}(z,t)$ and $\hat{P}_{\mathrm{p}}(z,t)$ are the nonlinear electric polarization at signal and pump frequencies. According to the form of the fields, they are given by:

$$\hat{P}_{\mathrm{s}}(z,t) = -\epsilon_0\chi \sum_{m,q} \mathcal{E}_{\mathrm{s},m}\mathcal{E}_{\mathrm{s},q}\left[\hat{s}_m(t)\,\hat{s}_q(t)\,e^{i(k_{\mathrm{s},m}+k_{\mathrm{s},q})z} + \hat{s}_m^\dagger(t)\,\hat{s}_q^\dagger(t)\,e^{-i(k_{\mathrm{s},m}+k_{\mathrm{s},q})z}\right] \tag{3.15}$$

$$\hat{P}_{\mathrm{p}}(z,t) = \epsilon_0\chi \sum_{j,m} \mathcal{E}_{\mathrm{p},j}\mathcal{E}_{\mathrm{s},m}\left[\hat{s}_m^\dagger(t)\,\hat{p}_j(t)\,e^{i(k_{\mathrm{p},j}-k_{\mathrm{s},m})z} + \hat{s}_m(t)\,\hat{p}_j^\dagger(t)\,e^{-i(k_{\mathrm{p},j}-k_{\mathrm{s},m})z}\right] \tag{3.16}$$

where χ is the relevant nonlinear susceptibility and the dispersion of the nonlinear susceptibility has been neglected. The interaction Hamiltonian becomes therefore:

$$\hat{H}_{\mathrm{I}} = -A_{\mathrm{I}} \int_{-l/2}^{+l/2} \mathrm{d}z \left[\hat{E}_{\mathrm{p}}(z,t)\,\hat{P}_{\mathrm{p}}(z,t) + \hat{E}_{\mathrm{s}}(z,t)\,\hat{P}_{\mathrm{s}}(z,t)\right]. \tag{3.17}$$

Substitution of the expressions for the field and the polarization into the interaction Hamiltonian yields:

$$\hat{H}_{\mathrm{I}} = 2i\epsilon_0\chi l A_{\mathrm{I}} \sum_{j,m,q} \mathcal{E}_{\mathrm{p},j}\mathcal{E}_{\mathrm{s},m}\mathcal{E}_{\mathrm{s},q}F_{j,m,q}\left(\hat{p}_j(t)\,\hat{s}_m^\dagger(t)\,\hat{s}_q^\dagger(t) - \hat{p}_j^\dagger(t)\,\hat{s}_m(t)\,\hat{s}_q(t)\right), \tag{3.18}$$

where we defined the phase-mismatch factor:

$$F_{j,m,q} = \frac{\sin\Phi_{j,m,q}}{\Phi_{j,m,q}}, \tag{3.19}$$

being

$$\Phi_{j,m,q} = \frac{1}{2}\left(k_{\mathrm{p},j} - k_{\mathrm{s},m} - k_{\mathrm{s},q}\right)l, \tag{3.20}$$

the phase-mismatch angle. In Eq. (3.18), only the terms that approximatively preserve momentum conservation have been retained.

3.1.4 The Heisenberg equations

The total Hamiltonian of the system is given by:

$$\hat{H} = \hat{H}_0 + \hat{H}_{\mathrm{I}}, \tag{3.21}$$

where:

$$\hat{H}_0 = \sum_j \hbar\omega_{\mathrm{p},j}\hat{p}_j^\dagger\hat{p}_j + \sum_m \hbar\omega_{\mathrm{s},m}\hat{s}_m^\dagger\hat{s}_m, \tag{3.22}$$

is the free evolution Hamiltonian. The Heisenberg equations for pump and signal boson operators are:

$$i\hbar\frac{d\hat{p}_j}{dt} = \left[\hat{p}_j, \hat{H}\right], \tag{3.23}$$

$$i\hbar\frac{d\hat{s}_m}{dt} = \left[\hat{s}_m, \hat{H}\right], \tag{3.24}$$

that, making use of (3.9) and (3.18), can be written as:

$$i\hbar\frac{d\hat{p}_j}{dt} = \hbar\omega_{\mathrm{p},j}\hat{p}_j - 2i\epsilon_0\chi A_{\mathrm{I}} l\sum_{m,q}\mathcal{E}_{\mathrm{p},j}\mathcal{E}_{\mathrm{s},m}\mathcal{E}_{\mathrm{s},q}F_{j,m,q}\hat{s}_m\hat{s}_q, \tag{3.25}$$

$$i\hbar\frac{d\hat{s}_m}{dt} = \hbar\omega_{\mathrm{s},m}\hat{s}_m + 4i\epsilon_0\chi A_{\mathrm{I}} l\sum_{j,q}\mathcal{E}_{\mathrm{p},j}\mathcal{E}_{\mathrm{s},m}\mathcal{E}_{\mathrm{s},q}F_{j,m,q}\hat{p}_j\hat{s}_q^\dagger, \tag{3.26}$$

Up to here we considered the Hamiltonian dynamics of the fields in the crystal. Nevertheless the optical cavity has losses, which must be incorporated into the description. According to the input-output formalism of quantum optics, losses occur at a single mirror at rates γ_{s} and γ_{p}, for the signal and pump fields, respectively. They are obtained from pump and signal power transmission coefficients of the cavity output mirror, T_{p} and T_{s}, according to the relation $\gamma_{\mathrm{f}} = \frac{cT_{\mathrm{f}}}{2L}$ ($\mathrm{f} = \mathrm{p}$ for pump field, $\mathrm{f} = \mathrm{s}$ for signal field). Then, the equations of motion are transformed into the following quantum Langevin equations:

$$\frac{d\hat{p}_j}{dt} = -\left(\gamma_{\mathrm{p}} + i\omega_{\mathrm{p},j}\right)\hat{p}_j + \gamma_{\mathrm{p}}p_{\mathrm{ext},j}\mathrm{e}^{-i(\omega_{\mathrm{p}}+j\Omega_{\mathrm{p}})t} - \frac{\kappa}{2}\sum_{m,q}F_{j,m,q}\hat{s}_m\hat{s}_q + \sqrt{2\gamma_{\mathrm{p}}}\,\hat{p}_{\mathrm{in},j}, \tag{3.27}$$

$$\frac{d\hat{s}_m}{dt} = -\left(\gamma_{\mathrm{s}} + i\omega_{\mathrm{s},m}\right)\hat{s}_m + \kappa\sum_{j,q}F_{j,m,q}\hat{p}_j\hat{s}_q^\dagger + \sqrt{2\gamma_{\mathrm{s}}}\hat{s}_{\mathrm{in,m}}, \tag{3.28}$$

where the losses for pump γ_{p} on one hand, and signal γ_{s} on the other hand are supposed occur at the same rates for all modes, the complex numbers $p_{\mathrm{ext},q}$ account for the classical external pump and the "in" operators correspond to quantum fields entering the cavity through the coupling mirror. When that input is vacuum, the case we consider, the "in" operators verify $\langle\hat{p}_{\mathrm{in},m}(t)\rangle = \langle\hat{s}_{\mathrm{in},m}(t)\rangle = 0$ and the following correlations:

$$\left\langle\hat{p}_{\mathrm{in},m}(t)\,\hat{p}_{\mathrm{in},m'}^\dagger\left(t'\right)\right\rangle = \left\langle\hat{s}_{\mathrm{in},m}(t)\,\hat{s}_{\mathrm{in},m'}^\dagger\left(t'\right)\right\rangle = \delta_{m,m'}\delta\left(t-t'\right), \tag{3.29}$$

$$\left\langle\hat{p}_{\mathrm{in},m}(t)\,\hat{s}_{\mathrm{in},m'}^\dagger\left(t'\right)\right\rangle = 0. \tag{3.30}$$

The coupling constant κ is real and it is:

$$\kappa = 2\chi l \frac{A_{\mathrm{I}}}{A_{\mathrm{s}}\sqrt{A_{\mathrm{p}}}} \left(\frac{\omega_0}{n_0 L}\right)^{3/2} \sqrt{\frac{\hbar}{\epsilon_0}} \tag{3.31}$$

taking the assumption that $\mathcal{E}_{\mathrm{s},m} = \mathcal{E}_{\mathrm{s},0}\ \forall m$ and $\mathcal{E}_{\mathrm{p},q} = \mathcal{E}_{\mathrm{p},0}\ \forall q$, which is a very good approximation as far as pulses are not too short (say, larger than 30 fs in the visible).

Passing to the pump-interaction picture, the fields operators (also the input noise terms) are rewritten as:

$$\hat{p}_j(t) = \tilde{p}_j\, \mathrm{e}^{-i(\omega_{\mathrm{p}} + j\Omega_p)t}, \tag{3.32}$$

$$\hat{s}_m(t) = \tilde{s}_m\, \mathrm{e}^{-i\left(\frac{1}{2}\omega_{\mathrm{p}} + m\Omega_p\right)t}, \tag{3.33}$$

which, substituted in (3.27) and (3.28), yield the following evolution equations (after dropping the tildes for simplicity):

$$\begin{aligned} \frac{d\hat{p}_j}{dt} &= -\left(\gamma_{\mathrm{p}} + i\Delta_{\mathrm{p},j}\right)\hat{p}_j + \gamma_{\mathrm{p}} p_{\mathrm{ext},j} - \frac{\kappa}{2}\sum_{m,q} F_{j,m,q}\mathrm{e}^{i(j-m-q)\Omega_{\mathrm{p}}t}\hat{s}_m\hat{s}_q \\ &\quad + \sqrt{2\gamma_{\mathrm{p}}}\,\hat{p}_{\mathrm{in},j}, \end{aligned} \tag{3.34}$$

$$\frac{d\hat{s}_m}{dt} = -\left(\gamma_{\mathrm{s}} + i\Delta_{\mathrm{s},m}\right)\hat{s}_m + \kappa\sum_{j,q} F_{j,m,q}\mathrm{e}^{-i(j-m-q)\Omega_{\mathrm{p}}t}\hat{p}_j\hat{s}_q^{\dagger} + \sqrt{2\gamma_{\mathrm{s}}}\hat{s}_{\mathrm{in,m}}, \tag{3.35}$$

where:

$$\Delta_{\mathrm{p},j} = \omega_{\mathrm{p},j} - (\omega_{\mathrm{p}} + j\Omega_{\mathrm{p}}) = 2\Delta + j\left(\Omega - \Omega_{\mathrm{p}}\right), \tag{3.36}$$

$$\Delta_{\mathrm{s},m} = \omega_{\mathrm{s},m} - \left(\frac{1}{2}\omega_{\mathrm{p}} + m\Omega_{\mathrm{p}}\right) = \Delta + m\left(\Omega - \Omega_{\mathrm{p}}\right), \tag{3.37}$$

and keeping in mind the phase-matching condition $\omega_{\mathrm{p},0} = 2\omega_{\mathrm{s},0}$:

$$\Delta = \omega_{\mathrm{s},0} - \frac{1}{2}\omega_{\mathrm{p}} = \frac{1}{2}\left(\omega_{\mathrm{p},0} - \omega_{\mathrm{p}}\right). \tag{3.38}$$

For a high finesse cavity the condition $\gamma_{\mathrm{p}}, \gamma_{\mathrm{s}} \ll \Omega \sim \Omega_{\mathrm{p}}$ is satisfied, therefore only the terms that cancel the exponential factor $j - m - q = 0$ contribute significantly to the evolution of the fields. In other terms, this is the condition for energy conservation of each parametric process. The evolution equations (3.34) and (3.35) then become:

$$\frac{d\hat{p}_j}{dt} = -\left(\gamma_{\mathrm{p}} + i\Delta_{\mathrm{p},j}\right)\hat{p}_j + \gamma_{\mathrm{p}} p_{\mathrm{ext},j} - \frac{\kappa}{2}\sum_{m} f_{j,m}\hat{s}_m\hat{s}_{j-m} + \sqrt{2\gamma_{\mathrm{p}}}\,\hat{p}_{\mathrm{in},j}, \tag{3.39}$$

$$\frac{d\hat{s}_m}{dt} = -\left(\gamma_{\mathrm{s}} + i\Delta_{\mathrm{s},m}\right)\hat{s}_m + \kappa\sum_{q} f_{m+q,m}\hat{p}_{m+q}\hat{s}_m^{\dagger} + \sqrt{2\gamma_{\mathrm{s}}}\hat{s}_{\mathrm{in,m}}, \tag{3.40}$$

where the phase-mismatch factors are now redefined:

$$f_{j,m} = \frac{\sin\phi_{j,m}}{\phi_{j,m}}, \tag{3.41}$$

$$\phi_{j,m} = \frac{1}{2}\left(k_{\mathrm{p},j} - k_{\mathrm{s},m} - k_{\mathrm{s},j-m}\right)l. \tag{3.42}$$

For the calculation of phase-mismatch term (3.42), let's consider the standard approximation consisting in Taylor expanding $k_{\mathrm{p},j}$ and $k_{\mathrm{s},m}$ around their phase-matched values $2k_0 = 2\omega_0\, n\,(2\omega_0)$ and $k_0 = \omega_0\, n\,(\omega_0)$:

$$\begin{aligned} k_{\mathrm{p},j} &= 2k_0 + k'_{\mathrm{p}}\left(\omega_{\mathrm{p},j} - 2\omega_0\right) + \frac{1}{2}k''_{\mathrm{p},j}\left(\omega_{\mathrm{p},j} - 2\omega_0\right)^2 \\ &= 2k_0 + 2k'_{\mathrm{p}}\Delta + 2k''_{\mathrm{p}}\Delta^2 + j\left(k'_{\mathrm{p}} + 2k''_{\mathrm{p}}\Delta\right)\Omega + \frac{1}{2}k''_{\mathrm{p},j}j^2\Omega^2, \qquad (3.43) \\ k_{\mathrm{s},m} &= k_0 + k'_{\mathrm{s}}\left(\omega_{\mathrm{s},m} - \omega_0\right) + \frac{1}{2}k''_{\mathrm{s},m}\left(\omega_{\mathrm{s},m} - \omega_0\right)^2 \\ &= k_0 + k'_{\mathrm{s}}\Delta + k''_{\mathrm{s}}\Delta^2 + m\left(k'_{\mathrm{s}} + k''_{\mathrm{s}}\Delta\right)\Omega + \frac{1}{2}k''_{\mathrm{s},m}m^2\Omega^2, \qquad (3.44) \end{aligned}$$

where $k'_{\mathrm{p}} = \left(\partial k_{\mathrm{p}}/\partial\omega\right)_{\omega=2\omega_0}$ and $k'_{\mathrm{s}} = \left(\partial k_{\mathrm{s}}/\partial\omega\right)_{\omega=\omega_0}$ are the inverse of the group velocities at the phase-matched pump and signal frequencies and $k''_{\mathrm{p}} = \left(\partial^2 k_{\mathrm{p}}/\partial\omega^2\right)_{\omega=2\omega_0}$ and $k''_{\mathrm{s}} = \left(\partial^2 k_{\mathrm{s}}/\partial\omega^2\right)_{\omega=\omega_0}$ are responsible for group velocity dispersion. From these expressions the phase-mismatch term can be written as:

$$\begin{aligned} \phi_{j,m} &= l\left[\left(k'_{\mathrm{p}} - k'_{\mathrm{s}}\right)\Delta + \frac{1}{2}\left(2k''_{\mathrm{p}} - k''_{\mathrm{s}}\right)\Delta^2 + \frac{1}{2}j\left(k'_{\mathrm{p}} - k'_{\mathrm{s}} + \left(2k''_{\mathrm{p}} - k''_{\mathrm{s}}\right)\Delta\right)\Omega\right. \\ &\quad \left. + \frac{1}{4}j^2\left(k''_{\mathrm{p}} - k''_{\mathrm{s}}\right)\Omega^2 + \frac{1}{2}m\left(j - m\right)k''_{\mathrm{s}}\Omega^2\right]. \qquad (3.45) \end{aligned}$$

This expression can be simplified noting that the inequality $\left|\left(2k''_{\mathrm{p}} - k''_{\mathrm{s}}\right)\Delta\right| \ll \left|k'_{\mathrm{p}} - k'_{\mathrm{s}}\right|$ is in general always verified. Therefore Eq. (3.45) reads:

$$\phi_{j,m} = l\left[\left(k'_{\mathrm{p}} - k'_{\mathrm{s}}\right)\Delta + \frac{1}{2}j\left(k'_{\mathrm{p}} - k'_{\mathrm{s}}\right)\Omega + \frac{1}{4}j^2\left(k''_{\mathrm{p}} - k''_{\mathrm{s}}\right)\Omega^2 + \frac{1}{2}m\left(j - m\right)k''_{\mathrm{s}}\Omega^2\right]. \qquad (3.46)$$

Let's notice that the phase-mismatch verifies the symmetry $\phi_{m,m+q} = \phi_{q,m+q}$, hence:

$$f_{m+q,m} = f_{m+q,q}. \qquad (3.47)$$

This property will reveal to be important for the problem connected to the threshold of SPOPOs.

In order to relate the term $p_{\mathrm{ext},j}$ to the actual pump parameters as given by Eq. (3.5), we note that Eq. (3.39) with $\kappa = 0$ describes a passive ring resonator. Ignoring quantum fluctuations, the asymptotic solution is $\langle\hat{p}_j\rangle = p_{\mathrm{ext},j}$. Plugging this solution into Eq. (3.7) we obtain:

$$E_{\mathrm{p}}^{\mathrm{passive}}(z,t) = i\sum_j \mathcal{E}_{\mathrm{p},j}p_{\mathrm{ext},j}e^{i\left(k_{\mathrm{p},j}z - \omega_{\mathrm{p},j}t\right)} + \mathrm{H.c.} \qquad (3.48)$$

However this expression must coincide with the one obtained assuming that the cavity is pumped by the external field (3.5). As the cavity is resonant the following relation is obtained:

$$\mathcal{E}_{\mathrm{p},j}p_{\mathrm{ext},j} = \frac{t_{\mathrm{p}}}{1 - r_{\mathrm{p}}}\left(\frac{P}{2\epsilon_0 c}\right)^{\frac{1}{2}}\alpha_j, \qquad (3.49)$$

where t_{p} and $r_{\mathrm{p}} = \sqrt{1 - t_{\mathrm{p}}^2}$ are the transmission and reflection coefficients at the coupling mirror. As high finesse is assumed $t_{\mathrm{p}} \ll 1$ and $r_{\mathrm{p}} \simeq 1 - \frac{1}{2}t_{\mathrm{p}}^2$, hence:

$$\mathcal{E}_{\mathrm{p},j}p_{\mathrm{ext},j} = 2\left(\frac{P}{2\epsilon_0 c T_{\mathrm{p}}}\right)^{\frac{1}{2}}\alpha_j, \qquad (3.50)$$

where $T_\mathrm{p} = t_\mathrm{p}^2$ is the transmission factor of the coupling mirror. Finally putting $\mathcal{E}_{\mathrm{p},j} = \sqrt{\frac{\hbar\omega_0}{\epsilon_0 n_0 A_\mathrm{p} L}}$ we obtain:

$$p_{\mathrm{ext},j} = 2\sqrt{\frac{n_0 A_\mathrm{p} L P}{2cT_\mathrm{p}\hbar\omega_0}}\alpha_j. \tag{3.51}$$

Equations (3.39) and (3.40) constitute the general model of a resonant SPOPO.

3.1.5 The resonant model

In order to have well behaved subharmonic pulses and the SPOPO working in a phase-locked regime, the amount of the detuning is required to be smaller than an admissible limit. In fact in presence of mode-dependent detunings, Eqs. (3.39) and (3.40) can hardly admit phase-locked solutions. A rough estimate of the maximal admissible detunings could be achieved imposing that $|\Delta_{\mathrm{p},j_\mathrm{max}}|/\gamma_\mathrm{p} \ll 1$ and $|\Delta_{\mathrm{s},m_\mathrm{max}}|/\gamma_\mathrm{s} \ll 1$, where j_max and m_max are the largest values of q and m approximatively fixed by the pump and single combs spectral width, respectively. While we don't know yet the features of the signal combs, it is possible to estimate the pump spectral width that is basically determined by the external pump properties. Assuming pump pulses of 100 fs duration produced by a laser cavity of 1 m length, j_max is of the order of 10^4. By recalling Eq. (3.36) and that $\gamma_\mathrm{p} = T_\mathrm{p}\Omega/4\pi$ ($T_\mathrm{p} = t_\mathrm{p}^2$ is the power transmissivity of the output coupler for the pump field), the constraint $|\Delta_{\mathrm{p},j_\mathrm{max}}|/\gamma_\mathrm{p} \ll 1$ is equivalent to:

$$\left|\frac{\Omega - \Omega_\mathrm{p}}{\Omega}\right| \ll 10^{-6}, \tag{3.52}$$

for mirror transmissivities of about 0.1. For a ring cavity $\Omega = 2\pi c/L$, while $\Omega_\mathrm{p} = 2\pi c/L_\mathrm{p}$ (where L_p denotes the effective cavity length of the pumping laser), therefore the previous constraint amounts to ask in terms of cavity lengths:

$$\left|\frac{L - L_\mathrm{p}}{L_\mathrm{p}}\right| \ll 10^{-6}, \tag{3.53}$$

which require an adjustment of the SPOPO cavity length with a precision better than 100 nm. Another argument to understand the physical reasons to this limitation is that the incertitude on the OPO cavity length should be smaller than the spatial extension of the pump pulse:

$$\Delta L \ll c\Delta t. \tag{3.54}$$

If $\Delta t \simeq 100$ fs, then $\Delta L \ll 100$ nm which is in a good agreement with the former estimate. For shorter pulses (say 10 fs) or for better output couplers (say $T_\mathrm{p} = 0.01$), this estimate imposes precisions of 1 nm. This poses serious problems for the operation of SPOPOs pumped by ultrashort pulses.

Leaving the challenge for high precision synchronization to experimentalists, in the following we will consider that the SPOPO cavity length is perfectly matched to the pumping laser cavity: $\Omega = \Omega_\mathrm{p}$. In the case of perfect synchronization, the bias detuning term (see Eq. (3.38)) is also null. Consequently Eqs. (3.39) and (3.40) becomes:

$$\frac{d\hat{p}_j}{dt} = -\gamma_\mathrm{p}\hat{p}_j + \gamma_\mathrm{p} p_{\mathrm{ext},j} - \frac{\kappa}{2}\sum_m f_{j,m}\hat{s}_m\hat{s}_{j-m} + \sqrt{2\gamma_\mathrm{p}}\,\hat{p}_{\mathrm{in},j}, \tag{3.55}$$

$$\frac{d\hat{s}_m}{dt} = -\gamma_\mathrm{s}\hat{s}_m + \kappa\sum_q f_{m+q,m}\hat{p}_{m+q}\hat{s}_m^\dagger + \sqrt{2\gamma_\mathrm{s}}\hat{s}_{\mathrm{in,m}}. \tag{3.56}$$

3.1.6 The SPOPO below threshold

Equations (3.55) and (3.56) are nonlinear in the pump and signal bosonic operators and are usually solved by linearization of the operators $\hat{p}_q(t)$ and $\hat{s}_m(t)$ around their steady state values [Graham1968]:

$$\hat{p}_j(t) = \langle \hat{p}_j \rangle + \delta\hat{p}_j(t), \tag{3.57}$$

$$\hat{s}_m(t) = \langle \hat{s}_m \rangle + \delta\hat{s}_m(t), \tag{3.58}$$

where $\delta\hat{p}_j(t)$ and $\delta\hat{s}_m(t)$ represents field fluctuations around the steady state solutions. Below threshold signal modes are almost not excited and $\langle \hat{s}_m \rangle = 0$, therefore, at the 0-th order in the field fluctuations, Eq. (3.55) admits the solution:

$$\langle \hat{p}_j \rangle = p_{\mathrm{ext},j}, \tag{3.59}$$

while, at the first order eqs. (3.55) and (3.56) read as:

$$\frac{d}{dt}\delta\hat{p}_j(t) = -\gamma_{\mathrm{p}}\delta\hat{p}_j + \sqrt{2\gamma_{\mathrm{p}}}\delta\hat{p}_{\mathrm{in},j} - \frac{\kappa}{2}\sum_m f_{j,m}\delta\hat{s}_m\,\delta\hat{s}_{j-m}, \tag{3.60}$$

$$\begin{aligned}\frac{d}{dt}\delta\hat{s}_m(t) &= -\gamma_{\mathrm{s}}\delta\hat{s}_m + \kappa\sum_q f_{m+q,m}\langle\hat{p}_{m+q}\rangle\,\delta\hat{s}_m{}^{\dagger} + \sqrt{2\gamma_{\mathrm{s}}}\delta\hat{s}_{\mathrm{in},m} \\ &\quad + \kappa\sum_q f_{m+q,m}\,\delta\hat{s}_m{}^{\dagger}\,\delta\hat{p}_{m+q}.\end{aligned} \tag{3.61}$$

Neglecting the second order nonlinear term in Eq. (3.60), the solution for pump field fluctuations is readily obtained:

$$\delta\hat{p}_j(t) \simeq \sqrt{2\gamma_{\mathrm{p}}}\int_{-\infty}^{t} \mathrm{d}t'\delta\hat{p}_{\mathrm{in},j}(t')\,\mathrm{e}^{\gamma_{\mathrm{p}}(t-t')}, \tag{3.62}$$

where $\delta\hat{p}_j(t)$ is a new noise term that verify the following properties:

$$\langle \delta\hat{p}_j(t) \rangle = 0, \tag{3.63}$$

$$\langle \delta\hat{p}_j(t)\,\delta\hat{p}_r(t') \rangle = \delta_{j,r}e^{-|t-t'|}, \tag{3.64}$$

trivially obtained from Eqs. (3.29) and (3.30). The quantity $|p_{\mathrm{ext},q}|^2$ gives the number of intracavity pump photons at frequency $\omega_{\mathrm{p},j}$ coming from the pumping laser, and this number is normally huge. Hence, given that the noise term $\delta\hat{p}_j(t)$ is of order one, see Eq. (3.64), one can neglect it in Eq. (3.62) so that $\langle \hat{p}_j(t) \rangle = p_{\mathrm{ext},j}$.

However, at first order in Eq. (3.61), the pump fluctuations don't play any role in the evolution of signal field thanks to the fact that below threshold $\langle \hat{s}_m \rangle = 0$. Taking in mind that below threshold $\hat{s}_m(t) = \delta\hat{s}_m(t)$ and making use of Eq. (3.51), we finally obtain the linearized Langevin equation for the signal field:

$$\boxed{\frac{d\hat{s}_m}{dt} = -\gamma_{\mathrm{s}}\hat{s}_m + \sqrt{2\gamma_{\mathrm{s}}}\hat{s}_{\mathrm{in},m} + \gamma_{\mathrm{s}}\sigma\sum_q f_{m+q,m}\alpha_{m+q}\hat{s}_q^{\dagger},} \tag{3.65}$$

where:

$$\sigma = \sqrt{P/P_0}, \tag{3.66}$$

and

$$P_0 = \frac{\epsilon_0 c^3 n_0^2 T_\mathrm{s}^2 T_\mathrm{p}}{32\left(\omega_0 \chi l\right)^2}\left(\frac{A_\mathrm{s}}{A_\mathrm{I}}\right)^2, \tag{3.67}$$

is a reference irradiance, equal to the cw OPO threshold as shown in the next chapter (see section 4.3), and we made use of $\gamma_\mathrm{s} = \frac{cT_\mathrm{s}}{2L}$. Making use of Eq. (3.13) we can write:

$$P_0 = \frac{\epsilon_0 c^3 n_0^2 T_\mathrm{s}^2 T_\mathrm{p}}{32\left(\chi l \omega_0\right)^2}\left(1 + \frac{A_\mathrm{s}}{2A_\mathrm{p}}\right)^2. \tag{3.68}$$

The corresponding power $W_0 = A_\mathrm{p} P_0$, which is proportional to $\left(1 + \frac{A_\mathrm{s}}{2A_\mathrm{p}}\right)^2 A_\mathrm{p}$, plays the role of threshold power and is thus an important quantity. The minimum of W_0 occurs at $A_\mathrm{p} = A_\mathrm{s}/2$, as could be expected according to the nature of the nonlinear interaction, in which two signal photons interact with one pump photon. For this optimized setting we obtain:

$$P_0 = \frac{\epsilon_0 c^3 n_0^2 T_\mathrm{s}^2 T_\mathrm{p}}{8\left(\chi l \omega_0\right)^2}. \tag{3.69}$$

The linearized Langevin equations (3.65) in the below threshold regime is the general model that has been considered in order to study the problem of the threshold (see Chapter 4) and quantum properties (Chapter 5) of SPOPO devices. In the following we will directly consider the field operator in the interaction picture and assuming the conditions for a resonant operation satisfied.

3.2 Doubly resonant linear cavity

In this section we retrieve the quantum model for quasi-degenerate type I SPOPO in which both pump and signal are resonated inside a linear cavity (Fabry-Perot) of length L. The intracavity field is always supposed to be a superposition of plane waves propagating along $\mathbf{u}_z$.

3.2.1 Longitudinal modes of the resonator

The boundary condition imposed by the linear cavity to the intracavity field give origin to stationary longitudinal modes that are written as:

$$U_m^{\mathrm{lin}}(z,t) = \begin{cases} \frac{1}{\sqrt{n(\omega_m)}}\, u_m \sin\left(k_m z - \omega_m t\right), & z \in \left[-\frac{l}{2}, \frac{l}{2}\right] \\ u_m \sin\left(k_m^{\mathrm{vac}} z - \omega_m t + \phi_m\right), & z \notin \left[-\frac{l}{2}, \frac{l}{2}\right] \end{cases}, \tag{3.70}$$

where $k_m^{\mathrm{vac}} = \omega_m / c$ is the wavenumber in vacuum, $k_m = n(\omega_m)\, k_m^{\mathrm{vac}}$, $n(\omega_m)$ is the refractive index of the crystal at frequency ω_m, u_m is a classical complex amplitude, the transmission factor $1/\sqrt{n(\omega_m)}$ is due to the flux conservation keeping in count that reflection at the entrance facet is absent, and ϕ_m is a suitable phase. If the crystal is the only refractive element inside the cavity, the frequencies ω_m verify the following resonance condition:

$$\omega_m = m\,\frac{\pi c}{\left[n(\omega_m) - 1\right] l + L}, \tag{3.71}$$

with $m \in \mathbb{N}$. As for the ring cavity case, Eq. (3.71) put in evidence that the dispersion of the free spectral range need to be compensated by extra refractive elements in order to

achieve an optimal synchronized operation. Under the hypothesis of dispersion compensation, however, is always possible to describe the intracavity pump and signal frequency combs by means of eqs. (3.3) and (3.4).

3.2.2 The fields

Assuming the fields linearly polarized respectively along $\mathbf{u}_y$ for the pump and $\mathbf{u}_z$ for the signal, let's write the total intracavity field as in Eq. (3.6). Using the basis of longitudinal cavity modes, signal and pump field can be expanded, inside a crystal which extends from $z = -l/2$ to $z = l/2$, as:

$$\hat{E}_{\mathrm{p}}(z,t) = i\sum_m \mathcal{E}_{\mathrm{p},m}\hat{p}_m(t)\sin\left(k_{\mathrm{p},m}\left(z+L/2\right)\right)\mathrm{e}^{-i\omega_{\mathrm{p},m}t} + \mathrm{H.c.}, \tag{3.72}$$

$$\hat{E}_{\mathrm{s}}(z,t) = i\sum_m \mathcal{E}_{\mathrm{s},m}\hat{s}_m(t)\sin\left(k_{\mathrm{s},m}\left(z+L/2\right)\right)\mathrm{e}^{-i\omega_{\mathrm{s},m}t} + \mathrm{H.c.}, \tag{3.73}$$

where $\mathcal{E}_{\mathrm{f},m} = \sqrt{\frac{\hbar\omega_{\mathrm{f},m}}{\epsilon_0 n\left(\omega_{\mathrm{f},m}\right)A_{\mathrm{f}}L}}$, $\mathrm{f} = \mathrm{p},\mathrm{s}$ are single photon fields, and A_{f} is the transverse area of pump ($\mathrm{f} = \mathrm{p}$) or signal ($\mathrm{f} = \mathrm{s}$) fields. The boson operators $\hat{p}_j$ and $\hat{s}_m$ verify the usual commutation relations (3.9).

3.2.3 The interaction Hamiltonian

The interaction Hamiltonian (3.17) for a doubly resonant linear cavity is straightforwardly obtained from the expressions (3.72) and (3.73) keeping in mind that, in this case, the polarizations at pump and signal frequencies are:

$$\begin{aligned}\hat{P}_{\mathrm{p}}(z,t) &= \epsilon_0\sum_{j,m}\mathcal{E}_{\mathrm{p},j}\mathcal{E}_{\mathrm{s},m}\hat{p}_j(t)\hat{s}^\dagger(t)\times \\ &\times \sin\left(k_{\mathrm{p},j}(z+L/2)\right)\sin\left(k_{\mathrm{s},j}(z+L/2)\right)\mathrm{e}^{-i(\omega_{\mathrm{p},j}-\omega_{\mathrm{s},m})t} + \mathrm{H.c.} \qquad (3.74)\\ \hat{P}_{\mathrm{s}}(z,t) &= \epsilon_0\sum_{j,m}\mathcal{E}_{\mathrm{s},j}\mathcal{E}_{\mathrm{s},m}\hat{s}_j(t)\hat{s}(t)\times \\ &\times \sin\left(k_{\mathrm{s},j}(z+L/2)\right)\sin\left(k_{\mathrm{s},j}(z+L/2)\right)\mathrm{e}^{-i(\omega_{\mathrm{s},j}+\omega_{\mathrm{s},m})t} + \mathrm{H.c.} \qquad (3.75)\end{aligned}$$

After having expanded, in terms of exponentials, the sinus factors, it is worth to introduce new signal and pump boson operators:

$$\hat{p}_{j,\mathrm{new}}(t) = \hat{p}_j(t)\,e^{+ik_{\mathrm{p},j}L/2},\ \hat{p}^\dagger_{j,\mathrm{new}}(t) = \hat{p}^\dagger_j(t)\,e^{-ik_{\mathrm{p},j}L/2}, \tag{3.76}$$

$$\hat{s}_{m,\mathrm{new}}(t) = \hat{s}_m(t)\,e^{+ik_{\mathrm{s},m}L/2},\ \hat{s}^\dagger_{m,\mathrm{new}}(t) = \hat{s}^\dagger_m(t)\,e^{-ik_{\mathrm{s},m}L/2}. \tag{3.77}$$

By neglecting all the terms that will not satisfy the phase-matching condition, then, $\hat{H}_{\mathrm{I}}$ can be put in the form:

$$\hat{H}_I = \frac{i\epsilon_0\chi l A_{\mathrm{I}}}{2}\sum_{j,m,q}\mathcal{E}_{\mathrm{p},j}\mathcal{E}_{\mathrm{s},m}\mathcal{E}_{\mathrm{s},q}F_{j,m,q}\hat{p}_j\hat{s}^\dagger_m\hat{s}^\dagger_q\mathrm{e}^{-i(\omega_{\mathrm{p},j}-\omega_{\mathrm{s},m}-\omega_{\mathrm{s},q})t} + \mathrm{H.c.}, \tag{3.78}$$

with:

$$F_{j,m,q} = \frac{\sin\left(\left(k_{\mathrm{p},j}-k_{\mathrm{s},m}-k_{\mathrm{s},q}\right)\frac{l}{2}\right)}{\left(k_{\mathrm{p},j}-k_{\mathrm{s},m}-k_{\mathrm{s},q}\right)\frac{l}{2}}. \tag{3.79}$$

However, like in the end of Section 3.1.4, for high finesse cavities, we can make the rotating wave approximation, which leads to:

$$\hat{H}_I = \frac{i\epsilon_0 \chi l A_{\mathrm{I}}}{2} \sum_{j,m} \mathcal{E}_{\mathrm{p},j} \mathcal{E}_{\mathrm{s},m} \mathcal{E}_{\mathrm{s},j-m} f_{j,m} \hat{p}_j \hat{s}_m^\dagger \hat{s}_{j-m}^\dagger + \mathrm{H.c.}, \tag{3.80}$$

with

$$f_{j,m} = \frac{\sin\left(\left(k_{\mathrm{p},j} - k_{\mathrm{s},m} - k_{\mathrm{s},j-m}\right)\frac{l}{2}\right)}{\left(k_{\mathrm{p},j} - k_{\mathrm{s},m} - k_{\mathrm{s},j-m}\right)\frac{l}{2}}. \tag{3.81}$$

3.2.4 The Heisenberg equations

From the Hamiltonian (3.80) it is, now, easy to retrieve the Heisenberg equations for pump and signal field operators:

$$i\hbar \frac{d\hat{p}_j}{dt} = -\frac{i\epsilon_0 \chi l A_{\mathrm{I}}}{2} \sum_m \mathcal{E}_{\mathrm{p},j} \mathcal{E}_{\mathrm{s},m} \mathcal{E}_{\mathrm{s},j-m} f_{j,m} \hat{s}_m \hat{s}_{j-m}, \tag{3.82}$$

$$i\hbar \frac{d\hat{s}_m}{dt} = i\epsilon_0 \chi l A_{\mathrm{I}} \sum_q \mathcal{E}_{\mathrm{p},m+q} \mathcal{E}_{\mathrm{s},m} \mathcal{E}_{\mathrm{s},q} f_{m+q,q} \hat{p}_j \hat{s}_q^\dagger, \tag{3.83}$$

From Eqs. (3.82) and (3.83), it is, now, possible to retrieve the quantum Langevin equations for signal and pump operators that reads:

$$\frac{d\hat{p}_j}{dt} = -\gamma_{\mathrm{p}} \hat{p}_j + \gamma_{\mathrm{p}} p_{\mathrm{ext},j} - \frac{\kappa}{2} \sum_m f_{j,m} \hat{s}_m \hat{s}_{j-m} + \sqrt{2\gamma_{\mathrm{p}}}\, \hat{p}_{\mathrm{in},j}, \tag{3.84}$$

$$\frac{d\hat{s}_m}{dt} = -\gamma_{\mathrm{s}} \hat{s}_m + \kappa \sum_q f_{m+q,m} \hat{p}_{m+q} \hat{s}_m^\dagger + \sqrt{2\gamma_{\mathrm{s}}} \hat{s}_{\mathrm{in,m}}, \tag{3.85}$$

where, in this case, the coupling constant κ is:

$$\kappa = \sqrt{2}\chi l \frac{A_{\mathrm{I}}}{A_{\mathrm{s}}\sqrt{A_{\mathrm{p}}}} \left(\frac{\omega_0}{n_0 L}\right)^{3/2} \sqrt{\frac{\hbar}{\epsilon_0}}. \tag{3.86}$$

3.2.5 The SPOPO below threshold

Below threshold, the same arguments discussed in Section 3.1.6 apply. Therefore, while the signal modes are almost in the vacuum state, the main contribution to the pump field is given by its classical component $\langle \hat{p}_{\mathrm{in},j}(t) \rangle = p_{\mathrm{ext},j}$. Keeping in mind that for a linear cavity the pump field has been written as in Eq. (3.72), the expression (3.50) is slightly modified in:

$$\frac{1}{2} \mathcal{E}_{\mathrm{p},j} p_{\mathrm{ext},j} = 2 \left(\frac{P}{2\epsilon_0 c T_{\mathrm{p}}}\right)^{\frac{1}{2}} \alpha_j, \tag{3.87}$$

from which directly follows:

$$p_{\mathrm{ext},j} = 2\sqrt{\frac{n_0 A_{\mathrm{p}} L P}{c T_{\mathrm{p}} \hbar \omega_0}}\, \alpha_j. \tag{3.88}$$

The Langevin equation for the signal field, therefore, reads:

$$\boxed{\frac{d\hat{s}_m}{dt} = -\gamma_{\mathrm{s}} \hat{s}_m + \sqrt{2\gamma_{\mathrm{s}}} \hat{s}_{\mathrm{in},m} + \gamma_{\mathrm{s}} \sigma \sum_q f_{m+q,m} \alpha_{m+q} \hat{s}_q^\dagger,} \tag{3.89}$$

where:

$$\sigma = \sqrt{P/P_0}, \tag{3.90}$$

and

$$P_0 = \frac{\epsilon_0 c^3 n_0^2 T_\mathrm{s}^2 T_\mathrm{p}}{128\left(\omega_0 \chi l\right)^2}\left(\frac{A_\mathrm{s}}{A_\mathrm{I}}\right)^2. \tag{3.91}$$

P_0 is a reference power per unit area which has the role of c.w. OPO threshold, defined in a way similar to the case considered in the previous section. Since the linear geometry, we used $\gamma_\mathrm{s} = \frac{cT_\mathrm{s}}{4L}$, being T_s the power transmission coefficient through the output coupler, to get Eq. (3.91). The corresponding power $W_0 = A_\mathrm{p} P_0$ plays the role of threshold power.

As in section 3.1, making use of Eq. (3.13) and for the optimized setting corresponding to $A_\mathrm{p} = A_\mathrm{s}/2$ we obtain:

$$P_0 = \frac{\epsilon_0 c^3 n_0^2 T_\mathrm{s}^2 T_\mathrm{p}}{32\left(\chi l \omega_0\right)^2}. \tag{3.92}$$

For the doubly resonant linear cavity case, then, we obtain a threshold that is lower than the doubly resonant ring cavity of a factor 4. This occurrence is consistent with the fact that in a linear cavity the signal field passes through the crystal two times together with the pump field, thus feeling a parametrical gain proportional to $(2l)^2$, which corresponds to an increase of the intra-cavity power of the same factor 4.

The experimental setting of a OPO cavity, that is resonant both for the pump and signal fields may result difficult, since the condition of synchronization have to be kept for all the frequencies of the combs. From this point of view, the situation is partially simplified by implementing an OPO cavity that is resonant only for the signal field. However, since the pump field is no more resonating, a higher threshold should be expected. In the next sections we are going to analyze, then, this different configuration both for the ring and linear geometries.

3.3 Singly resonant ring cavity

Let's consider a ring cavity of length L which is not resonant for the pump field. In this case the pump field cannot be quantified inside the cavity and, consequently, the derivation of the Langevin equation for the pump and signal filed operators becomes more involved. Nevertheless, in the below threshold and linearized fluctuations regime, the final evolution equation is formally equivalent to Eq. (3.65). We suppose the same phase matching operation as the previous cases. The intracavity fields are considered of fixed linear polarization as in (3.6).

3.3.1 The fields

The resonating signal field is expanded on the usual basis of longitudinal cavity modes, while the pump field, that in general is the superposition of continuous modes, is quantized in a box of length L_p, with periodic boundary conditions, that at the end will be assumed $L_\mathrm{p} \to +\infty$:

$$\hat{E}_\mathrm{p}(z,t) = i\sum_j \mathcal{E}(\nu_j)\left[\hat{p}_j^{(+)}(t)\, e^{i\kappa_j z} + \hat{p}_j^{(-)}(t)\, e^{-i\kappa_j z}\right] e^{-i\nu_j t} + \mathrm{H.c.}, \tag{3.93}$$

$$\hat{E}_\mathrm{s}(z,t) = i\sum_m \mathcal{E}_{\mathrm{s},m}\hat{s}_m(t)\, \mathrm{e}^{i(k_{\mathrm{s},m} z - \omega_{\mathrm{s},m} t)} + \mathrm{H.c.}, \tag{3.94}$$

where the superscripts $(\pm)$ label the propagation direction. The fields have been written in the interaction picture under the hypothesis that no detuning of the pump respect to the cavity modes occurs.

However, since the counter-propagating pump component labeled with $(-)$ is never phase matched with the signal field, Eq. (3.93) can be written in a simpler form:

$$\hat{E}_{\mathrm{p}}(z,t) = i\sum_{j}\mathcal{E}(\nu_j)\,\hat{p}_j(t)\,\mathrm{e}^{i(\kappa_j z-\nu_m t)} + \mathrm{H.c.}, \tag{3.95}$$

where the superscript $(+)$ has been understood. The signal single photon field amplitude is $\mathcal{E}_{\mathrm{s},m} = \sqrt{\frac{\hbar\omega_{\mathrm{s},m}}{2\epsilon_0 n(\omega_{\mathrm{s},m})A_{\mathrm{s}}L}}$ and the pump single photon field amplitude is $\mathcal{E}(\nu_j) = \sqrt{\frac{\hbar\nu_j}{2\epsilon_0 n(\nu_j)A_{\mathrm{p}}L}}$. The frequencies ν_j are given by $\nu_j = j\frac{2\pi c}{L_{\mathrm{p}}}$ and the wavenumbers $\kappa_j = \frac{n(\nu_j)\nu_j}{c}$, with $n(\nu_j)$ the crystal refractive index.

3.3.2 The interaction Hamiltonian

The interaction Hamiltonian $\hat{H}_{\mathrm{I}}$ is calculated as usual as:

$$\hat{H}_{\mathrm{I}} = -A_{\mathrm{I}}\int_{-l/2}^{+l/2}\mathrm{d}z\left[\hat{E}_{\mathrm{p}}(z,t)\,\hat{P}_{\mathrm{p}}(z,t) + \hat{E}_{\mathrm{s}}(z,t)\,\hat{P}_{\mathrm{s}}(z,t)\right], \tag{3.96}$$

where A_{I} is the effective area of interaction corresponding to the three-mode overlapping integral across the transverse plane. According to (3.94) and (3.95) and neglecting the terms that will not satisfy the phase-matching conditions, the polarization at signal frequencies is:

$$\hat{P}_{\mathrm{s}}(z,t) = \epsilon_0\chi\sum_{j,m}\mathcal{E}(\nu_j)\,\mathcal{E}_{\mathrm{s},m}\hat{p}_j(t)\,\hat{s}_m^{\dagger}(t)\,\mathrm{e}^{i(\kappa_j-k_{\mathrm{s},m})z}\mathrm{e}^{-i(\nu_j-\omega_{\mathrm{s},m})t} + \mathrm{H.c.}, \tag{3.97}$$

therefore:

$$\begin{aligned}\hat{E}_{\mathrm{s}}(z,t)\,\hat{P}_{\mathrm{s}}(z,t) = &-i\epsilon_0\chi\sum_{j,m,q}\mathcal{E}(\nu_j)\,\mathcal{E}_{\mathrm{s},m}\mathcal{E}_{\mathrm{s},q}\hat{p}_j\hat{s}_m^{\dagger}\hat{s}_q^{\dagger}\mathrm{e}^{i(\kappa_j-k_{\mathrm{s},m}-k_{\mathrm{s},q})z}\mathrm{e}^{-i(\nu_j-\omega_{\mathrm{s},m}-\omega_{\mathrm{s},q})t}\\ &+\mathrm{H.c.}\end{aligned} \tag{3.98}$$

Similarly, for the polarization at pump frequencies:

$$\hat{P}_{\mathrm{p}}(z,t) = -\epsilon_0\chi\sum_{m,q}\mathcal{E}_{\mathrm{s},m}\mathcal{E}_{\mathrm{s},q}\hat{s}_m(t)\,\hat{s}_q(t)\,\mathrm{e}^{i(k_{\mathrm{s},m}+k_{\mathrm{s},q})z}\mathrm{e}^{-i(\omega_{\mathrm{s},m}+\omega_{\mathrm{s},q})t} + \mathrm{H.c.} \tag{3.99}$$

Since the product $\hat{E}_{\mathrm{p}}\hat{P}_{\mathrm{p}}$ has the same expression as Eq. (3.98), the interaction Hamiltonian is easily evaluated from (3.96):

$$\hat{H}_{\mathrm{I}} = 2i\epsilon_0\chi A_{\mathrm{I}}l\sum_{j,m,q}\mathcal{E}(\nu_j)\,\mathcal{E}_{\mathrm{s},m}\mathcal{E}_{\mathrm{s},q}F_{j,m,q}\hat{p}_j\hat{s}_m^{\dagger}\hat{s}_q^{\dagger}\mathrm{e}^{-i(\nu_j-\omega_{\mathrm{s},m}-\omega_{\mathrm{s},q})t} + \mathrm{H.c.}, \tag{3.100}$$

where we defined:

$$F_{j,m,q} = \frac{\sin\left(\kappa_j - k_{\mathrm{s},m} - k_{\mathrm{s},q}\right)\frac{l}{2}}{\left(\kappa_j - k_{\mathrm{s},m} - k_{\mathrm{s},q}\right)\frac{l}{2}}. \tag{3.101}$$

3.3.3 The Heisenberg equations

The time evolution for the pump field operators is given by the following Heisenberg equations:

$$\frac{d\,\hat{p}_j}{dt} = -\frac{2\epsilon_0\chi A_{\mathrm{I}} l}{\hbar}\sum_{m,q}\mathcal{E}\left(\nu_j\right)\mathcal{E}_{\mathrm{s},m}\mathcal{E}_{\mathrm{s},q}\hat{s}_m\hat{s}_q F_{j,m,q}\mathrm{e}^{i(\nu_j-\omega_{\mathrm{s},m}-\omega_{\mathrm{s},q})t}, \tag{3.102}$$

$$\frac{d\,\hat{s}_m}{dt} = \frac{4\epsilon_0\chi A_{\mathrm{I}} l}{\hbar}\sum_{j,q}\mathcal{E}\left(\nu_j\right)\mathcal{E}_{\mathrm{s},m}\mathcal{E}_{\mathrm{s},q}\hat{s}_q^{\dagger}\hat{p}_j F_{j,m,q}\mathrm{e}^{-i(\nu_j-\omega_{\mathrm{s},m}-\omega_{\mathrm{s},q})t}. \tag{3.103}$$

Integration of Eq. (3.102) yields:

$$\begin{aligned}\hat{p}_j\left(t\right) &= \hat{p}_j^{(0)} - \frac{2\epsilon_0\chi A_{\mathrm{I}} l}{\hbar}\sum_{m,q}\mathcal{E}\left(\nu_j\right)\mathcal{E}_{\mathrm{s},m}\mathcal{E}_{\mathrm{s},q}F_{j,m,q}\\ &\quad\times\int_0^t \mathrm{d}t\,\hat{s}_m\left(t'\right)\hat{s}_q\left(t'\right)\mathrm{e}^{i(\nu_j-\omega_{\mathrm{s},m}-\omega_{\mathrm{s},q})t'},\end{aligned} \tag{3.104}$$

where $\hat{p}_j^{(0)}$ is the pump field that has not yet interacted with the crystal. Since the nonlinear interaction can be assumed instantaneous respect to the oscillating term $\mathrm{e}^{i(\nu_j-\omega_{\mathrm{s},m}-\omega_{\mathrm{s},q})t'}$, it is possible to make use of the Wigner-Weisskopft approximation, that leads to:

$$\begin{aligned}\hat{p}_j\left(t\right) &= \hat{p}_j^{(0)} - \frac{2\epsilon_0\chi A_{\mathrm{I}} l}{\hbar}\sum_{m,q}\mathcal{E}\left(\nu_j\right)\mathcal{E}_{\mathrm{s},m}\mathcal{E}_{\mathrm{s},q}F_{j,m,q}\hat{s}_m\left(t\right)\hat{s}_q\left(t\right)\int_0^t \mathrm{d}t\,\mathrm{e}^{i(\nu_j-\omega_{\mathrm{s},m}-\omega_{\mathrm{s},q})t'}\\
&= \hat{p}_j^{(0)} - \frac{2\epsilon_0\chi A_{\mathrm{I}} l}{\hbar}\sum_{m,q}\mathcal{E}\left(\nu_j\right)\mathcal{E}_{\mathrm{s},m}\mathcal{E}_{\mathrm{s},q}F_{j,m,q}\hat{s}_m\left(t\right)\hat{s}_q\left(t\right)\\
&\quad\times\mathrm{e}^{-\frac{i}{2}(\omega_{\mathrm{s},m}+\omega_{\mathrm{s},q}-\nu_j)}\frac{\sin\left(\omega_{\mathrm{s},m}+\omega_{\mathrm{s},q}-\nu_j\right)t}{\frac{1}{2}\left(\omega_{\mathrm{s},m}+\omega_{\mathrm{s},q}-\nu_j\right)}\\
&\simeq \hat{p}_j^{(0)} - \frac{4\pi\epsilon_0\chi A_{\mathrm{I}} l}{\hbar}\sum_{m,q}\mathcal{E}\left(\nu_j\right)\mathcal{E}_{\mathrm{s},m}\mathcal{E}_{\mathrm{s},q}F_{j,m,q}\hat{s}_m\left(t\right)\hat{s}_q\left(t\right)\\
&\quad\times\delta\left(\omega_{\mathrm{s},m}+\omega_{\mathrm{s},q}-\nu_j\right),\end{aligned} \tag{3.105}$$

where in the last row the sign "$\simeq$" has to be understood in the sense of weak convergence of the approximation below:

$$\frac{\sin\left(\omega_{\mathrm{s},m}+\omega_{\mathrm{s},q}-\nu_j\right)t}{\frac{1}{2}\left(\omega_{\mathrm{s},m}+\omega_{\mathrm{s},q}-\nu_j\right)} \simeq 2\pi\delta\left(\omega_{\mathrm{s},m}+\omega_{\mathrm{s},q}-\nu_j\right). \tag{3.106}$$

that will become meaningful in the continuum limit $L_{\mathrm{p}}\to+\infty$. After substituting (3.105) in (3.103), the signal field equation becomes

$$\begin{aligned}\frac{d\,\hat{s}_m}{dt} &= \frac{4\epsilon_0\chi A_I l}{\hbar}\sum_{j,q}\mathcal{E}\left(\nu_j\right)\mathcal{E}_{s,m}\mathcal{E}_{s,q}F_{m,q}^j\hat{s}_q^{\dagger}\left(t\right)\hat{p}_j^{(0)}\mathrm{e}^{-i(\nu_j-\omega_{s,m}-\omega_{s,q})t}\\
&\quad-\pi\left(\frac{4\epsilon_0\chi A_I l}{\hbar}\right)^2\sum_{j,q}\mathcal{E}\left(\nu_j\right)\mathcal{E}_{s,m}\mathcal{E}_{s,q}F_{m,q}^j\hat{s}_q^{\dagger}\left(t\right)\mathrm{e}^{-i(\nu_j-\omega_{s,m}-\omega_{s,q})t}\\
&\quad\times\sum_{n,r}\mathcal{E}\left(\nu_j\right)\mathcal{E}_{s,n}\mathcal{E}_{s,r}F_{n,r}^j\hat{s}_n\left(t\right)\hat{s}_r\left(t\right)\delta\left(\omega_{s,n}+\omega_{s,r}-\nu_j\right).\end{aligned} \tag{3.107}$$

In order to perform the passage to the continuum, let's define the continuum pump operators as:

$$\hat{p}^{(0)}\left(\nu_j\right) \equiv \sqrt{\frac{L_p}{2\pi c}}\,\hat{p}_j^{(0)}, \tag{3.108}$$

which verify:

$$\left[\hat{p}^{(0)}\left(\nu_j\right), \left(\hat{p}^{(0)}\left(\nu_k\right)\right)^{\dagger}\right] = \frac{L_{\mathrm{p}}}{2\pi c}\,\delta_{j,k} \overset{L_{\mathrm{p}}\to+\infty}{\longrightarrow} \delta\left(\nu_j - \nu_k\right). \tag{3.109}$$

Keeping in mind that $\mathcal{E}\left(\nu_j\right) = \sqrt{\frac{\hbar\nu_j}{2\epsilon_0 n(\nu_j) A_{\mathrm{p}} L_{\mathrm{p}}}}$, Eq. (3.107) becomes

$$\begin{aligned}
\frac{d\,\hat{s}_m}{dt} &= 2\frac{A_{\mathrm{I}}}{\sqrt{A_{\mathrm{p}}}}\chi l\sqrt{\frac{\epsilon_0}{\pi\hbar c}}\sum_{j,q}\frac{2\pi c}{L_{\mathrm{p}}}\sqrt{\frac{\nu_j}{n\left(\nu_j\right)}}\mathcal{E}_{\mathrm{s},m}\mathcal{E}_{\mathrm{s},q}F_{j,m,q}\hat{s}_q^{\dagger}\hat{p}^{(0)}\left(\nu_j\right)\mathrm{e}^{-i(\nu_j-\omega_{\mathrm{s},m}-\omega_{\mathrm{s},q})t} \\
&\quad -\pi\left(\frac{4\epsilon_0\chi A_{\mathrm{I}} l}{\hbar}\right)^2\frac{\hbar}{4\pi\epsilon_0 c A_{\mathrm{p}}}\sum_{j,q}\frac{2\pi c}{L_{\mathrm{p}}}\frac{\nu_j}{n\left(\nu_j\right)}\mathcal{E}_{\mathrm{s},m}\mathcal{E}_{\mathrm{s},q}F_{j,m,q}\hat{s}_q^{\dagger}\mathrm{e}^{-i(\nu_j-\omega_{\mathrm{s},m}-\omega_{\mathrm{s},q})t} \\
&\quad \times\sum_{n,r}\mathcal{E}_{\mathrm{s},n}\mathcal{E}_{\mathrm{s},r}F_{j,n,r}\hat{s}_n\hat{s}_r\delta\left(\omega_{\mathrm{s},n}+\omega_{\mathrm{s},r}-\nu_j\right).
\end{aligned} \tag{3.110}$$

In the limit $L_p \to +\infty$, the sums over j are transformed into integrals:

$$\begin{aligned}
\frac{d\,\hat{s}_m}{dt} &= 2\frac{A_{\mathrm{I}}}{\sqrt{A_{\mathrm{p}}}}\chi l\sqrt{\frac{\epsilon_0}{\pi\hbar c}}\sum_{q}\mathcal{E}_{\mathrm{s},m}\mathcal{E}_{\mathrm{s},q}\hat{s}_q^{\dagger}I_{m,q}^{(1)} \\
&\quad - 4\left(\chi l\right)^2\left(\frac{A_{\mathrm{I}}}{\sqrt{A_{\mathrm{p}}}}\right)^2\frac{\epsilon_0}{\hbar c}\sum_{q,n,r}\mathcal{E}_{\mathrm{s},m}\mathcal{E}_{\mathrm{s},q}\mathcal{E}_{\mathrm{s},n}\mathcal{E}_{\mathrm{s},r}\hat{s}_q^{\dagger}\hat{s}_n\hat{s}_r I_{m,q}^{(2)},
\end{aligned} \tag{3.111}$$

where:

$$I_{m,q}^{(1)} = \int \mathrm{d}\nu\sqrt{\frac{\nu}{n\left(\nu\right)}}\frac{\sin\left[\left(k(\nu)-k_{\mathrm{s},m}-k_{\mathrm{s},q}\right)\frac{l}{2}\right]}{\left(k(\nu)-k_{\mathrm{s},m}-k_{\mathrm{s},q}\right)\frac{l}{2}}\hat{p}^{(0)}\left(\nu\right)\mathrm{e}^{-i(\nu-\omega_{\mathrm{s},m}-\omega_{\mathrm{s},q})t} \tag{3.112}$$

$$\begin{aligned}
I_{m,q}^{(2)} &= \int \mathrm{d}\nu\,\delta\left(\nu-\omega_{\mathrm{s},m}-\omega_{\mathrm{s},q}\right)\frac{\nu}{n\left(\nu\right)}\frac{\sin\left[\left(k(\nu)-k_{\mathrm{s},m}-k_{\mathrm{s},q}\right)\frac{l}{2}\right]}{\left(k(\nu)-k_{\mathrm{s},m}-k_{\mathrm{s},q}\right)\frac{l}{2}} \\
&\quad \times\frac{\sin\left[\left(k(\nu)-k_{\mathrm{s},n}-k_{\mathrm{s},r}\right)\frac{l}{2}\right]}{\left(k(\nu)-k_{\mathrm{s},n}-k_{\mathrm{s},r}\right)\frac{l}{2}}\mathrm{e}^{-i(\nu-\omega_{\mathrm{s},m}-\omega_{\mathrm{s},q})t}.
\end{aligned} \tag{3.113}$$

The second integral is trivial. On the other side, $I_{m,q}^{(1)}$ requires some manipulations. Dividing the interval of integration in a sum of frequency intervals of width Ω and centered at frequencies $\omega_{p,r} = 2\omega_0 + r\Omega,\ r \in \mathbb{Z}$, integral $I_{m,q}^{(1)}$ reads:

$$I_{m,q}^{(1)} = \sum_r \int_r \mathrm{d}\nu\sqrt{\frac{\nu}{n\left(\nu\right)}}\frac{\sin\left[\left(k(\nu)-k_{\mathrm{s},m}-k_{\mathrm{s},q}\right)\frac{l}{2}\right]}{\left(k(\nu)-k_{\mathrm{s},m}-k_{\mathrm{s},q}\right)\frac{l}{2}}\hat{p}^{(0)}\left(\nu\right)\mathrm{e}^{-i(\nu-\omega_{\mathrm{s},m}-\omega_{\mathrm{s},q})t}, \tag{3.114}$$

where:

$$\int_r \mathrm{d}\nu\, f\left(\nu\right) \equiv \int_{\omega_{\mathrm{p},r}-\Omega/2}^{\omega_{\mathrm{p},r}+\Omega/2}\mathrm{d}\nu\, f\left(\nu\right). \tag{3.115}$$

In each interval r, each function $f(\nu)$ of the frequency ν can be approximated by the corresponding value at the center of the interval $f(\omega_{\mathrm{p},r})$. The integral $I^{(1)}_{m,q}$, thus, can be approximated by:

$$I^{(1)}_{m,q} \simeq \mathrm{e}^{i(\omega_{\mathrm{s},m}+\omega_{\mathrm{s},q})t} \sum_r \sqrt{\frac{\omega_{\mathrm{p},r}}{n\left(\omega_{\mathrm{p},r}\right)}} \frac{\sin\left[\left(k(\omega_{\mathrm{p},r}) - k_{\mathrm{s},m} - k_{\mathrm{s},q}\right)\frac{l}{2}\right]}{\left(k(\omega_{\mathrm{p},r}) - k_{\mathrm{s},m} - k_{\mathrm{s},q}\right)\frac{l}{2}} \int_r \mathrm{d}\nu\, \hat{p}^{(0)}\left(\nu\right) \mathrm{e}^{-i\nu t}. \tag{3.116}$$

Let's define new pump operators as follows:

$$\sqrt{2\pi}\mathrm{e}^{-i\omega_{\mathrm{p},r}t}\hat{p}_{\mathrm{in},r}\left(t\right) \equiv \int_r \mathrm{d}\nu\, \hat{p}^{(0)}\left(\nu\right) \mathrm{e}^{-i\nu t}, \tag{3.117}$$

which verify the following property:

$$\begin{aligned}
\left\langle \hat{p}_{\mathrm{in},r_1}\left(t_1\right)\left[\hat{p}_{\mathrm{in},r_2}\left(t_2\right)\right]^\dagger \right\rangle &= \frac{1}{2\pi} e^{i\left(\omega_{\mathrm{p},r_1}t_1 - \omega_{\mathrm{p},r_2}t_2\right)} \\
&\quad \times \int_{r_1}\mathrm{d}\nu_1 \int_{r_2}\mathrm{d}\nu_2 e^{i(\nu_2 t_2 - \nu_1 t_1)} \left\langle \hat{p}^{(0)}\left(\nu_1\right)\left[\hat{p}^{(0)}\left(\nu_2\right)\right]^\dagger \right\rangle \\
&= \frac{1}{2\pi} e^{i\left(\omega_{\mathrm{p},r_1}t_1 - \omega_{\mathrm{p},r_2}t_2\right)} \int_{r_1} d\nu_1 \int_{r_2} d\nu_2 e^{i(\nu_2 t_2 - \nu_1 t_1)} \delta\left(\nu_1 - \nu_2\right) \\
&= \delta_{r_1,r_2} \frac{1}{2\pi} e^{i\omega_{\mathrm{p},r_1}(t_1 - t_2)} \int_{r_1} d\nu_1 e^{i\nu_1(t_2 - t_1)} \\
&= \delta_{r_1,r_2} \frac{\sin\left[\frac{\Omega}{2}\left(t_2 - t_1\right)\right]}{\pi\left(t_2 - t_1\right)} \simeq \delta_{r_1,r_2}\delta\left(t_1 - t_2\right),
\end{aligned} \tag{3.118}$$

where $\left\langle \hat{p}^{(0)}\left(\nu_1\right)\left[\hat{p}^{(0)}\left(\nu_2\right)\right]^\dagger \right\rangle = \delta\left(\nu_1 - \nu_2\right)$ and the term δ_{r_1,r_2} appears because the double integral vanishes if $r_2 \neq r_1$, being the domains of integration on ν_1 and ν_2 non-overlapping in that case. With these definitions $I^{(1)}_{m,q}$ becomes

$$I^{(1)}_{m,q} \simeq \sqrt{2\pi} \sum_r \sqrt{\frac{\omega_{\mathrm{p},r}}{n\left(\omega_{\mathrm{p},r}\right)}} \frac{\sin\left[\left(k(\omega_{\mathrm{p},r}) - k_{\mathrm{s},m} - k_{\mathrm{s},q}\right)\frac{l}{2}\right]}{\left(k(\omega_{\mathrm{p},r}) - k_{\mathrm{s},m} - k_{\mathrm{s},q}\right)\frac{l}{2}} \mathrm{e}^{-i(\omega_{\mathrm{p},r} - \omega_{\mathrm{s},m} - \omega_{\mathrm{s},q})t} \hat{p}_{\mathrm{in},r}\left(t\right). \tag{3.119}$$

The equation of the motion for $\hat{s}_m\left(t\right)$ is readily retrieved after using Eq. (3.119), the rotating wave approximation (RWA) and after having defined $k_{p,n+r} \equiv k\left(\omega_{p,n+r}\right) = k\left(\omega_{s,n} + \omega_{s,r}\right)$:

$$\begin{aligned}
\frac{d\,\hat{s}_m}{dt} &= 2\sqrt{2}\frac{A_{\mathrm{I}}}{\sqrt{A_{\mathrm{p}}}}\chi l \sqrt{\frac{\epsilon_0}{\hbar c}} \sum_q \sqrt{\frac{\omega_{\mathrm{p},m+q}}{n\left(\omega_{\mathrm{p},m+q}\right)}} f_{m,q}\mathcal{E}_{\mathrm{s},m}\mathcal{E}_{\mathrm{s},q}\hat{p}_{\mathrm{in},m+q}\hat{s}^\dagger_q \\
&\quad -4\left(\chi l\right)^2 \left(\frac{A_{\mathrm{I}}}{\sqrt{A_{\mathrm{p}}}}\right)^2 \frac{\epsilon_0}{\hbar c} \sum_{q,n,r} \frac{\omega_{\mathrm{p},m+q}}{n\left(\omega_{\mathrm{p},m+q}\right)} \mathcal{E}_{\mathrm{s},m}\mathcal{E}_{\mathrm{s},q}\mathcal{E}_{\mathrm{s},n}\mathcal{E}_{\mathrm{s},m+q-n} \\
&\quad \times f_{m,q}f_{n,m+q-n}\hat{s}^\dagger_q\hat{s}_n\hat{s}_{m+q-n},
\end{aligned} \tag{3.120}$$

where the phase-mismatch factor has been defined:

$$f_{m,q} = \frac{\sin\left[\left(k_{\mathrm{p},m+q} - k_{\mathrm{s},m} - k_{\mathrm{s},q}\right)\frac{l}{2}\right]}{\left(k_{\mathrm{p},m+q} - k_{\mathrm{s},m} - k_{\mathrm{s},q}\right)\frac{l}{2}}. \tag{3.121}$$

As remarked in previous sections, we can assume that $\omega_{\mathrm{p},m} \simeq 2\omega_0$ and $\mathcal{E}_{\mathrm{s},m} = \sqrt{\frac{\hbar\omega_0}{2\epsilon_0 n_0 A_{\mathrm{s}} L}}$ for all m, therefore Eq. (3.120) becomes

$$\frac{d\,\hat{s}_m}{dt} = g\sum_q f_{m,q}\hat{p}_{\mathrm{in},m+q}\hat{s}^\dagger_q - \frac{g^2}{2}\sum_{q,n,r} f_{m,q}f_{n,m+q-n}\hat{s}^\dagger_q\hat{s}_n\hat{s}_{m+q-n}, \tag{3.122}$$

where the coupling constant g has been defined as:

$$g = 2\chi \frac{A_{\mathrm{I}}}{A_{\mathrm{s}}\sqrt{A_{\mathrm{p}}}} \frac{l}{L} \left(\frac{\omega_0}{n_0}\right)^{3/2} \sqrt{\frac{\hbar}{\epsilon_0 c}}. \tag{3.123}$$

Accounting for the cavity losses that occur at a single mirror at rate γ_{s}, we finally obtain the quantum Langevin equations for signal operators:

$$\begin{aligned} \frac{d\hat{s}_m}{dt} &= -\gamma_{\mathrm{s}}\hat{s}_m(t) + \sqrt{2\gamma_{\mathrm{s}}}\hat{s}_{\mathrm{in},m}(t) + g\sum_q f_{m,q}\hat{s}_q^{\dagger}(t)\,\hat{p}_{\mathrm{in},m+q}(t) \\ &\quad -\frac{g^2}{2}\sum_n\sum_q f_{m,q}f_{n,m+q-n}\hat{s}_q^{\dagger}(t)\,\hat{s}_n(t)\,\hat{s}_{m+q-n}(t), \end{aligned} \tag{3.124}$$

where $\hat{s}_{\mathrm{in},m}(t)$ corresponds to the field at signal frequencies entering the cavity through the coupling mirror. When that input is coherent or vacuum, the case we consider, those "in" operators verify the following correlation:

$$\left\langle \hat{s}_{\mathrm{in},m}(t)\,\hat{s}_{\mathrm{in},m'}^{\dagger}(t')\right\rangle = \delta_{m,m'}\delta(t-t'), \tag{3.125}$$

and thus behave as $\hat{p}_{\mathrm{in},r}^{(\pm)}(t)$, see (3.118).

3.3.4 Relation between the intracavity pump field and the external pump field

Before to approach the formulation of the Langevin equations for the field operators in the below threshold regime, it is worth to clarify the relationship between the intra cavity pump field and the external pump described by Eq. (3.5). Starting from the original definition of the input pump field, which is analogous to (3.95), we rewrite this expression in order to make explicit the passage to continuous frequencies when the quantization box of the pump field is let toward infinity:

$$\begin{aligned} \hat{E}_{\mathrm{in,p}}(z,t) &= i\sum_j \mathcal{E}_{\mathrm{in},j}(\nu_j)\,\hat{p}_{\mathrm{in},j}\mathrm{e}^{i(\kappa_j z-\nu_j t)} + \mathrm{H.c.} \\ &= i\sum_j \sqrt{\frac{2\pi c}{L_p}}\sqrt{\frac{\hbar\nu_j}{2\epsilon_0 n(\nu_j)A_{\mathrm{p}}L_{\mathrm{p}}}}\,\hat{p}_{\mathrm{in}}(\nu_j)\,\mathrm{e}^{i(\kappa_j z-\nu_j t)} + \mathrm{H.c.} \\ &= i\sum_j \frac{2\pi c}{L_{\mathrm{p}}}\sqrt{\frac{\hbar\nu_j}{4\pi\epsilon_0 c n(\nu_j)A_{\mathrm{p}}L_{\mathrm{p}}}}\,\hat{p}_{\mathrm{in}}(\nu_j)\,\mathrm{e}^{i(\kappa_j z-\nu_j t)} + \mathrm{H.c.}, \end{aligned} \tag{3.126}$$

where we substituted $\hat{p}_{\mathrm{in},j} = \sqrt{\frac{2\pi c}{L_{\mathrm{p}}}}\,\hat{p}_{\mathrm{in}}(\nu_j)$. In the limit $L_{\mathrm{p}} \to +\infty$, we have:

$$\begin{aligned} \hat{E}_{\mathrm{in,p}}(z,t) &= i\int \mathrm{d}\nu \sqrt{\frac{\hbar\nu}{4\pi\epsilon_0 c n(\nu)A_{\mathrm{p}}L_{\mathrm{p}}}}\,\hat{p}_{\mathrm{in}}(\nu)\,\mathrm{e}^{i(\kappa(\nu)z-\nu t)} + \mathrm{H.c.} \\ &= i\sum_r \int_r \mathrm{d}\nu \sqrt{\frac{\hbar\nu}{4\pi\epsilon_0 c n(\nu)A_{\mathrm{p}}L_{\mathrm{p}}}}\,\hat{p}_{\mathrm{in}}(\nu)\,\mathrm{e}^{i(\kappa(\nu)z-\nu t)} + \mathrm{H.c.} \\ &= i\sum_r \sqrt{\frac{\hbar\nu_r}{4\pi\epsilon_0 c n(\nu_r)A_{\mathrm{p}}L_{\mathrm{p}}}}\,\mathrm{e}^{i\kappa_r z}\int_r \mathrm{d}\nu\,\hat{p}_{\mathrm{in}}(\nu)\,\mathrm{e}^{-i\nu t} + \mathrm{H.c.} \end{aligned} \tag{3.127}$$

After the redefinition:

$$\sqrt{2\pi}\mathrm{e}^{-i\omega_{\mathrm{p},r}t}\hat{p}_{\mathrm{in},r}(t) \equiv \int_r \mathrm{d}\nu\, \hat{p}_{\mathrm{in}}(\nu)\, \mathrm{e}^{-i\nu t}, \tag{3.128}$$

we finally get:

$$\hat{E}_{\mathrm{in,p}}(z,t) = i\sum_r \sqrt{\frac{\hbar\omega_0}{\epsilon_0 c n_0 A_{\mathrm{p}}}}\hat{p}_{\mathrm{in},r}(t)\mathrm{e}^{i(\kappa_r z-\omega_{\mathrm{p},r}t)} + \mathrm{H.c.} \tag{3.129}$$

By demanding that the intracavity pump field equals the external pump field given by Eq. (3.5), we find that the following equality has to be satisfied:

$$\sqrt{\frac{\hbar\omega_0}{\epsilon_0 A_{\mathrm{p}} n_0 c}}\,\hat{p}_{\mathrm{in},r}(t) = \sqrt{\frac{P}{2\epsilon_0 c}}\,\alpha_r, \tag{3.130}$$

with P the average power per unit area of the mode-locked pump laser and $\sum_m |\alpha_m|^2 = 1$. Finally we obtain:

$$\hat{p}_{\mathrm{in},r}(t) = \sqrt{\frac{n_0 A_{\mathrm{p}} P}{2\hbar\omega_0}}\,\alpha_r \tag{3.131}$$

3.3.5 The SPOPO below threshold

Below threshold signal modes are almost not excited and the pump "in" fields can be approximated by their classical mean values as their fluctuation part gives rise to smaller terms, which are neglected for the same reasons in section 3.1.6.

According to Eq. (3.117), Eq. (3.131) corresponds to the case when the external pump is a frequency comb in which all its components are monochromatic with frequencies $\omega_{\mathrm{p},r}$, as assumed since the beginning (see Eq. (3.5)). The linearized equations for the SPOPO below threshold, then, become

$$\boxed{\frac{d\hat{s}_m(t)}{dt} = -\gamma_{\mathrm{s}}\hat{s}_m(t) + \gamma_{\mathrm{s}}\sigma\sum_q f_{m,q}\alpha_{m+q}\hat{s}_q^{\dagger}(t) + \sqrt{2\gamma_{\mathrm{s}}}\hat{s}_{\mathrm{in},m}(t)\,,}\tag{3.132}$$

where:

$$\sigma = \sqrt{P/P_0} \tag{3.133}$$

and

$$P_0 = \frac{\epsilon_0 c^3 n_0^2 T_{\mathrm{s}}^2}{8\left(\chi l\omega_0\right)^2}\left(\frac{A_{\mathrm{s}}}{A_{\mathrm{I}}}\right)^2. \tag{3.134}$$

P_0 is a reference power per unit area, equal to the cw OPO threshold obtained by using $\gamma_{\mathrm{s}} = \frac{cT_{\mathrm{s}}}{2L}$, being T_{s} the power transmission coefficient through the output coupler, to get Eq. (3.134). Hence the linearized equations (3.132) formally coincide with those for a SPOPO with resonant cavity for the pump, Eq. (3.65), with the only difference of the definition of the reference power per unit area P_0. The corresponding power $W_0 = A_{\mathrm{p}}P_0$ plays the role of threshold power.

As in section 3.1, making use of Eq. (3.13) and for the optimized setting corresponding to $A_{\mathrm{p}} = A_{\mathrm{s}}/2$ we obtain:

$$P_0 = \frac{\epsilon_0 c^3 n_0^2 T_{\mathrm{s}}^2}{2\left(\chi l\omega_0\right)^2}. \tag{3.135}$$

As expected, in this case, the threshold is higher than the doubly resonant case of a factor $4/T_{\mathrm{p}}$. We will detail in Section 3.5 the origin such a factor, even if, from a physical point of view, it is ascribable to the fact that the intra cavity pump power is lower in a non resonant configuration.

3.4 Singly resonant linear cavity

In this section we develop the quantum theory of a quasi-degenerate (idler and signal coincide) type I SPOPO in which only the signal field is resonated inside a cavity. Unlike section 3.3, we consider here a linear cavity (Fabry-Perot like). Anyway, as will be clear in the end of this demonstration, the geometry of the cavity influences only the cw OPO threshold P_0 but not the formal appearance of the evolution equations. As in the previous section 3.3, the treatment of this case is more involved than that for resonant case (see section 3.2) as the pump field cannot be quantized inside the OPO cavity.

3.4.1 The fields

The signal field inside the nonlinear crystal, which extends from $z = -l/2$ to $z = +l/2$, is written as:

$$\hat{E}_{\mathrm{s}}(z,t) = i\sum_{q}\mathcal{E}_{\mathrm{s},q}\sin\left(k_{\mathrm{s},q}z'\right)\hat{s}_q(t)\,e^{-i\omega_{\mathrm{s},q}t} + \mathrm{H.c.}, \tag{3.136}$$

where $z' = z + L/2$ and $\mathcal{E}_{\mathrm{s},q} = \sqrt{\frac{\hbar\omega_{\mathrm{s},q}}{\epsilon_0 n(\omega_{\mathrm{s},q})A_{\mathrm{s}}L}}$. On the contrary, the pump field is not affected by the cavity and hence it is given by a continuum of modes. We shall use the common approach of quantizing the pump field in a line of length L_{p} with periodic boundary conditions and, in the end of the calculations, we will make $L_{\mathrm{p}} \to \infty$. As in (3.93), we thus write:

$$\hat{E}_{\mathrm{p}}(z,t) = i\sum_{j}\mathcal{E}(\nu_j)\left[\hat{p}_j^{(+)}(t)\,e^{i\kappa_j z} + \hat{p}_j^{(-)}(t)\,e^{-i\kappa_j z}\right]e^{-i\nu_j t} + \mathrm{H.c.}, \tag{3.137}$$

where the superscripts $(\pm)$ label the propagation direction and must not be confused with their usual meaning of labeling positive and negative frequency parts. $\mathcal{E}(\nu_j) = \sqrt{\frac{\hbar\nu_j}{2\epsilon_0 A_{\mathrm{p}}L_{\mathrm{p}}n(\nu_j)}}$ are single photon field amplitudes. As in the previous section, the frequencies ν_j are given by $\nu_j = j\frac{2\pi c}{L_{\mathrm{p}}}$, $j \in \mathbb{N}$, and the wavenumbers $\kappa_j = \frac{n(\nu_j)\nu_j}{c}$, with $n(\nu_j)$ the crystal refractive index. The fields are, again written as a superposition of plane waves, but the treatment is still approximately valid for Gaussian beams as commented before.

3.4.2 The interaction Hamiltonian

The interaction Hamiltonian $\hat{H}_{\mathrm{I}}$ is calculated as usual as:

$$\hat{H}_{\mathrm{I}} = -A_{\mathrm{I}}\int_{-l/2}^{+l/2}\mathrm{d}z\left[\hat{E}_{\mathrm{p}}(z,t)\,\hat{P}_{\mathrm{p}}(z,t) + \hat{E}_{\mathrm{s}}(z,t)\,\hat{P}_{\mathrm{s}}(z,t)\right], \tag{3.138}$$

where A_{I} is the effective area of interaction corresponding to the three-mode overlapping integral across the transverse plane. In the case of Gaussian beams as commented in section 3.1,

$$\frac{1}{A_{\mathrm{I}}} = \frac{1}{A_{\mathrm{s}}} + \frac{1}{2A_{\mathrm{p}}}. \tag{3.139}$$

The nonlinear electric polarization at signal and pump frequencies, $\hat{P}_{\mathrm{s}}(z,t)$ and $\hat{P}_{\mathrm{p}}(z,t)$ are given by:

$$\hat{P}_{\mathrm{p}}(z,t) = \epsilon_0 \chi\, \hat{E}_{\mathrm{s}}(z,t)\, \hat{E}_{\mathrm{s}}(z,t)\Big|_{\substack{\text{terms oscillating at optical}\\ \text{frequencies around } \pm 2\omega_0}} \tag{3.140}$$

$$\hat{P}_{\mathrm{s}}(z,t) = \varepsilon_0 \chi\, \hat{E}_{\mathrm{p}}(z,t)\, \hat{E}_{\mathrm{s}}(z,t)\Big|_{\substack{\text{terms oscillating at optical}\\ \text{frequencies around } \pm \omega_0}} \tag{3.141}$$

where χ is the relevant nonlinear susceptibility (whose dispersion is neglected). It is then lengthy but simple to arrive to the following form of the interaction Hamiltonian:

$$\begin{aligned}\hat{H}_{\mathrm{I}}(t) &= i\frac{\varepsilon_0 \chi l A_{\mathrm{I}}}{2} \sum_m \sum_q \sum_j \mathcal{E}(\nu_j)\, \mathcal{E}_{\mathrm{s},m} \mathcal{E}_{\mathrm{s},q} F^j_{m,q} e^{-i(k_{\mathrm{s},m}+k_{\mathrm{s},q})L/2} \\ &\quad \times \hat{s}^\dagger_m(t)\, \hat{s}^\dagger_q(t) \left[\hat{p}^{(+)}_j(t) + \hat{p}^{(-)}_j(t)\right] e^{i(\omega_{\mathrm{s},m}+\omega_{\mathrm{s},q}-\nu_j)t} + \mathrm{H.c.},\end{aligned} \tag{3.142}$$

where we defined the phase-mismatch factor:

$$F_{j,m,q} = \frac{\sin\left[(\kappa_j - k_{\mathrm{s},m} - k_{\mathrm{s},q})\frac{l}{2}\right]}{(\kappa_j - k_{\mathrm{s},m} - k_{\mathrm{s},q})\frac{l}{2}}. \tag{3.143}$$

In (3.142) we dropped highly phase mismatched terms, as usual. It is convenient to define new signal boson operators through

$$\hat{s}_{m,\mathrm{new}}(t) = \hat{s}_m(t)\, e^{+ik_{\mathrm{s},m}L/2},\ \ \hat{s}^\dagger_{m,\mathrm{new}}(t) = \hat{s}^\dagger_m(t)\, e^{-ik_{\mathrm{s},m}L/2}, \tag{3.144}$$

in terms of which the interaction Hamiltonian becomes as (3.142) but without the exponential $e^{-i(k_{\mathrm{s},m}+k_{\mathrm{s},q})L/2}$. In the following we work with the new operators but omit the superscript "new".

3.4.3 The Heisenberg equations

The time evolution of the pump and signal operators is ruled by the following Heisenberg equations:

$$\frac{d\hat{p}^{(\pm)}_j(t)}{dt} = -\frac{\epsilon_0 \chi l A_{\mathrm{I}}}{2\hbar} \sum_m \sum_q \mathcal{E}(\nu_j)\, \mathcal{E}_{\mathrm{s},m} \mathcal{E}_{\mathrm{s},q} F_{j,m,q} \hat{s}_m(t)\, \hat{s}_q(t)\, e^{-i(\omega_{\mathrm{s},m}+\omega_{\mathrm{s},q}-\nu_j)t}, \tag{3.145}$$

$$\frac{d\hat{s}_m(t)}{dt} = \frac{\epsilon_0 \chi l A_{\mathrm{I}}}{\hbar} \sum_q \sum_j \mathcal{E}(\nu_j)\, \mathcal{E}_{\mathrm{s},m} \mathcal{E}_{\mathrm{s},q} F_{j,m,q} \hat{s}^\dagger_q(t) \left[\hat{p}^{(+)}_j(t) + \hat{p}^{(-)}_j(t)\right] e^{i(\omega_{\mathrm{s},m}+\omega_{\mathrm{s},q}-\nu_j)t}. \tag{3.146}$$

Integration of the pump equations yields:

$$\begin{aligned}\hat{p}^{(\pm)}_j(t) &= \hat{p}^{(\pm)}_{\mathrm{free},j} - \frac{\epsilon_0 \chi l A_{\mathrm{I}}}{2\hbar} \sum_m \sum_q \mathcal{E}(\nu_j)\, \mathcal{E}_{\mathrm{s},m} \mathcal{E}_{\mathrm{s},q} F_{j,m,q} \\ &\quad \times \int_0^t \mathrm{d}t' \hat{s}_m(t')\, \hat{s}_q(t')\, e^{-i(\omega_{\mathrm{s},m}+\omega_{\mathrm{s},q}-\nu_j)t'},\end{aligned} \tag{3.147}$$

where $\hat{p}^{(\pm)}_{\mathrm{free},j} = \hat{p}^{(\pm)}_j(0)$ is the source-free part of the pump (the field impinging the nonlinear crystal). As before, the Wigner-Weisskopf approximation permits to bring the signal

operators outside the integral and to consider their values at the present time. As in (3.105), within this approximation we obtain:

$$\hat{p}_j^{(\pm)}(t) \simeq \hat{p}_{\mathrm{free},j}^{(\pm)}(t) - \frac{\pi\epsilon_0\chi A_\mathrm{I} l}{\hbar}\sum_m\sum_q \mathcal{E}(\nu_j)\,\mathcal{E}_{\mathrm{s},m}\mathcal{E}_{\mathrm{s},q}F_{j,m,q}\hat{s}_m(t)\,\hat{s}_q(t)\,\delta(\omega_{\mathrm{s},m}+\omega_{\mathrm{s},q}-\nu_j), \tag{3.148}$$

where, in the last row, we made the approximation (3.106) that has to be understood as a week convergence. After substituting Eq. (3.148), the signal field equations become:

$$\begin{aligned}\frac{d\hat{s}_m(t)}{dt} &= \frac{\epsilon_0\chi l A_\mathrm{I}}{\hbar}\sum_q\sum_j \mathcal{E}(\nu_j)\,\mathcal{E}_{\mathrm{s},m}\mathcal{E}_{\mathrm{s},q}F_{j,m,q}\hat{s}_q^\dagger(t)\left[\hat{p}_{\mathrm{free},j}^{(+)}(t)+\hat{p}_{\mathrm{free},j}^{(-)}(t)\right]e^{i(\omega_{\mathrm{s},m}+\omega_{\mathrm{s},q}-\nu_j)t}\\ &-2\pi\left(\frac{\epsilon_0\chi l A_\mathrm{I}}{\hbar}\right)^2\sum_q\sum_j \mathcal{E}(\nu_j)\,\mathcal{E}_{\mathrm{s},m}\mathcal{E}_{\mathrm{s},q}F_{j,m,q}\hat{s}_q^\dagger(t)\,e^{i(\omega_{\mathrm{s},m}+\omega_{\mathrm{s},q}-\nu_j)t}\\ &\times\sum_n\sum_r \mathcal{E}(\nu_j)\,\mathcal{E}_{\mathrm{s},n}\mathcal{E}_{\mathrm{s},r}F_{j,n,r}\hat{s}_n(t)\,\hat{s}_r(t)\,\delta(\omega_{\mathrm{s},n}+\omega_{\mathrm{s},r}-\nu_j).\end{aligned} \tag{3.149}$$

For the passage to the continuum we will follows the steps already detailed in section 3.3, for this reason in the following we will rapidly report the treatment for the present case. After the definition of continuum pump operators:

$$\hat{p}_{\mathrm{free}}^{(\pm)}(\nu_j) = \sqrt{\frac{L_\mathrm{p}}{2\pi c}}\hat{p}_{\mathrm{free},j}^{(\pm)}, \tag{3.150}$$

which verify:

$$\left[\hat{p}_{\mathrm{free}}^{(\pm)}(\nu_j),\left(\hat{p}_{\mathrm{free}}^{(\pm)}(\nu_k)\right)^\dagger\right] = \frac{L_\mathrm{p}}{2\pi c}\delta_{j,k} \underset{L_\mathrm{p}\to\infty}{\longrightarrow} \delta(\nu_j-\nu_k), \tag{3.151}$$

the sums over j are transformed into integrals taking in mind that $\mathcal{E}(\nu_j) = \sqrt{\frac{\hbar\nu_j}{\epsilon_0 A_\mathrm{p} L_\mathrm{p} n(\nu_j)}}$:

$$\begin{aligned}\frac{d\hat{s}_m(t)}{dt} &= \frac{A_\mathrm{I}}{\sqrt{A_\mathrm{p}}} l\chi\sqrt{\frac{\epsilon_0}{4\pi\hbar c}}\sum_q \mathcal{E}_{\mathrm{s},m}\mathcal{E}_{\mathrm{s},q}\hat{s}_q^\dagger(t)\,I_{m,q}^{(1)}\\ &-\frac{A_\mathrm{I}^2}{A_\mathrm{p}}(l\chi)^2\frac{\epsilon_0}{2\hbar c}\sum_n\sum_r\sum_q \mathcal{E}_{\mathrm{s},m}\mathcal{E}_{\mathrm{s},q}\mathcal{E}_{\mathrm{s},n}\mathcal{E}_{\mathrm{s},r}\hat{s}_q^\dagger(t)\,\hat{s}_n(t)\,\hat{s}_r(t)\,I_{m,q}^{(2)},\end{aligned} \tag{3.152}$$

where

$$I_{m,q}^{(1)} = \int \mathrm{d}\nu\sqrt{\frac{\nu}{n(\nu)}}\frac{\sin\left[\left(k(\nu)-k_{\mathrm{s},m}-k_{\mathrm{s},q}\right)\frac{l}{2}\right]}{\left(k(\nu)-k_{\mathrm{s},m}-k_{\mathrm{s},q}\right)\frac{l}{2}}\left[\hat{p}_{\mathrm{free}}^{(+)}(\nu)+\hat{p}_{\mathrm{free}}^{(-)}(\nu)\right]e^{i(\omega_{\mathrm{s},m}+\omega_{\mathrm{s},q}-\nu)t}, \tag{3.153}$$

and $I_{m,q}^{(2)}$ is defined in Eq. (3.113). Integration of $I_{m,q}^{(1)}$ is performed as in the previous section. First we write the integral as a sum over frequency intervals of width Ω (the free spectral range of the SPOPO cavity) and centered at frequencies $\omega_{\mathrm{p},r} = 2\omega_0 + r\Omega$, $r\in\mathbb{Z}$. Then approximating the function $k(\nu)$ by $k_{\mathrm{p},r} = k(\omega_{\mathrm{p},r})$ and $\sqrt{\frac{\nu}{n(\nu)}}$ by $\sqrt{\frac{\omega_{\mathrm{p},r}}{n(\omega_{\mathrm{p},r})}}$ and defining new pump operators as follows:

$$\sqrt{2\pi}e^{-i\omega_{\mathrm{p},r}t}\hat{p}_{\mathrm{in},r}^{(\pm)}(t) = \int_r \mathrm{d}\nu e^{-i\nu t}\hat{p}_{\mathrm{free}}^{(\pm)}(\nu). \tag{3.154}$$

the integral results to be:

$$I_{m,q}^{(1)} \simeq \sqrt{2\pi}\sum_r \sqrt{\frac{\omega_{\mathrm{p},r}}{n\left(\omega_{\mathrm{p},r}\right)}}\frac{\sin\left[\left(k_{\mathrm{p},r}-k_{\mathrm{s},m}-k_{\mathrm{s},q}\right)\frac{l}{2}\right]}{\left(k_{\mathrm{p},r}-k_{\mathrm{s},m}-k_{\mathrm{s},q}\right)\frac{l}{2}} e^{i\left(\omega_{\mathrm{s},m}+\omega_{\mathrm{s},q}-\omega_{\mathrm{p},r}\right)t}\left[\hat{p}_{\mathrm{in},r}^{(+)}\left(t\right)+\hat{p}_{\mathrm{in},r}^{(-)}\left(t\right)\right]. \tag{3.155}$$

where $k_{\mathrm{p},r} = k\left(\omega_{\mathrm{p},r}\right) = k\left(2\omega_0 + r\Omega\right)$. The new pump operators verify the following property:

$$\left\langle \hat{p}_{\mathrm{in},r_1}^{(\pm)}\left(t_1\right)\left(\hat{p}_{\mathrm{in},r_2}^{(\pm)}\left(t_2\right)\right)^{\dagger}\right\rangle = \delta_{r_1,r_2}\frac{\sin\left[\frac{\Omega}{2}\left(t_2-t_1\right)\right]}{\pi\left(t_2-t_1\right)} \simeq \delta_{r_1,r_2}\delta\left(t_1-t_2\right). \tag{3.156}$$

In the RWA and taking in mind that $k\left(\omega_{\mathrm{s},n}+\omega_{\mathrm{s},r}\right) = k\left(\omega_{\mathrm{p},n+r}\right) = k_{\mathrm{p},n+r}$, the equations of motion for $\hat{s}_m\left(t\right)$ become:

$$\begin{aligned}\frac{d\hat{s}_m\left(t\right)}{dt} &= g\sum_q f_{m,q}\hat{s}_q^{\dagger}\left(t\right)\left[\hat{p}_{\mathrm{in},m+q}^{(+)}\left(t\right)+\hat{p}_{\mathrm{in},m+q}^{(-)}\left(t\right)\right] \\ &\quad -g^2\sum_n\sum_q f_{m,q}f_{n,m+q-n}\hat{s}_q^{\dagger}\left(t\right)\hat{s}_n\left(t\right)\hat{s}_{m+q-n}\left(t\right),\end{aligned} \tag{3.157}$$

were we defined the phase-mismatch factor:

$$f_{m,q} = \frac{\sin\left[\left(k_{\mathrm{p},m+q}-k_{\mathrm{s},m}-k_{\mathrm{s},q}\right)\frac{l}{2}\right]}{\left(k_{\mathrm{p},m+q}-k_{\mathrm{s},m}-k_{\mathrm{s},q}\right)\frac{l}{2}}, \tag{3.158}$$

and the coupling constant:

$$g = \chi\frac{A_{\mathrm{I}}}{A_{\mathrm{s}}\sqrt{A_{\mathrm{p}}}}\frac{l}{L}\left(\frac{\omega_0}{n_0}\right)^{3/2}\sqrt{\frac{\hbar}{\epsilon_0 c}} \tag{3.159}$$

For obtaining (3.157), we made the usual assumption of negligible dispersion of the single photon amplitude $\mathcal{E}_{\mathrm{s},m} = \mathcal{E}_{\mathrm{s}} = \sqrt{\frac{\hbar\omega_0}{\epsilon_0 n_0 A_{\mathrm{s}} L}}$ and $\omega_{\mathrm{p},m} = 2\omega_0$ for all m.

Since the optical cavity has losses, which occur at a single mirror at rate γ_{s}, the equations of motion must be transformed into the following quantum Langevin equations:

$$\begin{aligned}\frac{d\hat{s}_m\left(t\right)}{dt} &= -\gamma_{\mathrm{s}}\hat{s}_m\left(t\right)+\sqrt{2\gamma_{\mathrm{s}}}\hat{s}_{\mathrm{in},m}\left(t\right)+g\sum_q f_{m,q}\hat{s}_q^{\dagger}\left(t\right)\left[\hat{p}_{\mathrm{in},m+q}^{(+)}\left(t\right)+\hat{p}_{\mathrm{in},m+q}^{(-)}\left(t\right)\right] \\ &\quad -g^2\sum_n\sum_q f_{m,q}f_{n,m+q-n}\hat{s}_q^{\dagger}\left(t\right)\hat{s}_n\left(t\right)\hat{s}_{m+q-n}\left(t\right),\end{aligned} \tag{3.160}$$

where $\hat{s}_{\mathrm{in},m}\left(t\right)$ corresponds to the field at signal frequencies entering the cavity through the coupling mirror. When that input is coherent or vacuum, the case we consider, the "in" operators verify the following correlation:

$$\left\langle \hat{s}_{\mathrm{in},m}\left(t\right)\hat{s}_{\mathrm{in},m'}^{\dagger}\left(t'\right)\right\rangle = \delta_{m,m'}\delta\left(t-t'\right). \tag{3.161}$$

3.4.4 The SPOPO below threshold

Below threshold signal modes are almost not excited and the double sum in (3.160) can be neglected. Also, the pump "in" fields can be approximated by their classical mean values as their fluctuation part gives rise to smaller terms, which are neglected for the same reasons

as before. Hence, we write $\hat{p}^{(-)}_{\mathrm{in},m}(t) = 0$ (unidirectional pumping). On the other hand, the relationship between the input pump field and the external classical pump has been retrieved explicitly in Section 3.3.4:

$$\hat{p}^{(+)}_{\mathrm{in},m}(t) = \sqrt{\frac{n_0 A_\mathrm{p} P}{2\hbar\omega_0}}\alpha_m, \tag{3.162}$$

with P the average power per unit area of the mode-locked pump laser and $\sum_m |\alpha_m|^2 = 1$. The linearized equations for the SPOPO below threshold then become

$$\boxed{\frac{d\hat{s}_m(t)}{dt} = -\gamma_\mathrm{s}\hat{s}_m(t) + \gamma_\mathrm{s}\sigma\sum_q f_{m,q}\alpha_{m+q}\hat{s}^\dagger_q(t) + \sqrt{2\gamma_\mathrm{s}}\hat{s}_{\mathrm{in},m}(t),} \tag{3.163}$$

where σ is defined as in (3.90) and:

$$P_0 = \frac{\epsilon_0 c^3 n_0^2 T_\mathrm{s}^2}{8(\chi l\omega_0)^2}\left(\frac{A_\mathrm{s}}{A_\mathrm{I}}\right)^2. \tag{3.164}$$

In order to obtain (3.164), we used $\gamma_\mathrm{s} = \frac{cT_\mathrm{s}}{4L}$, being T_s the power transmission coefficient through the output coupler, to arrive to Eq. (3.164)). Making use of Eq. (3.139) we can write:

$$P_0 = \frac{\epsilon_0 c^3 n_0^2 T_\mathrm{s}^2}{8(\chi l\omega_0)^2}\left(1 + \frac{A_\mathrm{s}}{2A_\mathrm{p}}\right)^2. \tag{3.165}$$

The minimum of this function occurs at $A_\mathrm{p} = A_\mathrm{s}/2$. For this optimized setting we obtain:

$$P_0 = \frac{\varepsilon_0 c^3 n_0^2 T_\mathrm{s}^2}{2(\chi l\omega_0)^2}. \tag{3.166}$$

3.5 Conclusions

In this last section we want to summarize the main results about the quantum model of a SPOPO. Its validity falls in the domain where the hypothesis of perfect synchronization between the mode-locked laser and the OPO cavity and the below threshold regime are verified. Let's stress again that, when $\langle\hat{s}_m\rangle = 0$, it is not necessary that the pump field has negligible fluctuations since they are weighted by a vacuum signal field. It is sufficient, then, to require the pump contains a large number of photons. Being negligible the parametric interaction from the point of view of the intracavity pump field, the linearized Langevin equations for the signal field reads:

$$\frac{d\hat{s}_m}{dt} = -\gamma_\mathrm{s}\hat{s}_m + \gamma_\mathrm{s}\sigma\sum_q f_{m+q,q}\alpha_{m+q}\hat{s}^\dagger_q + \sqrt{2\gamma_\mathrm{s}}\hat{s}_{\mathrm{in},m}, \tag{3.167}$$

The phase-matching factor $f_{m+q,m}$ is defined as:

$$f_{m+q,m} = \frac{\sin\phi_{m,q}}{\phi_{m,q}}, \tag{3.168}$$

with a mismatch angle, $\phi_{m+q,m}$, defined as:

$$\phi_{m,q} = l(k_{\mathrm{p},m+q} - k_{\mathrm{s},m} - k_{\mathrm{s},q}). \tag{3.169}$$

Keeping in mind that, by Taylor expanding $\phi_{m,q}$ in ω around the phase-matched frequencies ω_0 and$2\omega_0$, respectively for signal and pump field, and arresting the series up to the second order,Eq. (3.169) can be written as in Eq. (3.46), we can further simplify the notation by writing:

$$\phi_{m,q} = \beta_1 (m+q) + \beta_{2\mathrm{p}} (m+q)^2 - \beta_{2\mathrm{s}} \left(m^2 + q^2\right), \tag{3.170}$$

where we imposed $\Delta = 0$ (resonant case) and where we defined:

$$\beta_1 = \frac{1}{2} l\Omega \left(k'_{\mathrm{p}} - k'_{\mathrm{s}}\right), \tag{3.171}$$

$$\beta_{2\mathrm{p}} = \frac{1}{4} l\Omega^2 k''_{\mathrm{p}}, \tag{3.172}$$

$$\beta_{2\mathrm{s}} = \frac{1}{4} l\Omega^2 k''_{\mathrm{s}}, \tag{3.173}$$

which are the temporal walk-off between pump and signal pulses and the pump and signal group velocity dispersion, respectively.

The coupling constant σ reads:

$$\sigma = \sqrt{\frac{P}{P_0}}, \tag{3.174}$$

where P is the external average laser irradiance (power per unit area) and P_0 is a normalization factor representing the c.w. threshold for a simple-mode OPO, as we will see in Chapter 4, and defined as:

$$\boxed{P_0 = \Pi_0 \frac{\epsilon_0 c^3 n_0^2 T_{\mathrm{s}}^2}{(\chi l \omega_0)^2}} \tag{3.175}$$

being Π_0 different for each cavity configuration and specified in Table 3.1. From a physical point of view, it is very easy to understand the differences between the thresholds according to the geometry of the cavity and the resonant or not resonant operation of the pump. In particular, in the doubly resonant operation the intracavity pump power is higher than that in the singly resonant case. In fact, for a field resonating inside a cavity (no matter what kind of geometry), we have:

$$E(t) = \sqrt{T_{\mathrm{p}}} E_{\mathrm{in}} + \sqrt{1 - T_{\mathrm{p}}} E(t), \tag{3.176}$$

that suddenly leads to:

$$E(t) \simeq \frac{T_{\mathrm{p}}}{2} E_{\mathrm{in}}, \tag{3.177}$$

for cavities of high finesse, where $T_{\mathrm{p}} \ll 1$ is the usual transmission coefficient of the coupling mirror at the pump frequencies. Therefore the c.w. threshold in a doubly resonant configuration results to be lower of a factor $T_{\mathrm{p}}/4$ with respect to a singly resonant cavity.

Π_0	Doubly resonant	Simply resonant
Linear cavity	$T_{\mathrm{p}}/32$	1/2
Ring cavity	$T_{\mathrm{p}}/8$	1/2

Table 3.1: Coefficient for retrieving the cw threshold P_0 in the different cases discussed along this chapter.

For what concerns the geometric configuration of the cavity, if the pump and signal field are simultaneously resonating, in a linear cavity the signal field passes through the non-linear crystal two times per round-trip with respect to the ring cavity case. Therefore the first configuration is equivalent that of a ring cavity of same length but with a non-linear crystal two time thicker. Since, from Eq. (3.175), the c.w. is inversely proportional to the square of the crystal thickness (l), the threshold in the linear geometry have to be smaller of a factor 4 with respect to the ring geometry. In the simply resonant configuration with a linear geometry, since the pump is not resonating, the signal field cannot see a gain during his second backward passage through the non-linear crystal, therefore a threshold equal to the simply resonant ring cavity is perfectly expected.

CHAPTER 4

Classical linear dynamics of SPOPO below threshold

Contents

In this chapter we consider in detail the classical linear dynamics of SPOPOs in the below threshold regime. In particular, we show that this problem can be decomposed over a basis of combs of frequencies evolving with different evolution rates Λ_k and the threshold is attained when the comb with the faster dynamics starts oscillating. Such results are obtained by diagonalizing the matrix which couples the each mode of the pump comb to each mode of the signal comb. This problem can be solved both numerically and analytically. In the last case, the diagonalization can be analytically performed thanks to the fact that the coupling matrix can be substituted, without loss of information, with a gaussian function. This occurs only when specific conditions are met. We then analyze the solutions obtained in different experimental configurations such as different

kind of non-linearities, different kinds of phase-matching or different sizes of crystals, comparing the results form the analytical and the numerical approach. We find, then, how the choice of the experimental parameters affects the spectrum of the coupling matrix and consequently the dynamics of the modes on which the intra-cavity field has been decomposed. Surprisingly, it turns out that it is almost completely characterized by a small subset of combs with respect to the about 10^5 modes involved during the evolution.

4.1 Determination of the oscillation threshold

The classical counterpart of Eq. (3.167) is obtained by removing the input noise terms and replacing the operators by complex numbers:

$$\frac{ds_m}{dt} = -\gamma_s s_m + \gamma_s \sigma \sum_q f_{m+q,m} \alpha_{m+q} s_m^*, \tag{4.1}$$

and completed by its adjoint:

$$\frac{ds_m^*}{dt} = -\gamma_s s_m^* + \gamma_s \sigma \sum_q f_{m+q,m} \alpha_{m+q}^* s_m. \tag{4.2}$$

Arranging the complex numbers s_m and s_m^* in vector form:

$$\mathbf{s} = \begin{pmatrix} \vdots \\ s_{-2} \\ s_{-1} \\ s_0 \\ s_1 \\ s_2 \\ \vdots \end{pmatrix} \quad \text{and} \quad \mathbf{s}^* = \begin{pmatrix} \vdots \\ s_{-2}^* \\ s_{-1}^* \\ s_0^* \\ s_1^* \\ s_2^* \\ \vdots \end{pmatrix}, \tag{4.3}$$

eqs. (4.1) and (4.2) can be written as:

$$\frac{d}{dt} \begin{pmatrix} \mathbf{s} \\ \mathbf{s}^* \end{pmatrix} = -\gamma_s \left(I - \sigma \widetilde{\mathcal{L}} \right) \begin{pmatrix} \mathbf{s} \\ \mathbf{s}^* \end{pmatrix}, \tag{4.4}$$

where I is the identity matrix, $\widetilde{\mathcal{L}}$ is the block matrix:

$$\widetilde{\mathcal{L}} = \left(\begin{array}{c|c} \mathbf{0} & \mathcal{L}_{m,q} \\ \hline \mathcal{L}_{m,q}^* & \mathbf{0} \end{array} \right), \tag{4.5}$$

and

$$\mathcal{L}_{m,q} = f_{m+q,m} \alpha_{m+q}. \tag{4.6}$$

Recalling the property (3.47), it is easy to show that the operator $\mathcal{L}$ is a symmetric matrix. In fact it satisfies the following equalities:

$$\mathcal{L}_{m,q}^T = \mathcal{L}_{q,m} = f_{m+q,q} \alpha_{m+q} \overset{(3.47)}{=} f_{m+q,m} \alpha_{m+q} = \mathcal{L}_{m,q}. \tag{4.7}$$

As a consequence, the operator $\tilde{\mathcal{L}}$ in (4.4), that couples $\mathbf{s}$ to $\mathbf{s}^*$, is self-adjoint and all its eigenvalues are real numbers. In the most general case, the normalized pump spectral

amplitudes $\{\alpha_m\}$ are complex numbers, nevertheless, for all that cases in which the pump field can be supposed to have only a global phase and no frequency dependent phase component, they are purely real numbers. Typically, the situation for which complex spectral amplitudes need to be considered occurs for chirped pump field and it will be analyzed in the last section of this chapter (see section 4.4). For the following the pump field will be considered real and this implies that $\mathcal{L}^{\dagger}_{m,q} = \mathcal{L}_{m,q}$.

Let's consider the solution of Eq. (4.4) in the form:

$$s_m(t) = \sum_k S^{(1)}_{k,m} e^{\lambda_k t}, \quad s^*_m(t) = \sum_k S^{(2)}_{k,m} e^{\lambda_k t}, \tag{4.8}$$

where $S^{(1)}_{k,m}$ and $S^{(2)}_{k,m}$ are complex numbers and $\{\lambda_k\}_{k\in\mathbb{N}}$ is the spectrum of $\tilde{\mathcal{L}}$. Since λ_k are real, the number $S^{(2)}_{k,m}$ is the complex conjugated of $S^{(1)}_{k,m}$ and in the following they will be denoted as $S_{k,m}$ and $S^*_{k,m}$. Substitution of eqs. (4.8) in (4.4) yields:

$$\lambda_k S_{k,m} = -\gamma_s S_{k,m} + \gamma_s \sigma \sum_q \mathcal{L}_{m,q} S^*_{k,q}, \tag{4.9}$$

$$\lambda_k S^*_{k,m} = -\gamma_s S^*_{k,m} + \gamma_s \sigma \sum_q \mathcal{L}_{m,q} S_{k,q}. \tag{4.10}$$

For fixed SPOPO parameters (γ_s, σ and $f_{m+q,m}$), λ_k and $S_{k,m}$ depend on the pump spectrum $\{\alpha_m\}$.

Let's consider the solution of (4.9) and (4.10) represented by $\{\lambda_k, S_{k,m}\}$. It is straightforward to verify that also the set:

$$\lambda'_k = -2\gamma_s - \lambda_k, \quad S'_{k,m} = iS_{k,m} \tag{4.11}$$

is a solution. We can state the following:

Proposition 3 *The state in quadrature with any eigenstate of (4.9) and (4.10) is an eigenstate too. In particular the solution* $\boxed{S'_{0,m} = iS_{0,m}}$ *has the lowest eigenvalue admitted* $\boxed{\lambda'_0 = -2\gamma_s}$*, being $S_{0,m}$ the solution that is undamped at threshold (i.e. $\lambda_0 = 0$).*

In fact, for any other solution $\lambda_k \neq \lambda_0$, since $\lambda_{k,m} + \lambda'_{k,m} = 2\gamma_s$, if $\lambda'_{k,m} < -2\gamma_s$ then $\lambda_k > 0$ and vice-versa thus contradicting the initial assumption that the SPOPO is at threshold.

Let's assume, now, that the only control parameter is the total pump power σ and that the pump power spectrum $\{\alpha_m\}$ is fixed. Be σ_{th} the pumping power for which the SPOPO is at threshold (thus a $\lambda_0 = 0$ exists) and $\sigma_r = r\sigma_{th}$, with $0 \leq r < 1$, a generic pumping power below the threshold condition. It is, then, verified the following:

Proposition 4 *If it exists an order relation between the eigenvalues at threshold, the same relation exists for any value of the pumping power below threshold.*

For the demonstration, let's take any two eigenvalues that, for $r = 1$ (the oscillation threshold), satisfy the inequality $\lambda_k(1) > \lambda_j(1)$. For each of them, Eq. (4.9) reads:

$$\lambda_k(1) S_{k,m}(1) = -\gamma_s S_{k,m}(1) + \gamma_s \sigma_{th} \sum_q \mathcal{L}_{m,q} S^*_{k,q}(1). \tag{4.12}$$

At different pumping power $r < 1$, instead, the same equation reads:

$$\lambda_k(r) S_{k,m}(r) = -\gamma_s S_{k,m}(r) + r\gamma_s \sigma_{th} \sum_q \mathcal{L}_{m,q} S^*_{k,q}(r). \tag{4.13}$$

Eq. (4.13) is solved by setting:

$$S_{k,m}(r) = S_{k,m}(1), \tag{4.14}$$

$$\lambda_k(r) = (r-1)\gamma_s + r\lambda_k(1). \tag{4.15}$$

While the first condition implies that the eigenvectors are not affected by the pumping level, the second directly proves that $\lambda_k(r) > \lambda_j(r)$ and therefore the eigenvalues are ordered as they are at threshold. This means, also, that λ_0 is the largest eigenvalue and that $\lambda'_0(r)$ is the smallest one for any r, and that they are given by:

$$\lambda_0(r) = (r-1)\gamma_s, \tag{4.16}$$

$$\lambda_0(r)' = -(r+1)\gamma_s. \tag{4.17}$$

The solution of equations (4.9) and (4.10) and, consequently, the determination of threshold and the corresponding state that will be oscillate first can be connected to the diagonalization of the matrix $\mathcal{L}_{m,q}$. Its eigenvalues Λ_k and eigenvectors $\vec{L}_k$ of components $L_{k,m}$ are obtained from the following system of algebraic equations:

$$\Lambda_k L_{k,m} = \sum_q \mathcal{L}_{k,q} L_{k,q}. \tag{4.18}$$

Since, for not chirped pump fields, this matrix is self-adjoint and real, the solutions of (4.18) are all real. Moreover, since γ_s and σ are also real, two sets of solutions to Eqs. (4.9) and (4.10) exists, which are related to the solutions of Eq. (4.18) according to:

$$\begin{gathered} S^{(+)}_{k,m} = L_{k,m}, \quad S^{(-)}_{k,m} = iL_{k,m}, \\ \lambda^{(\pm)}_k = \gamma_s(-1 \pm \sigma\Lambda_k). \end{gathered} \tag{4.19}$$

Let us label by index $k = 0$ the solution of maximum value of $|\Lambda_k|$: $|\Lambda_0| = \max\{|\Lambda_k|\}$. When $\sigma\,|\Lambda_0| < 1$, all the rates $\lambda^{(\pm)}_k$ are negative, which implies that the null solution for the steady state signal field is stable. For simplicity of notation, Λ_0 will be assumed to be positive in the following, but in the case of negativity the null eigenvalue at threshold would be $\lambda^{(-)}_0$ instead of $\lambda^{(+)}_0$.

Hence $\lambda^{(+)}_0$ is the largest eigenvalue and the condition $\lambda^{(+)}_0 = 0$ sets the SPOPO oscillation threshold, which then occurs when σ takes the value $1/\Lambda_0$, i.e. for a pump irradiance $P = P_{\rm th}$ equal to:

$$P_{\rm th} = P_0/\Lambda_0^2, \tag{4.20}$$

where P_0 is defined in Eq. (3.175).

The value of Λ_0, and therefore of the SPOPO threshold, depends on the exact shape of the phase matching curve and on the exact spectrum of the pump laser. As will be shown in section 4.3 through the diagonalization of matrix $\mathcal{L}$, the theoretical SPOPO threshold is extremely low, of the order of the cw single mode threshold divided by the number of pump modes. Let us now define the normalized amplitude pumping rate r by:

$$r = \sqrt{P/P_{\rm th}}, \tag{4.21}$$

or $r = \sigma\Lambda_0$, so that threshold occurs at $r = 1$. In terms of Eq. (4.21) the eigenvalues λ_k become:

$$\lambda_k^{(\pm)} = \gamma_s \left(-1 \pm r \frac{\Lambda_k}{\Lambda_0} \right). \tag{4.22}$$

4.1.1 Monochromatic pumping: determination of the cw oscillation threshold

In the case of monochromatic pumping, the spectral pump amplitudes are expressed by $\alpha_m = \delta_{m,m_0}$, where m_0 corresponds to the pumped mode (with $m_0 \in \mathbb{Z}$). In this case the matrix elements of $\mathcal{L}$(see Eq. (4.6)) are

$$\mathcal{L}_{m,q} = f_{m,m+q}\delta_{m+q,m_0}, \tag{4.23}$$

and the linearized equations (4.4) become

$$\frac{d}{dt}\begin{pmatrix} s_m \\ s^*_{m_0-m} \end{pmatrix} = \begin{pmatrix} -\gamma_s & \gamma_s\sigma f_{m,m_0} \\ \gamma_s\sigma f_{m,m_0} & -\gamma_s \end{pmatrix}\begin{pmatrix} s_m \\ s^*_{m_0-m} \end{pmatrix}, \tag{4.24}$$

where the property $f_{m-m_0,m_0} = f_{m,m_0}$ has been used. The eigenvalues of Eq. (4.24) are:

$$\lambda^{(\pm)} = \gamma_s \left(-1 \pm \sigma f_{m,m_0} \right). \tag{4.25}$$

This result expresses the fact that the couples of modes m and $m_0 - m$ attain the oscillation for the same pump irradiance:

$$P_{\text{th}}(m, m_0 - m) = P_0 / f^2_{m,m_0}. \tag{4.26}$$

In general, since $f^2_{m,m_0-m} \leq 1$, $P_{\text{th}} \geq P_0$. The two modes that have a lower threshold and that attain first the oscillation are those for which f^2_{m,m_0} is maximum. This circumstance explains the role that the shape of the phase-matching and, in particular, the second order dispersion have in the modal selection. In fact, from Eq. (3.46) (with $\Delta = 0$, i.e. the resonant case), the phase-mismatch angle reads:

$$\phi_{m,m_0-m} = l\left[\frac{1}{2} m_0 \left(k'_p - k'_s \right)\Omega + \frac{1}{4} m_0^2 \left(k''_p - k''_s \right)\Omega^2 + \frac{1}{2} m \left(m_0 - 2m \right) k''_s \Omega^2 \right]. \tag{4.27}$$

The function f_{m,m_0} depends on m as far as $k''_s \neq 0$, otherwise the modal selection would not occur. Of course this argument is valid in the case where higher order dispersion are negligible, on the contrary they should be considered and modal selection could be still possible. If the pump field is tuned to the phase-matching frequency so that $m_0 = 0$, the lowest threshold occurs at $m = 0$ as well because $f^2_{0,0} = 1$ and equals P_0 that therefore coincides to the cw degenerate operation of an OPO.

4.1.2 Pulsed operation

In the regime for which the pump field is a cw train of ultrashort pulses (about 100 fs) the pump spectrum $\{\alpha_{m,q}\}$ is not monochromatic. In particular it will be assumed a Gaussian spectral profile:

$$\alpha_m = \frac{1}{\pi^{1/4}\sqrt{N_p}} e^{-\frac{1}{2}\left(\frac{m-\mu_p}{N_p}\right)^2} \tag{4.28}$$

with N_p the number of pump modes (the pump bandwidth in units of the free spectral range Ω), which verifies the normalization condition $\sum_m |\alpha_m|^2 = 1$, and μ_p an offset of the maximum of the spectrum from the phase matching frequency.

Using the properties of Fourier transform, the classical uncertainty relation between the time duration of each pulse of the cw train, say τ_p, and the spectral bandwidth Δ_p in the conjugate space is given by:

$$\tau_\mathrm{p}\Delta_\mathrm{p} = 1. \tag{4.29}$$

For a 100 fs pump pulse it is easy to show that $N_\mathrm{p} \sim 10^5$. The number of longitudinal modes involved in the nonlinear process is of the same order of magnitude and, accordingly, the linear problem (4.9) and (4.10) consists in a computationally too large number of algebraic equations to solve at the same time. However, in the next subsection, we will show that the linear problem can be simplified by exploiting its scalability.

4.1.3 Scalability of the linear problem

In the general case one must diagonalize numerically the linear problem, which in fact constitutes its true solution. The real difficulty with this comes from the fact that the matrix to be diagonalized contains a huge number of elements, typically on the order of $10^5 \times 10^5$, which is definitely too much. The situation can be dramatically simplified from the computational viewpoint by noting that a scale transformation affecting the SPOPO parameters allows diagonalization of a much smaller matrix.

Under the assumption that $\mathcal{L}_{m,q}$ is a smoothest function over its indices, the scalability of the problem can be proved after replacing the sum over q in (4.18) by an integral:

$$\Lambda_k L_k(m) = \int \mathrm{d}q \mathcal{L}(m,q) L_k(q). \tag{4.30}$$

Explicitly, the form of function $\mathcal{L}$, using Eq. (3.170), is:

$$\mathcal{L}(m,q) = \frac{\sin\left[\beta_1(m+q) + \beta_{2\mathrm{p}}(m+q)^2 - \beta_{2\mathrm{s}}\left(m^2+q^2\right)\right]}{\beta_1(m+q) + \beta_{2\mathrm{p}}(m+q)^2 - \beta_{2\mathrm{s}}(m^2+q^2)} \frac{1}{\pi^{1/4}\sqrt{N_\mathrm{p}}} e^{-\frac{1}{2}\left(\frac{m+q-\mu_\mathrm{p}}{N_\mathrm{p}}\right)^2}, \tag{4.31}$$

where it has been assumed a Gaussian form for the pump spectrum (other choices can be taken, such as sech). Let's now consider a second set of parameters defined by

$$\beta_1' = c\beta_1,\ \beta_{2\mathrm{p}}' = c^2\beta_{2\mathrm{p}},\ \beta_{2\mathrm{s}}' = c^2\beta_{2\mathrm{s}}, \tag{4.32}$$

$$N_\mathrm{p}' = c^{-1}N_\mathrm{p},\ \mu_\mathrm{p}' = c^{-1}\mu_\mathrm{p}, \tag{4.33}$$

with c a (large and) positive real, which, in its turn, defines a new problem. Denoting by $\mathcal{L}'$ the matrix corresponding to:

$$\begin{aligned}\mathcal{L}'(m,q) &= \frac{\sin\left[c\beta_1(m+q) + c^2\beta_{2\mathrm{p}}(m+q)^2 - c^2\beta_{2\mathrm{s}}\left(m^2+q^2\right)\right]}{c\beta_1(m+q) + c^2\beta_{2\mathrm{p}}(m+q)^2 - c^2\beta_{2\mathrm{s}}(m^2+q^2)} \\ &\times \frac{1}{\pi^{1/4}\sqrt{N_\mathrm{p}/c}} e^{-\frac{1}{2}\left[\frac{(m+q)-\mu_\mathrm{p}/c}{N_\mathrm{p}/c}\right]^2},\end{aligned} \tag{4.34}$$

it is evident that:

$$\mathcal{L}'(m,q) = \sqrt{c}\mathcal{L}(cm, cq), \tag{4.35}$$

for which, the eigenvalue problem is then:

$$\Lambda'_k L'_k(m) = \int \mathrm{d}q \mathcal{L}'(m,q) L'_k(q). \tag{4.36}$$

Using (4.35), the following change of variables

$$x = cm,\ y = cq, \tag{4.37}$$

leads to

$$\left(\sqrt{c}\Lambda'_k\right) L'_k(x/c) = \int \mathrm{d}y \mathcal{L}(x,y) L'_k(y/c).$$

Finally, comparison with (4.30) immediately yields

$$\Lambda_k = \sqrt{c}\Lambda'_k, \tag{4.38}$$

$$L_{k,m} = L'_k(m/c). \tag{4.39}$$

These two relations are very useful as they allow to compute numerically eigenvalues and eigenvectors of a real problem represented by $\mathcal{L}$ in terms of the corresponding ones of a toy problem represented by $\mathcal{L}'$ because, according to (4.35), the support of $\mathcal{L}'$ is much reduced as compared with that of $\mathcal{L}$. In any case the value for c must be chosen adequately in the sense that the diagonalization of the toy problem can be cast in the integral form (4.36) so as to keep $\mathcal{L}'$ a smooth function of (m,q).

4.2 Diagonalization of the linear problem

The solutions of Eqs. (4.9) and (4.10) below/at threshold are strictly connected to the diagonalization (4.18) of the matrix $\mathcal{L}$ according to relations (4.19). Apart from very simple cases in which the pump spectrum has special shapes, as could be the monochromatic pump, the diagonalization of $\mathcal{L}$ does not presents a direct, analytical solution. The two approaches that can be envisaged in order to avoid this difficulty consist either in the "brutal attack" with a numerical diagonalization or by using an opportune approximation in order to reduce the solution of Eq. (4.18) to a simpler problem.

In the first case, we have seen that the numerical diagonalization can be a computationally heavy task when a pump comb consisting of 10^5 modes is considered. Luckily, in the precedent section, we have seen that the problem (4.9)-(4.10) shows a scaling property grace to which it is possible to reduce it to the diagonalization of a matrix smaller of a factor c respect to the original one. In the other case, the analytical approach consists in approximating the matrix $\mathcal{L}$ around the phase-matched frequency ω_0 with a Gaussian-shaped function thanks to the fact that $\mathcal{L}$ has a compact support. Diagonalization of the new function is trivial since its solutions are well known [Gradshteyn].

4.2.1 The coupling matrix

Keeping in mind the quantum Langevin equations for the evolution of longitudinal modes boson operators $\hat{s}_m$ (see Eq. (3.167)), it is evident that the matrix $\mathcal{L}_{m,q} = f_{m+q,m}\alpha_{m+q}$ represents the coupling between a generic pair of longitudinal modes m-q. The two contribution to $\mathcal{L}$ represented by $f_{m+q,m}$ and α_{m+q} resumes, respectively, the crystal contribution

and the pump contribution. From a physical point of view, the first term ($f_{m+q,m}$) represents the momentum conservation in three photon interaction according the selection rule:

$$\vec{k}_{\mathrm{p}} = \vec{k}_{\mathrm{s}} + \vec{k}_{\mathrm{s}'}, \tag{4.40}$$

where the sum of the linear momenta of signal and idler photons (that in our case are indistinguishable) must equals the momentum of pump photon and $f_{m+q,m} = 1$. In effect, this selection rule does not need to be strictly observed as suggested by the functional dependence of the phase-mismatching angle (3.169) on the cardinal sinus. In fact, for imperfect phase-matching (i.e. $\phi_{m,q} \neq 0$), the contribution of the crystal is still appreciable as far as $\phi_{m,q}$ is small respect to 2π. This is the typical situation that occurs in presence of quasi phase-matched laser beams. Because of the broadband nature of the interacting fields, the phase-matching condition can be satisfied by several couples of signal photons, whose ensemble forms a locus of points corresponding to a constant value of the phase-mismatch angle $\phi_{m,q}$. If we write Eq. (3.170) in a opportune reference frame ($m + q = x$ and $m - q = y$), the phase-mismatch angle reads:

$$\phi_{m,q} = \left(\beta_{2\mathrm{p}} - \frac{1}{2}\beta_{2\mathrm{s}}\right) x^2 - \beta_{2\mathrm{s}}\, y^2 + \beta_1 x, \tag{4.41}$$

thus showing that these lines can be either ellipses, hyperboles or parabolas according to the values of the parameters β_1, $\beta_{2\mathrm{p}}$ and $\beta_{2\mathrm{s}}$. In particular, we get ellipses if the condition $(\beta_{2\mathrm{p}} - \frac{1}{2}\beta_{2\mathrm{s}})\beta_{2\mathrm{s}} > 0$, hyperbolas in the opposite case and parabolas in the case where equality is verified. From Eq. (4.41) the role of the difference between group velocities β_1 represents only a translation in the plane $\{x, y\}$.

For typical non-linear crystals, in the transparency region, the main contribution to the second derivative of the wavevector

$$\frac{\partial^2 k}{\partial \omega^2} = \frac{1}{c}\left[2n'(\omega) + \omega n''(\omega)\right] \tag{4.42}$$

is given by the first term, that is always positive and, thus, $\beta_{2\mathrm{s}} > 0$. This is a consequence of the fact that the optical region were the crystal is operated is closer to the red-shifted resonance than to the blue-shifted one. However this does not prevent the existence of crystals where this condition could be no more satisfied. Since, the inequality $\beta_{2\mathrm{p}} > \frac{1}{2}\beta_{2\mathrm{s}}$ is verified too, for typical operation, the hyperbolic configuration is a more common situation than the elliptical one.

On the other side, the term α_{m+q}, representing the pump spectrum, reflects the energy conservation law. Each pump photon of energy $\hbar\omega_{\mathrm{p},m+q}$ is parametrically down-converted in a couple of signal photons of energy $\hbar(\omega_{\mathrm{s},m} + \omega_{\mathrm{s},q})$ according to:

$$\omega_{\mathrm{p},m+q} = \omega_{\mathrm{s},m} + \omega_{\mathrm{s},q}. \tag{4.43}$$

Because of energy conservation, in the plane $\{m, q\}$, the quantity $m + q$ has to be constant and the pump selects a portion of the matrix $f_{m,m+q}$ given by the intersection of $f_{m,m+q}$ with a straight band oriented along the direction $m+q = 2\bar{m}$, where $\bar{m}$ corresponds to the maximum of the pump spectrum. Hence, if the pump spectrum is centered at the phase-matching frequency $2\omega_0$ (the case we consider) $\bar{m} = 0$ and the matrix $\mathcal{L}$ is given by a portion of the upper branch of the hyperbola crossing $\{m = 0, q = 0\}$ whose width is selected by the pump bandwidth Δ_{p} along the direction $m - q = 0$.

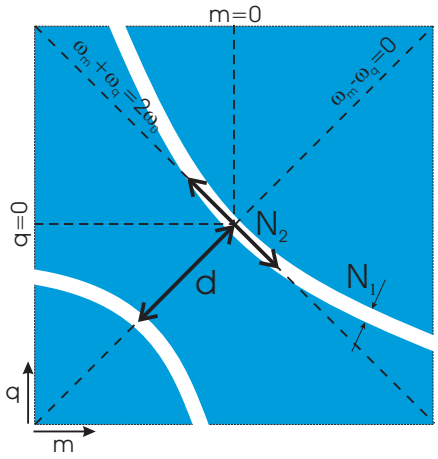

Figure 4.1: Schematization of the phase-matching matrix $f_{m+q,m}$.

In Figure 4.1 a scheme of the phase-matching matrix is represented in the space of $\{m, q\}$ assuming an hyperbolic case. Since m and q are integer numbers which unambiguously identify the signal frequency $\omega_{s,m}$ and $\omega_{s,q}$ according to Eq. (3.4), all the quantities represented in this figure are scaled over the cavity free spectral range Ω. Therefore, the hyperbolas have two branches whose width is N_1 (or $\Delta_1 = N_1\Omega$) and whose minimum distance is given by d along the direction $m - q = 0$. As remarked above, we are assuming that the maximum of the pump spectrum occurs at the phase-matched frequency $2\omega_0$ which corresponds to the point $(m = 0, q = 0)$. Therefore the energy conservation rule selects a slice of the phase-matching matrix whose direction is $m + q = 0$ or, in terms of frequencies, $\omega_{s,m} + \omega_{s,q} = 2\omega_0$. Because of the selection acted by the pump, the final coupling matrix $\mathcal{L}$ has a compact support characterized by two typical width represented

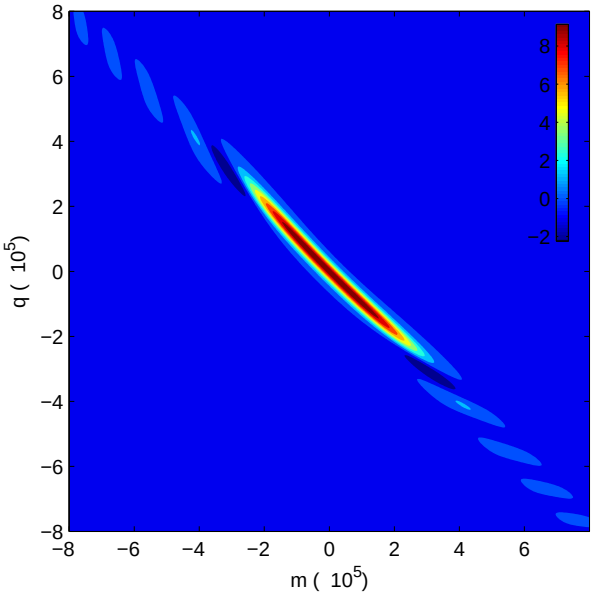

Figure 4.2: Matrix $\mathcal{L}$ resulting from the product of α_{m+q} and $f_{m+q,m}$.

by N_1 and N_2 (respectively Δ_1 and Δ_2). In Figure 4.2 we traced the matrix $\mathcal{L}$ resulting from the product of the pump and the phase-matching terms. As we can see, the coupling matrix consists of a bell-shaped main part and oscillating lateral tails due to the cardinal sinus dependence of the exact matrix. Therefore, the statement that $\mathcal{L}$ has a compact support is not completely exact, because in principle non-null oscillations occurs at frequencies whose values have not an upper limit. However, it is always possible to show that the error committed in diagonalization by choosing a limited domain for $\mathcal{L}$ is small, provided that this domain is enough large to contain sufficient information of the exact matrix.

4.2.2 Gaussian approximation and analytical diagonalization

The role of the pump spectrum $\{\alpha_m\}$ is to select from $f_{m+q,m}$ a slice, so that the broader the pump spectrum the less selective it is. When the pump is centered at the phase-matching frequency and it is not so broad, for example on the order of the width of the phase-mismatch factor along the axis $m-q=0$, the resulting matrix $\mathcal{L}$ is well confined within an "ellipse" whose principal axes are oriented along the direction $m+q=0$ and $m-q=0$. This allows an approximated description that leads to an analytical solution of the diagonalization problem. In fact, we can make the assumption that the coupling matrix is described by:

$$\mathcal{L}_{m,q} = \mathrm{e}^{-\frac{1}{2}\left(\frac{m+q}{N_1}\right)^2} \mathrm{e}^{-\frac{1}{2}\left(\frac{m-q}{N_2}\right)^2} \frac{1}{\pi^{1/4}\sqrt{N_\mathrm{p}}} \mathrm{e}^{-\frac{1}{2}\left(\frac{m+q}{N_\mathrm{p}}\right)^2}, \tag{4.44}$$

where the phase-mismatch factor has been approximated by the following Gaussian function:

$$f_{m+q,m} = \mathrm{e}^{-\frac{1}{2}\left(\frac{m+q}{N_1}\right)^2} \mathrm{e}^{-\frac{1}{2}\left(\frac{m-q}{N_2}\right)^2} \tag{4.45}$$

and the pump spectrum has been assumed to be a Gaussian spectrum like in (4.28). Notice that the exact coupling matrix can be exchanged with the matrix in (4.44) without loosing too much information as far as the oscillating tails have a negligible contribution (see Figure 4.2).

In the following, after having retrieved the expressions for the characteristic widths (N_1, N_2, d), we will define also a criterion able to discriminate between the situations where this approximation is correct and situations where deviation from "Gaussianity" is more critical. The characteristic widths are found by comparing a suitable approximation of the exact coupling matrix around the phase-matched frequency ω_0 with the matrix considered in (4.44). The idea to substitute the phase-matching matrix with a Gaussian function, characterized by two widths, has been already used in [Bennink2002, Wasilewski2006a] for the study of the dynamics of a system consisting in a simple passage pulsed OPA. We will return in the next chapter on the similarities between the two problems and the consequences from a quantum point of view.

Along the axis $m+q=0$, after the rotation $x=m+q$, $y=m-q$, the matrix (3.168) reads:

$$f_{m+q=0} = \frac{\sin\left(\frac{1}{2}\beta_{2\mathrm{s}}y^2\right)}{\frac{1}{2}\beta_{2\mathrm{s}}y^2}. \tag{4.46}$$

Since, around the point $y=0$, a function $\sin(y^2)/y^2$ can be approximated by the function $\mathrm{e}^{-y^2/\eta}$, where the parameter η can be opportunely chosen so that the results

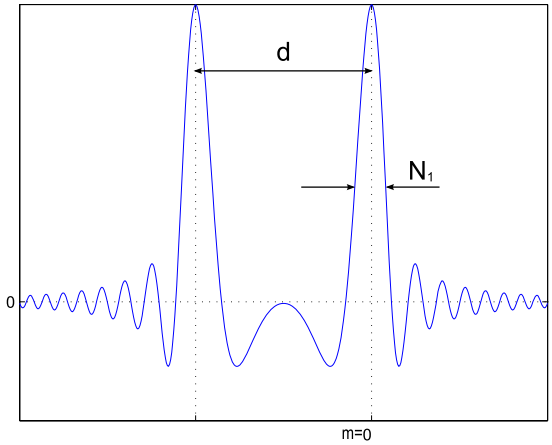

Figure 4.3: Section of the matrix $f_{m+q,m}$ along the axis $m - q = 0$.

from diagonalization of matrix (4.44) match optimally to the results of diagonalization of the original matrix (4.6). In our case $\eta = 12$, then the comparison with Eq. (4.45) leads to:

$$N_2 = \frac{2\sqrt{3}}{\sqrt{|\beta_{2s}|}}. \tag{4.47}$$

On the other side, along the axis $m - q = 0$, after the same rotation as above, the matrix (3.168) reads:

$$f_{m-q=0} = \frac{\sin\left[\left(\beta_{2p} - \frac{1}{2}\beta_{2s}\right)x^2 + \beta_1 x\right]}{\left(\beta_{2p} - \frac{1}{2}\beta_{2s}\right)x^2 + 2\beta_1 x}, \tag{4.48}$$

that has been traced in Figure 4.3.

At small x and keeping in mind that in typical situations[2] $|2\beta_{2p} - \beta_{2s}| \ll |\beta_1|$, the function $f_{m-q=0}$ can be approximated by $e^{-(\beta_1 x)^2/5}$. Therefore, after comparison with Eq. (4.45), we obtain:

$$N_1 = \frac{\sqrt{5/2}}{|\beta_1|}. \tag{4.49}$$

The values of x for which $f_{m-q=0}$ has the two principal maxima are, instead, obtained when the argument is zero. Since the first maximum is at $x = 0$ and the second is found at $x = -|\beta_1|/|\beta_{2p} - \frac{1}{2}\beta_{2s}|$, the distance d between the maxima is:

$$d = \frac{|\beta_1|}{|\beta_{2p} - \frac{1}{2}\beta_{2s}|}. \tag{4.50}$$

If we adopted different approximations for $\sin(x)/x$ and $\sin(x^2)/x^2$, other values of the numerical constants in Eqs. (4.47), (4.49) and (4.50) would be obtained. N_1 and N_2 are a measure of the spectral response of the crystal, in the frequency domain they define the following bandwidths

$$\Delta_1 = N_1\Omega, \quad \Delta_2 = N_2\Omega, \tag{4.51}$$

[2]For typical crystals $|k'_p - k'_s| \sim 10^{-10} - 10^{-9}\,\mathrm{sm}^{-1}$ and k''_p, $|k''_s| \sim 10^{-25} - 10^{-24}\,\mathrm{s}^2\mathrm{m}^{-1}$.

which are independent from the free spectral range. In fact, according to Eqs. (4.49), (4.47), (4.51) and keeping in mind the expressions for β-parameters (see Eqs. (3.171), (3.172) and (3.173)), we have:

$$\Delta_1 = \frac{\sqrt{10}}{|k'_{\rm p} - k'_{\rm s}|l}, \quad \Delta_2 = \frac{4\sqrt{3}}{\sqrt{|k''_{\rm s}|l}}. \tag{4.52}$$

In their turn the bandwidths define the two characteristic times:

$$\tau_1 \equiv \frac{1}{\Delta_1} = \frac{|k'_{\rm p} - k'_{\rm s}|l}{\sqrt{10}}, \tag{4.53}$$

$$\tau_2 \equiv \frac{1}{\Delta_2} = \frac{\sqrt{|k''_{\rm s}|l}}{4\sqrt{3}}, \tag{4.54}$$

which depend on the crystal properties only. Under typical conditions[1], these times are on the order of $\tau_1 \sim 100\,\text{fs}$ and $\tau_2 \sim 5\,\text{fs}$ for a crystal length $l = 1\,\text{mm}$, and in general $\tau_2 \ll \tau_1$ whenever $l \gtrsim 0.1\,\mu\text{m}$.

The Gaussian approximation introduced with Eq. (4.44) has a limited validity according to the values of the pump bandwidth and the crystal parameters (β_1, $\beta_{2\rm p}$, $\beta_{2\rm s}$ and l). As remarked above, in fact, the Gaussian approximation can be performed each time the interplay between the pump spectrum and the phase-matching is opportune. More quantitatively speaking, we have to demand that the two branches of the hyperbola in Figure 4.1 are sufficiently separated each other, which is traduced by imposing $d \gg \Delta_1$ (for example $d \gtrsim 10\Delta_1$), and that the pump width is sufficiently smaller than the width of each branch along the direction $m - q = 0$ in order that the secondary maxima of $f_{m,m+q}$ do not show up, which is traduced by demanding that $\Delta_p \lesssim \Delta_1$. These conditions lead to the following bounds:

$$\frac{\beta_1^2}{|\beta_{2\rm p} - \frac{1}{2}\beta_{2\rm s}|} \gtrsim 20, \quad 2|\beta_1|N_{\rm p} \lesssim 1. \tag{4.55}$$

In terms of the crystal parameter and of the pump pulse duration $\tau_{\rm p}$, from these relations, we obtain the two constraints

$$l \gtrsim 20\,\frac{|k''_{\rm p} - \frac{1}{2}k''_{\rm s}|}{\left(k'_{\rm p} - k'_{\rm s}\right)^2}, \tag{4.56}$$

$$\tau_{\rm p} \gtrsim |k'_{\rm p} - k'_{\rm s}|l, \tag{4.57}$$

that have to be satisfied independently. Condition (4.56) is very easily fulfilled and as we will see in the next section, for a BIBO crystal under typical operation, this inequality reads $l > 50\,\mu\text{m}$. On the contrary, condition (4.57) is not always met. For example for a BIBO crystal under typical conditions this inequality reads $\tau_{\rm p} > 400\,l\,\text{fs} \times \text{mm}^{-1}$. Hence, for a crystal of length $l = 1mm$, $\tau_{\rm p}$ should be larger than 400 fs in order the Gaussian approximation is valid, while for $l = 0.1\,\text{mm}$ the condition is met for $\tau_{\rm p} > 40\,\text{fs}$. Let's note that condition (4.57) is connected with the walk-off between signal and pump modes along their propagation inside the crystal so that the smaller the difference between group velocities or the crystal length, the less restrictive condition (4.57) becomes.

Under the approximation (4.44), the eigenvalue problem (4.18) admits an exact solution in the continuous limit where the discrete variables m and q become continuous variables

and the sum is replaced by the integral:

$$\int_{-\infty}^{+\infty} \mathrm{d}q\, \mathcal{L}\,(m,q)\, L_k\,(q) = \Lambda_k L_k\,(m)\,. \tag{4.58}$$

The passage to the continuum is justified if Δ_1 is much greater then the free spectral range Ω. Since typically $\beta_1 \sim 10^{-4}$, from Eqs. (3.171) and (4.51), it directly follows $N_1 \gg 1$ and, then, the matrix $\mathcal{L}$ can be considered a function that smoothly varies over m and q. The eigenvalues are given by (see Appendix A):

$$\Lambda_k = \Lambda_0 \rho^k, \tag{4.59}$$

where:

$$\Lambda_0 = \pi^{1/4}\sqrt{2N_\mathrm{p}}\frac{\tau_\mathrm{p}}{\tau_2 + \sqrt{\tau_1^2+\tau_\mathrm{p}^2}}, \tag{4.60}$$

$$\rho = \frac{\tau_2 - \sqrt{\tau_1^2+\tau_\mathrm{p}^2}}{\tau_2 + \sqrt{\tau_1^2+\tau_\mathrm{p}^2}}, \tag{4.61}$$

which is a geometric progression of ratio ρ. As discussed above, unless $l < 0.1\,\mu$m, τ_2 is much smaller than τ_1, hence the quantity

$$\rho \sim -1 + 2\sqrt{\frac{\tau_2^2}{\tau_1^2+\tau_\mathrm{p}^2}} \tag{4.62}$$

is very close to, but larger than, -1. Equation (4.59) corresponds, then, to an alternating geometric progression of ratio ρ, whose first element is $\Lambda_0 > 0$.

The eigenvectors are (see Appendix A):

$$L_{k,m} = \frac{1}{\sqrt{k!2^k\pi^{1/2}N_\mathrm{s}}} e^{-\frac{1}{2}\left(\frac{m}{N_\mathrm{s}}\right)^2} H_k\left(\frac{m}{N_\mathrm{s}}\right), \tag{4.63}$$

where H_k is the Hermite polynomial of order k, and N_s is the number of signal modes given by:

$$\frac{1}{N_\mathrm{s}^2} = \frac{2}{N_2}\sqrt{\frac{1}{N_1^2}+\frac{1}{N_\mathrm{p}^2}}. \tag{4.64}$$

Alternatively, $N_\mathrm{s} = (\Omega\tau_\mathrm{s})^{-1}$ in terms of the signal pulse duration τ_s (corresponding to $k = 0$), which is given by:

$$\tau_\mathrm{s}^2 = 2\tau_2\sqrt{\tau_1^2+\tau_\mathrm{p}^2}. \tag{4.65}$$

We see that the free spectral range Ω just appears as a proportionality factor in Λ_k (through $\sqrt{2N_\mathrm{p}}$ in Λ_0, keeping in mind that $N_\mathrm{p} = (\Omega\tau_\mathrm{p})^{-1}$), but does not affect the signal pulse duration τ_s.

The strict validity of these results requires the fulfilling of condition (4.57) that, according to the definition of τ_1 (see Eq. (4.53)) becomes $\tau_\mathrm{p} > \sqrt{10}\,\tau_1$. Hence, within the strict domain of validity, $\tau_\mathrm{p}^2 \gg \tau_1^2$ ("long" pump pulses), so that $\Lambda_0^2 \simeq 2\sqrt{\pi}N_\mathrm{p}$ is roughly the (huge) number of pump modes and $\tau_\mathrm{s} \simeq \sqrt{2\tau_2\tau_\mathrm{p}}$ (note that the signal pulse duration τ_s should be quite smaller than the pump pulse duration τ_p as $\tau_2 \ll \tau_\mathrm{p}$).

According to Eq. (4.20), the predicted SPOPO threshold, in the limit of "long" pump pulses, is roughly the c.w. single mode threshold P_0 divided by the number of pump modes. Under a physical point of view, the reason resides in the fact that parametric down-conversion can be considered, with a good level of approximation, instantaneous respect to the pump pulse duration, therefore the efficiency of the nonlinear interaction is directly proportional to the pump peak power that, for a mode-locked beam, is the result of contribution of all the modes present in the pump spectrum. For example, if $N_\mathrm{p} = 2 \times 10^4$ (corresponding to $\tau_\mathrm{p} = 100\,\mathrm{fs}$ and a cavity length $L = 2$) and considering the case already discussed (a $100\,\mu$m-thick BIBO based linear SPOPO pumped at $0.4\,\mu$m), we obtain threshold pump irradiances $P_\mathrm{th}^{(\mathrm{singly})} = 31.7 \times 10^{-3}$, 3.96, and $31.7\,\mathrm{kW\,cm^{-2}}$ for $T_\mathrm{s} = T_\mathrm{p} = 0.01$, 0.05, and 0.1, respectively. For a typical pump beam radius of $70\,\mu$m these irradiances lead to the following pump threshold powers $W_\mathrm{th}^{(\mathrm{singly})} = 0.02$,2.2, and 18 mW, respectively.

4.2.3 General case: numerical diagonalization

In the general case, and in particular when the Gaussian limit discussed above is not met, $\mathcal{L}$ has to be diagonalized numerically. However, as explained, the size of this matrix prevents numerical procedure in practice. As demonstrated in section 4.1.3, the eigenproblem, univocally defined by $(\beta_1, \beta_{2\mathrm{p}}, \beta_{2\mathrm{s}}, N_\mathrm{p}, \mu_\mathrm{p})$, can be rescaled according to Eqs. (4.32) and (4.33) allowing the diagonalization of a matrix $\mathcal{L}'$ that is much smaller respect to the original coupling matrix. The necessary condition for the validity of Eqs. (4.38) and (4.39) is that also $\mathcal{L}'$ be a smooth function over the variables m' and q'. According to the same reasoning used in section 4.2.2, this is true when $N_1' \gg 1$ and, consequently, the choice of the scaling parameter c have to be done in order to respect (even if not strictly) this inequality.

Keeping in mind these observations, we applied numerical diagonalization for studying typical experimental situations in several configurations, eventually comparing the results with predictions that can be obtained with the analytical model. In particular, we considered both BIBO and $KNbO_3$ crystals in configurations involving different pump pulse durations τ_p, cavity lengths L, crystal thicknesses l and phase-matching conditions, such as critical or non-critical, that give rise to different dispersion properties. When these parameters satisfy the conditions (4.56) and (4.57), we found confirmation that the analytical description obtained in the Gaussian approximation describes very well the results obtained via numerical approach. On the other side, when that conditions get violated, deviations from the the analytical results are found.

4.3 Application to BIBO and KNbO3 based SPOPOs

The connection between the linear problem (4.18) and the threshold of a SPOPO permits to have access to the dynamical properties of the system below/at threshold. According to Eq. (4.6), since the coupling matrix is the product of the phase-matching matrix and the pump spectrum, they can be, somehow, controlled acting on the type of phase-matching or of the pump field.

Under the hypothesis of Fourier-transform-limited pump pulses, the spectrum of the pump field can be assumed to be in the Gaussian form as in Eq. (4.28) whose bandwidth is

connected to the time duration of the pulse according to the classical incertitude relation (4.29). In our analysis we considered a Gaussian pump spectrum, limiting our study to the dependence of the threshold on Δ_{p} (or τ_p) without considering spectra different from Eq. (4.28).

For what concerns the phase-matching, several choices are possible such as the type of the non-linear crystal, its thickness, the type of phase-matching. For tunable ultra-short pulse generation, continuous operation of a SPOPO has been demonstrated by Piskarskas *et al.* [Piskarskas1988] in a doubly resonant oscillator configuration using a $Ba_2NaNb_5O_{12}$ crystal as the gain medium. Although the doubly resonant configuration results in low oscillation threshold, it is very sensitive to perturbations since the requirements for simultaneous resonance for both the generated fields demands a high stability on the pump laser and the OPO cavity. Resonating only one of the generated fields in a singly resonant oscillator can greatly relax the tolerances on the pump laser and OPO cavity, as we have already discussed in Section 3.1.5. On the other side, the price to pay is for an order-of-magnitude increase in the oscillation threshold condition. Edelstein *et al.* [Edelstein1989] and Wachman *et al.* [Wachman1990], first, experimentally demonstrated the operation of a c.w. singly resonant SPOPO using potassium titanyl phosphate (KTP) as the gain medium and colliding-pulse mode-locked dye laser as the pump source. In the quest for more efficient pulse compression, several experimental strategies, leading to the choice of different kind of nonlinear crystals, type of phase-matching, have been explored. Among the great variety of crystals, the most exploited have been KTP, BBO and LBO, and more recently BIBO [Ghotbi2004]. In contrast to the restrictions of standard birefringent phase-matching, quasi-phase-matching offers several advantages, since PPLN crystals presents high conversion gain (17 pm/V [Galvanauskas1997]) and a relatively large transparency range thus leading to better pulse compression. Synchronously pumped OPO based on PPLN has been demonstrated, instead, in [McGowan1998]. On the other side, in experiments such as the generation of pulsed squeezed light [Slusher1987, Wenger2004], commonly the choice has fallen on the nonlinearity of $KNbO_3$ crystals.

We performed numerical calculations on the nonlinearities of BIBO and $KNbO_3$ crystals for different reasons. The first crystal has been chosen since this work aims at providing a theoretical support to the experiment set up at Laboratorie Kastler Brossel where a BIBO based SPOPO is operated in the femtosecond regime. BIBO crystals, in fact, present at the same time very high resistance to optical damage and the same nonlinearities of KTP [Ebrahimzadeh1991]. On the other side, $KNbO_3$ is a nonlinearity that have been not explored for applications like SPOPOs and consequently can represent a new situation.

4.3.1 Phase-matching conditions

In accordance with the model developed in Chapter 3, a collinear, degenerate type I phase-matching will be considered only.

For a BIBO crystal, the Sellmeyer coefficients corresponding to equations:

$$n_i^2(\lambda) = A_i + \frac{B_i}{\lambda^2 - C_i} - D_i\lambda^2, \tag{4.66}$$

can be found in [Nikogosyan2005] and are reported in Table 4.1. Notice that, in eq. (4.66),

the indices $i = x, y, z$ represent the coordinates in the crystal reference frame and λ have to be expressed in μm.

i	A_i	B_i	C_i	D_i
x	3.0722	0.0324	0.0315	0.0133
y	3.1669	0.0372	0.0348	0.0175
z	3.6525	0.0511	0.0370	0.0266

Table 4.1: Sellmeier coefficients for BIBO

Since BIBO is a biaxial crystal, the type I collinear and degenerate phase matching condition ($o \to e + e$) at the pump wavelength λ_0,

$$\frac{2\pi}{\lambda_0}\left(n_o(\lambda_0) + n_e(2\lambda_0)\right) = 0, \tag{4.67}$$

in the general case requires to solve the intersection between the plane determined by the pump wavevector $\overrightarrow{k} = \sin\theta\cos\phi\,\mathbf{u}_x + \sin\theta\sin\phi\,\mathbf{u}_y + \cos\theta\,\mathbf{u}_z$ and the ellipsoid of the refraction indexes whose principal axes are determined by eqs. (4.66). This problem can be simplified considering a ordinary pump field polarized along the direction $\mathbf{u}_x$ and propagating along a direction laying in the plane yOz (i.e. $\phi = \pi$) so that $n_o \equiv n_x$ and

$$n_e(\theta) = \left(\frac{\sin^2(\pi-\theta)}{n_y^2} + \frac{\cos^2(\pi-\theta)}{n_z^2}\right)^{-1/2}. \tag{4.68}$$

Using Sellmeier's coefficients and for a pump at $0.4\,\mu$m, we obtain that such phase-matching occurs at an angle $\pi - \theta = 151°$, in agreement with [Ghotbi2004]. Once determined the ordinary and extraordinary refraction indexes, respectively for the propagation of the pump and signal fields inside the crystal, we can retrieve the values of the dispersion parameters. In fact, from $k(\omega) = \omega\, n(\omega/c)$, the inverse of the group velocity $k'(\omega)$ and of the group velocity dispersion (GVD) $k''(\omega)$ are:

$$k' = \frac{n(\lambda) - \lambda\frac{dn}{d\lambda}}{c}, \tag{4.69}$$

$$k'' = \frac{\lambda^3\frac{d^2n}{d\lambda^2}}{2\pi c^2}, \tag{4.70}$$

where the r.h.s. must be evaluated at $\omega = 2\pi c/\lambda$. Therefore, for a $0.4\,\mu$m pump field and a $0.8\,\mu$m signal field, the dispersion parameter up to the second order in the perturbative expansion around the phase matched frequencies are:

$$k'_{\mathrm{s}} = 6.2664 \times 10^{-9}\,\mathrm{s\,m^{-1}}, \quad k''_{\mathrm{s}} = 1.6420 \times 10^{-25}\,\mathrm{s^2\,m^{-1}}, \tag{4.71}$$

$$k'_{\mathrm{p}} = 6.6537 \times 10^{-9}\,\mathrm{s\,m^{-1}}, \quad k''_{\mathrm{p}} = 4.7248 \times 10^{-25}\,\mathrm{s^2\,m^{-1}}. \tag{4.72}$$

In the case of noncritical phase-matching, the phase mismatch is minimized by adjusting the crystal temperature so that the phase velocities of pump and signal fields are equal. Under the simplificative assumption that the fields propagate along one of the crystal directions $\{\mathbf{u}_x, \mathbf{u}_y, \mathbf{u}_z\}$, the only possibility to find noncritical phase-matching at room temperature is a situation where the pump field is polarized along $\mathbf{u}_y$, the signal

i	A_i	B_i	C_i	D_i
x	4.4308	0.10044	0.054084	0.019592
y	4.8355	0.12839	0.056342	0.025379
z	4.9873	0.15149	0.064143	0.028775

Table 4.2: Sellmeier coefficients for $KNbO_3$

field along $\mathbf{u}_z$ and at a pumping wavelength of $\lambda_\mathrm{p} \simeq 0.589\,\mu$m. In such a case, then, the dispersion parameters are:

$$k'_\mathrm{s} = 6.0390 \times 10^{-9}\,\mathrm{s\,m^{-1}}, \quad k''_\mathrm{s} = 2.5606 \times 10^{-25}\,\mathrm{s^2\,m^{-1}}, \tag{4.73}$$

$$k'_\mathrm{p} = 6.1603 \times 10^{-9}\,\mathrm{s\,m^{-1}}, \quad k''_\mathrm{p} = 2.1917 \times 10^{-25}\,\mathrm{s^2\,m^{-1}}\,. \tag{4.74}$$

Let's consider now a $KNbO_3$ crystal. The Sellmeier's coefficients given in Table 4.2 can be found, for example, at [SellmeierKNbO3].

As for the previous case, $KNbO_3$ is a biaxial crystal too. Therefore, for sake of simplicity, we will assume a pump field propagating in the plane xOy (then $\theta = 0$) and polarized along $\mathbf{u}_z$ so that $n_o \equiv n_z$. On the other side, the signal field, polarized along a direction orthogonal to the plane determined by $\{\overrightarrow{k}_\mathrm{p}, \mathbf{u}_z\}$, sees an extraordinary refraction index given by:

$$n_e(\phi) = \left(\frac{\cos^2(\pi - \phi)}{n_x^2} + \frac{\sin^2(\pi - \phi)}{n_y^2} \right)^{-1/2}. \tag{4.75}$$

For a $0.4\,\mu$m pumping (and at room temperature), we found a phase-matching for an angle $\phi \simeq 20°$. Therefore, using Eqs. (4.69) and (4.70), we obtain:

$$k'_\mathrm{s} = 7.6301 \times 10^{-9}\,\mathrm{s\,m^{-1}}, \quad k''_\mathrm{s} = 1.1845 \times 10^{-25}\,\mathrm{s^2\,m^{-1}}, \tag{4.76}$$

$$k'_\mathrm{p} = 7.7629 \times 10^{-9}\,\mathrm{s\,m^{-1}}, \quad k''_\mathrm{p} = 4.4721 \times 10^{-25}\,\mathrm{s^2\,m^{-1}}\,. \tag{4.77}$$

For a noncritical phase-matching at room temperature two favorable situations close to $0.4\,\mu$m exist. In the first case, the pump field is polarized along $\mathbf{u}_x$, the signal along $\mathbf{u}_z$ and the phase-matching occurs at $\lambda_\mathrm{p} \simeq 0.431\,\mu$m. In the second case, the pump field is polarized along $\mathbf{u}_x$, the signal along $\mathbf{u}_y$ and the phase-matching occurs at $\lambda_\mathrm{p} \simeq 0.496\,\mu$m. Finally the dispersion parameters (4.69) and (4.70), in the two cases, have been reported in Table 4.3.

	$\lambda_\mathrm{p} \simeq 0.431\,\mu$m	$\lambda_\mathrm{p} \simeq 0.496\,\mu$m
k'_s ($\times 10^{-9}\,\mathrm{s\,m^{-1}}$)	7.9868	7.6779
k''_s ($\times 10^{-25}\,\mathrm{s^2\,m^{-1}}$)	2.7869	1.3196
k'_p ($\times 10^{-9}\,\mathrm{s\,m^{-1}}$)	9.1762	8.4323
k''_p ($\times 10^{-25}\,\mathrm{s^2\,m^{-1}}$)	1.5945	1.0536

Table 4.3: Dispersion parameters for noncritical phase-matching of $KNbO_3$ at room temperature

As we shall see in the next paragraph, the conditions (4.56) and (4.57) can be satisfied/violated not only by playing with pump pulse duration or crystal thickness, but

also with an opportune choice of the phase-matching conditions which, among several possibilities, represent already some significative examples.

4.3.2 The case: $\tau_p = 100$fs, $L = 4$m, $l = 0.1$mm

The first parametrical setup we consider is the one corresponding to a ring cavity pumped by a c.w. train of 100 fs pulses at 0.4 μm and filled with a nonlinear crystal of thickness of about 0.1 mm, because this is the setup adopted for the real experiment. The pump spectrum is assumed to be Gaussian as expressed in eq. (4.28).

Critically phase-matched BIBO

Let's consider the case of $BIBO$ crystal critically phase-matched at a pump wavelength of 0.4 μm discussed in Section 4.3.1. Using the values of the dispersion parameters of the crystal in Eqs. (4.71) and (4.72), the limits of validity of the Gaussian approximation, represented by Eqs. (4.56) and (4.57), reads $l > 50\,\mu$m and $\tau_p > 40$ fs and are both satisfied. The matrix $\mathcal{L}$ corresponding to this parametric case has been traced in Figure 4.4(a) in a frequency representation (where the labels m and q represents the order of the longitudinal cavity mode expressed in eq. (3.4)), which is the actual matrix to be diagonalized, while in Figure 4.4(b) the wavelength representation is displayed.

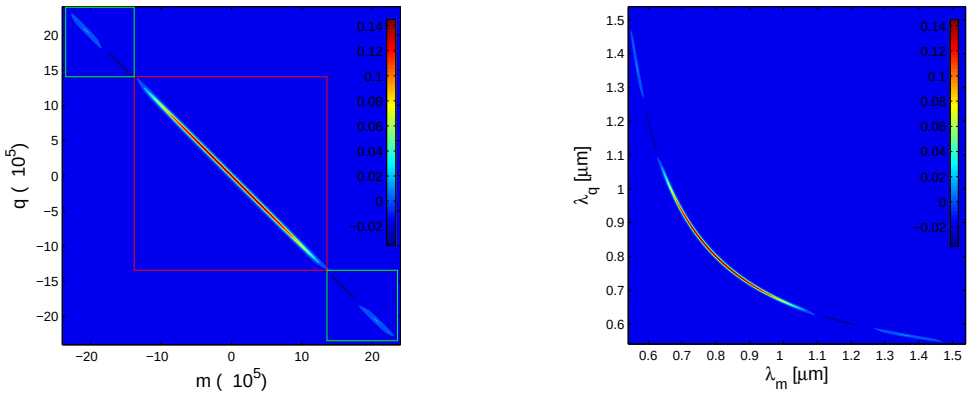

(a) (b)

Figure 4.4: Appearance of $\mathcal{L}$ matrix in the case of critically phase-matched BIBO of 0.1 mm of thickness, in a ring cavity of 4 m, pumped at 0.4 μm by a cw train of 100 fs pulses. In (b) the axes are wavelengths.

The characteristic times, evaluated from Eqs. (4.53) and (4.54), are $\tau_1 \simeq 12.25$ fs and $\tau_2 \simeq 1.17$ fs, in agreement with the previous statement that for typical configuration $\tau_2 \ll \tau_1$. As explained in Section 4.1.3, since the numerical solution of the linear problem (4.18) is a highly demanding task in terms of CPU resources, the best solution is to exploit the scaling property illustrated in that section. Such a property, however, is valid only in the case where the rescaled coupling matrix is still a smooth function over the domain of integers. Figures 4.4(a) and 4.4(b) have been traced over a grid of 4800×4800 points, with a scaling parameter $c = 1000$. In this situation, from Eq. (4.49), the rescaled width $N_1' \simeq 170$ is much bigger than 1, thus guaranteeing the smoothness of $\mathcal{L}$. If we wanted

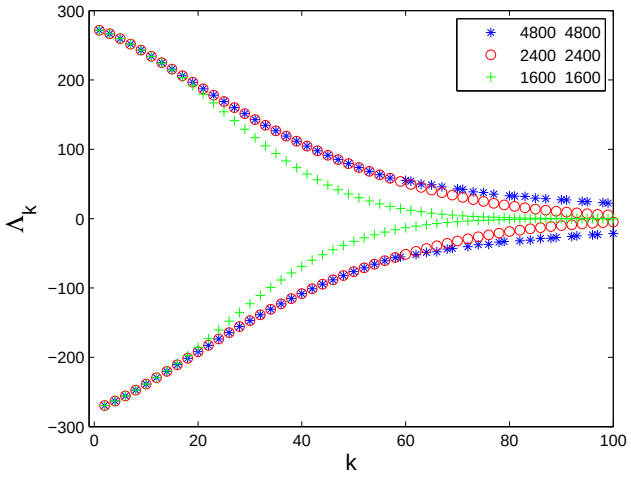

Figure 4.5: Comparison between the spectrum of eigenvalues retrieved for a grid of 1600×1600 points, a grid of 2400×2400 points and a grid of 4800×4800 points.

further reduce the dimension of the matrix to diagonalize, we could increase the scaling parameter c but at the expenses of the validity of the integral approximation (4.30). The last remark, on the numerical method adopted for diagonalizing the coupling matrix, is concerned with the fact that, at fixed scaling, the dimension of the grid over which is drawn $\mathcal{L}$ plays an important role from the point of view of the diagonalization and, obviously, there is a minimum dimension below of which is not possible to go. With reference to Figure 4.4(a), a diagonalization performed on a grid of 2400×2400 points (corresponding, approximatively, to the red box) gives a spectrum that is correct only for the first highest eigenvalues (the first 59 eigenvalues), for $k > 59$ discrepancies between the 4800×4800 become evident, as it can be appreciated in Figure 4.5.

The reason is easy to understand. In fact, over the 2400×2400-grid, the zones where there is a residual information about the phase-matching (boxed in green) are neglected. The progressive enlarging of the dimension of $\mathcal{L}$ leads to successive corrections which make converge the numerical spectrum toward the exact solution obtained for an infinite space. In the case presented of a 4800×4800 coupling matrix discrepancies are almost negligible and affect eigenvalues for very high k.

In the light of these observations, we performed numerical diagonalization over a grid of 4800×4800 points and with a scaling parameter of $c = 1000$. The results of such numerical diagonalization are presented in Figures 4.6 and 4.7 where the spectrum of eigenvalues and the four eigenvectors, corresponding to the four highest $|\Lambda_k|$, have been compared with the analytical results obtained from (4.60), (4.62) and (4.63). The comparison of the analytical eigenspectrum (represented by red dots) with the corresponding numerical solution (in blue stars) - that we consider the "exact" solution in the sense previously explained - evidences a good agreement between the two curves. In particular the highest eigenvalue, which is the one connected to the SPOPO threshold, is $\Lambda_{\text{analyt},0} \simeq 269.11$ from Eq. (4.60) and $\Lambda_{\text{num},0} \simeq 271,71$ from the numerical diagonalization, with a relative error of about the 0.1% respect to the true value $\Lambda_0 \equiv \Lambda_{\text{num},0}$. However, from Figure 4.6, there is a substantial difference between the analytical spectrum and the numerical one that presents little deviations from the geometric progression. The reason resides in

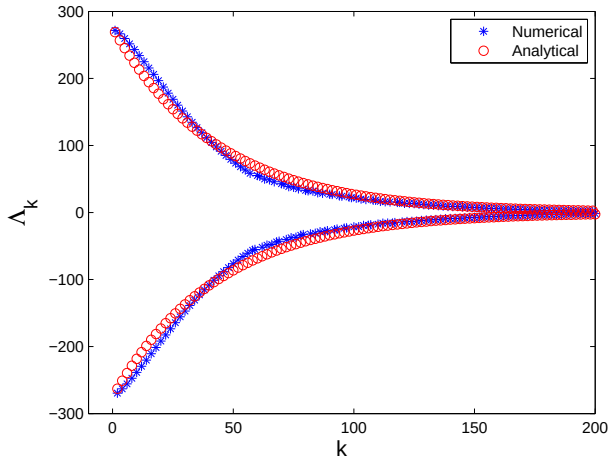

Figure 4.6: Comparison between the numerical and analytical solutions of the eigenspectrum.

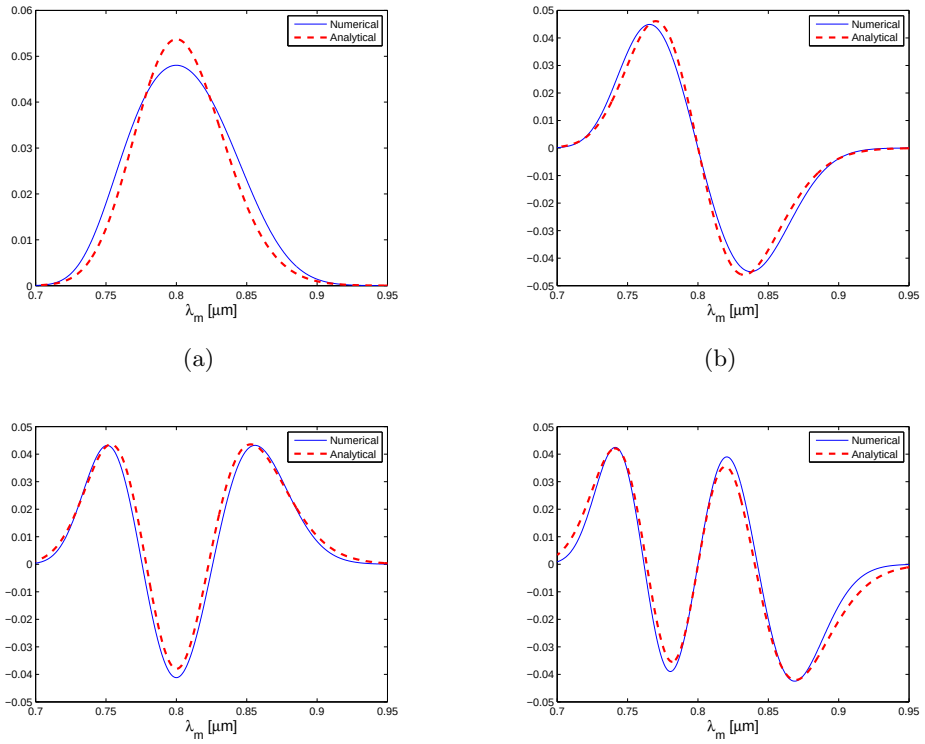

Figure 4.7: Comparison between the numerical and analytical solutions of the first four eigenvectors.

the fact that, even if the parameters respect the bounds for the Gaussian approximation, the coupling matrix $\mathcal{L}$ cannot be completely considered as the Gaussian (4.44) because the presence of the small oscillations (boxed in green in Figure 4.4(a)) due to the "sinc" modulation. The maximum relative error does not exceeds 10% for $k < 50$, while in the interval $50 < k < 200$ does not exceeds the 30%. For $k > 200$ the discrepancy between

the numerical and the analytical curves can exceed the 30%, mainly for two reasons. The first is ascribed to the fact that the analytical curve does not faithfully represent the true solution and the relative error becomes more and more significative since for $k > 200$ the eigenvalues become small numbers as they converge to 0 for $k \to \infty$. The second reason resides in the fact that even the numerical solution cannot be considered as the correct one since we diagonalized $\mathcal{L}$ in a truncated space. However, since we assumed a temporal dependence of the type $\mathrm{e}^{-\Lambda_k t}$ for the solutions of eq. (4.4), this is not a great problem because on a dynamical point of view the evolution of the intracavity field, below threshold, will be steered by the solutions (i.e. the eigenvectors) connected to the greatest values of $|\Lambda_k|$, while for small $|\Lambda_k|$ the dynamics of the corresponding solution is less important respect to the global behavior of the system. This last remark, therefore, lay in emphasis the role of the diagonalization of the matrix $\mathcal{L}$ in simplifying the description of the dynamics of a system, such a SPOPO, where many modes evolves and interact each other. In fact, since not all the eigenmodes are equally important in the evolution of the system, from a set of about 10^5 modes generated by parametric interaction, it is possible to extract a finite set of eigenmodes (or frequency combs). In the next chapter we will see, not only, that these objects embody almost all the dynamical properties of a SPOPO but also all the quantum effects generated by the intracavity parametric interaction.

The eigenvectors $\overrightarrow{L}_k$ (for $k = 0, 1, 2, 3$) connected to the four highest $|\Lambda_k|$, traced in Figure 4.7 with the blue line, are the solutions obtained form the numerical diagonalization of $\mathcal{L}$. Let's note that the eigenvectors $\overrightarrow{L}_k$ should appear as combs made up by a discrete number of frequencies while, in the figure, they have been traced by means of a continuous line which represents their envelopes.

As expected, since we are considering a parametrical situation that satisfies the conditions (4.56) and (4.57), the eigenvectors are close to Hermite-Gauss polynomials given by eq. (4.63). In fact, the numerical solution is fitted by a Gauss-Hermite function having $N_\mathrm{s} \simeq 236 \times 10^3$ and the scalar product $\overrightarrow{L}_0 \cdot \overrightarrow{GH}_0(N_\mathrm{s} = 236.88 \times 10^3) \simeq 0.9991$ can be considered as an indicator of the quality of the fit ($GH_{k,m}$ corresponds to polynomials (4.63)). Keeping in mind that $\tau_\mathrm{s} = (N_\mathrm{s}\Omega)^{-1}$, the time duration of the generated signal pulse is about $\tau_\mathrm{s} \simeq 11.1\,\mathrm{fs}$ which is an order of magnitude smaller than the pump pulse width. In fact, from eq. (4.65), we expect a pulse compression of the signal field since τ_2 is much smaller than τ_p and τ_1. From a physical point of view, this effect is directly connected to the fact that the parametric conversion has a broadband gain proportional to the spectral width Δ_2 that is about one order of magnitude greater than the pump bandwidth Δ_p.

On the other side, the analytical solutions are obtained from eq. (4.63) once calculated the signal pulse width $\tau_\mathrm{s} \simeq 9.3\,\mathrm{fs}$ from the crystal coherences τ_1 and τ_2 given by eqs. (4.53) and (4.54) (respectively 12.25 fs and 1.17 fs). Notice that these coherences are expressed in terms of the crystal dispersion parameters k' and k'' when the Gaussian approximation of the coupling matrix is considered. They have been traced in Figure 4.7 with the dotted red line. In particular, the scalar product with the numerical solution amounts to about 0.9954.

As shown in Section 4.1, from a dynamical point of view, when all parameters are real, in particular when the pump field is assumed to be not chirped, two kind of solutions, $S^{(+)}_{k,m}$ and $S^{(-)}_{k,m}$, of eq. (4.4) are admitted according eqs. (4.19). For a given k and assuming for a

while that $\Lambda_k > 0$, the solution $S^{(+)}_{k,m}$ will attain its threshold/amplification (i.e. $\lambda^{(+)}_k \geq 0$) when $\sigma\Lambda_k \geq 1$. At the same time, the solution $S^{(-)}_{k,m}$, in quadrature with the previous one, cannot attain its threshold/amplification (i.e. $\lambda^{(-)}_k \geq 0$) since the condition $\sigma\Lambda_k \geq -1$ is not satisfied. Conversely, the opposite situation occurs when $\Lambda_k < 0$. Since the spectrum of eigenvalues is approximatively an oscillating geometric progression, the first mode that will attain the oscillation, by increasing from 0 the pump power, is $S^{(+)}_{0,m}$ whose threshold coincides with P_{th} (see eq. (4.20)). Above this value the condition for oscillation will be attained by the other solutions in the order $\overrightarrow{S}^{(-)}_1, \overrightarrow{S}^{(+)}_2, \ldots, \overrightarrow{S}^{(-)}_{2k-1}, \overrightarrow{S}^{(+)}_{2k}, \ldots$. However, as for lasers, the first mode that attains the threshold kills the oscillations of all the others and it is the only one to be amplified for pump powers above P_{th}. In the ambit of a below threshold theory, all the solutions are dumped, nevertheless these properties will be reveal important from quantum point of view. From eq. (4.20), a threshold of $W_{\text{th}} = 4.1\,\text{mW}$ is readily obtained for the corresponding eigenvalue $\Lambda_0 = 271.71$ in the case of ring cavity singly resonant SPOPO with $T_s = 0.01$ and a beam waist of $70\,\mu\text{m}$.

Non-critically phase-matched BIBO

In the case of non critically phase-matched BIBO, at room temperature, the pump field must be tuned at a wavelength of $0.589\,\mu\text{m}$. In this situation, eqs. (4.56) and (4.57) reads $l > 0.1\,\text{mm}$ and $\tau_p > 12\,\text{fs}$. Even if the condition on l is only just verified, also this parametrical situation satisfies the Gaussian approximation . We will give later an explication showing that, for such situation, the bound on the crystal thickness can be not strictly observed for particular values of the pump pulse duration in order to still consider the Gaussian approximation valid. The results obtained from the diagonalization of the coupling matrix shows a good agreement with the analytical solutions as discussed in the previous parametrical case and does not represent a new situation. For the spectrum of eigenvalues, the numerical diagonalization of $\mathcal{L}$ gives $\Lambda_0 \simeq 272.9$ that have to be compared with the analytical result $\Lambda_0 \simeq 270.1$, with a relative error of about the 1%. Therefore, in the case of a ring cavity singly resonant SPOPO with $T_s = 0.01$ and a beam of $70\,\mu\text{m}$, a threshold of $4.1\,\text{mW}$ is obtained. For what concerns the eigenvectors, the agreement between the numerical and the analytical solutions is quantified by the scalar product which amounts to 0.9950 while, from eq. (4.65), the signal pulse duration is about $\tau_s \simeq 12.1\,\text{fs}$.

Critically phase-matched KNbO3

For the $KNbO_3$ crystal critically phase-matched at a pump wavelength of $0.4\,\mu\text{m}$ discussed in Section 4.3.1 the conditions (4.56) and (4.57) reads $l > 0.4\,\text{mm}$ and $\tau_p > 13.3\,\text{fs}$. While the condition on the pump pulse duration is largely satisfied, since we are considering a $0.1\,\text{mm}$-thick crystal, the bound on l is violated. A priori, then, we would expect that the numerical diagonalization of $\mathcal{L}$ leads to results that are in disagreement with Eqs. (4.59) and (4.63). In fact, observing the phase-matching matrix, shown in Figure 4.8(a), is characterized by coherences $\tau_1 \simeq 4.2\,\text{fs}$ and $\tau_2 \simeq 1.0\,\text{fs}$, obtained by using the dispersion parameters of the crystal in (4.76) and (4.77). Since τ_1 is about one order of magnitude smaller than the cases previously shown, in the frequency domain this is translated in a spectral width Δ_1 that is one order of magnitude bigger (about $2.38 \times 10^{14}\,\text{s}^{-1}$). On

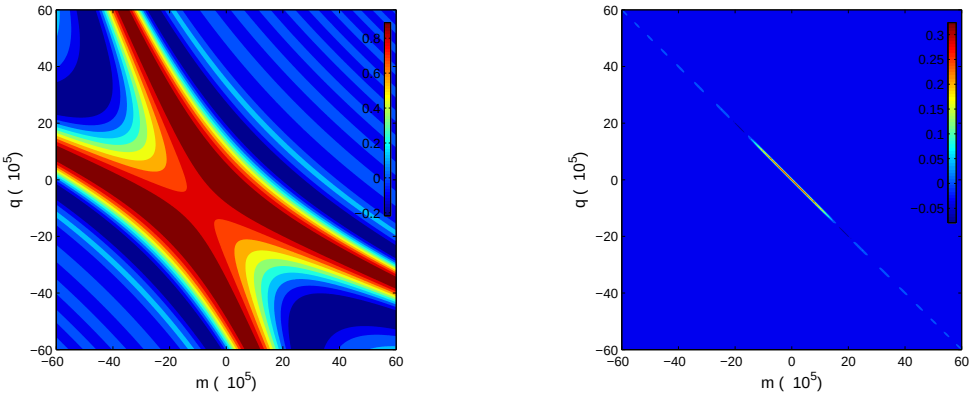

(a) (b)

Figure 4.8: Critically phase-matched $KNbO_3$ of 0.1 mm of thickness, in a ring cavity of 4 m, pumped at 0.4 μm by a c.w. train of 100 fs pulses. Appearance of the phase-matching matrix (a) and of the coupling matrix $\mathcal{L}$ (b) in the frequency representation.

the other hand, the distance d between the branches of the hyperbola evaluated along the direction $m - q = 0$, in the frequency domain, is about $6.84 \times 10^{14}\,\mathrm{s}^{-1}$. In order the Gaussian approximation to be valid, we imposed the condition that $d \gtrsim 10\Delta_1$ that in this situation is not satisfied. However, this situation is not dramatic since, on the other hand, the pump bandwidth $\Delta_p \simeq 10^{13}\,\mathrm{s}^{-1}$ is one order of magnitude smaller than Δ_1 and thus the energy conservation constraint selects only a small slice around the phase-matched principal maximum (corresponding to $m = q = 0$), without including "sinc" oscillations or the second branch of the hyperbole that would play a role in deviations from the Gaussian limit. Resulting from the interplay between the phase-matching condition and the energy conservation, the coupling matrix, shown in Figure 4.8(b), consists in a bell-shaped function centered in $m = q = 0$ that still can be thought as Gaussian function similarly to the previous cases, therefore we expect that the numerical solutions are in accord with the analytical ones. The spectrum of the eigenvalues has been traced in Figure 4.9, where the numerical and the analytical solutions are compared. Like in the previous cases the agreement is confirmed by the fact that the relative error between the numerical and analytical eigenvalues does not exceed the 10% for $k < 50$ and it is less than the 30% for $k < 200$ while for the maximum eigenvalue the relative error is less then the 1%. In particular we have $\Lambda_0 \simeq 273.37$ which gives a threshold of $W_{\mathrm{th}} \simeq 0.44\,\mathrm{mW}$ for a ring cavity singly resonant SPOPO with $T_{\mathrm{s}} = 0.01$ and a beam waist of 70 μm. In Figure 4.10 are compared, instead, the eigenvectors obtained numerically and analytically. The compatibility of the two results is confirmed by a scalar product of about 0.9906, which, therefore, puts into evidence the fact that the solutions obtained in the Gaussian approximation are able to describe the numerical results in a parametrical situation that seems to violate the condition on the crystal thickness. Introducing the values of the crystal coherences τ_1 and τ_2 in Eq. (4.65), the signal pulse width results to be about $\tau_{\mathrm{s}} \simeq 10.0\,\mathrm{fs}$.

4.3.3 Non-Gaussian configurations

We have seen in the previous subsection that, for parametrical configurations satisfying the bounds (4.56) and (4.57), the analytical solutions (4.59) and (4.63) describe with enough accuracy the results obtained from the numerical diagonalization of the coupling matrix. However, in particular conditions (for example for special choices of the nonlinearities or of the phase-matching conditions as it is the case of the critically phase-matched $KNbO_3$), parametrical setups violating these bounds could exist. In such cases the efficacy of the analytical prediction rapidly run out and the numerical diagonalization is the only support. In a first instance, then, understanding how and how much such predictions deviate from the "true" solutions is an important issue. Nevertheless, we will see in the next chapter that configurations violating the Gaussian limits are even desirable for certain applications. Therefore, learning to master the parameters at stake in order to enhance the wanted effects becomes a critical point. In the case of the $KNbO_3$ the choice of the phase-matching conditions leads to a violation of the condition (4.56) on the crystal thickness that, however, reveals to be not critical since the pump bandwidth is small enough to prevent deviations from Gaussian solutions. Then, the condition (4.57) on the pump pulse duration results to be a stronger constraint. Moreover, the violation of the Gaussian limits by means of the good choice of the nonlinearities or the phase-matching operation may results too difficult or too tough to be properly mastered and it is clear that such way should be engaged as "extrema ratio". On the other hand, acting over the crystal length l or the pump pulse duration τ_p represent a more flexible manner to master the "Gaussianity" of the problem also in view of an experimental implementation.

Critically phase-matched BIBO with $l = 5$mm

For the parametrical situation illustrated above, where a critically phase-matched 0.1 mm-thick BIBO crystal is pumped at 0.4 μm, the bound (4.57) reads $\tau_p \gtrsim 40$ fs which is largely verified for a c.w. train of 100 fs pulses. In fact the numerical solutions obtained from the diagonalization of $\mathcal{L}$ results to be well described by Eqs. (4.59) and (4.63). However,

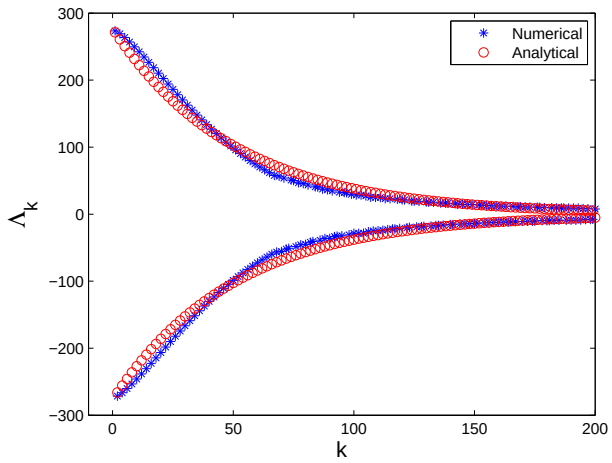

Figure 4.9: Comparison between the numerical and analytical solutions of the eigenspectrum.

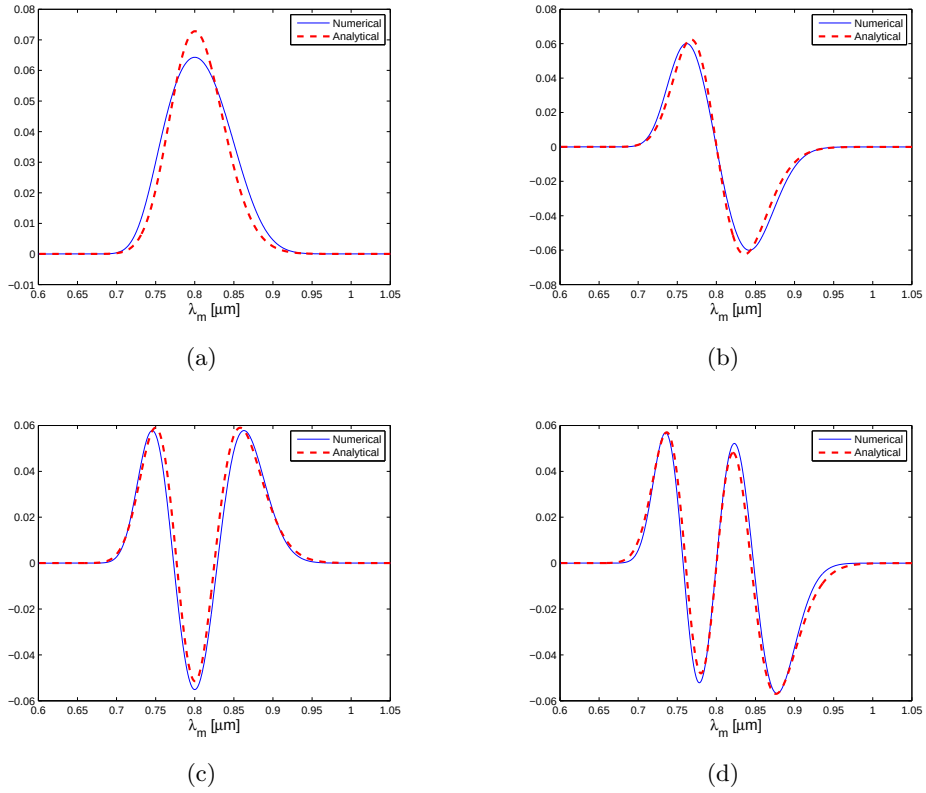

Figure 4.10: Comparison between the numerical and analytical solutions of the first four eigenvectors.

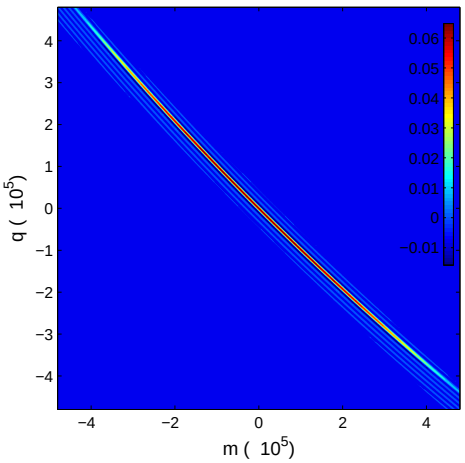

Figure 4.11: Appearance of $\mathcal{L}$ matrix in the case of critically phase-matched BIBO of 5 mm of thickness, in a ring cavity of 4 m, pumped at 0.4 μm by a c.w. train of 100 fs pulses.

from Eq. (4.57), the choice of a thicker crystal permits to violate such limit. A strongly non-Gaussian configuration can be obtained in correspondence of a 5 mm-thick crystal. In such case the Gaussian limit for the pump pulse duration reads $\tau_p \gtrsim 1.94 \times 10^{-12}$ s, which is violated for 100 fs pump pulses. The coupling matrix corresponding to this situation is illustrated in Figure 4.11.

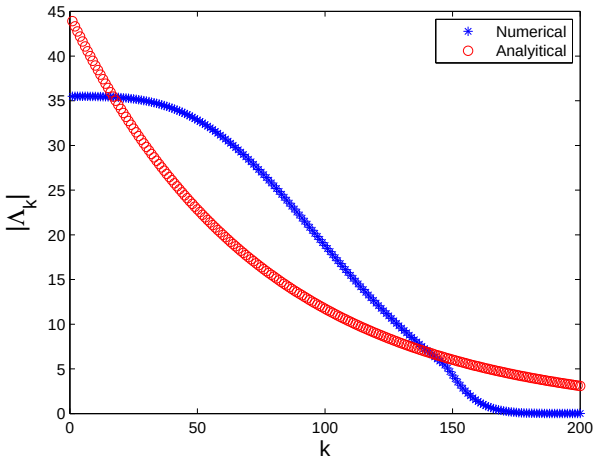

Figure 4.12: Comparison between the numerical and analytical solutions of the absolute value of the eigenspectrum.

In terms of frequencies, a non-Gaussian configuration occurs when the pump spectral width Δ_p is sufficiently greater than the bandwidth Δ_1 of the phase-matching function. In this case, indeed, the pump is large enough to select not only the main peak of the cardinal sinus modulation of the phase-matching matrix, but also the secondary maxima, as one could easily realize by comparing Figure 4.11 with the Gaussian case represented in Figure 4.4(a). This has an important consequence for what concerns the eigenvectors and eigenvalues of $\mathcal{L}$ that have been reported in Figures 4.12 and 4.13. In Figure 4.12, the spectrum of the eigenvalues obtained from the analytical solution (4.59) (red circles) shows a great discrepancy with the eigenvalues obtained from numerical diagonalization of $\mathcal{L}$. In particular, the eigenvalues flatten around the critical value $\Lambda_0 \simeq 36$ in the first part of the spectrum (for $k < 50$), while the Gaussian approximation predicts always a geometric progression-like behavior with a critical eigenvalue $\Lambda_{\text{Gauss},0} \simeq 44$. On the other hand, in Figure 4.13, the eigenvectors retrieved in the Gaussian approximation (4.63) do no more fit the numerical solutions which still preserve a shape similar to Gauss-Hermite functions, but, nevertheless, are affected by a small modulation of the spectral amplitude. From a physical point of view, the Gaussian limit corresponds to the optimal circumstance where the length of the nonlinear crystal is sufficiently small to prevent the pump and signal pulses from spatially separate inside the crystal because of the difference between their group velocities. In other terms, this amount to require the temporal walk-off, between pump and signal pulses, be not greater than the pump temporal width τ_p. In this way, all the pump energy is optimally transferred, inside the crystal, towards the signal pulse. On the contrary, when we are considering a non-Gaussian configuration, the overlapping between the pump and signal pulses is not perfect all along the crystal, thus preventing an optimal energy exchange between the two fields. At the light of this interpretation, it is quite natural, then, to expect threshold that is higher (and consequently a Λ_0 which is lower) than the prediction of the Gaussian approach. Therefore, if the temporal walk-off is big enough, we can manage to approach the eigenvalues of several eigenmodes simply because we are making energetically disadvantageous the coupling between the pump and signal field.

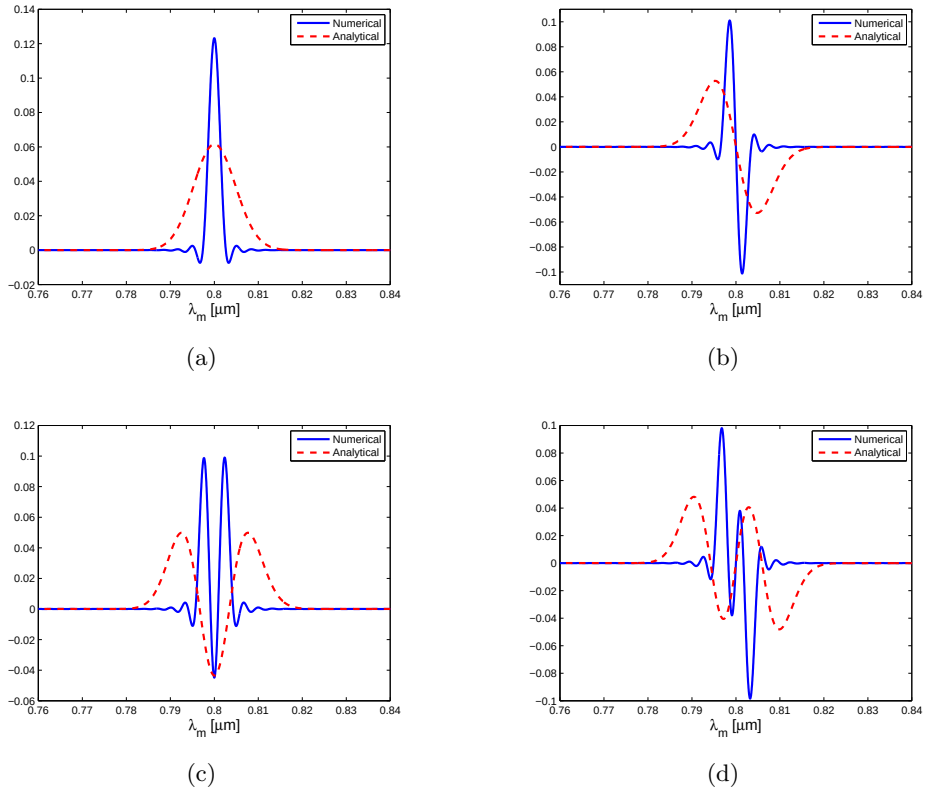

Figure 4.13: Comparison between the numerical and analytical solutions of the first four eigenvectors.

We can explain this result in different way, too. Let's notice that the critical eigenvalue obtained by means of the Gaussian approach (see Eq. (4.60)) depends on the number of modes in the pump pulse N_{p}. Since we observed that, beyond the Gaussian limit, the spectral width of the pump field is greater than the phase-matching bandwidth Δ_1, not all the N_{p} pump modes are equally phase-matched and, then, not all can transfer energy towards the signal modes. We see, therefore, that this picture confirms a lower threshold (or higher Λ_0) for a non-Gaussian configuration. Moreover, we think that the modulation of the spectral amplitude of the eigenvectors of $\mathcal{L}$ can be equally be ascribed to the cardinal sinus modulation of the phase-matching matrix, which is impressed on the signal modes by means of the not equally phase-matched pump modes. However, we have not yet completely understood this mechanism, which deserves a more accurate study.

The dependence on the crystal thickness l

The passage from a Gaussian to a non-Gaussian regime can be performed, then, simply by increasing the crystal length in order to induce a temporal walk-off between the pump and signal pulses. It is interesting, hence, to study how the threshold behaves as a function of l. A priori, the analytical results obtained in the Gaussian approximation when the condition $\tau_{\mathrm{p}} \ll |k'_{\mathrm{p}} - k'_{\mathrm{s}}|l$ is violated are not supposed to be in agreement with the numerical solutions. Indeed, in the situation considered above, with $l = 5$mm, the value of Λ_0 obtained by the analytical approach is in complete disagreement with the numerical value. Nevertheless,

let's consider Eq. (4.60) in the limit of very large l. Since from Eq. (4.53), in such case, $\tau_1 \gg \tau_\mathrm{p}$, then Λ_0 asymptotically converges to:

$$\Lambda_0 \simeq \pi^{1/4}\sqrt{20N_\mathrm{p}}\frac{\tau_\mathrm{p}}{|k'_\mathrm{p}-k'_\mathrm{s}|}\frac{1}{l}. \tag{4.78}$$

This expression suggests that the product $\Lambda_0\, l$ is constant for values of l compatible with a non-Gaussian regime. In Figure 4.14, then, we report the values of this product as a function of the crystal thickness. For $l \lesssim 1$mm the analytical solution, as expected, is in good agreement with the numerical one, while for greater thicknesses the discrepancy is significative. This is an expected results, since, the analytical solution for the critical eigenvalue has not validity when the condition (4.57) is violated. However, the fact that also the analytical solution reaches asymptotically, for increasing l, a plateau suggests a $1/l$-like behavior of Λ_0. A possible interpretation, in the light of what we have observed above, is that the number of pump modes actually involved is smaller than the nominal value N_p, in agreement to the observation that, when the pump pulse width is smaller than τ_1 (or equivalently $\Delta_\mathrm{p} \gg \Delta_1$) not all the pump modes are phase matched.

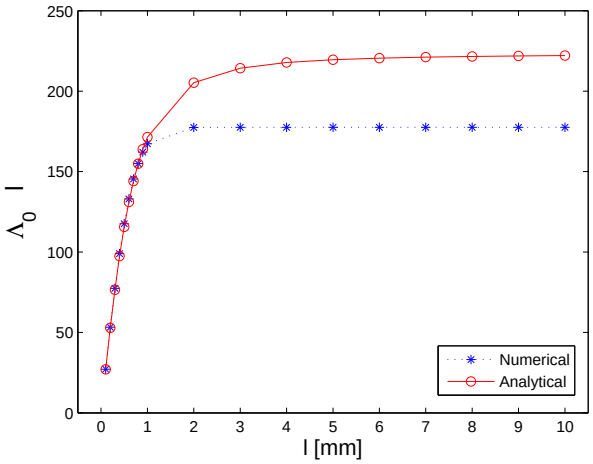

Figure 4.14: Dependence of the product $\Lambda_0 \times l$ on the crystal length l for numerical and analytical solutions.

4.4 SPOPO injected with a chirped pump field

In Section 4.1, the assumption of real dynamical constants and the property of the coupling matrix to be self-adjoint lead to two sets of solutions $\{\vec{S}_k^{(+)}, \vec{S}_k^{(-)}\}$, of Eq. (4.4), satisfying conditions (4.19). In general, these conditions do not hold any longer when γ_s, γ_p, σ and $\mathcal{L}$ are not real. In particular this situation occurs when $\mathcal{L}$ is complex, usually in presence of frequency dependent pump field phase.

The chirp is usually understood as the time dependence of its instantaneous frequency. For example, a pulse with a Gaussian envelope and quadratic temporal phase:

$$E(t) = |E(t)|\mathrm{e}^{i\Phi(t)} = E_0\mathrm{e}^{-at^2+ibt^2}, \tag{4.79}$$

is associated with an instantaneous frequency which varies linearly in time:

$$\omega(t) = \frac{\partial \Phi}{\partial t} = 2bt. \tag{4.80}$$

Intrinsically connected to a nontrivial dependence of the spectral phase $\phi(\omega)$, defined as:

$$E(\omega) = |E(\omega)|\mathrm{e}^{i\phi(\omega)}, \tag{4.81}$$

on the frequency components ω, in the Fourier space, the chirp can be explained by the presence of a dispersion of the group velocity which causes different delays for each spectral components. The expansion of the spectral phase around the phase-matched frequency $2\omega_0$ gives:

$$\varphi(\omega_{\mathrm{p},m}) = \varphi(\omega_{\mathrm{p},0}) + \left.\frac{\partial \varphi}{\partial \omega}\right|_{\omega=2\omega_0} (\omega_{\mathrm{p},m} - 2\omega_0) + \frac{1}{2}\left.\frac{\partial^2 \varphi}{\partial \omega^2}\right|_{\omega=2\omega_0} (\omega_{\mathrm{p},m} - 2\omega_0)^2 + \dots, \tag{4.82}$$

that, after Eq. (3.36) and under the assumption that the pump field is resonant with the OPO cavity (i.e. $\Delta \simeq 0$), can be rewritten as:

$$\varphi(\omega_{\mathrm{p},m}) = \phi_0 + \phi_1\, m + \phi_2\, m^2 + \dots, \tag{4.83}$$

where $\phi_0 = \varphi(\omega_{\mathrm{p},0})$, $\phi_1 = \Omega \left.\frac{\partial \varphi}{\partial \omega}\right|_{2\omega_0}$ and $\phi_2 = \frac{1}{2}\Omega^2 \left.\frac{\partial \varphi}{\partial \omega}\right|_{2\omega_0}$.

Arresting the expansion up to the second order and neglecting the factor ϕ_1 since it represents a simple time delay, the pump field defined in Eq. (3.5) can be cast as:

$$E_{\mathrm{ext}}(t) = i\sqrt{\frac{P}{2\varepsilon_0 c}} \sum_m \alpha_m e^{-i(2\omega_0 + m\Omega_{\mathrm{p}})t} \mathrm{e}^{i\phi_2\, m^2} + \text{c.c.}. \tag{4.84}$$

The quadratic dependence of the field phase on $\omega_{\mathrm{p},m}$ corresponds to a group delay

$$\tau(\omega_{\mathrm{p},m}) = \left.\frac{\partial \varphi}{\partial \omega}\right|_{2\omega_0} \simeq \phi_2\, (\omega_{\mathrm{p},m} - 2\omega_0) \tag{4.85}$$

linearly varying with the spectral components also known as second-order chirping. From Eq. (4.84) directly descends the fact that

$$\boxed{\mathcal{L}^{\mathrm{ch}}_{m,q} = \mathcal{L}_{m,q}\mathrm{e}^{i\phi_2\,(m+q)^2}} \tag{4.86}$$

is a complex matrix. In such case the classical couterpart of the linearized Langevin equations for the resonant signal field are (see Eq. (4.4)):

$$\frac{d}{dt}\begin{pmatrix} \mathbf{s} \\ \mathbf{s}^* \end{pmatrix} = -\gamma_{\mathrm{s}} \left(I - \sigma \tilde{\mathcal{L}}^{\mathrm{ch}}\right) \begin{pmatrix} \mathbf{s} \\ \mathbf{s}^* \end{pmatrix}, \tag{4.87}$$

where $\mathbf{s}$ is the vector defined in Eq. (4.3) and:

$$\tilde{\mathcal{L}}^{\mathrm{ch}} = \begin{pmatrix} \mathbf{0} & \mathcal{L}^{\mathrm{ch}}_{m,q} \\ \mathcal{L}^{\mathrm{ch}}_{m,q}{}^* & \mathbf{0} \end{pmatrix}, \tag{4.88}$$

which is, still, a self-adjoint matrix. Then, all its eigenvalues Λ, are real numbers. As for its eigenvectors Ψ, denoting them as:

$$\Psi \equiv \begin{pmatrix} \vec{L} \\ \vec{L}' \end{pmatrix}, \tag{4.89}$$

they verify:

$$\mathcal{L}^{\mathrm{ch}} \cdot \vec{L}' = \Lambda \vec{L}, \tag{4.90}$$

$$\mathcal{L}^{\mathrm{ch}\,*} \cdot \vec{L} = \Lambda \vec{L}'. \tag{4.91}$$

Since Λ is real, by complex conjugating Eq. (4.90) and comparing with Eq. (4.91), we find that:

$$\vec{L}' = \vec{L}^*, \tag{4.92}$$

and relations (4.90) and (4.91) becomes:

$$\mathcal{L}^{\mathrm{ch}} \cdot \vec{L}^* = \Lambda \vec{L}, \tag{4.93}$$

$$\mathcal{L}^{\mathrm{ch}\,*} \cdot \vec{L} = \Lambda \vec{L}^*. \tag{4.94}$$

Multiplying by $-i$ Eq. (4.93) and by i Eq. (4.94), we obtain the following:

$$\mathcal{L}^{\mathrm{ch}} \cdot \left(-i\vec{L}\right) = (-\Lambda)\left(i\vec{L}\right), \tag{4.95}$$

$$\mathcal{L}^{\mathrm{ch}\,*} \cdot \left(i\vec{L}\right) = (-\Lambda)\left(-i\vec{L}^*\right), \tag{4.96}$$

from which it follows that if $\Psi = \mathrm{col}\left(\vec{L}, \vec{L}^*\right)$ is the eigenvector of $\widetilde{\mathcal{L}}$ with eigenvalue Λ, then, $\Psi' = \mathrm{col}\left(i\vec{L}, -i\vec{L}^*\right)$ is eigenvector with eigenvalue $\Lambda' = -\Lambda$ as well. This result is equivalent to the one obtained for the real case in Section 4.1, since two eigenvectors in quadrature, $\Psi_k^{(+)}$ and $\Psi_k^{(-)}$, correspond to a positive Λ_k and a negative $-\Lambda_k$. However, if in the real case the diagonalization of $\widetilde{\mathcal{L}}$ is directly related to the diagonalization of one of its blocks (i.e. $\mathcal{L}^{\mathrm{ch}}$), a priori this is not possible for a complex $\widetilde{\mathcal{L}}$. Anyway, provided that $\left(\vec{L}, \vec{L}^*\right)$ is an eigenvector of $\mathcal{L}^{\mathrm{ch}}$, by multiplying Eq. (4.94) from the left by $\mathcal{L}^{\mathrm{ch}}$ and introducing Eq. (4.93), a simplification can be achieved noting that the following relation:

$$\left(\mathcal{L}^{\mathrm{ch}} \cdot \mathcal{L}^{\mathrm{ch}\,*}\right) \cdot \vec{L} = \Lambda^2 \vec{L} \tag{4.97}$$

permits to get the eigenvectors and the eigenvalues of $\widetilde{\mathcal{L}}$ apart from a global phase. Let's denote with $\vec{L}_{\mathrm{aux}}$ the eigenvectors obtained from Eq. (4.97) (with eigenvalue Λ^2) and by $\vec{L} = \mathrm{e}^{i\eta}\vec{L}_{\mathrm{aux}}$ the eigenvector of (4.93) and (4.94) with a phase η. In order to determine η, we make use of Eq. (4.93):

$$\mathcal{L}^{\mathrm{ch}} \cdot \left(\mathrm{e}^{i\eta}\vec{L}_{\mathrm{aux}}\right) = \Lambda\left(\mathrm{e}^{i\eta}\vec{L}_{\mathrm{aux}}\right), \tag{4.98}$$

which, written in terms of its components, leads to:

$$\Lambda^{-1}\frac{\left(\mathcal{L}^{\mathrm{ch}} \cdot \vec{L}^*_{\mathrm{aux}}\right)_m}{\left(\vec{L}^*_{\mathrm{aux}}\right)_m} = \mathrm{e}^{2i\eta}. \tag{4.99}$$

Since Λ is determined from Eq. (4.97) up to a sign, two values for the phase η, differing by $\pi/2$, are obtained, in accordance with the fact that the eigenspectrum of $\widetilde{\mathcal{L}}$ is made up by couples of eigenvalues $\Lambda_\pm = \pm\sqrt{\Lambda^2}$. Then we obtain:

$$\Lambda_\pm^{-1}\frac{\left(\mathcal{L}^{\mathrm{ch}} \cdot \vec{L}^*_{\mathrm{aux}}\right)_m}{\left(\vec{L}^*_{\mathrm{aux}}\right)_m} = \mathrm{e}^{2i\eta_\pm}, \tag{4.100}$$

with $\eta_- = \eta_+ + \pi/2$, which finally determine the searched eigenvectors.

Vectors $\vec{L}$ and $\vec{L}^*$ are not eigenvectors of the matrix $\widetilde{\mathcal{L}}$, hence their orthogonality must be studied. We can prove the following:

Proposition 5 *Given any two eigenvectors Ψ_k^+ and Ψ_l^+ (or Ψ_k^- and Ψ_l^-) with eigenvalues Λ_k^+ and Λ_l^+ (or Λ_k^- and Λ_l^-), then:*

$$\vec{L}_k^* \cdot \vec{L}_l = \delta_{k,l}. \tag{4.101}$$

Writing Eq. (4.93) in terms of its components and using the symmetry $\mathcal{L}^{\text{ch}}_{m,q} = \mathcal{L}^{\text{ch}}_{q,m}$, we obtain:

$$\sum_q \mathcal{L}^{\text{ch}}_{m,q} L^*_{k,q} = \sum_q L^*_{k,q} \mathcal{L}^{\text{ch}}_{q,m} = \Lambda_k L_{k,m}, \tag{4.102}$$

which, in vector form, reads:

$$\vec{L}_k^* \cdot \mathcal{L}^{\text{ch}} = \Lambda_k \vec{L}_k. \tag{4.103}$$

By computing the quantity $\vec{L}_l^* \cdot \mathcal{L}^{\text{ch}} \cdot \vec{L}_k^*$ and using alternatively (4.93) and (4.103), we obtain:

$$\Lambda_k \vec{L}_l^* \cdot \vec{L}_k = \Lambda_l \vec{L}_l \cdot \vec{L}_k^*. \tag{4.104}$$

Since Λ_k and Λ_l are real, the phase of $\vec{L}_l^* \cdot \vec{L}_k$ and $\vec{L}_l \cdot \vec{L}_k^*$ must coincide, but, as they are complex-conjugate, both must be real and the equal. Thus we obtain:

$$(\Lambda_k - \Lambda_l)\, \vec{L}_l^* \cdot \vec{L}_k = 0, \tag{4.105}$$

from which directly follows (4.101). The relation (4.105) can result problematic when $\Lambda_k = \Lambda_l$, with $k \neq l$, in which case the subspace spanned by the two vectors is degenerate and on can find suitable new vectors satisfying Eq. (4.101). However, such situation is very exotic since in usual experimental situations the eigenspectrum is never degenerate (as we have seen in Section 4.3). In the following we will show a second property that will be useful in the next chapter.

Proposition 6 *Given a complete set of eigenvectors of $\widetilde{\mathcal{L}}$, it is possible to write:*

$$\mathcal{L}_{m,q} = \sum_k 2\Lambda_k L_{k,m} L_{k,q}, \tag{4.106}$$

$$\mathcal{L}^*_{m,q} = \sum_k 2\Lambda_k L^*_{k,m} L^*_{k,q}. \tag{4.107}$$

This proposition follows directly from the spectral theorem. In fact, for a given set of eigenvectors $\{\Psi_k^{(+)}, \Psi_k^{(-)}\}$ with eigenvalues $\Lambda_\pm$, the matrix $\widetilde{\mathcal{L}}$ can be written as:

$$\widetilde{\mathcal{L}} = \sum_k \Lambda_k \Psi_k^{(+)} \otimes \left(\Psi_k^{(+)}\right)^\dagger + \sum_k (-\Lambda_k)\, \Psi_k^{(-)} \otimes \left(\Psi_k^{(-)}\right)^\dagger, \tag{4.108}$$

which becomes:

$$\begin{aligned} \widetilde{\mathcal{L}} &= \sum_k \Lambda_k \left\{ \begin{pmatrix} \vec{L}_k \\ \vec{L}_k^* \end{pmatrix} \otimes \begin{pmatrix} \vec{L}_k^\dagger, & \vec{L}_k^{*\,\dagger} \end{pmatrix} - \begin{pmatrix} i\vec{L}_k \\ -i\vec{L}_k^* \end{pmatrix} \otimes \begin{pmatrix} -i\vec{L}_k^\dagger, & i\,\vec{L}_k^{*\,\dagger} \end{pmatrix} \right\} \\ &= \sum_k 2\Lambda_k \begin{pmatrix} \mathbf{0} & \vec{L}_k \otimes \vec{L}_k^{*\,\dagger} \\ \vec{L}_k^* \otimes \vec{L}_k^\dagger & \mathbf{0} \end{pmatrix}, \end{aligned} \tag{4.109}$$

and straightforwardly demonstrates the proposition.

The properties we have shown here are useful for characterizing the classical dynamics of a SPOPO in presence of a chirped field by means of a decomposition over non monochromatic modes, similarly to the analysis we discussed in the previous sections in the case of not-chirped pump field. Moreover, from a quantum point of view, Proposition 6 is necessary for a complete equivalence of the modal-decomposition (see Section 5.1.1) of the signal output field with not-chirped cases. However, in this thesis we will not present the results for this case, which will be the object of future works.

CHAPTER 5

Quantum properties of SPOPO below threshold

Contents

In the previous chapter we have studied the classical behavior of the SPOPO intracavity field mean values in the below threshold regime. Its linear dynamics can be decomposed into a discrete basis of independently evolving frequency combs. The threshold of the device corresponds to the threshold of the mode with the faster dynamics and that, consequently, will attain the oscillation faster than the others. To some extent, therefore, from a classical point of view, the dynamics of the other modes has less importance. On the other hand, for a complete quantum characterization of the output field, below threshold, as announced in Section 2.2, we have to consider global quantum noise properties of whole the set of modes. We discover, then, that the SPOPO dynamics is formally equivalent to the dynamics of N single-mode OPOs, squeezing the noise fluctuations of the signal field in each one of the modes of the basis. Once verified the multi-mode character of

SPOPO systems, special combination of combs can be considered in order to put in evidence multi-mode non-classical correlations. The demonstration of their feasibility, under certain conditions, suggests SPOPOs as possible sources by means of which multi-partite entanglement can be investigated or protocols for the quantum communication can be implemented.

5.1 Multi-mode representations

As discussed in Chapter 2, from a classical point of view, the field generated by a SPOPO device which is the result of a coherent superposition of longitudinal modes can be always thought as single-mode provided that it is observed in the good basis (for example the one built starting from the vector (2.31)). Nevertheless, from a quantum point of view the situation is more complicated since the down-converted photons are generated not necessarily in a particular longitudinal mode but in a wide range of modes limited only by energy-conservation and phase-matching conditions. In fact, for a given photon in a general longitudinal mode of the signal field, one cannot trace back the pump photon who generated it since the energy and momentum selection rules allows several possibilities. Thus, an excitation in one longitudinal mode of the signal field could be connected to several different couples of down-converted photons and, a priori, the signal field cannot be more considered as a coherent superposition of modes since there are not-trivial quantum correlations distributed among its whole spectrum and, then, its "multimodicity" has to be thoroughly investigated.

Although the description of pulsed beams in the context of the parametric down-conversion, such as the mode-locked beam outgoing a SPOPO, involves a very large number of degree of freedom (about 10^5 modes for the case which we are interested to), their quantum properties do not necessarily involve all of them. As discussed in Section 2.2, one could construct a set of modes, as linear combination of the canonical ones, in order that, in such a modal picture, the global quantum state of the beam can be written as $\hat{\rho} = \hat{\rho}_{\text{exc}} \otimes \hat{\rho}_{\text{vac}}$, where $\hat{\rho}_{\text{exc}}$ is some nontrivial density operator of few excited modes and $\hat{\rho}_{\text{vac}}$ is the vacuum state density operator of the remaining modes. Therefore, the critical question is how to identify which modes are relevant in the quantum description of the considered field.

The interest in pulsed squeezed light and in general in two-photon quantum correlations in pulsed systems dates back to the first experimental realizations by Slusher *et al.* [Slusher1987] since nonclassical properties of quantum states find applications in quantum communication and quantum information protocols. In the small gain regime of parametric conversion of simple pulses, Law *et al.* [Law2000] have shown the existence of a finite but not null set of "special" two-photon modes (not monochromatic), among an infinite number of degrees of freedom, which contribute to and completely characterize pairwise entanglement. The set of these modes, as we will see, introduces a discretization of the continuum which is exact (not an approximation) and unique.

A simplified picture of the experimental situation considered by Law *et al.* consists of a single pump pulse impinging a degenerate optical parametric amplifier. If the field at the down-converted frequencies is initially in the vacuum state $|0\rangle$, the output state can

be written as:

$$|\psi_{\text{out}}\rangle = \hat{U}|\psi_{\text{in}}\rangle \simeq |0\rangle + \frac{1}{2}\int \mathrm{d}\omega\, \mathrm{d}\omega'\, \Psi\left(\omega,\omega'\right) \hat{a}^{\dagger}\left(\omega\right) \hat{a}^{\dagger}\left(\omega'\right) |0\rangle, \tag{5.1}$$

where $\Psi\left(\omega,\omega'\right)$ is the symmetric two-photon wave function given by the product of the spectral pump amplitude at the frequency $\omega+\omega'$ and the phase-matching function at the down-converted frequencies. By performing the Schmidt decomposition, Ψ can be put in the form:

$$\Psi\left(\omega,\omega'\right) = \sum_{n=0}^{\infty} \sqrt{\lambda_n}\psi_n\left(\omega\right)\psi_n^{*}\left(\omega'\right), \tag{5.2}$$

where λ_n and $\psi_n\left(\omega\right)$ are the solutions of the integral eigenvalue equation:

$$\int \mathrm{d}\omega'\, \Psi\left(\omega,\omega'\right)\psi_n\left(\omega'\right) = \lambda_n\psi_n\left(\omega\right). \tag{5.3}$$

The mathematical properties of the eigenvalues and eigenvectors of Eq. (5.3) can be found more detailed in [Tricomi1967, Parker2000]. Here we will limit to remark that for quadratically integrable kernels, such as Ψ in equation (5.3), the spectrum of eigenvalues $\{\lambda_n\}_{n\in\mathbb{N}}$ has infinitely many nonzero values and have no accumulation points (i.e. the eigenvalues do not form a continuous set) except at zero. The use of Schmidt decomposition for continuous variables has been previously discussed in problems focused to quantify entanglement for two-photon wave-functions [Parker2000, Huang1996].

The decomposition performed suggests the introduction of a set of field operators defined by:

$$\hat{b}_n = \int \mathrm{d}\omega\, \psi_n\left(\omega\right)\hat{a}\left(\omega\right), \tag{5.4}$$

which are not monochromatic. These operators satisfy standard bosonic commutation relations $[\hat{b}_n, \hat{b}_m^{\dagger}] = \delta_{n,m}$, which directly follow from the orthogonality of the eigenfunctions $\psi_n\left(\omega\right)$ and, unlike the canonical set of annihilation operators $\hat{a}\left(\omega\right)$, they forms a discrete set. In terms of $\hat{b}_n$ the two-photon wave-function reads:

$$|\psi_{\text{out}}\rangle = \hat{U}|\psi_{\text{in}}\rangle \simeq |0\rangle + \frac{1}{2}\sum_{n=0}^{\infty} \sqrt{\lambda_n}\, {\hat{b}_n^{\dagger}}^2 |0\rangle, \tag{5.5}$$

in which the continuous integral in Eq. (5.1) has been replaced by an infinite discrete summation. The wave-function (5.5) can be obtained from the perturbative expansion of the multimode squeezing operator of the form:

$$\hat{U} = \bigotimes_{n=0}^{\infty} \exp\left\{\frac{\sqrt{\lambda_n}}{2}\left[{\hat{b}_n^{\dagger}}^2 - \hat{b}_n^2\right]\right\}. \tag{5.6}$$

This result has been retrieved with a different approach in [Xin1990] by disentangling the N-mode squeezing operator defined in general manner as:

$$\hat{S}_{\text{N}}\left(\xi\right) \equiv \exp\left\{\frac{1}{2}\left[{\hat{a}^{\dagger}}^{\text{T}}\xi\hat{a}^{\dagger} - \hat{a}^{\text{T}}\xi\hat{a}\right]\right\}, \tag{5.7}$$

where $\hat{a} \equiv (\hat{a}_1, \ldots, \hat{a}_{\text{N}})^{\text{T}}$ and ξ is a symmetric $N \times N$ matrix.

The advantages of using the Schmidt-mode representation are now clear. In fact, according to the picture (5.5) or (5.6), two-photon correlations - which in the specific case

of degenerate parametric conversion correspond to the squeezing properties of the beam - appear only in Schmidt modes and the decomposition identifies precisely in which modes photons go as pairs. On the other hand, the values of λ_n determines the occupation probability of the corresponding mode. Since the analytical properties of the eigenspectrum of (5.3) require it to converge asymptotically towards zero, only a finite set of λ_n's will have a significant value. Therefore the representation (5.5) gives an information about the effective dimension of the Hilbert space in which the state of the signal field lives. In the eventuality that only one eigenvalue has a not null value, a single modal description of the field completely characterizes the considered quantum state. The "pulse mode" in which the Schmidt operator $\hat{b}_n$ generates or destroys a photon is easily retrieved from the definition of the field operator:

$$\hat{E}^{(+)}(t,x) = \int \mathrm{d}\omega \sqrt{\frac{\hbar\omega}{2\epsilon_0 cn(\omega)}}\hat{a}(\omega)\,\mathrm{e}^{-i\omega(t-\frac{x}{c})}. \tag{5.8}$$

By using the completeness of $\psi_n(\omega)$, the field operator takes the simple form:

$$\hat{E}^{(+)}(t,x) = \sum_n \hat{b}_n u_n\left(t-\frac{x}{c}\right), \tag{5.9}$$

when the "pulse mode" is defined as:

$$u_n(t) \equiv \int \mathrm{d}\omega \sqrt{\frac{\hbar\omega}{2\epsilon_0 cn(\omega)}}\psi_n(\omega)\mathrm{e}^{-i\omega t}. \tag{5.10}$$

The multi-modal approach depicted above turn out to be a powerful tool for a meaningful and complete characterization of the quantum state of an optical pulse. In 2002, R. S. Bennink and R. Boyd [Bennink2002], on the basis of the results obtained in [Xin1990], extended the approach of Law *et al.* to multi-mode squeezed light generated by parametric down-conversion. A similar approach was independently developed by Opatrný [Opatrný2002] for the complete characterization of the quantum state of solitons in optical fibers. The approach used by Bennink and Boyd not only introduces the concept of eigenmodes of the squeezing, which have the same physical interpretation of the Schmidt modes, and provide insight into the correlations which exist in multi-mode squeezed fields, but also gives information on the mode structure of the local oscillator that should be used in order to measure the smallest quadrature noise. In fact, although the importance of mode matching in homodyne detection was already known (see for example [LaPorta1991, Kim1994, Werner1995, Levandovsky1999]), the typical experimental setups were suboptimal while, in such cases, the shaping of the local oscillator according the multi-mode theory suggested by Bennink and Boyd lead to a great improvement of squeezed light measurements in accordance with the results of the theory.

A modal decomposition as the one discussed above in the case of small gain exists also in a generalized form, far from the perturbative limit, as long as the multi-mode evolution remains linear in the field operators. This usually happens when the pumping fields are strong enough that their quantum fluctuations and pump depletion may be neglected. In such case the evolution of the field can be written as a Bogoliubov transformation [Ekert1991] which connects the the output field operator $\hat{a}_{\mathrm{out}}(\omega)$ to the input field operator $\hat{a}_{\mathrm{in}}(\omega)$:

$$\hat{a}_{\mathrm{out}}(\omega) = \int \mathrm{d}\omega' \left[C(\omega,\omega')\,\hat{a}_{\mathrm{in}}(\omega') + S(\omega,\omega')\,\hat{a}_{\mathrm{in}}(\omega)^{\dagger}\right]. \tag{5.11}$$

The reduction of linear Bogoliubov transformations is given by the Bloch-Messiah theorem for bosons [Braunstein2005] which is a formal extension of the original result for fermions [Ring1980]. For the transformation (5.11) the Bloch-Messiah reduction leads to the decomposition:

$$C\left(\omega,\omega'\right) = \sum_{n=0}^{\infty}\zeta_n\psi_n\left(\omega\right)\phi_n^*\left(\omega'\right), \tag{5.12}$$

$$S\left(\omega,\omega'\right) = \sum_{n=0}^{\infty}\xi_n\psi_n\left(\omega\right)\phi_n^*\left(\omega'\right), \tag{5.13}$$

where $\psi_n\left(\omega\right)$ and $\phi_n\left(\omega\right)$ are two independent orthonormal sets of functions and ζ_n and ξ_n are two parameters which have to satisfy:

$$\zeta_n^2 - \xi_n^2 = 1, \tag{5.14}$$

which comes from the fact that the output operators must satisfy the canonical commutation relations. Analogously to Eq. (5.4), we can define a discrete set of field operators according to:

$$\hat{b}_{\mathrm{in},n} = \int \mathrm{d}\omega\,\psi_n\left(\omega\right)\hat{a}_{\mathrm{in}}\left(\omega\right), \tag{5.15}$$

$$\hat{b}_{\mathrm{out},n} = \int \mathrm{d}\omega\,\phi_n\left(\omega\right)\hat{a}_{\mathrm{out}}\left(\omega\right), \tag{5.16}$$

whose evolution is completely characterized by the following transformation:

$$\hat{b}_{\mathrm{out},n} = \hat{b}_{\mathrm{in},n}\mathrm{cosh}r + \hat{b}_{\mathrm{in},n}^{\dagger}\mathrm{sinh}r, \tag{5.17}$$

with $\zeta_n = \mathrm{cosh}r$, $\xi_n = \mathrm{sinh}r$ and r a real number. It is clear then, from Eq. (5.17), that the Bloch-Messiah reduction permits the description of a multi-mode optical field by means of a discrete set of squeezing modes evolving independently, generalizing the result obtained in the limit of small gain represented by Eq. (5.6). One of the most relevant implications of this theorem is that any optical circuit, characterized by a linear input-output relation, can be equivalently obtained with a system made of a linear multi-port interferometer (performing a linear local transformation) followed by the parallel application of a set of single-mode squeezers and then another multi-port interferometer as shown in Figure 5.1. As a consequence the number of independent modes, in the Bloch-Messiah reduced form, represents an intrinsic and irreducible resource of squeezing of any given multi-port optical device. A smaller number of squeezers will not result sufficient for the device construction. In the same manner than the λ_n's of the Schmidt-mode representation, the minimum number of Bloch-Messiah modes necessary to completely characterize the optical system is intrinsically connected to its "multimodicity" since it determines the effective dimension of the Hilbert space in which the quantum state of the system can be written, as in the beginning of this section, by means of a density operator $\hat{\rho} = \hat{\rho}_{\mathrm{exc}} \otimes \hat{\rho}_{\mathrm{vac}}$.

As an example we can consider the field generated by a two-mode down-converter through an interaction Hamiltonian of the form:

$$\hat{H}_2 \propto \left(\hat{a}_1^{\dagger}\hat{a}_2^{\dagger} - \hat{a}_1\hat{a}_2\right). \tag{5.18}$$

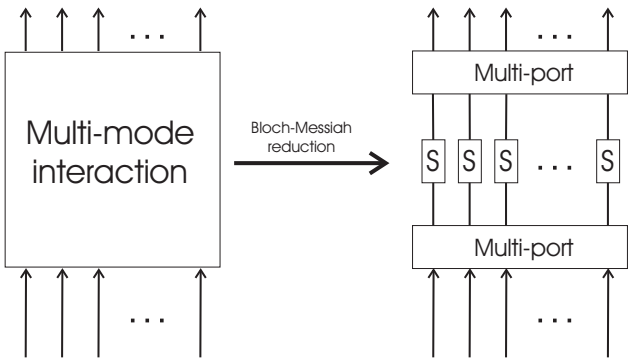

Figure 5.1: An arbitrary complicated multi-mode interaction may be decomposed by Bloch-Messiah reduction into an input linear multi-port followed by an irreducible number of squeezers and an output multi-port coupler.

The Bloch-Messiah theorem states the equivalence with an optical system formed by two squeezers acting on the two independently evolving modes:

$$\hat{v}_+ = \frac{\hat{a}_1 + \hat{a}_2}{\sqrt{2}}, \quad \hat{v}_- = \frac{\hat{a}_1 - \hat{a}_2}{\sqrt{2}}, \tag{5.19}$$

and mixed at a 50/50 beam splitter. We discover, therefore, that the equivalence between squeezing and entanglement, discussed in the Section 1.3.5, finds in the Bloch-Messiah theorem an elegant generalization to multi-mode bosonic fields.

In its original form the Bloch-Messiah theorem was introduced by Braunstein for discrete bosonic linear systems [Braunstein2005] and only later was extended to continuous system. In particular it has been adapted by Wasilewski *et al.* to the characterization of the spectral properties of squeezed light produced be means of pulsed, single-pass degenerate parametric down-conversion [Wasilewski2006a] and of the quantum entanglement of Stokes light in single-pass stimulated Raman scattering by atomic-ensembles [Wasilewski2006b].

5.1.1 Definition of "super-modes" in SPOPOs

In the case we are interested in, instead of the simple passage of one short impulsion through a nonlinear medium, a mode-locked coherent field (described by a comb of frequencies) interacts with a nonlinear medium inside a cavity which is supposed to be resonant with all the frequencies of the comb. Therefore, in contrast to the situations analyzed in [Law2000, Wasilewski2006a], we are in a context of a system with a discrete, but still huge, number of degrees of freedom represented by the longitudinal modes of the comb whose evolution is described by the discrete set of bosonic operators $\{\hat{s}_m\}_{m\in\mathbb{Z}}$. As seen in previous chapters, in a typical experimental situation the mode-locked beam pumping a SPOPO consists of about 10^5 longitudinal modes. Following the evolution of each degree of freedom and characterizing the quantum properties of such field is not convenient, therefore making a multi-mode approach to the problem advisable for a compact and complete description.

The study of the linear dynamics of a SPOPO system we performed in Chapter 4 already evidenced the fact that the eigenvectors of the coupling matrix $\mathcal{L}$ follow independent evolutions with the rates λ_k (see Eq. (4.19)). In fact, if the coupling matrix is written in its normal form $\mathcal{L} = L^\dagger D L$, where D is the diagonal matrix whose entries are the eigenvalues

$\{\Lambda_k\}$ of $\mathcal{L}$ and L is the unitary matrix constructed with the eigenvectors $\{L_{k,m}\}$ of $\mathcal{L}$, the multi-modal evolution described by Eq. (4.4) assumes the expression:

$$\frac{d}{dt}\begin{pmatrix}\mathbf{S}\\ \mathbf{S}^*\end{pmatrix} = -\gamma_s\left(\widetilde{I}-\sigma\widetilde{D}\right)\begin{pmatrix}\mathbf{S}\\ \mathbf{S}^*\end{pmatrix} + \sqrt{2\gamma_s}\,\mathbf{S}_{in}, \tag{5.20}$$

where $\mathbf{S} = \mathrm{col}\{\hat{S}_0, \hat{S}_1, \ldots\}$ and $\mathbf{S}_{in} = \mathrm{col}\{\hat{S}_{in,0}, \hat{S}_{in,1}, \ldots\}$ are, respectively, the vector of intracavity signal operators and the vector of input signal operators, $\widetilde{I} = I \otimes I$ is the identity matrix and

$$\widetilde{D} = \begin{pmatrix}0 & D\\ D & 0\end{pmatrix}. \tag{5.21}$$

The modes $\mathbf{S}$ reveal, therefore, to be equivalent of the Schmidt modes or of the Bloch-Messiah modes discussed before and are defined as:

$$\hat{S}_k(t) = \sum_m L_{k,m}\hat{s}_m(t), \tag{5.22}$$

$$\hat{S}_{in,k}(t) = \sum_m L_{k,m}\hat{s}_{in,m}(t). \tag{5.23}$$

It is important to stress the fact that, likewise the Schmidt and Bloch-Messiah reduction, the modal formulation represented by (5.22) and (5.23) it is possible thanks to the linearization of the evolution equations due to small-fluctuations.

Since $\overrightarrow{L}_k \cdot \overrightarrow{L}_{k'} = \sum_m L_{k,m}L_{k',m} = \delta_{k,k'}$, one has trivially:

$$\left[\hat{S}_k(t), \hat{S}_k^\dagger(t)\right] = \delta_{k,k'}, \tag{5.24}$$

$$\left[\hat{S}_{in,k}(t), \hat{S}_{in,k}^\dagger(t')\right] = \delta_{k,k'}\delta(t-t'), \tag{5.25}$$

as well as the correlations:

$$\langle \hat{S}_{in,k}(t), \hat{S}_{in,k}^\dagger(t')\rangle = \delta_{k,k'}\delta(t-t'), \tag{5.26}$$

which have been obtained from the non-null correlations of the longitudinal mode operators $\hat{s}_m(t)$:

$$\langle \hat{s}_{in,m}(t)\hat{s}_{in,m'}^\dagger(t')\rangle = \delta_{m,m'}\delta(t-t'), \tag{5.27}$$

when the input is in the vacuum state. Hence $\hat{S}_k$ and $\hat{S}_{in,k}$ are the annihilation operators of the combination of signal modes of different frequencies corresponding to the mode $\overrightarrow{L}_k$. The corresponding creation operator applied to the vacuum state creates a photon in the mode $\overrightarrow{L}_k$ which we will call "super-mode" and which globally describes a frequency comb. Analogously one can define super-mode output operators:

$$\hat{S}_{out,k}(t) = \sum_m L_{k,m}\hat{s}_{out,m}(t), \tag{5.28}$$

where the output boson operator $\hat{s}_{out,m}(t)$ is related to the intracavity and input boson operators through the usual input-output relation of optical cavities [Gardiner1985] valid for very small transmission:

$$\hat{s}_{out,m}(t) + \hat{s}_{in,m}(t) = \sqrt{2\gamma_s}\,\hat{s}_m(t). \tag{5.29}$$

Starting from the linear quantum evolution of the super-mode operators (5.20), which reads:

$$\frac{d}{dt}\hat{S}_k = -\gamma_s \hat{S}_k + \gamma_s \sigma \Lambda_k \hat{S}_k^\dagger + \sqrt{2\gamma_s}\,\hat{S}_{\mathrm{in},k}, \tag{5.30}$$

$$\frac{d}{dt}\hat{S}_k^\dagger = -\gamma_s \hat{S}_k^\dagger + \gamma_s \sigma \Lambda_k \hat{S}_k + \sqrt{2\gamma_s}\,\hat{S}_{\mathrm{in},k}^\dagger. \tag{5.31}$$

we derive now a relation between the output super-mode operators $\hat{S}_{\mathrm{out},k}$ and the input super-mode operators $\hat{S}_{\mathrm{in},k}$. The quadrature hermitian operators $\hat{S}_k^{(\pm)}$ defined by:

$$\hat{S}_k^{(+)} = \hat{S}_k + \hat{S}_k^\dagger, \tag{5.32}$$

$$\hat{S}_k^{(-)} = -i\left(\hat{S}_k - \hat{S}_k^\dagger\right), \tag{5.33}$$

evolve according to the following equations:

$$\frac{d}{dt}\hat{S}_k^{(\pm)} = \lambda_k^{(\pm)}\hat{S}_k^{(\pm)} + \sqrt{2\gamma_s}\,\hat{S}_{\mathrm{in},k}^{(\pm)}, \tag{5.34}$$

where $\hat{S}_{\mathrm{in},k}^{(\pm)}$ and $\hat{S}_{\mathrm{out},k}^{(\pm)}$ have been defined as in (5.32) and (5.33) and λ_k are given by Eq. (4.19). These relations enable us to determine the intracavity quadrature operators in the Fourier domain $\widetilde{S}_k^{(\pm)}(\omega)$:

$$i\omega\widetilde{S}_k^{(\pm)}(\omega) = \lambda_k^{(\pm)}\widetilde{S}_k^{(\pm)}(\omega) + \sqrt{2\gamma_s}\,\widetilde{S}_k^{(\pm)}(\omega). \tag{5.35}$$

On the other side the usual input-output relation (5.29) on the coupling mirror which can be written as:

$$\tilde{s}_{\mathrm{out},m}(\omega) = -\tilde{s}_{\mathrm{in},m}(\omega) + \sqrt{2\gamma_s}\tilde{s}_m(\omega), \tag{5.36}$$

being $\tilde{s}_{\mathrm{out},m}(\omega)$ the Fourier transform of the output boson operator $\hat{s}_{\mathrm{out},m}(t)$, extends by linearity to any super-mode operator as the mirror is assumed to have a transmission independent of the mode frequency. One, then, obtains the following expression for the quadrature component in Fourier space of any signal super-mode:

$$\widetilde{S}_{\mathrm{out},k}^{(\pm)}(\omega) = v_k^{(\pm)}(\omega)\,\widetilde{S}_{\mathrm{in},k}^{(\pm)}(\omega), \tag{5.37}$$

$$v_k^{(\pm)}(\omega) = \frac{\gamma_s\left(1 \pm r\Lambda_k/\Lambda_0\right) - i\omega}{\gamma_s\left(-1 \pm r\Lambda_k/\Lambda_0\right) + i\omega}. \tag{5.38}$$

It is easy to compute the following correlations[3], corresponding to vacuum inputs, which follow straightforwardly from Eqs. (5.23) and (5.27):

$$\left\langle \widetilde{S}_{\mathrm{in},k}^{(+)}(\omega)\,\widetilde{S}_{\mathrm{in},l}^{(+)}(\omega_2)\right\rangle = \frac{1}{2\pi}\delta_{kl}\delta(\omega+\omega_2), \tag{5.39}$$

$$\left\langle \widetilde{S}_{\mathrm{in},k}^{(-)}(\omega)\,\widetilde{S}_{\mathrm{in},l}^{(-)}(\omega_2)\right\rangle = \frac{1}{2\pi}\delta_{kl}\delta(\omega+\omega_2), \tag{5.40}$$

$$\left\langle \widetilde{S}_{\mathrm{in},k}^{(+)}(\omega)\,\widetilde{S}_{\mathrm{in},l}^{(-)}(\omega_2)\right\rangle = i\frac{1}{2\pi}\delta_{kl}\delta(\omega+\omega_2), \tag{5.41}$$

$$\left\langle \widetilde{S}_{\mathrm{in},k}^{(-)}(\omega)\,\widetilde{S}_{\mathrm{in},l}^{(+)}(\omega_2)\right\rangle = -i\frac{1}{2\pi}\delta_{kl}\delta(\omega+\omega_2). \tag{5.42}$$

[3]Provided the Fourier transform have been defined like $\tilde{S}(\omega) = \frac{1}{2\pi}\int \mathrm{d}t\, \mathrm{e}^{-i\omega t}\hat{S}(t)$.

From these relations one can finally compute the corresponding output correlations:

$$\left\langle \widetilde{S}^{(+)}_{\mathrm{out},k}(\omega)\,\widetilde{S}^{(+)}_{\mathrm{out},l}(\omega_2)\right\rangle = \frac{v_k^{(+)}(\omega)\,v_l^{(+)}(-\omega)}{2\pi}\delta_{kl}\delta(\omega+\omega_2), \tag{5.43}$$

$$\left\langle \widetilde{S}^{(-)}_{\mathrm{out},k}(\omega)\,\widetilde{S}^{(-)}_{\mathrm{out},l}(\omega_2)\right\rangle = \frac{v_k^{(-)}(\omega)\,v_l^{(-)}(-\omega)}{2\pi}\delta_{kl}\delta(\omega+\omega_2), \tag{5.44}$$

$$\left\langle \widetilde{S}^{(+)}_{\mathrm{out},k}(\omega)\,\widetilde{S}^{(-)}_{\mathrm{out},l}(\omega_2)\right\rangle = i\frac{v_k^{(+)}(\omega)\,v_l^{(-)}(-\omega)}{2\pi}\delta_{kl}\delta(\omega+\omega_2), \tag{5.45}$$

$$\left\langle \widetilde{S}^{(-)}_{\mathrm{out},k}(\omega)\,\widetilde{S}^{(+)}_{\mathrm{out},l}(\omega_2)\right\rangle = -i\frac{v_k^{(-)}(\omega)\,v_l^{(+)}(-\omega)}{2\pi}\delta_{kl}\delta(\omega+\omega_2). \tag{5.46}$$

The relations retrieved above will result useful in the next section, when the multi-mode characterization of the quantum fluctuations of the field generated by a SPOPO will be approached.

5.2 Noise properties of super-modes

The modal decomposition illustrated in the previous section allows, then, a compact way to completely characterize the quantum state of the multi-mode light generated by a SPOPO. As for the dynamical properties discussed in Chapter 4, we learned that the eigenvalues Λ_k of the coupling matrix $\mathcal{L}$ are intrinsically connected to the dimension of the reduced Hilbert space in which the characterization of such system is still effective. Such characterization is carried out by the measure of the variance of the operators (5.28) by means of the usual balanced homodyne detection scheme. In this case the local oscillator is a coherent mode-locked multi-mode field $E_{\mathrm{L}}(t)$ having the same repetition rate as the pump laser:

$$E_{\mathrm{L}}(t) = E^{-}_{\mathrm{L}}(t) + E^{+}_{\mathrm{L}}(t), \tag{5.47}$$

$$E^{-}_{\mathrm{L}}(t) = i\epsilon_{\mathrm{L}}\sum_m e_m\,\mathrm{e}^{-i\omega_{\mathrm{s},m}t}, \tag{5.48}$$

$$E^{+}_{\mathrm{L}}(t) = \left[E^{-}_{\mathrm{L}}(t)\right]^*, \tag{5.49}$$

where $\sum_m |e_m|^2 = 1$, and ϵ_{L} is the LO field total amplitude factor. The output signal field exiting the SPOPO, $\hat{E}_{\mathrm{s,out}}(t)$, is combined with $E_{\mathrm{L}}(t)$ in a $50\% - 50\%$ beam splitter, and the intensity difference between the two output ports is measured. Writing the output field as:

$$\hat{E}_{\mathrm{s,out}}(t) = \hat{E}^{-}_{\mathrm{s,out}}(t) + \hat{E}^{+}_{\mathrm{s,out}}(t), \tag{5.50}$$

$$\hat{E}^{-}_{\mathrm{s},out}(t) = i\mathcal{E}_{\mathrm{out}}\sum_m \hat{s}_{\mathrm{out},m}(t)\,\mathrm{e}^{-i\omega_{\mathrm{s},m}t}, \tag{5.51}$$

$$\hat{E}^{+}_{\mathrm{s,out}}(t) = \left[\hat{E}^{-}_{\mathrm{s,out}}(t)\right]^{\dagger}, \tag{5.52}$$

the quantity $\mathcal{E}_{\mathrm{out}}$ is an appropriate proportionality constant which needs not to be fixed here. If sufficiently fast detectors were used, the measurement would give an instantaneous signal represented by the photocurrent operator:

$$\hat{i}(t) = \frac{1}{\epsilon_{\mathrm{L}}\mathcal{E}_{\mathrm{out}}}\left[E^{-}_{\mathrm{L}}(t)\hat{E}^{+}_{\mathrm{out},m}(t) + E^{+}_{\mathrm{L}}(t)\hat{E}^{-}_{\mathrm{out},m}(t)\right]. \tag{5.53}$$

When detectors are not so fast, they average over many pulses along their response time τ_{d} (we are considering inter-pulse separation on the order of few ns) and the photocurrent operator must be substituted by $\hat{i}_{\mathrm{H}}(t) = \frac{1}{\tau_{\mathrm{d}}}\int_{t-\tau_{\mathrm{d}}}^{t+\tau_{\mathrm{d}}} \mathrm{d}t'\, \hat{i}(t')$, which can be very well approximated by:

$$\hat{i}_{\mathrm{H}}(t) = \frac{1}{\epsilon_{\mathrm{L}}\mathcal{E}_{\mathrm{out}}}\left[e_m \hat{s}^{\dagger}_{\mathrm{out},m}(t) + e^{*}_m \hat{s}_{\mathrm{out},m}(t)\right], \tag{5.54}$$

where we considered that $\tau_{\mathrm{d}} \gg 2\pi/\Omega$ and used the fact that $\hat{s}_{\mathrm{out},m}(t)$ and $\hat{s}^{\dagger}_{\mathrm{out},m}(t)$ vary little during the time τ_{d} [Knöll1991], what roughly requires that $\tau_{\mathrm{d}} \ll \gamma_{\mathrm{s}}^{-1}$. Note that this case, that reads $2\pi/\Omega \ll \tau_{\mathrm{d}} \ll \gamma_{\mathrm{s}}^{-1}$, requires $T_{\mathrm{s}} \ll 1$ since $\gamma_{\mathrm{s}} = T_{\mathrm{s}}\Omega/4\pi$, being T_{s} the transmission factor of the single cavity mirror at which signal losses are assumed to be concentrated.

5.2.1 Homodyne detection in conditions of perfect mode-matching

Since the balanced homodyne detection scheme measures the variance of the fluctuations of the projection of the output field on the local oscillator mode, the mode-matching is a critical point for an optimal probing of the squeezed field. When the local oscillator is perfectly matched to one of the super-modes (5.28), the coefficients e_m of the LO field spectral decomposition are equal, apart from a global phase ϕ_{L}, to the coefficients $L_{k,m}$ of the k-th supermode and the photocurrent difference is given by:

$$\hat{i}_{\mathrm{H}}(t) = \mathrm{e}^{i\phi_{\mathrm{L}}}\hat{S}^{\dagger}_{\mathrm{out},k}(t) + \mathrm{e}^{-i\phi_{\mathrm{L}}}\hat{S}_{\mathrm{out},k}(t) = \hat{S}^{(+)}_{\mathrm{out},m}(t)\cos\phi_{\mathrm{L}} + \hat{S}^{(-)}_{\mathrm{out},m}(t)\sin\phi_{\mathrm{L}}. \tag{5.55}$$

The noise variance spectrum $V(\omega)$, associated to $\hat{i}_{\mathrm{H}}(t)$, defined as:

$$V(\omega) = \int_{-\infty}^{+\infty} \mathrm{d}\tau\, \mathrm{e}^{-i\omega\tau}\left\langle \hat{i}_{\mathrm{H}}(t+\tau)\,\hat{i}_{\mathrm{H}}(t)\right\rangle, \tag{5.56}$$

can be computed as:

$$\begin{aligned} V(\omega) &= \int_{-\infty}^{+\infty}\mathrm{d}\tau\,\mathrm{e}^{-i\omega\tau}\int_{-\infty}^{+\infty}\mathrm{d}\omega_1\mathrm{e}^{-i\omega_1(t+\tau)}\int_{-\infty}^{+\infty}\mathrm{d}\omega_2\,\mathrm{e}^{-i\omega_2\tau}\left\langle\tilde{i}_{\mathrm{H}}(\omega_1)\,\tilde{i}_{\mathrm{H}}(\omega_2)\right\rangle \\ &= \int_{-\infty}^{+\infty}\mathrm{d}\omega_1\int_{-\infty}^{+\infty}\mathrm{d}\omega_2\,\mathrm{e}^{i(\omega_1+\omega_2)t}\left\langle\tilde{i}_{\mathrm{H}}(\omega_1)\,\tilde{i}_{\mathrm{H}}(\omega_2)\right\rangle \underbrace{\int_{-\infty}^{+\infty}\mathrm{d}\tau\,\mathrm{e}^{-i(\omega-\omega_1)\tau}}_{2\pi\,\delta(\omega-\omega_1)} \\ &= 2\pi\int_{-\infty}^{+\infty}\mathrm{d}\omega_2\,\mathrm{e}^{i(\omega+\omega_2)t}\left\langle\tilde{i}_{\mathrm{H}}(\omega)\,\tilde{i}_{\mathrm{H}}(\omega_2)\right\rangle, \end{aligned} \tag{5.57}$$

provided the Fourier transform of $\hat{i}_{\mathrm{H}}(t)$ is defined as:

$$\tilde{i}_{\mathrm{H}}(\omega) = \frac{1}{2\pi}\int_{-\infty}^{+\infty}\mathrm{d}t\,\mathrm{e}^{-i\omega t}\,\hat{i}_{\mathrm{H}}(t). \tag{5.58}$$

Thus, the variances of the two quadratures relative to the super-mode operator $\hat{S}_k(t)$, which can be measured by changing the phase ϕ_{L} of the local oscillator (see Eq. (5.55)), are given by:

$$V_k^{(-)}(\omega) = v_k^{(-)}(\omega)\,v_k^{(-)}(-\omega) = \frac{\gamma_{\mathrm{s}}^2\left(1-r\Lambda_k/\Lambda_0\right)^2+\omega^2}{\gamma_{\mathrm{s}}^2\left(1+r\Lambda_k/\Lambda_0\right)^2+\omega^2}, \tag{5.59}$$

$$V_k^{(+)}(\omega) = v_k^{(+)}(\omega)\,v_k^{(+)}(-\omega) = V_k^{(-)}(\omega)^{-1}. \tag{5.60}$$

Equations (5.59) and (5.60) show that the device produces a minimum uncertainty state, that quantum noise reduction below the standard quantum limit (here equal to 1) is achieved for any super-mode characterized by a non-zero Λ_k and that the smallest fluctuations are obtained close to threshold ($r \simeq 1$) and at zero Fourier frequency:

$$V_{k,\min} = \left(\frac{\Lambda_0 - |\Lambda_k|}{\Lambda_0 + |\Lambda_k|} \right)^2 . \tag{5.61}$$

In particular, if one uses as the local oscillator a copy of the critical mode $k = 0$ (identical to the one oscillating just above the threshold $r = 1$) one then gets perfect squeezing just below threshold and at zero noise frequency, just like in the c.w. single mode case [4]. But modes of $k \neq 0$ may be also significantly squeezed, provided that $|\Lambda_k/\Lambda_0|$ is not much different from 1. In Section 4.3 we found that the eigenvalues Λ_k of the coupling matrix $\mathcal{L}$ form a discrete set asymptotically converging to zero. Consequently, among a huge number of super-modes, only a smaller set, corresponding to the most significant Λ_k, will contain almost all the information of the quantum state of the output signal field which could be approximatively factorized as $\hat{\rho}_{\rm exc} \otimes \hat{\rho}_{\rm vac}$. For example, in the case of the critically phase-matched BIBO analyzed in Section 4.3.2, the first 100 super-modes accounts for about the 92% of the signal quantum state. It is important to remark that, differently from a c.w. single mode OPO, the cavity does not naturally selects any special mode and the system behaves like a multi-mode device squeezing a large number of them.

5.2.2 Homodyne detection with a generic local oscillator

The optimal measuring of the noise variances associated to the super-modes requires the use of pulse shaping techniques of the local oscillator so that the mode-matching is the best possible, namely $e_m = \mathrm{e}^{i\phi_L} L_{k,m}$. In general, this can be a difficult task in experimental implementations. Therefore it is necessary to determine the actual noise measured with an arbitrary local oscillator. Form Eq. (5.53), the photocurrent difference $\hat{i}_{\rm H}(t)$ measured in a balanced homodyne detection will be proportional to:

$$\hat{i}_{\rm H}(t) = \sum_m \left[e_m \hat{s}^{\dagger}_{{\rm out},m}(t) + e^*_m \hat{s}_{{\rm out},m} \right] . \tag{5.62}$$

The projections of the local oscillator frequency comb onto the super-modes $\overrightarrow{L}_k$ are defined as:

$$\beta_k = \sum_m L_{k,m} e_m , \tag{5.63}$$

and its inverse:

$$e_m = \sum_k L_{k,m} \beta_k , \tag{5.64}$$

where the result $\sum_m L_{k,m} L_{k,n} = \delta_{m,n}$ involving the elements of a basis has been used. Substitution of Eq. (5.64) into (5.62) yields:

$$\hat{i}_{\rm H}(t) = \sum_k \left[{\rm Re}\left(\beta_k\right) \hat{S}^{(+)}_{{\rm out},k}(t) + {\rm Im}\left(\beta_k\right) \hat{S}^{(-)}_{{\rm out},k}(t) \right] , \tag{5.65}$$

[4] Notice that the unphysical results of perfect squeezing on the quadrature $\hat{S}^{(-)}_0$ and infinite noise fluctuations on the quadrature $\hat{S}^{(+)}_0$ have been obtained in the context of linear approximation of quantum Langevin equations. Considering the orders greater than one in the perturbative expansion will prevent the noise to diverge.

where the quadrature super-mode operators (5.32) and (5.33) have been used. The auto-correlation $\langle \tilde{\imath}_{\mathrm{H}}(\omega)\,\tilde{\imath}_{\mathrm{H}}(\omega_2)\rangle$ can be computed by using Eq. (5.37) and Eq. (5.65) and reads:

$$\begin{aligned}
&\langle \tilde{\imath}_{\mathrm{H}}(\omega)\,\tilde{\imath}_{\mathrm{H}}(\omega_2)\rangle = \\
&= \sum_{k,l}\Big\{\mathrm{Re}(\beta_k)\,\mathrm{Re}(\beta_l)\left\langle \tilde{S}^{(+)}_{\mathrm{out},k}(\omega)\,\tilde{S}^{(+)}_{\mathrm{out},l}(\omega_2)\right\rangle + \mathrm{Re}(\beta_k)\,\mathrm{Im}(\beta_l)\left\langle \tilde{S}^{(+)}_{\mathrm{out},k}(\omega)\,\tilde{S}^{(-)}_{\mathrm{out},l}(\omega_2)\right\rangle \\
&+\mathrm{Im}(\beta_k)\,\mathrm{Re}(\beta_l)\left\langle \tilde{S}^{(-)}_{\mathrm{out},k}(\omega)\,\tilde{S}^{(+)}_{\mathrm{out},l}(\omega_2)\right\rangle + \mathrm{Im}(\beta_k)\,\mathrm{Im}(\beta_l)\left\langle \tilde{S}^{(-)}_{\mathrm{out},k}(\omega)\,\tilde{S}^{(-)}_{\mathrm{out},l}(\omega_2)\right\rangle\Big\} \\
&= \frac{\delta(\omega+\omega_2)}{2\pi}\sum_k\Big\{(\mathrm{Re}\beta_k)^2\,v_k^{(+)}(\omega)\,v_k^{(+)}(-\omega) + (\mathrm{Im}\beta_k)^2\,v_k^{(-)}(\omega)\,v_k^{(-)}(-\omega) \\
&+i\,\mathrm{Re}(\beta_k)\,\mathrm{Im}(\beta_k)\left[v_k^{(+)}(\omega)\,v_k^{(-)}(-\omega) - v_k^{(-)}(\omega)\,v_k^{(+)}(-\omega)\right]\Big\}, \qquad (5.66)
\end{aligned}$$

where $v_k^{(\pm)}(\omega)$ are defined by Eq. (5.38) and we used the output correlation functions (5.43), (5.44), (5.45) and (5.46). It is then straightforward to compute the noise variance spectrum from Eq. (5.66), the final result reading:

$$\begin{aligned}
V(\omega) = \sum_k\Big\{&(\mathrm{Re}\beta_k)^2\,v_k^{(+)}(\omega)\,v_k^{(+)}(-\omega) + (\mathrm{Im}\beta_k)^2\,v_k^{(-)}(\omega)\,v_k^{(-)}(-\omega) \\
&+i\,\mathrm{Re}\beta_k\,\mathrm{Im}\beta_k\left[v_k^{(+)}(\omega)\,v_k^{(-)}(-\omega) - v_k^{(-)}(\omega)\,v_k^{(+)}(-\omega)\right]\Big\}. \qquad (5.67)
\end{aligned}$$

Equation (5.67) gives the general expression of the squeezing spectrum corresponding to a generic LO defined by its supermodal amplitudes β_k, Eq. (5.63). When the LO is proportional to the super-mode labeled by k, say $e_m = \mathrm{e}^{i\phi_{\mathrm{L}}}L_{k,m}$, and $\phi_{\mathrm{L}} = 0, \pi/2$, the two special quadratures (5.32) and (5.33) are selected and the results (5.59) and (5.60) are recovered.

5.2.3 Squeezing properties in BIBO based SPOPOs

By way of example we consider the case of a 0.1 μm thick BIBO crystal inside a 4 m ring OPO cavity pumped by a c.w. train of 100 fs pulses for a degenerate type I critically phase-matching operation at 0.4 μm pumping.

From Eq. (5.61), close to the threshold ($r \simeq 1$), the minimum noise fluctuations at zero Fourier frequency depend only on the eigenvalues Λ_k of the parametric interaction. Independently from the magnitude of the critical value Λ_0 (which for the specific case is about 272), the corresponding super-mode will show perfect squeezing, while the other super-modes will be squeezed according the ratio Λ_k/Λ_0.

In Figure 5.2(a) we report the minimum noise fluctuations given by Eq. (5.61) under the hypothesis of being able to perfectly mode-match the local oscillator to the corresponding super-mode. A significative number of super-modes, namely for $0 \le k \le 62$, shows a noise reduction better than -3 dB. In particular, for the first three super-modes (apart from the critical one) we obtain $V_{1,\min} \simeq -48$ dB, $V_{2,\min} \simeq -40$ dB and $V_{1,\min} \simeq -36$ dB. Notice that, since the oscillating character of the eigenspectrum $\{\Lambda_k\}$, the quadratures of $\hat{S}_k$ which are squeezed (anti-squeezed) are $\hat{S}^{(-)}_{2n}$ and $\hat{S}^{(+)}_{2n+1}$ ($\hat{S}^{(+)}_{2n}$ and $\hat{S}^{(-)}_{2n+1}$).

However, in experimental implementations, the mode-matching of the local oscillator to the quadrature to analyze can be a hard task. In fact, the super-modes have a generally

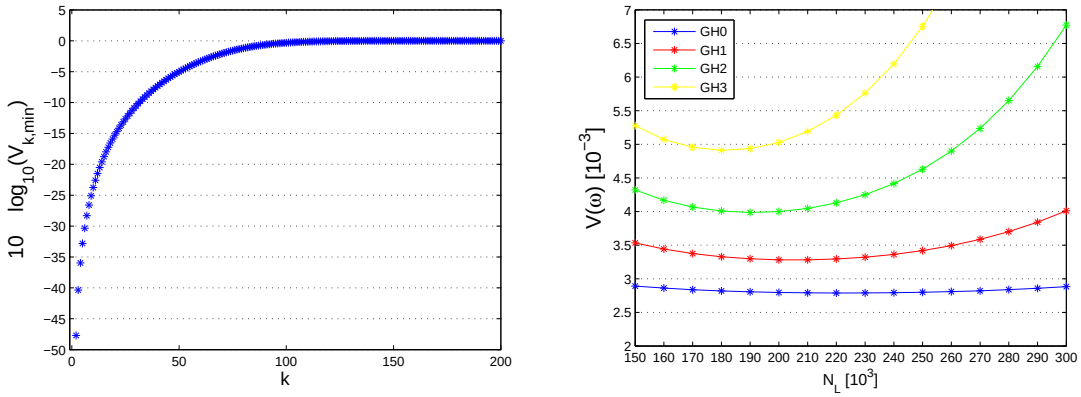

(a) (b)

Figure 5.2: 5.2(a) Noise variance at threshold ($r \simeq 1$) and $\omega = 0$, in decibels. Notice that, since in decibels $V_{0,\min} = -\infty$, the variances are traced for $k \geq 1$. 5.2(b) Maximum noise reduction measured by means of a Gauss-Hermite local oscillator in function of spectral width Δ_{LO}. The order of the G-H polynomial optimizes the projection of $k = 1, 2, 3$ and 4 super-modes on the local oscillator (respectively the cases blue, red, green and yellow).

complicated spectral form that can be theoretically retrieved from the analysis of the linear problem (4.9). A simpler situation occurs when the conditions for Gaussian approximation (4.56) and (4.57) are satisfied. In this case, we expect the super-mode to have a spectral form like (4.63) and the shaping of the local oscillator can result easier than the general case. While in the next section we will discuss in more detail the methods for shaping the local oscillator and we will outline a possible algorithm for experimentally retrieving the true shape of super-modes, here we consider a local oscillator shaped as a Gaussian-Hermite polynomial:

$$e_{k,m} = \frac{1}{\pi^{1/4} N_{\mathrm{L}}^{-1/2}} \mathrm{e}^{-\frac{1}{2}(m/N_{\mathrm{L}})^2} H_k\left(m/N_{\mathrm{L}}\right), \tag{5.68}$$

where N_{L} is the number of longitudinal modes of the local oscillator comb. In this case, the variance noise spectrum has to be evaluated using Eq. (5.67) and is given by the sum of all super-modes noise variance spectra weighted by the mode-matching parameter β_k, which describes how well each super-mode projects onto the local oscillator field. Since we expect Gaussian solutions for super-modes, for each k the local oscillator is almost orthogonal to every $L_{k',m}$ with $k' \neq k$. As an example we reported in Figure 5.2(b) the variances evaluated at zero Fourier frequency in correspondence of the first four Gauss-Hermite polynomials as functions of the spectral width of the local oscillator in the experimental conditions as above but considering the system below threshold ($r = 0.9$). The optimal N_L is found in correspondence of the minima of the curves, which represent the best noise reductions measurable with a local oscillator of the form (5.68). Such value, of course, is greater than the one obtained in the perfect case (see Section 5.2.1) because of a small contribution of the super-modes $k' \neq k$. In particular, for $e_{0,m}$, the maximum noise reduction is obtained for $N_{\mathrm{L}} = 220000$ with a variance $V_{\mathrm{GH0}}^{(-)} \simeq -25\,\mathrm{dB}$ that coincides with the noise reduction in the ideal situation $V_0^{(-)} \simeq -25\,\mathrm{dB}$. Hence, this result shows that

the mode-matching between the local oscillator and the super-mode $L_{0,m}$ is quite optimal what is confirmed by the fact that their scalar product is $\beta_0 \simeq 0.999$. For the other super-modes (i.e. $k = 1, 2, 3$) the optimal spectral width is obtained in correspondence of $N_{\mathrm{L}} \simeq 2 \times 10^5, 1.9 \times 10^5, 1.8 \times 10^5$, respectively. Therefore, even with the most trivial mode-shaping of the local oscillator, consisting of gaussian pulses of adjustable spectral width, it is possible to measure the squeezing of the output filed of a SPOPO with very high efficiencies and confirm again the quality of the Gaussian approximation introduced in the previous chapter.

5.2.4 Experimental shaping of the local oscillator

In general the super-modes characterizing the multi-mode output field of a SPOPO have not necessarily a Gauss-Hermite form and, however, even the simplest shaping, represented by Eq. (5.68), may be not an easy task to accomplish only by means of passive interferometric optics. In the context of ultra-short pulses, the use of Spatial Light Modulators (SLMs) represents a simple and compact method to shape the temporal mode of an optical pulse [Jiang2007, Huang2008, Supradeepa2008] that, thus, permits to overcome the difficulties relatives to the shaping of the mode-locked local oscillator we are considering. The principle of functioning of a SLM based pulse-shaper is illustrated in Figure 5.3. A given pulsed beam is sent on a first diffracting optical element that spatially separates the frequencies constituting it. Such frequency components, after, pass through the SLM which is a device that, electronically driven by a conventional interface (usually a VGA or DVI input), permits some form of spatially-varying modulation (for both amplitude and phase) according to the wanted output spectral shape. Finally they are recombined on a second diffractive optical element.

From an experimental point of view the knowledge of the theoretical form of the super-modes could be not sufficient and it could be more interesting to have direct access to their true shape since it does not straightforwardly coincide with the experimental one. For this reason an adaptive algorithm permitting to retrieve the true form of super-modes could be envisaged. Since each super-mode can be distinguished each other by their noise properties, which depend on the ratio $|\Lambda_k/\Lambda_0|$, the strategy that one could follow is simple: starting from an initial guess in the total space, say $\mathcal{H}$, if the local oscillator coincides with one super-mode the algorithm stops otherwise a feed-back loop will slightly change the initial guess and will check again until local oscillator matches a super-mode. Each time a particular super-mode $\vec{L}_k$ is found, the algorithm restarts with a new guess but in the

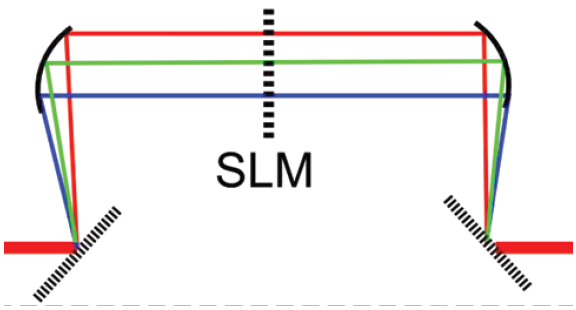

Figure 5.3: Sketch of a SLM based pulse shaper.

reduced space $\mathcal{H} - \text{span}\{\vec{L}_k\} \equiv \text{span}\{\vec{L}_k\}^{\perp}$. Then, it is worth to study better the noise properties of the points $L_{k,m}$ as functions of the pump field spectral amplitudes $\{e_{k,m}\}$.

For sake of simplicity, let's consider the case of real pump field. Then, the eigenvectors of the coupling matrix will be real too and, consequently, also the scalar products β_k will be real. Therefore, the sum in eq.(5.67) reduces only to the terms proportional to $\text{Re}\,(\beta_k)$. In the space of the pump spectral amplitude coefficients $\{e_m\}$, a point in the neighborhood of $\left\{\vec{L}_{\bar{k}}\right\}$ can be represented as:

$$e_m = \sqrt{1 - \sum_{k' \neq \bar{k}} \epsilon_{k',m}^2}\, L_{\bar{k},m} + \sum_{k' \neq \bar{k}} \epsilon_{k',m} L_{k,m}, \tag{5.69}$$

with $\epsilon_{k'} \ll 1$, $\forall\, k' \in \mathbb{N}$. Let's note that the condition $\sum_m |e_m|^2 = 1$ is satisfied. According to definition (5.63), the scalar products β_k are expressed as:

$$\beta_k = \sqrt{1 - \sum_{k' \neq \bar{k}} \epsilon_{k',m}^2}\, \delta_{k,\bar{k}} + \sum_{k' \neq \bar{k}} \epsilon_{k',m} \delta_{k',k}, \tag{5.70}$$

and thus the spectrum (5.67) can be written as:

$$V(\omega) = \left(1 - \sum_{k \neq \bar{k}} \epsilon_{k,m}^2\right) V_{\bar{k}}(\omega) + \sum_{k \neq \bar{k}} \epsilon_{k,m}^2 V_k(\omega), \tag{5.71}$$

where $V_k(\omega) \equiv v_k^{(\pm)}(\omega)\, v_k^{(\pm)}(-\omega)$. The first derivative of Eq. (5.71) with respect to a given ϵ_q reads:

$$\frac{\partial V}{\partial \epsilon_q} = 2\epsilon_q \left(V_q(\omega) - V_{\bar{k}}(\omega)\right), \quad q \neq \bar{k}, \tag{5.72}$$

and is equal to zero if for each $q \in \mathbb{N}$: $\epsilon_q = 0$; therefore, in the space of the parameters $\{e_m\}$ and with the constraint $\sum_m |e_m|^2 = 1$, the points $\left\{\vec{L}_k\right\}$ are stationary. Further, the Hessian matrix is given by:

$$\frac{\partial^2 V}{\partial \epsilon_q \partial \epsilon_m} = \begin{cases} 0, & \text{if } q \neq m \\ 2\left(V_q(\omega) - V_{\bar{k}}(\omega)\right), & \text{if } q = m \neq \bar{k} \end{cases} \tag{5.73}$$

Since the difference $V_q(\omega) - V_{\bar{k}}(\omega)$ can be greater or smaller than zero according to the sign of Λ_k/Λ_0, in general the Hessian matrix has not a definite sign and therefore the points $\left\{\vec{L}_k\right\}$ are saddle points. On the contrary, $\vec{L}_0$ and $\vec{L}_1$ are, respectively, a minimum and a maximum, since they corresponds to the maximum squeezing $V_0(\omega)$ and anti-squeezing $V_1(\omega)$ achievable for a given quadrature.

Hence, the properties expressed by Eqs. (5.72) and (5.73) of the noise variance spectra permit to recognize each super-mode from the level of squeezing measured by means of an algorithm of minimization (maximization). In particular, starting from an initial guess for the local oscillator parameters $\{e_{\text{guess},m}\}$, a homodyne detection scheme measures the noise level of a specific quadrature of the output signal field at a convenient frequency. Subsequently, the pulse shaper slightly changes the initial guess to another value $\{e_{\text{guess},m} + \epsilon_m\}$ and compares the output noise level with the previous one. This algorithm can be programmed in order to find the absolute minimum (maximum) represented by $\vec{L}_0$ ($\vec{L}_1$) and when accomplished, to restrict the parameter space excluding the super-mode just found

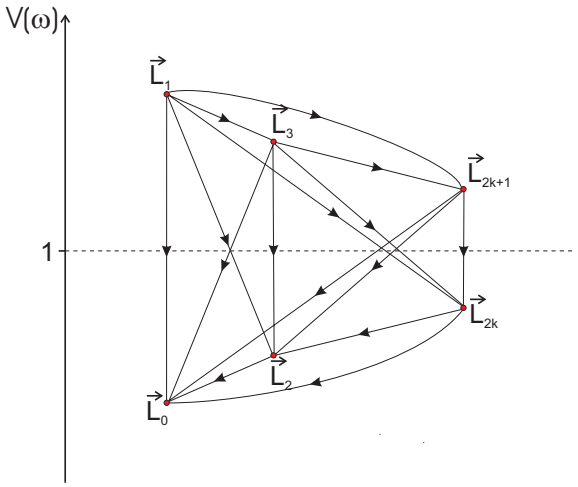

Figure 5.4: Bidimensional sketch of the structure of the parameters space $\{e_m\}$ and the main directions covered by an algorithm which minimizes the noise level of the output field. This particular structure permits any minimization (maximization) algorithm to find absolute minima (maxima). Starting, in fact, from a general point in this space (the initial guess) the minimization occurs along the arrows which lead towards points of progressively smaller noise variance. For example, starting from a guess about the point $\vec{L_3}$, the algorithm has many possible paths which lead to points of lower noise variance (i.e. $\vec{L}_0, \vec{L}_2, \ldots, \vec{L}_{2k}, \ldots$). Once it is in proximity of one of them, for example $\vec{L}_{2k}$, it can minimize the variance only evolving along the $2(k-1)$ possible paths towards the points $\vec{L}_0, \vec{L}_2, \ldots, \vec{L}_{2k-2}, \ldots$. It will stops only when, finally, it will be arrived in about $\vec{L}_0$

.

and restart the procedure. The particular structure of the parameter space (see Figure 5.4), in fact, assures that, sooner or later, the actual absolute minimum (maximum) will be discovered since the particular ordination of V_k. Starting from any point of the space $\{\alpha_m\}$, the algorithm, programmed for minimize (maximize) the noise level of the output field, will reach the closest saddle below the starting point which correspond to a general stationary $\vec{L}_k$. After that, the only possibility the algorithm has is to fall down (to rise up) towards any other saddle point which shows lower noise level and so on till the lowest possible noise level.

5.2.5 Conclusions

Since, by means of the super-modes basis it is possible to describe the quantum properties of the output field of a SPOPO in a compact and simple way, in this section we have studied their quantum properties. We studied the results of a standard balanced homodyne detection both for perfect and imperfect mode-matching of the local oscillator. Then, we have found that, among a huge variety, only a small but not null subset of this basis shows a significant reduction of the noise fluctuations below the standard quantum limit, hence, proving that a SPOPO is a multi-mode device. Finally, in the last part of this section, we approached the problem of experimentally implementing a system for controlling the wanted spectral shape of the local oscillator in order to optimize the mode-matching and suggested a possible scheme for experimentally retrieving the exact form of super-modes.

5.3 Two-mode correlations

One of the most appealing features of quantum mechanics is the existence of states formed by many parties for which the global wave-function cannot be factorized in a product of mono-partite wave-functions. Since they were originally introduced by Schrödinger [Schrödinger1935], such entangled states have been subject of animated scientific discussions. The two probably most significant contributions are represented by the works of Einstein *et al.* [EPR] and Bell [Bell1964]. Nowadays, the quantum correlations shared between two (or more) parties of a complex system are universally recognized as an important resource not only in the understanding of the fundamental principles of quantum mechanics, but also as resources for quantum information and quantum computation protocols which has not equals in classical mechanics. In principle, in fact, entanglement allows quantum teleportation [Bennett1993], quantum dense coding [Bennett1992a] or quantum key distribution [Bennett1984, Ekert1991, Bennett1992b]. The first experimental realizations of the EPR paradox and tests of the Bell's inequalities were performed on the entangled polarizations of two photons [Fry1976, Aspect1982]. Successively, in order to realize the original EPR paradox in continuous variables regimes, Reid proposed a schema for entangling the quadratures of the field with an OPO [Reid1989] that was experimentally implemented by Ou [Ou1992].

5.3.1 Perfect two-mode correlations

In the previous sections of this chapter we have shown the multi-modal character of the field produced by a synchronously pumped OPOs that, in the context of continuous variables regimes, could be, then, exploited as sources for entangling frequency combs. In order to see that, let's consider the interaction Hamiltonian below threshold and in the linear approximation:

$$\hat{H}_{\mathrm{I}} = \frac{i}{2}\hbar\kappa \sum_{m,q} \mathcal{L}_{m,q} \left(\hat{s}_m^{\dagger} \hat{s}_q^{\dagger} - \hat{s}_m \hat{s}_q \right). \tag{5.74}$$

Inverting Eq. (5.22) and its hermitian conjugate, the interaction Hamiltonian can be written in function of the super-mode operators:

$$\hat{H}_{\mathrm{I}} = \frac{i}{2}\hbar\kappa \sum_{k} \Lambda_k \hat{S}_k^{\dagger} \hat{S}_k^{\dagger} + \mathrm{H.c.}, \tag{5.75}$$

and is equivalent to the interaction Hamiltonian of independent squeezers. In general, the squeezing parameter Λ_k is different for each super-mode and the whole spectrum depends on the choice of the phase-matching properties of the crystal and on the shape of the pump width (see Eq. (4.6)). Nevertheless, as we have seen in Chapter 4 and discussed in Section 5.1, the sum rather than being infinite is usually limited to some number of super-modes as Λ_k is approximatively zero for most of them. Considering two specific super-modes $\hat{S}_j$ and $\hat{S}_l$ ($j \neq l$), let's define the two operators:

$$\hat{a} = \hat{S}_j \cos\theta + \hat{S}_l \sin\theta \tag{5.76}$$

$$\hat{b} = \hat{S}_j \sin\theta - \hat{S}_l \cos\theta \tag{5.77}$$

Hence, the contribution of $\hat{S}_j$ and $\hat{S}_l$ to the sum (5.75) can be written as:

$$\begin{aligned}\Lambda_j \hat{S}_j^2 + \Lambda_k \hat{S}_k^2 &= \hat{a}^2 \left(\Lambda_j \cos^2\theta + \Lambda_k \sin^2\theta\right) + \hat{b}^2 \left(\Lambda_j \sin^2\theta + \Lambda_k \cos^2\theta\right) \\ &+ 2\left(\Lambda_j - \Lambda_k\right) \hat{a}\,\hat{b} \cos\theta \sin\theta. \end{aligned} \tag{5.78}$$

The condition for having only crossed products is that $\Lambda_j \cos^2\theta + \Lambda_k \sin^2\theta = \Lambda_j \sin^2\theta + \Lambda_k \cos^2\theta = 0$ and one can verify that this occurs when $\Lambda_k = -\Lambda_j$, in which case $\cos 2\theta = 0 \Rightarrow \theta = \pi/4$, for instance. Then the two-modes contribution reads:

$$\Lambda_j \hat{S}_j^2 + \Lambda_k \hat{S}_k^2 = 2\Lambda_j \hat{a}\,\hat{b}. \tag{5.79}$$

Therefore, the super-modes $\hat{a}$ and $\hat{b}$ are entangled and detection in this special basis will show two-mode non-classical correlations. In general the condition $\Lambda_k = -\Lambda_j$ is not met, usually, in the case we already analyzed. In fact, a situation that seems favorable is that of non-Gaussian regimes we discussed in section 4.3.3, since one of the effects of the temporal walk-off in long crystals is to flatten a part of the eigenspectrum so that in a non-null subset of Λs they have very close values. This not perfect situation will be discussed in the following section.

We found that a favorable situation occurs when the pump field is detuned with respect to the phase-matched frequency ω_0 so that the offset parameter μ_p introduced in Eq. (4.28) is not null. In this case, the pump field selects from the phase-matching matrix a slice of width Δ_p around the frequency $\omega_0 + \mu_\mathrm{p}$.

Let's consider the realistic case of a 0.1 μm thick BIBO crystal inside a 4 m ring OPO cavity pumped by a c.w. train of 100 fs pulses for a degenerate type I critically phase-matching operation at 0.4 μm pumping. The resulting coupling matrix consists of two bell-shaped functions symmetric respect the axis $\omega_m - \omega_q = 0$, which have been boxed in Figure 5.5. The most significative eigenvalues satisfy (exactly) the condition $\Lambda_{2k+1} =$

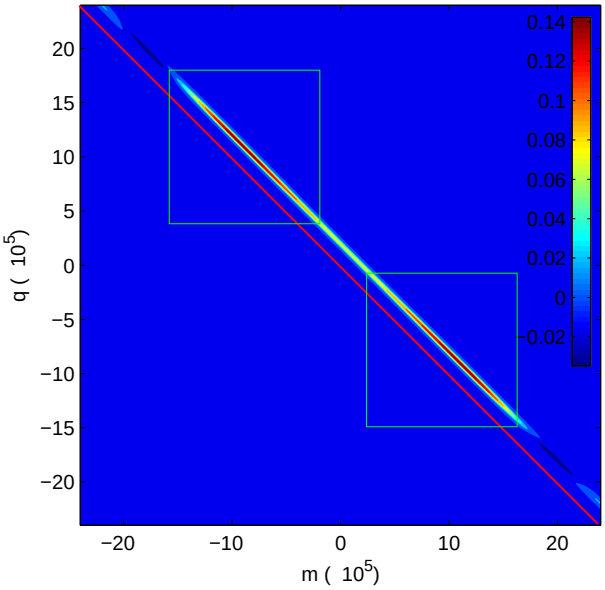

Figure 5.5: Coupling matrix when the pump field is mismatched of about $2\Delta_\mathrm{p}$ respect to the frequency ω_0.

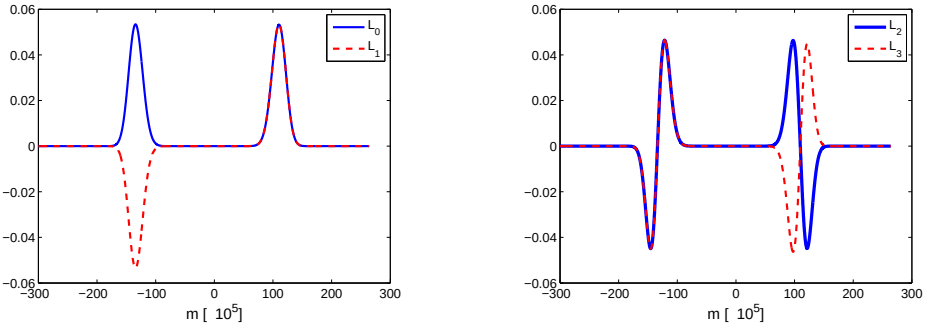

(a) (b)

Figure 5.6: Spectrum of the first four eigenvectors of the coupling matrix in the case $\mu_p = 2\Delta_p$.

$-\Lambda_{2k}$, while the fact the others are not exactly equal reflects only the necessity to have cut the space in which we diagonalized $\mathcal{L}$, as discussed in Section 4.3.2. Therefore, the couples of super-modes, obtained from the couples of super-modes $\hat{S}_{2k}$ and $\hat{S}_{2k+1}$ by means of the transformation (5.76), are entangled. The first four super-modes found by the diagonalization of $\mathcal{L}$ are represented in Figure 5.6. Notice that, since one half of the $2k+1$-th eigenvector has a phase of π with respect to the phase of the $2k$-th one and since the super-modes:

$$\hat{a}_k = \frac{\hat{S}_{2k} + \hat{S}_{2k+1}}{\sqrt{2}} \tag{5.80}$$

$$\hat{b}_k = \frac{\hat{S}_{2k} - \hat{S}_{2k+1}}{\sqrt{2}} \tag{5.81}$$

result to be entangled. Therefore, by manipulating the pump field, we are able to produce two well separated spectral bands of the signal field which have non-classical correlations. This situation corresponds to that of the non degenerate c.w. OPO where twin photons are generated at the signal and idler frequencies. From this point of view, the operators $\hat{a}_k$ and $\hat{b}_k$ create/annihilate a couple of twin distinguishable broadband photons in two different parts of the signal spectrum.

5.3.2 Imperfect two-mode correlations

Even if the situation discussed in the section above is very easy to obtain in order to produce two-mode quantum correlations, here we want to discuss a simpler way to "produce" entanglement. Since the optical field generated by a SPOPO is intrinsically multi-mode, we want to stress that one is not obliged to measuring noise correlations in a particular basis of super-modes. The basis of $\hat{S}_k$ results to be perfect for characterizing squeezing properties of the output signal field, but another set of super-modes could be more suitable for putting in evidence two-mode or multi-mode quantum correlation, exactly as we did above by defining the super-modes $\hat{a}_k$ and $\hat{b}_k$. The question we will try to answer in this section is the following: what will happen if we detect noise correlations between suitable linear combinations (like in the transformation (5.76)) of super-modes $\hat{S}_k$ associated to eigenvalues Λ_k which don't satisfy the condition $\Lambda_k = -\Lambda_j$ for perfect two-mode

correlations? Notice that this problem is equivalent to study what happens when we mix at a beam splitter two optical fields that are not equally squeezed, since the eigenvalues Λ_k determine the amount of squeezing of each super-mode. However, in the case of a SPOPO, we don't need to use two physically separate squeezers and a beam splitter, but we need only to choose the desired superposition of super-modes on which to perform our detections. These detections are standard homodyne detections which need, therefore, an suitable shaping of the local oscillator. For this reason the implementation of a pulse shaper is critical for an experimental realization of such measurements. Since the quantum state of the output signal field results factorized in the representation of the super-modes (5.22), if we limit our measurements to the subspace spanned by any couple of super-modes, for example $\{\hat{S}_1, \hat{S}_2\}$, we can neglect, for the sake of simplicity, all the terms in the interaction Hamiltonian (5.75) that are orthogonal to this space and consider only the evolution in it:

$$\hat{H}_I = \frac{i}{2}\hbar\kappa \left\{ \Lambda_1 \hat{S}_1^\dagger \hat{S}_1^\dagger + \Lambda_2 \hat{S}_2^\dagger \hat{S}_2^\dagger \right\} + \text{H.c.} \tag{5.82}$$

As we learned from the diagonalization of $\mathcal{L}$, its eigenvalues (or the squeezing parameter, from the point of view of Eq. (5.82)) form a decreasing progression which tends to zero and where Λ_k is positive if k is even or negative if k is odd. Even if the difference between Λ_1 and Λ_2 can be appreciable for typical configurations, for non-Gaussian regimes we have shown that a significative number of eigenvalues assumes values that are close each others. In such situations it is therefore reasonable to assume that the difference between the magnitude of the squeezing parameters $|\Lambda_1| - |\Lambda_2|$ is small. Also, let's suppose that $\Lambda_1 > 0 > \Lambda_2$ and $|\Lambda_1| > |\Lambda_2|$. By means of a rotation, new operators can be defined as follows:

$$\hat{a} = \frac{\hat{S}_1 + \hat{S}_2}{\sqrt{2}} \tag{5.83}$$

$$\hat{b} = \frac{\hat{S}_1 - \hat{S}_2}{\sqrt{2}} \tag{5.84}$$

The two-mode Hamiltonian (5.82), thus, become:

$$\hat{H}_I = \frac{i}{2}\hbar\kappa \left(\frac{\Lambda_1 + \Lambda_2}{2} \right) \left(\hat{a}^\dagger \hat{a}^\dagger + \hat{b}^\dagger \hat{b}^\dagger \right) + \frac{i}{2}\hbar\kappa \left(\Lambda_1 - \Lambda_2 \right) \hat{a}^\dagger \hat{b}^\dagger + \text{H.c.} \tag{5.85}$$

By defining:

$$\begin{cases} \Lambda_1 - \Lambda_2 \equiv 2\Lambda \\ \Lambda_1 + \Lambda_2 \equiv \epsilon \end{cases} \tag{5.86}$$

the interaction Hamiltonian becomes:

$$\hat{H}_I = \frac{i}{2}\hbar\kappa \left\{ \frac{\epsilon}{2} \left(\hat{a}^\dagger \hat{a}^\dagger + \hat{b}^\dagger \hat{b}^\dagger \right) + 2\Lambda \hat{a}^\dagger \hat{b}^\dagger \right\} + \text{H.c.} \tag{5.87}$$

The first term on the right hand side of eq. (5.87) is responsible for generation, in independent way, of couples of photons in the mode $\hat{a}$ and in the mode $\hat{b}$. Detection in each mode will give as result squeezed light. On the other side, detection of photons belonging to couples which are in different modes will give no correlations. Differently, the second term on the right hand of eq. (5.87) is responsible for generation of twin photons; therefore we expect to find quantum correlations between the modes $\hat{a}$ and $\hat{b}$. On the whole,

therefore, from a detection in the two modes we expect to find a melange of twin photons and uncorrelated photons which will decrease the amount of correlations that would be in the ideal case. In particular, this mixing depends on the relative magnitude of ϵ respect to Λ. In fact, solving the Heisenberg equations for the modes $\hat{a}$ and $\hat{b}$ gives squeezed joint quadratures:

$$\begin{aligned} \hat{P}_{a,\text{out}} + \hat{P}_{b,\text{out}} &= (\hat{P}_a + \hat{P}_b)e^{-(\Lambda-\epsilon/2)T} \\ \hat{X}_{a,\text{out}} - \hat{X}_{b,\text{out}} &= (\hat{X}_a - \hat{X}_b)e^{-(\Lambda-\epsilon/2)T} \end{aligned} \tag{5.88}$$

where $\hat{P}$ and $\hat{X}$ are respectively the phase and amplitude quadratures of modes $\hat{a}$ and $\hat{b}$, $T \equiv \kappa l/(2v)$ and l/v is the interaction time necessary to the field to go through the crystal (with l the crystal length and v the velocity of the optical field in the crystal. The squeezing on the joint quadratures (5.88) reflects the fact that the field phase and amplitude quadratures are not maximally entangled, situation that occurs when $\Lambda \to \infty$, for the simple passage interaction here considered, or at threshold when we consider also the effects of a cavity on the system evolution. Therefore, also in a not ideal situation, where the squeezing parameters are not equal, non-classical correlation can still be demonstrated. In order to put them in evidence, several criteria have been developed (for a short review see for example [Treps2004]). In the following we will discuss the Reid's criteria for EPR correlations [Reid1989] and the Giovannetti's criteria for separability [Giovannetti2003].

Reid's formulation for the EPR paradox

For observables maximally correlated it is possible to infer an observable of one subsystem from the result of measurement performed on a second subsystem spatially separated from the first, thus demonstrating an EPR paradox. According to Reid's argument [Reid1989] instead, for observables not maximally correlated, there will be an error in deducing information about the first system by a measure on the second one. However, it can be shown that it is still possible to obtain an EPR paradox proving the error is small enough compared to the Heisenberg uncertainty principle for two non-commuting observables. The estimator for proving the EPR paradox is given by the minimized inference errors respectively on the quadrature $\hat{X}_a$ by a measure of the quadrature $\hat{P}_b$ and on the quadrature $\hat{P}_a$ by a measure of the quadrature $\hat{X}_b$. It is possible to show that such inference errors are given by the product of the conditional variances for the phase and amplitude quadratures:

$$\Delta^2 X_a^c = \langle \hat{X}_{a,\text{out}}^2 \rangle - \frac{\langle \hat{X}_{a,\text{out}} \hat{P}_{b,\text{out}} \rangle}{\langle \hat{P}_{b,\text{out}}^2 \rangle}, \tag{5.89}$$

$$\Delta^2 P_a^c = \langle \hat{P}_{a,\text{out}}^2 \rangle - \frac{\langle \hat{P}_{a,\text{out}} \hat{X}_{b,\text{out}} \rangle}{\langle \hat{X}_{b,\text{out}}^2 \rangle}, \tag{5.90}$$

where the quadrature operators have been defined as:

$$\begin{cases} \hat{X}_a = \hat{a} + \hat{a}^\dagger, & \hat{P}_a = -i\left(\hat{a} - \hat{a}^\dagger\right) \\ \hat{X}_b = \hat{b} + \hat{b}^\dagger, & \hat{P}_b = -i\left(\hat{b} - \hat{b}^\dagger\right) \end{cases} \tag{5.91}$$

On the other side, in the Schrödinger picture, the evolution of the system is given applying the propagator generated by $\hat{H}_\text{I}$ to the vacuum state:

$$|\psi(t)\rangle = \exp\left\{-i\hat{H}_I t/\hbar\right\}|0\rangle \tag{5.92}$$

Since $\left[\hat{a}^\dagger\hat{a}^\dagger - \hat{a}\hat{a} + \hat{b}^\dagger\hat{b}^\dagger - \hat{b}\hat{b},\, \hat{a}^\dagger\hat{b}^\dagger + \hat{a}\hat{b}\right] = 0$, by means of the Campbell-Baker-Hausdorff formula we can disentangle the propagation operator, after an interaction time which corresponds to $\tau = l/v$:

$$\hat{U} = \mathrm{e}^{-i\hat{H}_I\tau/\hbar} = \mathrm{e}^{\frac{\epsilon}{2}\left(\hat{a}^\dagger\hat{a}^\dagger - \hat{a}\hat{a}\right)T}\mathrm{e}^{\frac{\epsilon}{2}\left(\hat{b}^\dagger\hat{b}^\dagger - \hat{b}\hat{b}\right)T}\mathrm{e}^{2\Lambda\left(\hat{a}^\dagger\hat{b}^\dagger - \hat{a}\hat{b}\right)T} \equiv \hat{U}_{a,a}\hat{U}_{b,b}\hat{U}_{a,b}, \tag{5.93}$$

where, again, we defined $T \equiv \kappa l/(2v)$.

Then, the evolution of the operators (5.91), after the parametric interaction in the crystal, is given applying the propagator (5.93):

$$\begin{aligned}
\hat{X}_{a,\mathrm{out}} &= \hat{U}\hat{X}_a\hat{U}^\dagger = \left[\cosh(\epsilon T)\ \hat{X}_a + \sinh(\epsilon T)\ \hat{P}_a\right]\cosh(2\Lambda T) \\
&+ \left[\cosh(\epsilon T)\ \hat{P}_b + \sinh(\epsilon T)\ \hat{X}_b\right]\sinh(2\Lambda T), \qquad (5.94)\\
\hat{P}_{a,\mathrm{out}} &= \hat{U}\hat{P}_a\hat{U}^\dagger = \left[\cosh(\epsilon T)\ \hat{P}_a + \sinh(\epsilon T)\ \hat{X}_a\right]\cosh(2\Lambda T) \\
&+ \left[\cosh(\epsilon T)\ \hat{X}_b + \sinh(\epsilon T)\ \hat{P}_b\right]\sinh(2\Lambda T), \qquad (5.95)
\end{aligned}$$

$$\begin{aligned}
\hat{X}_{b,\mathrm{out}} &= \hat{U}\hat{X}_b\hat{U}^\dagger = \left[\cosh(\epsilon T)\ \hat{P}_a + \sinh(\epsilon T)\ \hat{X}_a\right]\sinh(2\Lambda T) \\
&+ \left[\cosh(\epsilon T)\ \hat{X}_b + \sinh(\epsilon T)\ \hat{P}_b\right]\cosh(2\Lambda T), \qquad (5.96)\\
\hat{P}_{b,\mathrm{out}} &= \hat{U}\hat{P}_b\hat{U}^\dagger = \left[\cosh(\epsilon T)\ \hat{X}_a + \sinh(\epsilon T)\ \hat{P}_a\right]\sinh(2\Lambda T) \\
&+ \left[\cosh(\epsilon T)\ \hat{P}_b + \sinh(\epsilon T)\ \hat{X}_b\right]\cosh(2\Lambda T). \qquad (5.97)
\end{aligned}$$

Hence, minimized inference errors are:

$$\Delta^2\hat{X}_a^c = \frac{\cosh(\epsilon T)}{\cosh(2\Lambda T)}, \tag{5.98}$$

$$\Delta^2\hat{P}_a^c = \frac{\cosh(\epsilon T)}{\cosh(2\Lambda T)}. \tag{5.99}$$

According to quantum mechanics two non-commuting operators cannot be simultaneously measured with a certainty greater than that allowed by the uncertainty principle. In the Reid's original argumentation the product $\Delta\hat{X}_{a,\mathrm{out}}\Delta\hat{P}_{a,\mathrm{out}}$ is always less than one for equally squeezed optical beams. On the other hand, if not perfectly correlated photons are assumed to be detected, the amount of quantum correlations can be degraded. However, since:

$$\Delta\hat{X}_a^c\Delta\hat{P}_a^c = \frac{\cosh(\epsilon T)}{\cosh(2\Lambda T)}, \tag{5.100}$$

the EPR paradox can be still demonstrated provided ϵ is small enough. In particular, under the conditions we assumed at the beginning of this section ($|\Lambda_1| > |\Lambda_2|$), the inequality $\epsilon < 2\Lambda$ is always verified. Then the product of conditional variances (5.100) is always smaller than zero and EPR correlations are verified. However, the smaller ϵ is the greater the violation of the Heisenberg inequality is. Since a non-null ϵ degrades the quality of the EPR state generated, reducing its magnitude is a crucial ingredient for the generation of such a state. From this point of view, then, it turns out that non-Gaussian regimes are important resources for their realization.

Giovannetti's criterion and verification of entanglement in the parametric amplification case

For bipartite quantum systems, Giovannetti's criterion [Giovannetti2003] can be used as necessary condition to identify entangled systems. From the couples of evolved operators after the parametric evolution in Eqs. (5.94), (5.95), (5.96) and (5.97), two new operators acting respectively on each of the two Hilbert subspaces of $\hat{a}$ and $\hat{b}$ can be defined:

$$\hat{C}_1 = i\left[\hat{X}_{a,\text{out}}, \hat{P}_{a,\text{out}}\right], \tag{5.101}$$

$$\hat{C}_2 = -i\left[\hat{X}_{b,\text{out}}, \hat{P}_{b,\text{out}}\right]. \tag{5.102}$$

Let's introduce the following observables on the global Hilbert space:

$$\hat{u} = a_1\hat{X}_{a,\text{out}} + b_1\hat{P}_{b,\text{out}}, \tag{5.103}$$

$$\hat{v} = a_2\hat{P}_{a,\text{out}} + b_2\hat{X}_{b,\text{out}}, \tag{5.104}$$

where a_i, b_i are real parameters; if the considered state is a separable one, then the following inequality is verified:

$$\left\langle \Delta^2\hat{u}\right\rangle \left\langle \Delta^2\hat{v}\right\rangle \geq \tilde{O}^2, \tag{5.105}$$

with:

$$\tilde{O} = \frac{1}{2}\left(|a_1a_2|\ |\langle\hat{C}_1\rangle| + |b_1b_2|\ |\langle\hat{C}_2\rangle|\right). \tag{5.106}$$

If coherent vacuum inputs are considered, we have $\langle\hat{X}_{k,\text{out}}\rangle = 0 = \langle\hat{P}_{k,\text{out}}\rangle$ (for $k, m = a, b$), $\langle\hat{F}_a\hat{F}_b\rangle = 0$ (with $\hat{F} \in \{\hat{X}, \hat{P}\}$). Therefore, by using Eqs. (5.94), (5.95), (5.96) and (5.97), the variances of the operators $\hat{u}$ and $\hat{v}$ turn out to be:

$$\left\langle \Delta^2\hat{u}\right\rangle = \left(a_1^2 + b_1^2\right)\cosh\epsilon\cosh\left(2\Lambda\right) + 2a_1b_1\cosh\epsilon\sinh\left(2\Lambda\right), \tag{5.107}$$

$$\left\langle \Delta^2\hat{v}\right\rangle = \left(a_2^2 + b_2^2\right)\cosh\epsilon\cosh\left(2\Lambda\right) + 2a_2b_2\cosh\epsilon\sinh\left(2\Lambda\right). \tag{5.108}$$

On the other hand, operators $\hat{C}_1$ and $\hat{C}_2$ can be evaluated, from Eqs. (5.94), (5.95), (5.96) and (5.97), after very tedious algebra:

$$\begin{aligned}\hat{C}_1 = {} & i\left\{\cosh^2\left(2\Lambda T\right)\left[\hat{X}_a, \hat{P}_a\right] - \sinh^2\left(2\Lambda T\right)\left[\hat{X}_b, \hat{P}_b\right]\right. \\ & \left. + \frac{1}{2}\sinh\left(4\Lambda T\right)\left(\left[\hat{X}_a, \hat{X}_b\right] - \left[\hat{P}_a, \hat{P}_b\right]\right)\right\},\end{aligned} \tag{5.109}$$

$$\begin{aligned}\hat{C}_2 = {} & -i\left\{\cosh^2\left(2\Lambda T\right)\left[\hat{X}_b, \hat{P}_b\right] - \sinh^2\left(2\Lambda T\right)\left[\hat{X}_a, \hat{P}_a\right]\right. \\ & \left. - \frac{1}{2}\sinh\left(4\Lambda T\right)\left(\left[\hat{X}_a, \hat{X}_b\right] - \left[\hat{P}_a, \hat{P}_b\right]\right)\right\}.\end{aligned} \tag{5.110}$$

In the case defined by Eq. (5.91), $\left[\hat{F}_a, \hat{F}'_b\right] = 0$ (with $\hat{F}, \hat{F}' \in \{\hat{X}, \hat{P}\}$) and $\left[\hat{X}_k, \hat{P}_k\right] = 2i$ (with $k = a, b$), therefore $\hat{C}_1 = -2$, $\hat{C}_2 = 2$ and the operator $\tilde{O}^2$ is:

$$\tilde{O}^2 = \left(a_1^2a_2^2 + 2|a_1a_2b_1b_2| + b_1^2b_2^2\right). \tag{5.111}$$

When the special symmetrical conditions $a_1 = 1$, $a_2 = 1$, $b_1 = -1$ and $b_2 = -1$ are considered [5], we obtain:

$$\left\langle \Delta^2 \hat{u} \right\rangle \left\langle \Delta^2 \hat{v} \right\rangle = 4 \cosh^2 (\epsilon T)\, \mathrm{e}^{-4\Lambda T}, \tag{5.112}$$

$$\tilde{O}^2 = 4. \tag{5.113}$$

Therefore Giovannetti's criterion is satisfied for all values of Λ and ϵ according the following inequality:

$$\cosh^2 (\epsilon T)\, \mathrm{e}^{-4\Lambda T} \leq 1. \tag{5.114}$$

Similarly to the previous case, such inequality is satisfied for any values of ϵ and Λ. However, in situations where the squeezing parameters are very different from each others the quality of separability can be very degraded with respect to the case where $\epsilon = 0$ and $\Lambda \to +\infty$.

Entangled super-modes in the SPOPO case

In the case of synchronously pumped OPO, let's consider the usual case of a 0.1 mm thick BIBO crystal inside a 4 m ring OPO cavity pumped by a c.w. train of 100 fs pulses for a degenerate type I critically phase-matching operation at 0.4 μm pumping. In this situation, besides the evolution of quadrature operators described by the interaction Hamiltonian (5.82), we have to consider the effects of the cavity feed-back thus leading to the usual quantum Langevin equations for super-modes (5.34) whose solutions are expressed in the Fourier domain by Eqs. (5.37) and (5.38). From these solutions, one can chose any couple of $\hat{S}_{\mathrm{out},k}$ and $\hat{S}_{\mathrm{out},m}$ (with $k \neq m$) and mix them by means of the transformation (5.83) and (5.84), quantum correlations are expected to appear in the modes $\hat{a}$ and $\hat{b}$ according to the values of Λ_k and Λ_m. Giovannetti's criterion can be used to preview how much such modes are entangled. For this specific case all the operators will be defined directly in the Fourier domain and identified with a tilde signs. Supposing coherent vacuum input, the product of the variances of the $\hat{u}$ and $\hat{v}$ operators is readily obtained:

$$\left\langle \Delta^2 \widetilde{u} \right\rangle \left\langle \Delta^2 \widetilde{v} \right\rangle = 4\, v_k^{(-)}(\omega)\, v_k^{(-)}(-\omega)\, v_m^{(+)}(\omega)\, v_m^{(+)}(-\omega), \tag{5.115}$$

where the functions $v_k^{(\pm)}(\omega)$ have been defined in (5.38). The explicit expression of the operators $\widetilde{C}_1$ and $\widetilde{C}_2$ is instead:

$$\begin{aligned} \widetilde{C}_1 = & -\frac{1}{2}\Big\{ v_k^{(+)}(-\omega)\, v_k^{(-)}(\omega) + v_k^{(+)}(\omega)\, v_k^{(-)}(-\omega) \\ & + v_m^{(+)}(-\omega)\, v_m^{(-)}(\omega) + v_m^{(+)}(\omega)\, v_m^{(-)}(-\omega) \Big\} \end{aligned} \tag{5.116}$$

$$\begin{aligned} \widetilde{C}_2 = & -\frac{1}{2}\Big\{ v_k^{(+)}(-\omega)\, v_k^{(-)}(\omega) + v_k^{(+)}(\omega)\, v_k^{(-)}(-\omega) \\ & + v_m^{(+)}(-\omega)\, v_m^{(-)}(\omega) + v_m^{(+)}(\omega)\, v_m^{(-)}(-\omega) \Big\}. \end{aligned} \tag{5.117}$$

In figure 5.7 we report the difference $\langle \Delta^2 \widetilde{u} \rangle \langle \Delta^2 \widetilde{v} \rangle - \widetilde{O}^2$ for different couples of super-modes, namely the couples $\{\hat{S}_0, \hat{S}_1\}$, $\{\hat{S}_0, \hat{S}_{10}\}$, $\{\hat{S}_0, \hat{S}_{25}\}$ and $\{\hat{S}_0, \hat{S}_{50}\}$, under the assumption to be at threshold ($r = 1$). For small values of the difference $\epsilon = \Lambda_0 - \Lambda_k$ between the eigenvalues associated the quantum state associated to the couple of super-mode can be considered

[5] This choice of parameters guarantees $[\hat{u}, \hat{v}] = 0$.

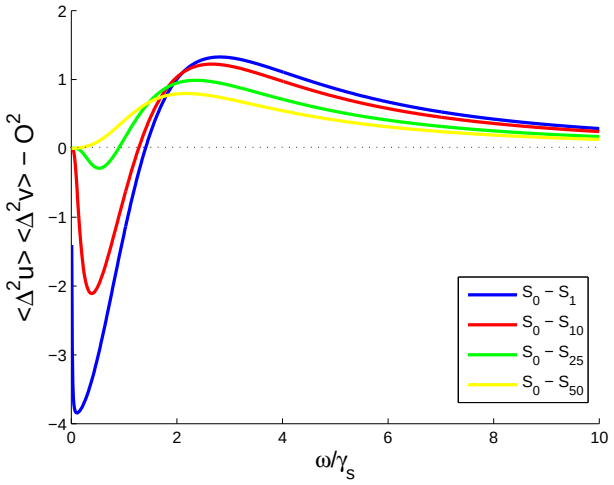

Figure 5.7: Giovannetti's estimator for separability evaluated for the couples of super-operators where the difference ϵ between the squeezing parameters increases. $\{\hat{S}_0, \hat{S}_1\}$ (blue line), $\{\hat{S}_0, \hat{S}_{10}\}$ (red line), $\{\hat{S}_0, \hat{S}_{25}\}$ (green line) and $\{\hat{S}_0, \hat{S}_{50}\}$ (yellow line). The quality of the entanglement between the modes obtained by mixing the super-modes which have approximatively equal squeezing parameters ($\Lambda_0 \simeq 272$ and $\Lambda_1 \simeq 269$, blue curve) is greater than situations where this difference is more significative ($\Lambda_{50} \simeq 76$, yellow curve).

inseparable since the Giovannetti's estimator assumes negative values in a frequency interval $0 < \omega \lesssim 1.41\gamma_s$ (in correspondence of the couple $\{\hat{S}_0, \hat{S}_1\}$). When ϵ increases, the region of negativity of the Giovannetti's estimator reduces too. In particular the couple of super-modes $\{\hat{S}_0, \hat{S}_{50}\}$ cannot be any longer considered entangled. Notice, however, that the great number of couples which still can be considered entangled witnesses, once again, the significant "multimodiciy" of a SPOPO.

5.4 Multi-mode entanglement

The entanglement shared between two parties enhances their capabilities to exchange information and to increase the security in communicating messages by means, for example, of quantum teleportation, quantum dense coding or quantum key distribution. Such communication schemes based on quantum protocols can be generalized to an arbitrary number of parties that share multipartite entanglement. For example optimal cloning can be achieved when a sender transfers quantum information to several receivers [Murao1999], or the parties share an information that can be retrieved only when all the parties cooperate (quantum secret sharing [Hillery1999]). The possibility of producing multipartite entanglement was experimentally demonstrated for the first time with the realization of GHZ states [Greenberger1990] of single-photon polarization [Bouwmeester1999], but a simple scheme for producing bipartite entangled states in continuous variable regimes had already been demonstrated by mixing independent squeezed states on beam splitter [Furusawa1998]. Multi-mode entanglement of continuous variables was first proposed by van Loock and Braunstein [vanLoock2000] and experimentally demonstrated in two different regimes [Aoki2003, Jing2003]. In their theoretical proposition N squeezed modes are

independently generated by N degenerate OPAs and coupled through a N-port beam splitter. Pfister *et al.* [Pfister2004] proposed a scheme where the simultaneous phase-matching of several second-order nonlinearities creating two-mode squeezing between N cavity field modes permits the use of a single OPA and no beam splitters. A similar scheme was recently reproposed by Menicucci *et al.* [Menicucci2007] showing the possibility of realizing an ultra-compact experimental setup involving only one OPO and no beam splitters. In both propositions a crucial point is the engineering of concurrent nonlinear interactions between (in principle) an arbitrary number of modes. The proposed set up seems to be rigid because of concurrent nonlinearities have to be designed expressly for a give number of input modes. Even if this complicated problem is solved using quasi-phase-matched materials [Pfister2004, Lifshitz2005], an experimental implementation could result of difficult feasibility when frequency combs of huge number of modes are considered, thus limiting the number of entangled modes.

In this section we will show that the scheme for the production of multi-mode entangled state proposed by Pfister without the beam-splitter network can be generalized to the class of multi-mode systems and in particular to OPOs that show multi-mode quantum character in spatial [Lopez2005, Navarrete2008] or temporal domain. While in the Pfister's proposal the engineering of the nonlinearities is necessary in order to obtain equal squeezing parameters for different modes, our purpose is to show that, even if, a priori, the squeezing parameters Λ_k are not exactly equal, quantum correlations can still exist, as we have discovered in Section 5.3.2 for the two-mode case. Further, under particular conditions (i.e. non-Gaussian regimes) one can make approaching the values of the squeezing parameters of a non-null set of super-modes, thus increasing the quantity and quality of non-classical correlations. Under this point of view, the advantage of a multi-mode system such a SPOPO is that one can use just typical nonlinearities (the one used in standard OPOs) in concomitance with a space or time multi-mode pump field.

On the other hand, a critical point is how measurements are realized. In the continuous variables regimes quantum fluctuations of the output field are projected onto a strong coherent local oscillator. Therefore the detection of the good entangled states presupposes the capability to shape the local oscillator in order to have access to that portion of Hilbert space where multi-mode entanglement is present. In Pfister's proposal this could be not too much critical for two reasons: primarily, the dimension of the total Hilbert space is exactly the dimension of the entangled state, secondarily, all the parties involved are easily physically separable by means of filters like polarizing beam splitters.

In the following we will analyze, first, the occurrence of three-mode and N-mode entanglement in the case of not equal squeezing parameters for a simple system such as the simple passage parametric interaction with a nonlinear crystal. We will find the eigenmodes of the Heisenberg evolution equations that result to be squeezed. Afterwards, we will consider the complete evolution equations for a SPOPO and we will show that for these eigenmodes is still possible to measure strong quantum correlations.

Three-mode entanglement

By restricting our measurement to the sub-space spanned by $\{\hat{S}_1, \hat{S}_2, \hat{S}_3\}$, where the subscripts 1,2 and 3 indicate a general tern chosen among all the possible super-modes, the

interaction Hamiltonian can be written as:

$$\hat{H}_I = \frac{i}{2}\hbar\kappa \left\{ \Lambda_1 \hat{S}_1^\dagger \hat{S}_1^\dagger + \Lambda_2 \hat{S}_2^\dagger \hat{S}_2^\dagger + \Lambda_3 \hat{S}_3^\dagger \hat{S}_3^\dagger \right\} + \text{H.c.} \tag{5.118}$$

As anticipated above, in the introduction to this section, we are starting from an interaction Hamiltonian where each term is weighted by a squeezing parameter Λ_k which is different for each mode. Differently, in the case considered in Pfister's work, the starting point is an Hamiltonian where the squeezing on each mode occurs with equal strength ($\Lambda_1 = \Lambda_2 = \Lambda_3$). This situation can be obtained by a proper engineering of the non-linearities. Our purpose is, instead, to release this condition and consider the general case of a standard non-linearities. In fact, for the case of SPOPOs, we have shown that it is possible to bring closer, simultaneously, a significant number of squeezing parameters by increasing the temporal walk-off between pump and signal pulses, that can be realized simply by controlling the crystal length l or the pump pulse duration τ_p. Therefore, our purpose in this section and in the next, is to obtain a general expression for the mode operators where three-mode or multi-mode entanglement is present, in a simple case where the effects of the cavity are temporarily neglected. By means of these expressions, then, we will discuss the specific case of SPOPOs, keeping in account for the cavity feed-back, showing that multi-mode entanglement can be still demonstrated for a large number of modes.

Let's assume, without loss of generality, that $-\Lambda_1 > \Lambda_2 > \Lambda_3 > 0$. The operators $\hat{a}$, $\hat{b}$ and $\hat{c}$ on which the measurement have to be performed are given by the following rotation:

$$\begin{pmatrix} \hat{a} \\ \hat{b} \\ \hat{c} \end{pmatrix} = B_{1,2}\left(\frac{1}{\sqrt{3}}\right) B_{2,3}\left(\frac{1}{\sqrt{2}}\right) = \begin{pmatrix} \frac{1}{\sqrt{3}} & \sqrt{\frac{2}{3}} & 0 \\ \frac{1}{\sqrt{3}} & -\frac{1}{\sqrt{6}} & \frac{1}{\sqrt{2}} \\ \frac{1}{\sqrt{3}} & -\frac{1}{\sqrt{6}} & -\frac{1}{\sqrt{2}} \end{pmatrix} \begin{pmatrix} \hat{S}_1 \\ \hat{S}_2 \\ \hat{S}_3 \end{pmatrix} \tag{5.119}$$

that is formally equivalent to a "tritter" [Braunstein1998b] mixing ports 1 and 2 of an angle of $\arccos\left(1/\sqrt{3}\right)$ and ports 2 and 3 of an angle of $\pi/4$ (see Figure 5.8). After the

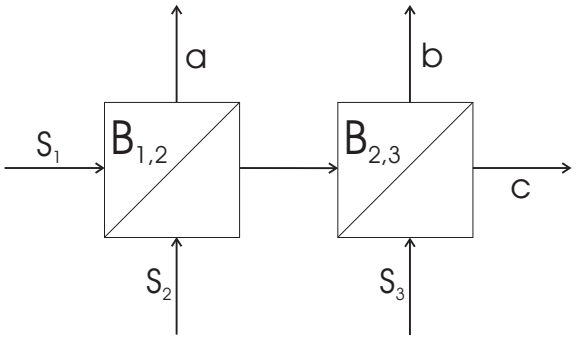

Figure 5.8: Equivalent representation of the transformation (5.119). The new super-mode operators $\hat{a}$, $\hat{b}$ and $\hat{c}$ are obtained by mixing the operators $\hat{S}_1$, $\hat{S}_2$ and $\hat{S}_3$ by means of two beam splitters $B_{1,2}$ (equivalent to a rotation of $\theta_{1,2} = \arccos(1/\sqrt{3})$) and $B_{2,3}$ (equivalent to a rotation of $\theta_{2,3} = \arccos(1/\sqrt{2})$).

transformation (5.119), the Hamiltonian (5.118) can be rewritten as:

$$\hat{H}_I = \frac{i}{2}\hbar\kappa \left\{ \left(\frac{\Lambda}{3} - \frac{2}{3}\epsilon_2\right) \hat{a}^{\dagger\,2} + \left(\frac{\Lambda}{3} - \frac{1}{6}\epsilon_2\right) \hat{b}^{\dagger\,2} + \left(\frac{\Lambda}{3} - \frac{2}{3}\epsilon_2 - \frac{1}{2}\epsilon_3\right) \hat{c}^{\dagger\,2} + \right.$$
$$\left. - \left(\frac{4}{3}\Lambda - \frac{2}{3}\epsilon_2\right) \hat{a}^\dagger\hat{b}^\dagger - \left(\frac{4}{3}\Lambda - \frac{2}{3}\epsilon_2\right) \hat{a}^\dagger\hat{c}^\dagger - \left(\frac{4}{3}\Lambda + \frac{1}{3}\epsilon_2 - \epsilon_3\right) \hat{b}^\dagger\hat{c}^\dagger \right\} + \text{H.c.} \tag{5.120}$$

where we defined $\Lambda_1 = -\Lambda$, $\Lambda_2 = \Lambda - \epsilon_2$ and $\Lambda_3 = \Lambda - \epsilon_3$. Notice that, in the symmetric situation where the three squeezing parameter are equally separated, the Hamiltonian (5.120) converges to Eq. (13) in [Pfister2004] for $\epsilon \to 0$. The system of Heisenberg equations, describing the evolution of the super-modes $\hat{a}$, $\hat{b}$ and $\hat{c}$ in a simple passage interaction, can be written as:

$$\frac{d}{dt}\begin{pmatrix}\hat{a}\\ \hat{b}\\ \hat{c}\end{pmatrix} = \kappa \begin{pmatrix} \frac{\Lambda-2\epsilon_2}{3} & -\frac{2\Lambda-\epsilon_2}{3} & -\frac{2\Lambda-\epsilon_2}{3} \\ -\frac{2\Lambda-\epsilon_2}{3} & \frac{\Lambda}{3} - \frac{\epsilon_2+3\epsilon_3}{6} & -\frac{2\Lambda+\epsilon_2-3\epsilon_3}{3} \\ -\frac{2\Lambda-\epsilon_2}{3} & -\frac{2\Lambda+\epsilon_2-3\epsilon_3}{3} & \frac{\Lambda}{3} - \frac{\epsilon_2+3\epsilon_3}{6} \end{pmatrix} \begin{pmatrix}\hat{a}^\dagger\\ \hat{b}^\dagger\\ \hat{c}^\dagger\end{pmatrix}. \tag{5.121}$$

As discussed in Section 4.3.3, when some parameters of the system (namely, the pump pulse width τ_p and the crystal thickness l) are changed in order to progressively approach a non-Gaussian regime – where the conditions (4.56) and (4.57) are no more verified – the values of an increasingly large number of eigenvalues approach each other. Therefore, we are allowed to suppose that ϵ_2 and ϵ_3 become negligible respect to Λ. In such case the eigenvalues of $\mathcal{M}$ are $(-\Lambda, \Lambda, \Lambda)$ and its eigenvectors, given by:

$$\begin{aligned} \hat{X}_{a,\mathrm{out}} + \hat{X}_{b,\mathrm{out}} + \hat{X}_{c,\mathrm{out}} &= (\hat{X}_a + \hat{X}_b + \hat{X}_c)e^{-\Lambda T}, \\ \hat{P}_{a,\mathrm{out}} - \hat{P}_{c,\mathrm{out}} &= (\hat{P}_a - \hat{P}_c)e^{-\Lambda T}, \\ \hat{P}_{b,\mathrm{out}} - \hat{P}_{c,\mathrm{out}} &= (\hat{P}_b - \hat{P}_c)e^{-\Lambda T}, \end{aligned} \tag{5.122}$$

are squeezed joint operators, whose common eigenstate is a three-mode entangled state that converges towards the GHZ state $\int \mathrm{d}x|x,x,x\rangle$ when $\Lambda \to \infty$. Notice that we labeled with "out" the operators outgoing the crystal after an interaction time l/v and we defined $T \equiv \kappa l/(2v)$. However ϵ_2 and ϵ_3 cannot be considered, in general, exactly zero even in a non-Gaussian regime and the operators (5.122) are no more eigenstates of $\mathcal{M}$. In this case the eigenvalues are $(-\Lambda, \Lambda - \epsilon_2, \Lambda - \epsilon_3)$ and the eigenvectors are:

$$\begin{aligned} \hat{v}_{1,\mathrm{out}} &= \left(\hat{X}_a + \hat{X}_b + \hat{X}_c\right) e^{-\Lambda T}, & \hat{v}_{4,\mathrm{out}} &= -\left(\hat{P}_a + \hat{P}_b + \hat{P}_c\right) e^{\Lambda T}, \\ \hat{v}_{2,\mathrm{out}} &= \left(2\hat{P}_a - \hat{P}_b - \hat{P}_c\right) e^{-(\Lambda-\epsilon_2)T}, & \hat{v}_{5,\mathrm{out}} &= \left(-2\hat{X}_a + \hat{X}_b + \hat{X}_c\right) e^{(\Lambda-\epsilon_2)T}, \\ \hat{v}_{3,\mathrm{out}} &= \left(\hat{P}_b - \hat{P}_c\right) e^{-(\Lambda-\epsilon_3)T}, & \hat{v}_{6,\mathrm{out}} &= -\left(\hat{X}_b - \hat{X}_c\right) e^{(\Lambda-\epsilon_3)T}. \end{aligned} \tag{5.123}$$

Hence, in the basis $\{\hat{v}_{1,\mathrm{out}}, \hat{v}_{2,\mathrm{out}}, \hat{v}_{3,\mathrm{out}}, \hat{v}_{4,\mathrm{out}}, \hat{v}_{5,\mathrm{out}}, \hat{v}_{6,\mathrm{out}}\}$, the evolved joint operators like in (5.122) are given by:

$$\begin{aligned} \hat{X}_{a,\mathrm{out}} + \hat{X}_{b,\mathrm{out}} + \hat{X}_{b,\mathrm{out}} &= \left(\hat{X}_a + \hat{X}_b + \hat{X}_c\right) e^{-\Lambda T}, \\ \hat{P}_{a,\mathrm{out}} - \hat{P}_{c,\mathrm{out}} &= \frac{1}{2}\left(\hat{v}_2 \mathrm{e}^{-(\Lambda-\epsilon_2)T} + \hat{v}_3 \mathrm{e}^{-(\Lambda-\epsilon_3)T}\right), \\ \hat{P}_{b,\mathrm{out}} - \hat{P}_{c,\mathrm{out}} &= \left(\hat{P}_b - \hat{P}_c\right) \mathrm{e}^{-(\Lambda-\epsilon_3)T}. \end{aligned} \tag{5.124}$$

From (5.124), we can conclude that the amount of quantum three-mode correlations and the reliability of the three-mode GHZ state corresponding to the system of modes (5.124) depend on how small the differences between the squeezing parameters, ϵ_2 and ϵ_3, are with respect to the amount of squeezing determined by Λ.

Generalization to N-mode entanglement

Let's now consider the interaction Hamiltonian corresponding to the parametric evolution in the N-dimensional Hilbert space spanned by the super-operators $\{\hat{S}_1, \ldots, \hat{S}_N\}$:

$$\hat{H}_I = \frac{i}{2}\hbar\kappa \left\{ \Lambda_1 \hat{S}_1^\dagger \hat{S}_1^\dagger + \ldots + \Lambda_N \hat{S}_N^\dagger \hat{S}_N^\dagger \right\} + \text{H.c.} \tag{5.125}$$

Like in the previous section, after the definition of new super-mode operators $\{\hat{a}_1, \ldots, \hat{a}_N\}$ according to the multi-mode transformation proposed by Braunstein [Braunstein1998b, vanLoock2000], we will express the evolution equations, for a simple passage interaction inside a non-linear crystal, in function of such operators in order to obtain the eigenmodes of squeezing (say $\{\hat{v}_1, \ldots, \hat{v}_N\}$). Then, we will write the joint-quadrature operators of the $\hat{a}_k$ operators in function of $\hat{v}_k$ operators in order to put in evidence multi-mode non-classical correlation.

The set of operators $\{\hat{a}_1, \ldots, \hat{a}_N\}$ giving N-mode quantum entanglement is obtained applying the following rotation [Braunstein1998b, vanLoock2000] to the operators $\{\hat{S}_k\}_{1 \le k \le N}$ (see Figure 5.9):

$$\mathcal{B}^N = B_{N-1,N}\left(\frac{1}{\sqrt{2}}\right) B_{N-2,N-1}\left(\frac{1}{\sqrt{3}}\right) \cdot \ldots \cdot B_{1,2}\left(\frac{1}{\sqrt{N}}\right) \tag{5.126}$$

where matrix $B_{k,l}(x)$ is an N-dimensional identity matrix where the entries $I_{k,k}$, $I_{k,l}$, $I_{l,k}$, $I_{l,l}$ have been replaced by the beam-splitter matrix:

$$\begin{pmatrix} x & \sqrt{1-x^2} \\ \sqrt{1-x^2} & -x \end{pmatrix} \tag{5.127}$$

In an explicit form, the matrix $\mathcal{B}^N$ reads:

$$\mathcal{B}_{ij}^N = \begin{cases} 0 & i \ge j+2 \\ \frac{1}{\sqrt{N}} & i = 1,\ j = 1, 2, \ldots, N \\ \sqrt{\frac{N-i+1}{N-i+2}} & i = j+1 \\ -\frac{1}{\sqrt{(N-i+1)(N-i+2)}} & i \le j \end{cases} \tag{5.128}$$

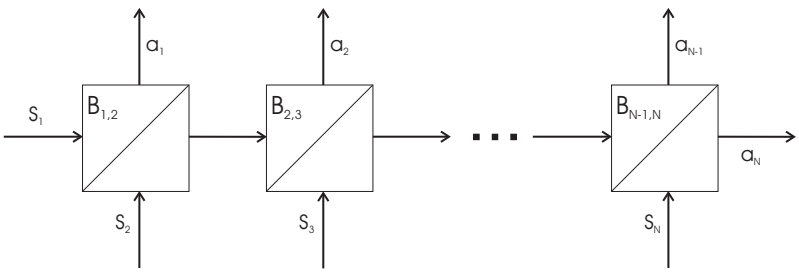

Figure 5.9: Equivalent representation of the transformation (5.126). The new super-mode operators $\hat{a}_1, \hat{a}_2, \ldots, \hat{a}_N$ are obtained by mixing the operators $\hat{S}_1, \hat{S}_2, \ldots \hat{S}_N$ by means of $N-1$ beam splitters.

After a change of basis by means of the transformation (5.126) and by defining $\Lambda_1 = -\Lambda$, $\Lambda_k = \Lambda - \epsilon_k$ for $k = \{2, \ldots, N\}$, the Hamiltonian (5.125) can be recast as:

$$\hat{H}_N = \hat{H}_N^{(0)} - \frac{i}{2}\hbar\kappa \left[\sum_{k=1}^{N} \sum_{p,q=1}^{N} \epsilon_k \mathcal{B}_{k,p}^N \mathcal{B}_{k,q}^N \hat{a}_p^\dagger \hat{a}_q^\dagger - \text{H.c.} \right] \tag{5.129}$$

where the first term on the right hand side is the "unperturbed" Hamiltonian like in [Pfister2004]:

$$\hat{H}_N^{(0)} = \frac{i}{2}\hbar\kappa \left[\frac{N-2}{N} \sum_{m=1}^{N} \hat{a}_m^{\dagger\,2} - \frac{2}{N} \sum_{p=1}^{N} \sum_{q>p}^{N} \hat{a}_p^\dagger \hat{a}_q^\dagger \right] + H.c. \tag{5.130}$$

In order to solve the Heisenberg equations in the N-dimensional case, we need to write in explicit form the corrections to the matrix $\mathcal{M} = \mathcal{M}^{(0)} + \kappa \sum_{k=1}^{N} \epsilon_k \mathcal{E}_{kij}^N$ which are proportional to the entries of the matrix $\mathcal{E}_{kij}^N = \mathcal{B}_{ki}^N \mathcal{B}_{kj}^N$ given below:

$$\mathcal{E}_{kij}^N = \begin{cases} 0 & i \leq k-2 \text{ or } j \leq k-2 \\ \frac{N-k+1}{N-k+2} & (i,j) = (k-1, k-1) \\ -\frac{1}{N-k+2} & i = k-1, j \geq k \;\text{ or }\; j = k-1, i \geq k \\ \frac{1}{(N-k+1)(N-k+2)} & i \geq k \text{ or } \; j \geq k \end{cases} \tag{5.131}$$

which, more explicitly, appears as:

$$\mathcal{E}_{kij}^N = \begin{pmatrix} 0 & \ldots & 0 & 0 & \ldots & \ldots & 0 \\ \vdots & \ddots & \vdots & \vdots & \ldots & \ldots & \vdots \\ 0 & \ldots & 0 & 0 & \ldots & \ldots & 0 \\ 0 & \ldots & 0 & \frac{N-k+1}{N-k+2} & -\frac{1}{N-k+2} & \cdots & -\frac{1}{N-k+2} \\ \vdots & \vdots & \vdots & -\frac{1}{N-k+2} & \frac{1}{(N-k+1)(N-k+2)} & \cdots & \frac{1}{(N-k+1)(N-k+2)} \\ \vdots & \vdots & \vdots & \vdots & \vdots & \ddots & \vdots \\ 0 & \ldots & 0 & -\frac{1}{N-k+2} & \frac{1}{(N-k+1)(N-k+2)} & \cdots & \frac{1}{(N-k+1)(N-k+2)} \end{pmatrix} \tag{5.132}$$

Hence, the eigenvalues of $\mathcal{M}$ are $\{-\Lambda, \Lambda - \epsilon_2, \ldots, \Lambda - \epsilon_N\}$ and the corresponding eigenvectors, in terms of quadratures of the super-mode operators $\{\hat{a}_1, \ldots, \hat{a}_N\}$, are:

$$\begin{aligned} \hat{v}_1(\tau) &= \sum_{k=1}^{N} \hat{X}_k \, e^{-\Lambda T}, \\ \hat{v}_l(\tau) &= \left[(N-1)\, \hat{P}_{l-1} - \sum_{k=l}^{N} \hat{P}_k \right] e^{-(\Lambda - \epsilon_l)T}, \\ \hat{v}_{N+1}(\tau) &= -\sum_{k=1}^{N} \hat{P}_k \, e^{\Lambda T}, \\ \hat{v}_{N+l}(\tau) &= \left[-(N-1)\, \hat{X}_{l-1} + \sum_{k=l}^{N} \hat{X}_k \right] e^{(\Lambda - \epsilon_l)T}, \end{aligned} \tag{5.133}$$

for $l = 2, \ldots, N$. As in the three-mode case, we can retrieve the evolved amplitude and phase quadrature operators, using the basis (5.133). In fact, by inverting Eq. (5.133) we obtain:

$$\begin{aligned}\hat{X}_k &= \frac{1}{N}\hat{v}_1 - \frac{1}{N-k+1}\hat{v}_{N+k+1} + \sum_{j=2}^{k}\frac{\hat{v}_{N+j}}{(N-j+2)(N-j+1)},\\ \hat{P}_k &= -\frac{1}{N}\hat{v}_{N+1} + \frac{1}{N-k+1}\hat{v}_{k+1} - \sum_{j=2}^{k}\frac{\hat{v}_j}{(N-j+2)(N-j+1)},\end{aligned} \tag{5.134}$$

for $k = 1, \ldots, N-1$, and for $k = N$:

$$\begin{aligned}\hat{X}_N &= \frac{1}{N}\hat{v}_1 + \sum_{j=2}^{N}\frac{\hat{v}_{N+j}}{(N-j+2)(N-j+1)},\\ \hat{P}_N &= -\frac{1}{N}\hat{v}_{N+1} - \sum_{j=2}^{N}\frac{\hat{v}_j}{(N-j+2)(N-j+1)}.\end{aligned} \tag{5.135}$$

Hence, the joint operators after parametric interaction are:

$$\begin{aligned}&\hat{X}_1(\tau) + \ldots + \hat{X}_N(\tau) = \sum_{k=1}^{N}\hat{X}_k\, e^{-\Lambda T},\\ &\hat{P}_k(\tau) - \hat{P}_{k+1}(\tau) = \frac{1}{N-k+1}\hat{v}_{k+1}e^{-(\Lambda-\epsilon_{k+1})T} - \frac{1}{N-k}\hat{v}_{k+2}e^{-(\Lambda-\epsilon_{k+2})T},\\ &\hat{P}_{N-1}(\tau) - \hat{P}_N(\tau) = \hat{v}_N e^{-(\Lambda-\epsilon_N)T},\end{aligned} \tag{5.136}$$

for $k = 1, \ldots, N-2$.

Similarly to the case of three-mode entanglement, this result shows that N-mode non-classical correlations are degraded in the case we mix N modes with different squeezing parameters. However, provided that $\epsilon_k \to 0$ for $k = 2, \ldots, N$, such correlations can still be significative and the N-mode quantum state corresponding to operators (5.136) converges towards the generalized N-mode GHZ state $\int \mathrm{d}x|x\rangle_1 \otimes \ldots \otimes |x\rangle_N$ in the limit of infinite squeezing $\Lambda \to +\infty$.

5.4.1 Multi-mode entanglement in the SPOPO case

In this section we consider the complete model for a SPOPO, in the realistic case of the BIBO nonlinear crystal, keeping into account not only the interaction Hamiltonian (5.75) but also the effects resulting from the cavity feedback and losses. The evolution for each super-mode $\hat{S}_k(t)$, described by (5.30) and (5.31), permits to obtain the corresponding Langevin equation for operators defined as like as in Eqs. (5.83) and (5.84), (5.119) or by means of the rotation (5.126) and finally retrieve the noise variance spectrum of the joint quadrature operators. In the following we will first consider the three-mode case and then we will generalize to an N-mode entangled state.

Three-mode entanglement

Starting from the evolution equations (5.30) and (5.31) for $k = 1, 2, 3$, let us mix now the operators $\hat{S}_1$, $\hat{S}_2$ and $\hat{S}_3$ by means of the tritter matrix (5.119) in order to obtain operators

$\hat{a}_1$, $\hat{a}_2$ and $\hat{a}_3$ and their corresponding Langevin equations. The vectors $\hat{\phi}_1$, $\hat{\phi}_2$ and $\hat{\phi}_3$ are constants of motion, as in (5.123), and in the Fourier space they are given by:

$$\begin{aligned}
\widetilde{\phi}_{\mathrm{out},1}(\omega) &= \mathcal{V}_1(\omega)\,\widetilde{\phi}_{\mathrm{in},1}(\omega)\,,\\
\widetilde{\phi}_{\mathrm{out},2}(\omega) &= \mathcal{V}_2(\omega)\,\widetilde{\phi}_{\mathrm{in},2}(\omega)\,,\\
\widetilde{\phi}_{\mathrm{out},3}(\omega) &= \mathcal{V}_3(\omega)\,\widetilde{\phi}_{\mathrm{in},3}(\omega)\,,
\end{aligned} \tag{5.137}$$

where:

$$\begin{aligned}
\mathcal{V}_1(\omega) &= \frac{\gamma^2(1-r)^2+\omega^2}{\gamma^2(1+r)^2+\omega^2},\\
\mathcal{V}_2(\omega) &= \frac{\gamma^2\left(1-r\left(1-\frac{\epsilon_2}{\Lambda}\right)\right)^2+\omega^2}{\gamma^2\left(1+r\left(1-\frac{\epsilon_2}{\Lambda}\right)\right)^2+\omega^2},\\
\mathcal{V}_3(\omega) &= \frac{\gamma^2\left(1-r\left(1-\frac{\epsilon_3}{\Lambda}\right)\right)^2+\omega^2}{\gamma^2\left(1+r\left(1-\frac{\epsilon_3}{\Lambda}\right)\right)^2+\omega^2}.
\end{aligned} \tag{5.138}$$

As before, we defined $\Lambda_1 = -\Lambda$, $\Lambda_2 = \Lambda - \epsilon_2$ and $\Lambda_3 = \Lambda - \epsilon_3$. Hence, the joint quadrature operators (5.124) have the following expressions:

$$\begin{aligned}
\widetilde{X}_{\mathrm{out},1}(\omega) + \widetilde{X}_{\mathrm{out},2}(\omega) + \widetilde{X}_{\mathrm{out},3}(\omega) &= \mathcal{V}_1(\omega)\,\widetilde{\phi}_{\mathrm{in},1}(\omega)\,,\\
\widetilde{P}_{\mathrm{out},1}(\omega) - \widetilde{P}_{\mathrm{out},3}(\omega) &= \frac{1}{2}\big(\mathcal{V}_2(\omega)\,\widetilde{\phi}_{\mathrm{in},2}(\omega) + \mathcal{V}_3(\omega)\,\widetilde{\phi}_{\mathrm{in},3}(\omega)\big),\\
\widetilde{P}_{\mathrm{out},2}(\omega) - \widetilde{P}_{\mathrm{out},3}(\omega) &= \mathcal{V}_3(\omega)\,\widetilde{\phi}_{\mathrm{in},3}(\omega)\,,
\end{aligned} \tag{5.139}$$

and the corresponding variances are expressed by:

$$\begin{aligned}
V_{\hat{X}_1+\hat{X}_2+\hat{X}_3}(\omega) &= \mathcal{V}_1(\omega)\,\mathcal{V}_1(-\omega)\,,\\
V_{\hat{P}_1-\hat{P}_3}(\omega) &= \frac{1}{2}\big(\mathcal{V}_2(\omega)\,\mathcal{V}_2(-\omega) + \mathcal{V}_3(\omega)\,\mathcal{V}_3(-\omega)\big),\\
V_{\hat{P}_2-\hat{P}_3}(\omega) &= \mathcal{V}_3(\omega)\,\mathcal{V}_3(-\omega)\,,
\end{aligned} \tag{5.140}$$

which have been obtained renormalizing the eigenvectors $\hat{\phi}_i$ for $i = 1, 2, 3$ and keeping in mind that the only non null correlations, for vacuum input state, are:

$$\left\langle \widetilde{\phi}_{\mathrm{in},i}(\omega)\,\widetilde{\phi}^{\dagger}_{\mathrm{in},j}(\omega')\right\rangle = \delta_{ij}\,\delta(\omega-\omega')\,. \tag{5.141}$$

Let's address to the case of a 0.1 μm thick BIBO crystal inside a 4 m ring OPO cavity pumped by a c.w. train of 100 fs pulses for a degenerate type I critically phase-matching operation at 0.4 μm pumping. Then the squeezing parameters for the first three supermodes are $\Lambda_1 = -272$, $\Lambda_2 = 269$ and $\Lambda_3 = 266$. At threshold ($r = 1$) and at the carrying frequency ($\omega = 0$) the variances for the joint quadrature operators (5.139) are $V_{\hat{X}_1+\hat{X}_2+\hat{X}_3} = 0$, $V_{\hat{P}_1-\hat{P}_3} = 5\times10^{-5}$ (i.e. about -43 dB) and $V_{\hat{P}_2-\hat{P}_3} = 9\times10^{-5}$ (i.e. about -40 dB). In typical configurations for BIBO based SPOPOs, therefore, we expect to find excellent quantum three-mode correlations between the quadratures defined in (5.119) even if there are small differences between the Λ_k and the use of a experimental configuration for which the system is in a non-Gaussian regime is not necessary.

Multi-mode entanglement

Let's consider, now, the evolution in the subspace $\{\hat{S}_1, \ldots, \hat{S}_N\}$ which is described by the equations (5.30) and (5.31) for $k = 1, \ldots, N$. The eigenvectors $\{\hat{\psi}_1, \ldots, \hat{\psi}_N\}$ introduced in (5.133) are constants of motion and, thus, we can write in the Fourier space:

$$\widetilde{v}_{\text{out},k}(\omega) = \mathcal{V}_k(\omega)\, \widetilde{v}_{\text{in},k}(\omega), \tag{5.142}$$

for $k = 1, \ldots, N$, where:

$$\mathcal{V}_k(\omega) = \frac{\gamma^2 \left(1 - r\left(1 - \frac{\epsilon_k}{\Lambda}\right)\right)^2 + \omega^2}{\gamma^2 \left(1 + r\left(1 - \frac{\epsilon_k}{\Lambda}\right)\right)^2 + \omega^2}, \tag{5.143}$$

with $\Lambda_1 = -\Lambda$, $\Lambda_k = \Lambda - \epsilon_k$, for $k = \{2, \ldots, N\}$. The joint quadrature operators (unnormalized) have, thus, the following expressions:

$$\begin{aligned}
&\widetilde{X}_{\text{out},1} + \ldots + \widetilde{X}_{\text{out},N} = \mathcal{V}_1(\omega)\, \widetilde{\phi}_{\text{in},1}, \\
&\widetilde{P}_{\text{out},k} - \widetilde{P}_{\text{out},k+1} = \frac{\mathcal{V}_{k+1}(\omega)}{N-k+1} \widetilde{\phi}_{\text{in},k+1} - \frac{\mathcal{V}_{k+2}(\omega)}{N-k} \widetilde{\phi}_{\text{in},k+2}, \\
&\widetilde{P}_{\text{out},N-1} - \widetilde{P}_{\text{out},N} = \mathcal{V}_N(\omega)\, \widetilde{\phi}_{\text{in},N},
\end{aligned} \tag{5.144}$$

where we omitted the frequency dependence of the operators. The variances corresponding to operators (5.144) are obtained considering a vacuum input state and correlations between $\hat{\phi}_k$ operators as in Eq. (5.141) for $i, j \in \{1, \ldots, N\}$. They result to be:

$$\begin{aligned}
&V_{\hat{X}_1 + \ldots + \hat{X}_N}(\omega) = |\mathcal{V}_1(\omega)|^2, \\
&V_{\hat{P}_k - \hat{P}_{k+1}}(\omega) = \frac{1}{\mathcal{N}_k} \left(\frac{|\mathcal{V}_{k+1}(\omega)|^2}{(N-k+1)^2} + \frac{|\mathcal{V}_{k+2}(\omega)|^2}{(N-k)^2} \right), \\
&V_{\hat{P}_{N-1} - \hat{P}_N}(\omega) = |\mathcal{V}_N(\omega)|^2,
\end{aligned} \tag{5.145}$$

for $k = 1, \ldots, N-2$. The factor $\mathcal{N}_k$ is chosen in order to make the shot noise level equal to one:

$$\mathcal{N}_k = \frac{1}{(N-k+1)^2} + \frac{1}{(N-k)^2}. \tag{5.146}$$

The joint operator $\hat{X}_1 + \ldots + \hat{X}_N$ at threshold and at zero analysis frequency is always perfectly squeezed. In Figure 5.10(a) we report the variances (5.145) of the joint quadrature operators for $N = 20$. The blue line correspond to the BIBO 0.1 mm-crystal case analyzed before for two-mode and three-mode entanglement. Non classical correlations for joint quadrature operators are included between about -15 dB for $k = 19$ and -37.5 dB for $k = 1$. The red and green lines, instead, represent the same case as before but with a crystal length of 0.65 mm and 5 mm. The degree of non classical correlations between each party of the output field is greatly increased by increasing the thickness of the crystal till about a minimum of about -97 dB for $k = 1$ and maximum of -52 dB for $k = 19$ in the case of 5 mm thick crystal. In fact, an increase of the crystal thickness has, on one side, the negative effect to rise upward the threshold of the system, while, from the multi-mode entanglement point of view, the spectrum of the squeezing parameters flatten and for a non-null subset of super-modes the associated values of Λ_k assume

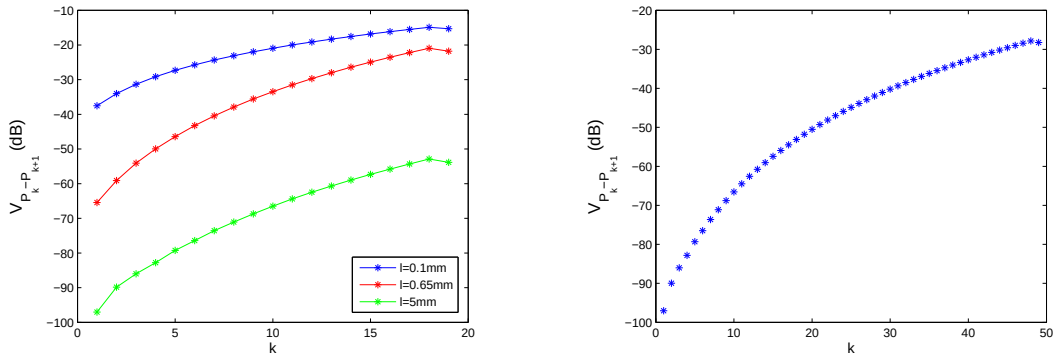

(a) (b)

Figure 5.10: (a) Variances of joint quadrature operators $V_{\hat{P}_k-\hat{P}_{k+1}}$ for $N = 20$ at $r = 1$ and $\omega = 0$ corresponding to three different thickness of a BIBO crystal. (b) Variances of joint quadrature operators $V_{\hat{P}_k-\hat{P}_{k+1}}$ for $N = 50$ at $r = 1$ and $\omega = 0$ for a 5 mm-thick BIBO crystal.

approximatively the same magnitude reflecting the fact that we are increasing the degree of correlations between the joint quadrature operators. In the case of $l = 5\,\text{mm}$ we can even realize a bigger multi-mode entangled state, with $N = 50$. In Figure 5.10(b) we show the variances for the joint quadrature operators, being the spread of squeezing between $-79\,\text{dB}$ and $-20\,\text{dB}$.

The results of this section as well as those of the one about the three-mode entanglement explains clearly that SPOPOs are systems which reveals marked multi-mode properties thus proving their great potential for producing multi-mode quantum states of very high dimensionality. Firstly, we do not need to produce N squeezed beams which are physically separated and mix them by means of a N-port interferometer, but the system naturally produces a beam which multi-mode. We need only to understand in which basis it shows N-mode entanglement and then perform the detection. From this point of view, a multi-mode device, and in particular a SPOPO, reveals to be a very compact source for the production of the quantum states needed in quantum communication protocols. Secondly, we learned that the condition of equal squeezing parameters required in [Pfister2004] can be slightly released. Consequently the engineering of non-linearities with perfectly equal coupling constant between the modes of an pump comb becomes less critical. Moreover, for a device such a SPOPO, we do not even need an engineering of the non-linear crystal, but use the standard non-linearities of c.w. OPOs, since the simple control of the temporal walk-off between the pump and signal pulses (by controlling the crystal length or the width of the pump pulse) permits us to increase (or decrease) the amount of correlations between the super-modes.

If the compactness of a SPOPO as source of multi-mode entangled states represents an advantage respect to standard schemes, on the other side the realization of a measurement of joint-quadrature correlations is a critical point. In fact, all along the section dedicated to multi-mode entanglement we supposed to restrict the space of interest to the space spanned by a limited number of super-modes. This situation can be realized only if the measure performed by a standard homodyne detection projects the global state of the

field considered over the space in which the multi-mode entanglement has to be evidenced. We need, therefore, techniques of shaping of the local oscillator as the one discussed in Section 5.2.4. Another difficulty affects the use of SPOPOs as multi-mode sources for multi-partite entangled states. Indeed, since the super-modes of the output signal field are degenerate for the carrying frequency ω_0, physical separation could result a difficult task. For what concerns spatial multi-mode OPOs it is still possible the use of filtering cavities (see for example [DelaubertPhD]), while for time multi-mode optical beams, at the best of our knowledge, there is still not an experimental evidence of frequency-filtering. A possible solution to this problem may come from [Schmidt2000, Opatrný2002]. Their proposal is based on the result that any discrete unitary operator can be constructed interferometrically [Reck1994]. The idea, basically, is to decompose the original pulse into quasi-monochromatic components, as illustrated in Figure 5.11, by means of a grating. Afterwards, each component is frequency shifted by an acusto-optical modulator (AOM) so that each channel has the same central frequency. These channels, then, interfere on a $2N$ port consisting of beam splitters and mirrors. By a proper choice of the $2N$ port parameters the output channels of such interferometer will consist of the physically separated modes $\hat{a}_k$. In principle, then, the output signal field which has N-mode quantum correlations among the modes $\hat{a}_k$ can be decomposed in N entangled parties which can be finally used for implementing protocols for quantum communication.

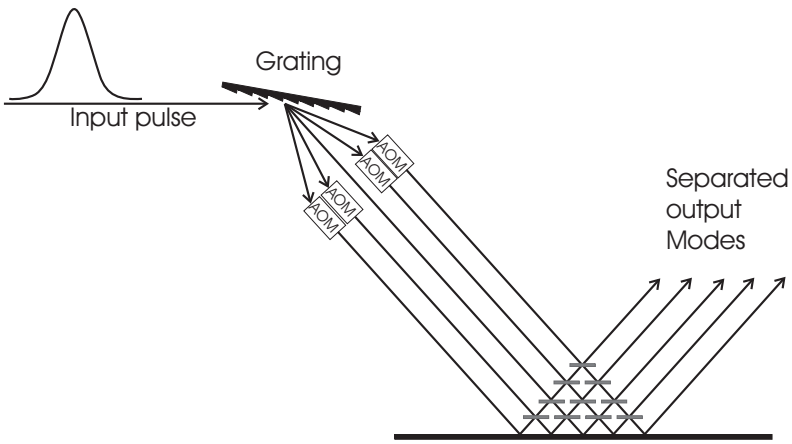

Figure 5.11: Scheme to separate individual non-monochromatic modes. The pulse is first decomposed into quasi-monochromatic channels. The frequency of each channel is then shifted by means of an AOM to the central frequency of the pulse. The resulting modes (with the same central frequency) then interfere on a $2N$ port [Opatrný2002].

Conclusions

Starting from the Heisenberg equations for pump, signal and idler intracavity field operators, we studied the evolution of the average values of the generated fields for a synchronously pumped optical parametric oscillator (SPOPO) in the below threshold regime. This problem depends on the solution of an eigenvalue equation from the spectrum of which we can extract information, for example, about the threshold and the shape of the super-mode that will oscillate at threshold. Not all the super-modes are equally important in the evolution of the system. When 10^5 pump modes generate by parametric interaction roughly 10^5 signal and idler modes, it is possible to extract in this huge, almost continuous, Hilbert space a finite set of simple objects: these are the eigen "super-modes", or "frequency combs", in which are concentrated all the quantum effects generated by the intracavity parametric interaction. Similar "super-modes" have been independently introduced by Wasilewski *et. al* [Wasilewski2006a] in the different context of transient degenerate down-conversion in a single-pass, single-pulse configuration. In their case, the "super-modes" are continuous linear superpositions of the annihilation operators in free space, whereas in our case, because of the resonant cavity, they are a discrete combination of modes. From the quantum point of view, parametric down conversion hamiltonian destroys a pump photon and creates two photons in any two of the about 10^5 temporal modes (in the case of 100 fs pulses) of the signal and idler according to the energy conservation and in a way that cannot be controlled from outside; in other words, in the standard representation of annihilation/creation field operators, such interaction hamiltonian is not diagonal. On the other side, all linear combinations of longitudinal mode annihilation/creation field operators which diagonalize the interaction hamiltonian, give rise to new special basis of operators which destroy a pump photon and produce two correlated photons in a single "super-mode". The novel aspect of our study is grounded on the fact that squeezing spectrum of a finite set of super-modes operators can be below the standard quantum limit, giving a clear image that the system is a highly quantum multi-mode system. In fact, not only the super-mode of minimum threshold is perfectly squeezed at threshold but, further, all the other super-modes have nonclassical character and are significantly squeezed provided that their threshold is sufficiently close to the minimum one. In effect, both numerical and analytical results show that a large number (in any case, greater than one) of super-modes whose threshold is close to the minimum one exists, thus proving the multi-modal character of this device. Hence, synchronously pumped OPOs reveal to be very interesting devices for studying frequency combs at the quantum level; their quantum multi-modal behavior could be exploited for generation of nonclassical states of the light used for implement optical time measurement of great sensitivity [Lamine2008]

or quantum information protocols. Moreover, the results illustrated at the end of this work (Section 5.4) prove that SPOPOs can be very promising devices for quantum state engineering. In fact, the quantum properties of super-modes depends on the spectrum of Λ_k which can be adjusted by means of the good choice of the number of modes or the spectral shape of the pump field as well as the form of the phase-matching. In this context one has to consider, then, the demonstration that a SPOPO, in principle, can produce generalized multi-mode GHZ states. One could go further. Keeping in mind that, in the scheme used in Section 5.4, we started from well defined transformations for obtaining the joint-quadrature operators which presents multi-mode entanglement, one could reverse the problem and try to understand which transformation and which parameters Λ_k are needed for generating a general quantum multi-mode state as like, for example, cluster states [Briegel2001]. Since the great manageability of SPOPOs, such a problem appears to have a promising solution and, even if not presented in this thesis, it is the object of our current research about the engineering of quantum states.

Acknowledgements

After this long adventure that brought me to the end of my doctorate, the number of people that directly or indirectly contributed to this important achieving is so huge that I will hardly succeed in the task of properly acknowledging their contribution in these few pages. From now on, hence, I apologize for possible omissions.

First of all I would like to thank the two structures, i.e. the Physics department of Università dell'Insubria and the Laboratoire Kastler-Brossel, and their directors who received and put me in the best favorable conditions for carrying out my research.

Sincere thanks to Professor Luigi A. Lugiato, supervisor of the Italian side of my work, who permitted this beautiful adventure to start. Thanks to Professor Claude Fabre, supervisor of the French side, who patiently followed my first steps in the world of quantum optics, for his countless suggestions and for his evergreen enthusiasm about Science and any sort of electronic device on the market.

I thank Marco Genovese and Emmanuel Rosencher who accepted to referee my work in spite of their obligations.

Thanks to the members of the quantum optics group in Como that received me with them and that gave to me the unique opportunity to learn and discuss about many problems concerning our work: to Alessandra Gatti for her illuminating clarifications, to Enrico Brambilla for his constant and patient support in problems concerning with physics and programming, to Lucia Caspani for the nice coffee-breaks.

The two years in Como, far away from home and the "old friends", rapidly elapsed thanks to the company of Betta, the "Red Scarf", and Emiliano. I am particulary grateful to Lorenzo Columbo for the time he dedicated to me for debugging codes for PDEs, for his unofficial supervision over my work about "cavity light bullets" and, above all, for the nice dinners and walks in the mountains we had together.

I want to thanks the members of the quantum optic group at LKB and in special way Nicolas Treps for his good mood, his simplicity and patience in explaining physics and French language, Thomas Coudreau who realized that my bike was needing a mudguard and gave to me his unused one. I thank also all the other members of the laboratory who every day contribute to the pleasant atmosphere, I will always keep with me the souvenir of discussions, lunches and laughes with them. Maybe I am missing someone in this very long list, but everyone left me something priceless as an encouragement, a smile, an advice, his friendship, his music or simply his time. Then, rigorously in alphabetical order, thanks to Taoufik Amri, Olivier Arcizet, Serge Begon, Monique Bonnamy, Alberto Bramati, Tristan Briant, Sidney Burks, Malo Cadoret, Pierre-François Cohadon, Vincent Delaubert, Benoit Gremaud, Saida Guellati, Alex Gumberidze, Antoine Heidmann, Gaelle Keller, Brahime

Lamin, Julien Laurat, Julien Lebar, Eric-Olivier Le Bigot, Jerome Lefrere, Charles Leyder, Valery Marachevsky, Letitia Morel, Jean-François Morizur, Jeremie Ortalo, Olivier Pinel, Sophie Schlesser, Csilla Szabo, Alexandros Tavernarakis.

I received the first welcome in Paris by Antonino Chiummo (M. Sciumò), with whom I shared not only the 4th floor in the hostel in Montrouge during my first year in France but also a sincere friendship in spite of the fact he will never admit it: I owe him a lot, above all "that famous" euro! After this first encounter suddenly I discovered that Paris gives hospitality to a huge community of Italian people and this situation occurs at a smaller scale at the LKB, where this community suddenly became my enlarged family abroad. Therefore I want to thank very much Martino Trassinelli and Francesco Intravaia for their advices about the bureaucracy and life in France, Pierre Verlot, Benoit Chalopin and Gabriel Lemarie for the nice time spent together to the point that they have been naturalized Italians by now. A big "thank you" to Estefania and Francesca for their happy company and to Pietro Lombardi and Ferruccio Pisanello who recently joined LKB. But the kernel of such family is represented by Riccardo Messina, Virginia D'Auria, Piernicola Spinicelli and Chiara Molinelli. I spent almost all my time in France with them either watching TV series, or going to the cinema, or to the museum, or simply having long walks in Paris. A countless number of hours have been spent together at Piernicola's home, having dinner, playing at the PS2 and having futile and endless discussions about any sort of issues... actually my work would have benefited more without these "time wasting", but it has to be acknowledged too.

I am very thankful to Germán de Valcárcel, since the first time I met him he revealed to be more than a collaborator, a patient and always optimist teacher and, above all, a sincere friend. Through him I had also the chance to meet his brilliant student Carlos Navarrete with whom I spent many pleasant days in Valencia visiting the city and its restaurants.

Thanks to "zia Chiara" for having kept updated her colleagues at the Institute Santarella about my research and my family that every day found out the means to support me despite the long distance that separates us. A great "thank you" to Chiarina who, with constance and patience, supported me during the periods of disappointment and frustration as well as those of enthusiasm and optimism.

Finally a grateful thought to "nonno Pippi" and "zio Matteo".

Appendix

A Solution of Fredholm integral with a Gaussian kernel

In Section 4.2 we have seen that the diagonalization of the matrix $\mathcal{L}_{m,q}$ can be reduced to the solution of the integral equation (4.58) with a Gaussian kernel. In this Appendix we retrieve the eigenvectors and the eigenvalues for this class of problem generally known as Fredholm integral equations. Let's consider, then, the integral equation:

$$\int_{-\infty}^{+\infty} \mathrm{d}y\, \mathrm{e}^{-\sigma_1^2(x+y)^2-\sigma_2^2(x-y)^2}\psi(y) = \lambda\psi(x), \tag{A-1}$$

and verify that the function $\mathrm{e}^{-\tau^2x^2}H_k(\sqrt{2}\tau x)$ satisfies Eq. (A-1), being $H_k(\sqrt{2}\tau x)$ the Hermite polynomial of order k-th and $\tau \equiv \sqrt{2\sigma_1\sigma_2}$. In fact, we have:

$$\begin{aligned}
&\int_{-\infty}^{+\infty} \mathrm{d}y\, \mathrm{e}^{-\sigma_1^2(x+y)^2-\sigma_2^2(x-y)^2}\mathrm{e}^{-\tau^2y^2}H_k(\sqrt{2}\tau y) = \\
&\quad = \int_{-\infty}^{+\infty} \mathrm{d}y\, \mathrm{e}^{-\left[\left(\sigma_1^2+\sigma_2^2\right)x^2+\left(\sigma_1^2+\sigma_2^2+\tau^2\right)y^2+2xy\left(\sigma_1^2-\sigma_2^2\right)\right]}H_k\left(\sqrt{2}\tau y\right) = \\
&\overset{\tau=\sqrt{2\sigma_1\sigma_2}}{=} \mathrm{e}^{-\left(\sigma_1^2+\sigma_2^2\right)x^2}\int_{-\infty}^{+\infty} \mathrm{d}y\, \mathrm{e}^{-\left[\left(\sigma_1^2+\sigma_2^2\right)y^2+2xy(\sigma_1+\sigma_2)(\sigma_1-\sigma_2)\right]} \times \\
&\quad \times \mathrm{e}^{\left[(\sigma_1-\sigma_2)^2x^2-(\sigma_1-\sigma_2)^2x^2\right]}H_k\left(\sqrt{2}\tau y\right) = \\
&\quad = \mathrm{e}^{-\left(\sigma_1^2+\sigma_2^2-(\sigma_1-\sigma_2)^2\right)x^2}\int_{-\infty}^{+\infty} \mathrm{d}y\, \mathrm{e}^{-\left[(\sigma_1+\sigma_2)y+(\sigma_1-\sigma_2)x\right]^2}H_k\left(\sqrt{2}\tau y\right).
\end{aligned} \tag{A-2}$$

After the making the substitutions:

$$\begin{cases}
\widetilde{y} = (\sigma_1+\sigma_2)\, y \\
\widetilde{x} = -(\sigma_1-\sigma_2)\, x \\
\mathrm{d}\widetilde{y} = \mathrm{d}y\,(\sigma_1+\sigma_2)
\end{cases} \tag{A-3}$$

We use the well known result [Gradshteyn]:

$$\int_{-\infty}^{+\infty} \mathrm{d}y\, \mathrm{e}^{-(x-y)^2}H_k(\alpha y) = \sqrt{\pi}\left(1-\alpha^2\right)^{k/2}H_k\left(\frac{\alpha x}{\sqrt{1-\alpha^2}}\right), \tag{A-4}$$

in Eq. (A-2), then obtaining:

$$\begin{aligned}
&\int_{-\infty}^{+\infty} \mathrm{d}y \, \frac{\mathrm{d}\widetilde{y}}{\sigma_1+\sigma_2} \mathrm{e}^{-(\widetilde{y}-\widetilde{x})^2} H_k\left(\frac{\sqrt{2}\tau\widetilde{y}}{\sigma_1+\sigma_2}\right) = \\
&= \frac{\sqrt{\pi}}{\sigma_1+\sigma_2}\left(1-\frac{2\tau^2}{(\sigma_1+\sigma_2)^2}\right)^{k/2} H_k\left(\frac{\sqrt{2}\tau}{\sigma_1+\sigma_2}\widetilde{x}\right) = \\
&= \frac{\pi}{\sigma_1+\sigma_2}\left(\frac{(\sigma_1-\sigma_2)^2}{(\sigma_1+\sigma_2)^2}\right)^{k/2} H_k\left(-\sqrt{2}\tau x\right). \qquad \text{(A-5)}
\end{aligned}$$

Therefore, we have:

$$\begin{aligned}
&\int_{-\infty}^{+\infty} \mathrm{d}y \, \mathrm{e}^{-\sigma_1^2(x+y)^2-\sigma_2^2(x-y)^2} \mathrm{e}^{-\tau^2 y^2} H_k(\sqrt{2}\tau y) = \\
&= \frac{\sqrt{\pi}}{\sigma_1+\sigma_2}(-1)^k\left(\frac{\sigma_1-\sigma_2}{\sigma_1+\sigma_2}\right)^k \mathrm{e}^{-\tau^2x^2} H_k\left(\sqrt{2}\tau x\right) = \\
&= \frac{\sqrt{\pi}}{2\sqrt{\sigma_1\sigma_2}} \frac{\mathrm{tgh}^k\left(\ln\sqrt{\sigma_2/\sigma_1}\right)}{\cosh\left(\ln\sqrt{\sigma_2/\sigma_1}\right)} \mathrm{e}^{-\tau^2x^2} H_k\left(\sqrt{2}\tau x\right). \qquad \text{(A-6)}
\end{aligned}$$

Bibliography

[Aoki2003] T. Aoki, N. Takei, H. Yonezawa, K. Wakui, T. Hiraoka, A. Furosawa, and P. van Loock, *Experimental Creation of a Fully Inseparable Tripartite Continuous-Variable State*, Phys. Rev. Lett. 91, 080404 (2003). Quoted p. 111

[Aspect1981] A. Aspect, P. Grangier and G. Roger, *Experimental tests of realistic local theories via Bell's theorem*, Phys. Rev. Lett. 47, 460 (1981). Quoted p. 9

[Aspect1982] A. Aspect, P. Grangier and G. Roger, *Experimental realization of Einstein-Podolsky-Rosen Gedankenexperiment: a new violation of Bell's inequalities*, Phys. Rev. Lett. 49, 91 (1982). Quoted p. 9, 103

[Banaszek1999] K. Banaszek, and K. Wódkiewicz, *Nonlocality of the Einstein-Podolsky-Rosen state in the phase space*, Acta Physica Slovaca 49, 491 (1999). Quoted p. 11

[Becker1974] M. F. Becker, D. J. Kuizenga, D. W. Phillion, A. E. Siegman, *Analytic expressions for ultrashort optical parametric oscillators*, J. Appl. Phys. 45, 3996 (1974). Quoted p. 16

[Bell1964] J. S. Bell, *On the Einstein-Podolsky-Rosen paradox*, Physics 1, 195 (1964). Quoted p. 9, 103

[Bennett1984] C. H. Bennett and G. Brassard, *Proceedings IEEE International Conference on Computers, Systems and Signal Processing*, IEEE Press, Los Alamos, Calif. 1984, p. 175. Quoted p. 103

[Bennett1992a] C. H. Bennett and S. J. Wiesner, *Communication via one- and two-particle operators on Einstein-Podolsky-Rosen states*, Phys. Rev. Lett. 69, 2881 (1992). Quoted p. 103

[Bennett1992b] C. H. Bennett, G. Bressard, and N. D. Mermin, *Quantum cryptography without Bell's theorem*, Phys. Rev. Lett. 68, 557 (1992). Quoted p. 103

[Bennett1993] C. H. Bennett, G. Brassard, C. Crépeau, R. Jozsa, A. Peres, and W. K. Wootters, *Teleporting an unknown quantum state via dual classical and Eistein-Podolsky-Rosen channels*, Phys. Rev. Lett. 70,1895 (1993). Quoted p. 103

[Bennink2002] Ryan S. Bennink, and Robert W. Boyd, *Improved measurement of multimode squeezed light via an eigenmode approach*, Phys. Rev. A 66, 053815 (2002). Quoted p. 64, 90

[Braunstein1998b] S. L. Braumstein, *Quantum error correction for communication with linear optics*, Nature 394, 47 (1998). Quoted p. 113, 115

[Braunstein2005] Samuel L. Braunstein, *Squeezing as an irreducible resource*, Phys. Rev. A 71, 055801 (2005). Quoted p. 91, 92

[Briegel2001] H. J. Briegel, and R. Raussendorf, *Persistent Entanglement in Arrays of Interacting Particles*, Phys. Rev. Lett. 86, 910 (2001). Quoted p. 124

[Boccara1980] C. Boccara, D. Fournier, and J. Badoz, *Termo-optical spectroscopy: detection by the "mirage effect"*, Appl. Phys. Letters 36, 130 (1980). Quoted p. 2

[Bouwmeester1999] D. Bouwmeester, J. Pan, M. Daniell, H. Weinfurter, and A. Zeilinger, *Observation of Three-Photon Greenberger-Horne-Zeilinger Entanglement*, Phys. Rev. Lett. 82, 1345 (1999). Quoted p. 111

[Caves1994] C. M. Caves and P. D. Drummond, *Quantum limits on bosonic communication rates*, Rev. Mod. Phys. 66, 481 (1994). Quoted p. 23

[Charbonnier1990] F. Charbonnier, *Capteur ò effet mirage à detecteur simple et à detecteur multiple: application au contrôle non destuctif avec excitation phototermique*, Thèse de doctorat de l'Université Paris 6 (1990). Quoted p. 2

[Cheung1991] E. C. Cheung and J. M. Liu, *Theory of a synchronously pumped optical paramteric oscillator in steady-state operation*, J. Opt. Soc. Am. B 7, 1385 (1990); E. C. Cheung and J. M. Liu, *Efficient generation of ultrashort wavelenght-tunable infrared pulses*, J. Opt. Soc. Am. B 8, 1491 (1991). Quoted p. 3, 16, 28

[Delaubert2006] V. Delaubert, N. Treps, C. C. Harb, P. K. Lam, and H.-A. Bachor, *Quantum measurements of spatial conjugate variables: displacement and tilt of a Gaussian beam*, Opt. Lett. 31, 1537 (2006). Quoted p. 23

[DelaubertPhD] V. Delaubert, *Quantum imaging with a small number of transverse modes*, PhD Thesis (Université Pierre et Marie Curie, Paris 2007). Quoted p. 121

[Drever1983] R. Drever, J. Hall, F. Kovalski, J. Hough, G. Ford, A. Munley, and H. Ward. *Laser phase and frequency stabilization using an optical resonator*, Appl. Phys. B 31, 97 (1983). Quoted p. 18

[Duan2000] L. Duan, G. Giedke, J. I. Cirac, and P. Zoller, *Inseparability criterion for countinuous variable systems*, Phys. Rev. Lett. 84, 2722 (2000). Quoted p. 10

[Ebrahimzadeh1991] M. Ebrahimzadeh, G. J. Hall and A. I. Ferguson, *Picosecond infrared optical parametric generation in KTP using a diode-laser-pumped solid-state laser*, Opt. Lett. 16, 1744 (1991). Quoted p. 16, 69

[Edelstein1989] D. C. Edelstein, E. S. Wachman, C. L. Tang, *Broadly tunable high repetition rate femtosecond optical parametric oscillator*, Appl. Phys. Lett. 54, 1728 (1989). Quoted p. 16, 69

[Ekert1991] A. K. Ekert and P. L. Knight, *Relationship between semiclassical and quantum-mechanical input-output theories of optical response*, Phys. Rev. A 43, 3934 (1991). Quoted p. 90, 103

[EPR] A. Einstein, B. Podolsky, and N. Rosen, *Can quantum-mechanical description be considered complete?*, Phys. Rev. 47, 777 (1935). Quoted p. 11, 103

[Fabre1989] C. Fabre, E. Giacobino, A. Heidmann, and S. Reynaud, *Noise characteristics of a non-degenerate optical parametric oscillator - application to quantum noise reduction*, J. Phys. France 50, 1209 (1989). Quoted p. 5

[Fabre2000] C. Fabre, J. B. Fouet, and A. Maître, *Quantum limits in the measurement of very small displacements in optical images*, Opt. Lett. 25, 76 (2000). Quoted p. 2

[Fabre2007] C. Fabre, N. Treps, H. A. Bachor, and P. K. Lam, *Quantum imaging techniques for improving information extraction from images*, pag. 323, in *Quantum information with continuous variables of atoms and light*, edited by N. J. Cerf, G. Leuchs and E. S. Polzik (2007). Quoted p. 2

[Forget2006] N. Forget, S. Bahbah, C. Drag, F. Bretenaker, M. Lefèbvre, and E. Rosencher, *Actively mode-locked optical parametric oscillator*, Opt. Lett. 31, 972 (2006). Quoted p. 17

[Fry1976] E. Fry and R. Thompson, *Experimetnal test of local hidden-variables theories*, Phys. Rev. Lett. 37, 465 (1976). Quoted p. 103

[Furusawa1998] A. Furusawa, J. L. Sørensen, S. L. Braunstein, C. A. Fuchs, H. J. Kimble, and E. S. Polzik, *Unconditional Quantum Teleportation*, Science 282, 706 (1998). Quoted p. 111

[Galvanauskas1997] A. Galvanauskas, M. A. Arbore, M. M. Fejer, M. E. Fermann, and D. Harter, *Fiber-laser-based femtosecond parametric generation in bulk periodically poled LiNbO3*, Opt. Lett. 22,105 (1997). Quoted p. 69

[Gardiner1985] C. W. Gardine and M. J. Collett, *Input and output in damped quantum systems: quantum stochastic differential equations and master equation*, Phys. Rev. A 31, 3761 (1985). Quoted p. 93

[Ghotbi2004] M. Ghotbi and Ebrahim-Zadeh, *Optical second harmonic generation properties of* BiB_3O_6Opt. Express **12**,6002 (2004). Quoted p. 69, 70

[Gigan2005] S. Gigan, L. Lopez, N. Treps, A. Maître, and C. Fabre, *Image transmission through a stable paraxial cavity*, Phys. Rev. A 72, 023804 (2005). Quoted p. 23

[Gigan2006] S. Gigan, L. Lopez, V. Delaubert, N. Treps, C. Fabre, and A. Maître, *Continuous-wave phase-sensitive parametric image amplification*, J. Mod. Opt. 53, 809 (2006). Quoted p. 23

[Giovannetti2003] V. Giovannetti, S. Mancini, D. Vitali, and P. Tombesi, *Characterizing the entanglement of bipartite quantum systems*, Phys. Rev. A 67, 022320 (2003). Quoted p. 10, 107, 109

[Glauber1963] R. Glauber, *Coherent and incoherent states of the radiation field*, The Phys. Rev. 31, 2766 (1963). Quoted p. 7

[Gradshteyn] I. S. Gradshteyn and I. M. Ryzhik, *Table of integrals, series and products*, edited by A. Jeffrey and D. Zwillinger, Elsevier (2007). Quoted p. 61, 127

[Graham1968] R. Graham and H. Haken, *Quantum theory of light propagation in a fluctuating laser-active medium*, Z. Phys. 213, 420 (1968). Quoted p. 36

[Grangier1998] P. Grangier, J.-A. Levenson, J.-P. Poizat, *Quantum non-demolition measurements in optics*, Nature 396, 537 (1998). Quoted p. 5

[Greenberger1990] D. M. Greenberger, M. A. Horne, A. Shimony, and A. Zeilinger, *Bell's theorem without inequalities*, Am. J. Phys. 58, 1131 (1990). Quoted p. 111

[Haken] H. Haken, *Synergetics: an introduction*, 3rd edition, Springer- Verlag, Berlin. Quoted p. 2

[Heidmann1987] A. Heidmann, R. Horowicz, S. Reynaud, E. Giacobino, C. Fabre, G. Camy, *Observation of Quantum Noise Reduction on Twin Laser Beams*, Phys. Rev. Lett. 59, 2555 (1987). Quoted p. 5, 16

[Hillery1999] M. Hillery, V. Bužek, and A. Berthiaume, *Quantum secret sharing*, Phys. Rev. A 59, 1829 (1999). Quoted p. 111

[Huang1996] H. Huang, and J. H. Eberly, *Correlations and One-quantum Pulse Shapes in Photon Pair Generation*, J. Mod. Opt. 40,915 (1996). Quoted p. 89

[Huang2008] C.-B. Huang, Z. Jiang, D. E. Leaird, J. Caraquitena, and A. M. Weiner, *Spectral line-by-line shaping for optical and microwave arbitrary waveform generations*, Laser&Photon. Rev. 2, 227 (2008). Quoted p. 100

[Incompleteness] For a review of experiments through 1987, see M. Redhead, *Incompleteness, nonlocality and realism*, Clarendon, Oxford (1987), pp. 107-113. For experiments through 1995, see A. M. Steinberg, P. G. Kwiat, and R. Y. Chiao, *Quantum optical tests of the foundations of physics*, in *Atomic, Molecular & Optical Physics Handbook*, AIP, New York (1996), pp. 907-909. Quoted p. 9

[Jiang2007] Z. Jiang, C.-B. Huang, D. E. Leaird, and A. M. Weiner, *Optical arbitrary waveform processing of more than 100 spectral comb lines*, Nature Photonics 1, 463 (2007). Quoted p. 100

[Jing2003] J. Jing, J. Zhang, Y. Yan, F. Zhao, C. Xie, and K. Peng, *Experimental Demonstration of Tripartite Entanglement and Controlled Dense Coding for Continuous Variables*, Phys. Rev. Lett. 90, 167903 (2003). Quoted p. 111

[Kim1994] C. Kim and P. Kumar, *Quadrature-Squeezed Light Detection Using a Self-Generated Matched Local Oscillator*, Phys. Rev. Lett. 73, 1605 (1994). Quoted p. 90

[Knöll1991] L. Knöll, W. Vogel, and D.-G. Welsch, *Resonators in quantum optics: a first-principles approach*, Phys. Rev. A 43, 543 (1991). Quoted p. 96

[Kojima1997] H. Kojima, E. Muto, H. Higuchi, and T. Yanagida, *Mechanics of single kinesin molecules measured by optical trapping nanometry*, Biophysical Journal 73, 2012 (1997). Quoted p. 2

[Kolobov1989] M. I. Kolobov, and I. V. Sokolov, *Squeezed states of light and noise-free optical images*, Phys. Lett. A 140, 101 (1989). Quoted p. 2

[Kolobov1995] M. I. Kolobov and L. A. Lugiato, *Noiseless amplification of optical images*, Phys. Rev. A 52, 4930 (1995). Quoted p. 2, 23

[Kolobov1999] M. I. Kolobov, *The spatial behavior of nonclassical light*, Rev. Mod. Phys. 71, 1539 (1999). Quoted p. 2

[Kolobv2000] M. I. Kolobov and C. Fabre, *Quantum limits on optical resolution*, Phys. Rev. Lett. 85, 3789 (2000). Quoted p. 23

[Lamine2008] B. Lamine, C. Fabre, and N. Treps, *Quantum improvement of time transfer between remote clocks*, Phys. Rev. Lett. 101, 123601 (2008). Quoted p. 123

[LaPorta1991] A. La Porta and R. E. Slusher, *Squeezing limits at high parametric gains*, Phys. Rev. A 44,2013 (1991). Quoted p. 90

[Lassen2007] M. Lassen, V. Delaubert, J. Janousek, K. Wagner, H.-A. Bachor, P. K. Lam, N. treps, P. Buchhave, C. Fabre, and C. C. Harb, *Tools for spatial multi-mode quantum information: modulation, detection and quantum correlations*, 98, 083602 (2007). Quoted p. 23

[Laurat2003] J. Laurat, T. Coudreau, N. Treps, A. Maître, and C. Fabre, *Conditional preparation of a quantum state in che continuous variable regime: generation of a sub-poissonian state from twin beams*, Phys. Rev. Lett. 91, 213601 (2003). Quoted p. 16

[Law2000] C. K. Law, I. A. Walmsley, and J. H. Eberly, *Continuous frequency entanglement: effective finite Hilbert space and entropy control*, Phys. Rev. Lett. 84,5304 (2000). Quoted p. 88, 92

[Levandovsky1999] D. Levandovsky, M. Vasilyev, and P. Kumar, *Perturbation theory of quantum solitons: continuum evolution and optimum squeezing by spectral filtering*, Opt. Lett. 24, 43 (1999). Quoted p. 90

[Levenson1993] J. A. Levenson, I. Abram, T. Rivera, P. Fayolle, J. C. Garreau, P. Grangier, *Quantum optical cloning amplifier*, Phys. Rev. Lett. 70, 267 (1993). Quoted p. 16

[Lifshitz2005] R. Lifshitz, A. Arie, and A. Bahabad, *Photonic Quasicrystals for Nonlinear Optical Frequency Conversion*, Phys. Rev. Lett. 95, 133901 (2005). Quoted p. 112

[Lopez2005] L. Lopez, S. Gigan, N. Treps, A. Maître, C. Fabre, and A. Gatti, *Multimode squeezing properties of a confocal optical parametric oscillator: Beyond the thin-crystal approximation*, Phys. Rev. A 72, 013806 (2005). Quoted p. 2, 23, 112

[Lopez2008] L. Lopez, N. Treps, B. Chalopin, C. Fabre, and A. Maître, *Quantum processing of images by continuous wave optical parametric amplification*, Phys. Rev. Lett. 100, 013604 (2008). Quoted p. 23

[Lugiato1995] L. A. Lugiato, A. Gatti, and H. Wiedemann, *Quantum fluctuations and nonlinear optical paterns*, proceedings of Les Houches summer school, 1995, edited by S. Reynaud, E. Giacobino and J. Zinn-Justin (North-Holland, Amsterdam, 1997). Quoted p. 2

[Lugiato2002] L. Lugiato, A. Gatti, and E. Brambilla, *Quantum imaging*, J. Opt. B: Quantum and Semiclassical Optics 4, S176 (2002). Quoted p. 2, 23

[Mak1992] G. Mak, Q. Fu, H. M. van Driel, *Externally pumped high repetition rate femtosecond infrared optical parametric oscillator*, Appl. Phys. Lett. 60, 542 (1992). Quoted p. 16

[Maker1990] G. T. Maker and A. I. Ferguson, *Doubly resonant optical parametric oscillator synchronously pumped by a frequency-doubled, mode-locked, and Q-switched diode laser pumped neodymium yttrium lithium fluoride laser*, Appl. Phys. Lett 56, 1614 (1990). Quoted p. 16

[Mancini2002] S. Mancini, V. Giovannetti, D. Vitali, and P. Tombesi, *Entangling macroscopic oscillators exploiting radiation pressure*, Phys. Rev. Lett. 88, 120401 (2002). Quoted p. 10

[Martinelli2003] M. Martinelli, N. Treps, S. Ducci, S. Gigan, A. Maître, and C. Fabre, *Experimental study of the spatial distribution of quantum corrlations in a confocal optical parametric oscillator*, Phys. Rev. A 67, 023808 (2003). Quoted p. 23

[Mattle1996] K. Mattle, H. Weinfurter, P. G. Kwiat, and A. Zeilinger, *Dense coding in experimental quantum communication*, Phys. Rev. Lett. 76, 4656 (1996). Quoted p. 23

[McCarty1992] M. J. McCarty and D. C. Hanna, *Continuous-wave mode-locked singly resonant optical parametric oscillator synchronously pumped by a laser-diode-pumped Nd:YLF laser*, Opt. Lett. 17, 402 (1992). Quoted p. 16

[McCarty1993] M. J. McCarty and D. C. Hanna, *All-solid-state synchronously pumped optical parametric oscillator*, J. Opt. Soc. Am. B 10, 2180 (1993). Quoted p. 16

[McGowan1998] C. McGowan, D. T. Reid, Z. E. Penman., M. Ebrahimzadeh, and W. Sibbet, *Femtosecond optical parametric oscillator based on periodically poled lithium niobate*, J. Opt. Soc. Am. B 15,694 (1998). Quoted p. 69

[Menicucci2007] N. Menicucci, S. T. Flammia, H. Zaidi, and O. Pfister, *Ultracompact generation of continuous-variable cluster states*, Phys. Rev. A, 76, 010302 (2007). Quoted p. 112

[Murao1999] M. Murao, D. Jonathan, M. B. Plenio, and V. Vedral, *Quantum telecloning and multiparticle entanglement*, Phys. Rev. A 59, 156 (1999). Quoted p. 111

[Navarrete2008] C. Navarrete-Benlloch, E. Roldán, and G. J. Valcárcel, *Noncritically squeezed light via spontaneous rotational symmetry breacking*, Phys. Rev. Lett. 100, 203601 (2008). Quoted p. 112

[Nikogosyan2005] D. N. Nikogosyan, *Nonlinear optical crystals. A complete survey*, Springer (2005). Quoted p. 69

[Opatrný2002] T. Opatrný, N. Korolkova, and G. Leuchs, *Mode structure and photon number correaltions in squeezed quantum pulses*, Phys. Rev. A 66, 053813 (2002). Quoted p. 90, 121

[Ou1992] Z. Y. Ou, S. F. Pereira, H. J. Kimble, and K. C. Peng, *Realization of the Einstein-Podolsky-Rosen paradox for continuous variables*, Phys. Rev. Lett. 68, 3663 (1992). Quoted p. 16, 23, 103

[Parker2000] S. Parker, S. Bose, and M. B. Plenio, *Entanglement quantification and purification in continuous-variable systems*, Phys. Rev. A 61, 032305 (2000). Quoted p. 89

[Pfister2004] O. Pfister, S. Feng, G. Jennings, R. Pooser, and D. Xie, *Multipartite continuous-variable entanglement from concurrent nonlinearities*, Phys. Rev. A 70, 020302 (2004). Quoted p. 112, 114, 116, 120

[Piskarskas1988] A. Piskarskas, V. J. Smil'gyavichyus and A. Umbrasas, Sov. Quantum Electron. 18, 155 (1988). Quoted p. 16, 69

[Putman1992] C. A. J. Putman, B. G. De Grooth, N. F. Van Hulst, and J. Greve, *A detailed analysis of the optical beam deflection technique for use in atomic force microscopy*, Hour. Appl. Phys. 72, 6 (1992). Quoted p. 2

[Reck1994] M. Reck, A. Zeilinger, H. J. Bernstein, and P. Bertani, *Experimental realization of any discrete unitary operator*, Phys. Rev. Lett. 73, 58 (1994). Quoted p. 121

[Reid1989] M. D. Reid, *Demonstration of the Einstein-Podolsky-Rosen paradox using nondegenerate parametric amplification*, Phys. Rev. A 40, 913 (1989). Quoted p. 10, 103, 107

[Ring1980] P. Ring and P. Schuck, *The nuclear many-body problem*, Springer-Verlag, New York (1980), p. 620. Quoted p. 91

[Roch1997] J.-F. Roch, K. VIgneron, P. Grelu, A. Sinatra, J.-P. Poizat, P. Grangier, *Quantum non demolition measurements using cold trapped atoms*, Phys. Rev. Lett. 78, 634 (1997). Quoted p. 5

[Rosenbluh1991] M. Rosenbluh, R. Shelby, *Squeezed optical solitons*, Phys. Rev. Lett. 66, 153 (1991). Quoted p. 16

[Schmidt2000] E. Schmidt, L. Knöll, and D. Welsch, *Nonclassical correlations in damped quantum solitons*, J. Opt. B: Quantum Semiclassical Opt. 2, 457 (2000). Quoted p. 121

[Schrödinger1935] E. Schrödinger, *Die gegenwärtige situation in der quantenmechanik*, Naturwissenschaften 23,807 (1935); English translation by J. D. Trimmer, *The present situation in quantum mechanics: a translation of Schrödinger's "Cat paradox" paper*, Proceedings of the American Philosophical Society 124, 323 (1980), reprinted in [Wheeler1983]. Quoted p. 103

[SellmeierKNbO3] `http://www.photox.co.uk/knbo3.htm`. Quoted p. 71

[Shelby1992] R. M. Shelby and M. Rosenbluh, *Generation of pulsed squeezed light in a mode-locked optical parametric oscillator*, Appl. Phys. B 55, 226 (1992). Quoted p. 16, 17

[Silberhorn2001] Ch. Silberhorn, P. K. Lam, O. Weiss, F. König, N. Korolkova, and G. Leuchs, *Quantum key distribution with bright entangled beams*, Phys. Rev. Lett. 86, 4267 (2001). Quoted p. 23

[Simon2000] R. Simon, *Peres-Horodecki separability criterion for continuous variable systems*, Phys. Rev. Lett. 84-2726 (2000). Quoted p. 10

[Slusher1985] R. E. Slusher, L. W. Hollberg, B. Yurke, J. C. Mertz, and J. F. Valley, *Observation of squeezed states by four wave mixing in an optical cavity*, Phys. Rev. Lett. 55, 2409 (1985). Quoted p. 12

[Slusher1987] R. E. Slusher, P. Grangier, A. LaPorta, B. Yurke, and M. J. Potasek, *Pulsed squeezed light*, Phys. Rev. Lett. 59, 2566 (1987). Quoted p. 5, 16, 69, 88

[Sokolov2001] I. Sokolov, M. Kolobov, A. Gatti, and L. Lugiato, *Quantum holographic teleportation*, Opt. Comm. 193, 175 (2001). Quoted p. 23

[Supradeepa2008] V. R. Supradeepa, C.-B. Huang, D. E. Leaird, and A. M. Weiner, *Femtosecondo pulse shaping in two dimensions: towards higher complexity optical waveforms*, Optics Express 16, 11878 (2008). Quoted p. 100

[Takeno2007] Y. Takeno, M. yukawa, H. Yonezawa, and A. Furusawa, *Observation of -9 dB quadrature squeezing with improvement of phase stability in homodyne measurement*, Optics Express 15, 4321 (2007). Quoted p. 16

[Cohen-Tannoudji] C. Cohen-Tannoudji, J. Dupont-Roc, and G. Grynberg, *Photons and Atoms. Introduction to quantum electrodynamics*, Wiley (1997). Quoted p. 19

[Treps2002] N. Treps, U. Andersen, B. Buchler, P. K. Lam, A. Maître, H.-A. Bachor, and C. Fabre, *Surpassing the standard quantum limit for high sensitivity measurements in optical images using non classical light*, Phys. Rev. Lett. 88, 203601 (2002). Quoted p. 2, 23

[Treps2003] N. Treps, N. Grosse, W. P. Bowen, C. Fabre, H.-A. Bachor, and P. K. Lam, *A quantum laser pointer*, Science 301, 940 (2003). Quoted p. 23

[Treps2004] N. Treps and C. Fabre, *Criteria of quantum correlation in the measurement of continuous variables in optics*, ArXiv:quant-ph/0407214v2 (2004). Quoted p. 9, 107

[Treps2005] N. Treps, V. Delaubert, A. Maître, J. M. Courty, and C. Fabre, *Quantum noise in multipixel image processing*, Phys. Rev. A 71, 013820 (2005). Quoted p. 15, 24, 25

[Tricomi1967] F. G. Tricomi, *Integral Equation*, Wiley, New York (1967). Quoted p. 89

[Vahlbruch2008] H. Vahlbruch, M. Mehmet, N. Lastzka, B. Hage, S. Chelkowski, A. Franzen, S. Gossler, K. Danzmann, and R. Schnabel, *Observation of squeezed light with 10dB quantum noise reduction*, Phys. Rev. Lett. 100, 033602 (2008). Quoted p. 12, 16

[vanEnk1999] S. J. van Enk, *Discrete formulation of teleportation of continuous variables*, Phys. Rev. A 60, 5095 (1999). Quoted p. 11

[vanLoock2000] P. van Loock and S. L. Braumstein, *Multipartite Entanglement for Continuous Variables: A Quantum Teleportation Network*, Phys. Rev. Lett. 84, 3482 (2000). Quoted p. 111, 115

[Wachman1990] E. S. Wachman, D. C. Edelstein, and C. L. Tang, *Continuous-wave mode-locked and dispersion-compensated femtosecond optical parametric oscillator*, Opt. Lett. 15, 136 (1990). Quoted p. 69

[Walls] D. F. Walls and Gerard J. Milburn, *Quantum Optics*, Springer (1994). Quoted p. 11, 21

[Wasilewski2006a] W. Wasilewski, A. I. Lvovsky, K. Banaszek, and C. Radzewicz, *Pulsed squeezed light: simultaneous squeezing of multiple modes*, Phys. Rev. A 73, 063819 (2006). Quoted p. 3, 64, 92, 123

[Wasilewski2006b] W. Wasilewski and M. G. Raymer, *Pairwise entanglement and readout of atomic-ensemble and optical wave-packet modes in traveling-wave Raman interactions*, Phys. Rev. A 73, 063816 (2006). Quoted p. 92

[Wenger2004] J. Wenger, J. Fiurášek, R. Tualle-Brouri, N. J. Cerf, and P. Grangier, *Pulsed squeezed vacuum measurements without homodyning*, Phys. Rev. A. 70, 053812 (2004). Quoted p. 69

[Werner1995] M. J. Werner, M. G. Raymer, and P. D. Drummond, *Ultrashort pulsed squeezing by optical parametric amplification*, Phys. Rev. A 52, 4202 (1995). Quoted p. 90

[Wheeler1983] J. A. Wheeler and W. H. Zurek, eds., *Quantum theory and measurement*, Princeton University PRess, Princeton (1983). Quoted p. 136

[Wu1986] L.A. Wu, H.J. Kimble, J. Hall, H. Wu, *Generation of Squeezed States by Parametric Down Conversion*, Phys. Rev. Lett. 57, 2520 (1986). Quoted p. 16

[Xin1990] Xin Ma, and William Rhodes, *Multimode squeeze operators and squeezed states*, Phys. Rev. A 41, 4625 (1990). Quoted p. 89, 90

Résumé

Ce mémoire présente une étudie théorique des propriétés dynamiques et quantiques d'un oscillateur paramétrique optique dégénéré de type I que est pompé de manière synchrone par un laser verrouillé en phase (SPOPO). Récemment, des SPOPO ont été exploité pour générer des impulsions optique de très bref durée et leurs propriétés temporelles ont été étudiées théoriquement. Ayant un très grand nombre de degrés de liberté, le champ sortant d'un SPOPO doit être caractérisé au moyen d'une analyse quantique multimodale. Par conséquent, nous développons d'abord un modèle multi-mode de ce système en déduisant des équations quantiques pour les opérateurs de champ intra-cavité. Ensuite, nous étudions les solutions stationnaires pour les champs générés. Celles-ci sont solution d'une équation aux valeurs propres dont le spectre donne des informations sur le nombre de modes "utiles" qui peuvent être extraits et qui condensent toutes les propriétés dynamiques et quantiques du champ intra-cavité et que nous appelons "super-modes". En fait, nous montrons que non seulement le super-mode de seuil le plus bas a (idéalement) des fluctuations parfaitement comprimées au seuil, mais aussi tout les autres super-modes, dont les seuils sont suffisamment proches du première, ont un caractère non-classique important. Cette propriété démontre clairement le fait qu'un SPOPO est un système fortement multi-mode. La dernière partie est consacrée à l'étude du champ de sortie sous le point de vue de la génération d'états intriqué multi-modes et à l'optimisation de ces états au moyen de configurations expérimentales spécifiques.

Mots-clef: oscillateur paramétrique optique, peignes de fréquences, impulsions de courte durée, variables continues, réduction de bruit, intrication, multi-mode.

Abstract

This Thesis studies, from a theoretical point of view, the dynamical and quantum properties of a type I degenerate optical parametric oscillator which is synchronously pumped by a mode-locked laser (SPOPO). In recent past, SPOPOs have been used for generating ultra-short optical pulses of tunable wavelength and their temporal properties have been investigated. Having a huge number of degrees of freedom, the output field of a SPOPO needs to be characterized via a multimodal quantum analysis. Then, we first develop a multimode model of the device, obtaining the quantum equations for the intra-cavity field operators. Afterwards, we study the steady state solutions of the average values of the generated fields that are the solutions of an eigenvalue equation. Its spectrum gives information about the "useful" number of modes in which are concentrated almost all the dynamical and quantum properties of the intra-cavity field and which we call "super-modes". Indeed, we show that not only the super-mode of minimum threshold is (ideally) perfectly squeezed at threshold, but that all the other super-modes have an important non-classical character provided that their thresholds are close enough to the minimum one. This circumstance gives the clear image that a SPOPO is a highly quantum multi-mode system. Finally, the last part of this Thesis is focused on the study of the output of a SPOPO from the point of view of the generation of highly multi-mode entangled states and their optimization by means of specific experimental configurations.

Keywords: optical parametric oscillator, frequency combs, ultra-short pulses, continuous variables, squeezing, entanglement, multi-mode.